Intravenously administered gene therapy for neuronopathic Gaucher disease

Giulia Massaro

Thesis submitted in fulfilment of the requirements for the degree of Doctor of Philosophy

University College London

Department of Pharmacology
UCL School of Pharmacy
29-39 Brunswick Square
London, WC1N 1AX

November 2017

I, Giulia Massaro confirm that the work presented in this thesis is my own. Where information has been derived from other sources, I confirm that this has been indicated in the thesis.

_____

Abstract

Gaucher disease is a lysosomal storage disorder caused by mutations in the *GBA1* gene encoding the enzyme glucocerebrosidase (GCase). Deficiency of GCase causes the accumulation of its substrate glucosylceramide in both visceral organs and the brain. Enzyme replacement therapy is successfully used to ameliorate the visceral pathology, however there is no treatment available for the lethal neurodegeneration. This research focuses on Gaucher disease type II, the most acute neuronopathic form, in which the neuropathology results in death during early infancy. The aim of this project is to intravenously administer adeno-associated viral vector (AAV) based gene therapy to a GCase-deficient mouse model of acute neuronopathic Gaucher disease and assess improvement in lifespan, behaviour, brain and visceral pathology.

The untreated *Gba1* knock-out mice die 12-14 days after birth following severe neurodegeneration. The AAV vector carrying the functional human *GBA1* gene under control of a ubiquitous promoter was intravenously administered to neonatal knock-out mice, with treated animals showing a significant increase in their lifespan ($p=0.0081$). Since the animals did not develop any evident pathological symptoms, they were sacrificed at 55 days of age for a short-term study. The neuropathology was ameliorated and several of the most affected areas of the brain were partially rescued. The analysis of liver, spleen, lung and heart tissues revealed promising improvements in the visceral pathology. A consequent long-term study was performed on 180-day-old treated mice, with the aim to compare intravenous and intracranial administration of the viral vector.

In order to enhance the therapeutic effects of the treatment and improve gene expression in the central nervous system, a novel construct where the *GBA1* gene is controlled by a neuron-specific promoter was administered to neonatal knock-out mice. The severe neurodegeneration was further rescued and the life span of treated animals increased.

Together, these encouraging results demonstrate that gene therapy could provide an effective treatment for the neuronopathic form of Gaucher disease, for which therapeutic needs are currently unmet.

Impact statement

The clinical impact of gene therapy is rapidly growing, as this field has the potential to provide treatment for a wide spectrum of diseases. Gaucher disease, although rare, is the most common lysosomal storage disorder (Belmatoug, 2012). Enzyme replacement therapy and substrate reduction therapy are effective in treating the visceral pathology of type I patients; however there is no cure for the neuronopathic forms of Gaucher disease. Gene therapy has shown the potential to address this unmet need. In the light of our promising findings, in 2015 the European Medicine Agency granted the Orphan Drug designation for AAV9-based gene therapy for neuronopathic Gaucher disease as a novel possible treatment.

Furthermore, systemic gene therapy could not only ameliorate the neuropathology but also be beneficial for type I cases. These patients present a wide range of symptoms with severe complications in different organs. Although enzyme replacement therapy has revolutionised the treatment of type I Gaucher disease (Pastores and Hughes, 2015), it has a number of drawbacks. This includes the need for repeated and regular infusions for the duration of the patient's life, which is both difficult and expensive and may fail to treat some tissues, such as the bones. Gene therapy has the potential to offer an alternative and unified treatment strategy that could overcome these issues through a single administration.

One of the principal limitations is the price of gene therapy trials, as the GMP vector manufacturing costs are extremely high. However, from a long-term economic perspective, gene therapy for Gaucher disease could be significantly less costly than a lifetime of enzyme replacement treatments. Nevertheless, as part of the gene therapy community we are confident that, as with all new technologies, further developments in research will ultimately decrease the cost of developing novel treatments.

Acknowledgements

After I graduated, I followed with great interest Dr. Rahim and Dr. Waddington research, hoping to move to London one day and join their team. Unfortunately, at that time the UCL Institute for Women's Health did not advertise any new PhD position and I was not able to find a suitable studentship. So I gave up, convinced I had lost my chance. However my brother, who I could not thank enough for his love and help, persuaded me to contact Dr. Rahim and Dr. Waddington despite the odds. Luckily I was the right person at the right time, and after a few months of uncertainty I got the position. So all my gratitude goes to Ahad and Simon that welcomed me in their office that morning and believed in my potential when they passed over to me their precious 'Gaucher project'. Over the course of the last three years they have constantly supported me, helping me to produce this work.

I would also like to thank the Gauchers Association for funding my PhD studentship and accepting me in their community, as well as all the collaborators who helped me along the way.

I would like to acknowledge everyone from the Waddington's group, and in particular Dany Perocheau for his invaluable patience and assistance. A big thank goes to Michael, who helped me infinite times bearing me in the lab and bearing with me at home. And of course thanks to Sam, Archie and everyone from the Pharmacology department, in whom I found great friends and fellows adventurers.

I thank from the bottom of my heart my family, who loves my unconditionally and without whose advices and sacrifices I would not be here. Grazie.

Last, but not least, I would like to honour the sacrifice of my animals to further the advancements of this scientific research, with the hope that our contribution will help Gaucher patients in the future.

Table of contents

List of figures

List of tables

Abbreviations

3D	Three-dimensional
AAV	Adeno-associated virus
BSA	Bovine serum albumin
CA1/CA2	Cornus ammonis region 1 and 2
CMV	Cytomegalovirus
CBE	Conduritol B epoxide
CD68	Cluster of Differentiation 68
cDNA	Complementary DNA
CENT2	Central lobule 2
CLN	Neuronal ceroid-lipofuscinosis
CNS	Central nervous system
dH_2O	Distilled water
DNA	Deoxyribonucleic acid
ER	Endoplasmic reticulum

FGF-2	Fibroblast growth factor 2
GAGs	Glycosaminoglycans
GalCer	Galactosylceramide
gc	Genome copies
GCase	β-glucocerebrosidase
GFAP	Glial fibrillary acidic protein
GFP	Green fluorescent protein
Gi	Gigantocellular nuclei
GlcCer	Glucosylceramide
GM	Monosialotetrahexosylganglioside
GUSB	β-glucuronidase
H&E	Hematoxylin and Eosin
IC	Intracranial
ICV	Intracerebroventricular
IT	Intrathecal
ITR	Inverted terminal repeat

IV	Intravenous
kb	Kilo base
KO	Knock-out
LAMP1	Lysosome-associated membrane protein 1
LIMP-2	Lysosome integral membrane protein 2
loxP	Locus of X(cross)-over in P1
M6P	Mannose-6-phosphate
MHC I	Major histocompatibility complexes class I
MPSs	Mucopolysaccharidoses
mRNA	Messenger RNA
NPC	Niemann-Pick disease type C
ns	Non-significant
P	Postnatal day
PEI	Polyethylenimine
PFA	Paraformaldehyde
rAAV	Recombinant AAV

RNA	Ribonucleic acid
S1BF	Somato-barrel field region 1
scAAV	Self-complementary AAv
SD	Standard deviation
SERCA	Sarco/endoplasmic reticulum ATPase
ssAAV	Single-stranded AAV
ssDNA	Single-stranded DNA
TNF- α	Tumor necrosis factor alpha
UPR	Unfolded protein response
UV	Ultraviolet
vg	Viral genome
vp	Viral particle
VPM/VPL	Ventral post medial/ventral post lateral thalamic nuclei
WPRE	Woodchuck post-transcriptional regulatory element
WT	Wild-type

1. Introduction

Gaucher disease is the most common lysosomal storage disorder (Lal and Sidransky, 2017). The disease is caused by mutations in the *GBA1* gene, which encodes for the lysosomal enzyme β-glucocerebrosidase, resulting in the accumulation of storage material in macrophages within visceral organs and in some cases the brain of affected patients. The spectrum of clinical manifestations is broad and there can be a lack of direct correlation between genotype and phenotype. However, Gaucher disease has historically been broadly classified into three distinct types according to the absence or presence and severity of central nervous system impairment. While there is a commercially available treatment that efficiently ameliorates the systemic manifestations, the neurological manifestations of the disease still remain incurable.

Extraordinary advances in the gene therapy field shed a light on the potential use of adeno-associated viruses as a therapeutic tool for the treatment of genetic diseases and in particular lysosomal storage disorders. Gaucher disease represents a feasible candidate for viral gene therapy applications. Taking into consideration the successful results of many preclinical studies on gene delivery to the central nervous system, gene therapy may be a promising clinical therapeutic option for the untreatable neuropathic forms of Gaucher disease.

The aim of this introductory chapter is to provide the reader with an overview of the main molecular and pathological features that characterise many lysosomal storage disorders, particularly Gaucher disease. Some of the current therapeutic options will be explored. Viral gene therapy and specifically gene delivery to the central nervous system will be examined. This chapter will conclude with a brief discussion of the rationale of the outlined research project.

1.1. Lysosomal Storage Disorders

Lysosomal storage disorders are monogenic metabolic diseases caused by the accumulation of biological materials in the late endosome/lysosome system (Platt, 2014). These include more than 60 different diseases, and even though they are referred to as rare their estimated combined frequency at birth is 1:7,500 (Cox and Cachon-Gonzalez, 2012). Traditionally, lysosomal storage diseases have been classified according to the substrate that accumulates in the cells (**Table 1**). However, these diseases are mainly caused by mutations in the genes encoding enzymatic hydrolases involved in the metabolism of macromolecules, so that the same metabolic pathway can be affected in different pathologies. Therefore, although caused by different genetic defects, distinctive disorders could be characterised by the accumulation of the same biological material (Prinetti et al., 2011). Moreover, the identification of novel defects in lysosomal enzymes and integral proteins involved in trafficking broadened the traditional classification of lysosomal storage disorders (Boustany, 2013).

In some ethnic groups, especially isolated communities and enclosed geographical areas, the incidence of lysosomal storage diseases or carrier frequency is drastically higher (Boustany, 2007). The known genetic defects involved in lysosomal storage diseases are numerous and even though lysosomal disorders are monogenic diseases, several diverse mutations have been identified in the same affected gene in different patients. The effects of distinctive mutations on the same gene are broad and can influence severity and onset of the disease. In fact, different mutations can lead to complete disruption of the enzymatic residual activity or only partially reduce it. The proximity of the mutation to the catalytic site of the enzyme, the distribution of stored substrate in specific tissues and the cell turnover rate are some of the factors that can influence the severity of the pathology. Taking these variations into consideration, it is clear that genetic analysis is not always enough to predict the symptoms, onset and progression of the disease, as the spectrum of the clinical manifestations is broad and there may not always be a direct genotype-phenotype correlation (Futerman and van Meer, 2004).

CLASS	DEFECTIVE ENZYME OR PROTEIN
Sphingolipidoses	
Fabry disease	α-Galactosidase A
Farber lipogranulomatosis	Ceramidase
Gaucher disease type I	β-Glucosidase
Gaucher disease types II and III	Saposin-C activator
Niemann–Pick disease types A and B	Sphingomyelinase
GM1-gangliosidosis: infantile, juvenile and adult variants	β-Galactosidase
GM2-gangliosidosis (Sandhoff): infantile and juvenile	β-Hexosaminidase A and B
GM2-gangliosidosis (Tay–Sachs): infantile, juvenile and adult variants	β-Hexosaminidase A
GM2-gangliosidosis (GM2-activator deficiency)	GM2-activator protein
GM3-gangliosidosis	GM3 synthase
Metachromatic leukodystrophy (late infantile, juvenile and adult)	Arylsulphatase A
Sphingolipid-activator deficiency	Sphingolipid activator
Mucopolysaccharidoses	
MPS I (Scheie, Hurler–Scheie and Hurler disease)	α-Iduronidase
MPS II (Hunter)	Iduronidase-2-sulphatase
MPS IIIA (Sanfilippo A)	Heparan N-sulphatase (sulphamidase)
MPS IIIB (Sanfilippo B)	N-acetyl-α-glucosaminidase
MPS IIIC (Sanfilippo C)	Acetyl-CoA; α-glucosamide N-acetyltransferase
MPS IIID (Sanfilippo D)	N-acetylglucosamine-6-sulphatase
MPS IVA (Morquio syndrome A)	N-acetylgalactosamine-6-sulphate sulphatase
MPS IVB (Morquio syndrome B)	β-Galactosidase
MPS VI (Maroteaux–Lamy)	N-acetylgalactosamine-4-sulphatase (arylsulphatase B)
MPS VII (Sly disease)	β-Glucuronidase
MPS IX	Hyaluronidase
Glycogen storage disease	

Pompe (glycogen storage disease type II)	α-Glucosidase
Oligosaccharidoses	
α-Mannosidosis	α-Mannosidase
β-Mannosidosis	β-Mannosidase
Fucosidosis	α-Fucosidase
Aspartylglucosaminuria	Aspartylglucosaminidase
Schindler disease	α-N-acetylgalactosaminidase
Sialidosis	α-Neuraminidase
Galactosialidosis	Lysosomal protective protein
Mucolipidosis II (I-cell disease); mucolipidosis III	Urine diphosphate-N-acetylglucosamine; lysosomal enzyme N-acetylglucosaminyl-1-phosphotransferase
Integral membrane protein	
Cystinosis	Cystinosin
Danon disease	Lysosome-associated membrane protein 2
Action myoclonus–renal failure syndrome	Lysosome membrane protein 2
Salla disease	Sialin
Niemann–Pick disease type C1	NPC-1 , NPC-2
Mucolipidosis IV	Mucolipin
Additional disease types	
Multiple sulphatase deficiency	Sulphatase-modifying factor 2
Niemann–Pick disease type C2	NPC-2
Wolman disease (infantile); cholesteryl ester storage disease	Lysosomal acid lipase
Galactosialidosis	Cathepsin A

Table 1 - Summary of the most common lysosomal storage disorders.

Classification of main lysosomal storage diseases and correspondent defective enzymes.

1.1.1. Pathobiology

The pathophysiology of lysosomal storage disorders is complex and still not fully understood. This is because the lysosomal compartment is involved in numerous

cellular mechanisms and several biological processes contribute to the propagation of pathology (**Figure 1**).

The endosome/lysosome system is a tightly connected cellular compartment and it is responsible for the degradation and recycling of extracellular substrates. Moreover, cellular components, such as protein aggregates, damaged cytosolic organelles and intracellular pathogens can be targeted for degradation in lysosomes through the formation of autophagosomes and consequent fusion and release of the damaged cellular material into the lysosomal compartment (Levine and Klionsky, 2004). Autophagy is a tightly controlled cellular mechanism; therefore it is not surprising that this process is dysregulated in many lysosomal storage disorders. Indications of the involvement of impaired autophagy in lysosomal storage disorders have been found in several animal models of Neuronal Ceroid Lipofuscinoses (Koike et al., 2005), Pompe disease (Fukuda et al., 2006) and Niemann-Pick type C (Ko et al., 2005).

Some of the macromolecules that accumulate in lysosomal storage disorders are involved in various signal transduction pathways, such as glycosaminoglycans (GAGs) in mucopolysaccharidoses, heparan sulphate in Hurler disease or galactosylceramide in Krabbe disease (Huizing et al., 2008). Metabolites produced from the degradation of GAGs have a similar structure to the bacterial endotoxin lipopolysaccharide. When this material accumulates it can activate the Toll like receptor 4 (TLR4), leading to the secretion of proinflammatory cytokines like TNF-α, and the proapoptotic signalling molecule ceramide (Simonaro et al., 2005). Ceramide synthesis is also upregulated in some ceroid lipofuscinosis, where the accumulation of CLN proteins activates the production of ceramide, contributing to the increased apoptosis (Haddad et al., 2012). Impairment of the fibroblast growth factor 2 signalling cascade due to the accumulation of heparan sulphate in neuronal precursor cells in Hurler syndrome promotes neurodegeneration and cell death (Pan et al., 2005). The aforementioned examples are only a few of the critical signal transduction pathways that can be impaired in lysosomal storage diseases, where dysfunctions in lipid rafts and trafficking result in cell death. However, the apoptotic pathway is not the only signalling mechanism that can be altered in lysosomal storage disorders. For instance, in Krabbe disease the accumulation of galactosylceramide's derivative psychosine activates the T-cell associated gene 8 (TDAG8) receptor, inhibiting physiological cytokinesis with consequent formation of

multinucleated ‘globoid’ cells (Esch et al., 2003).

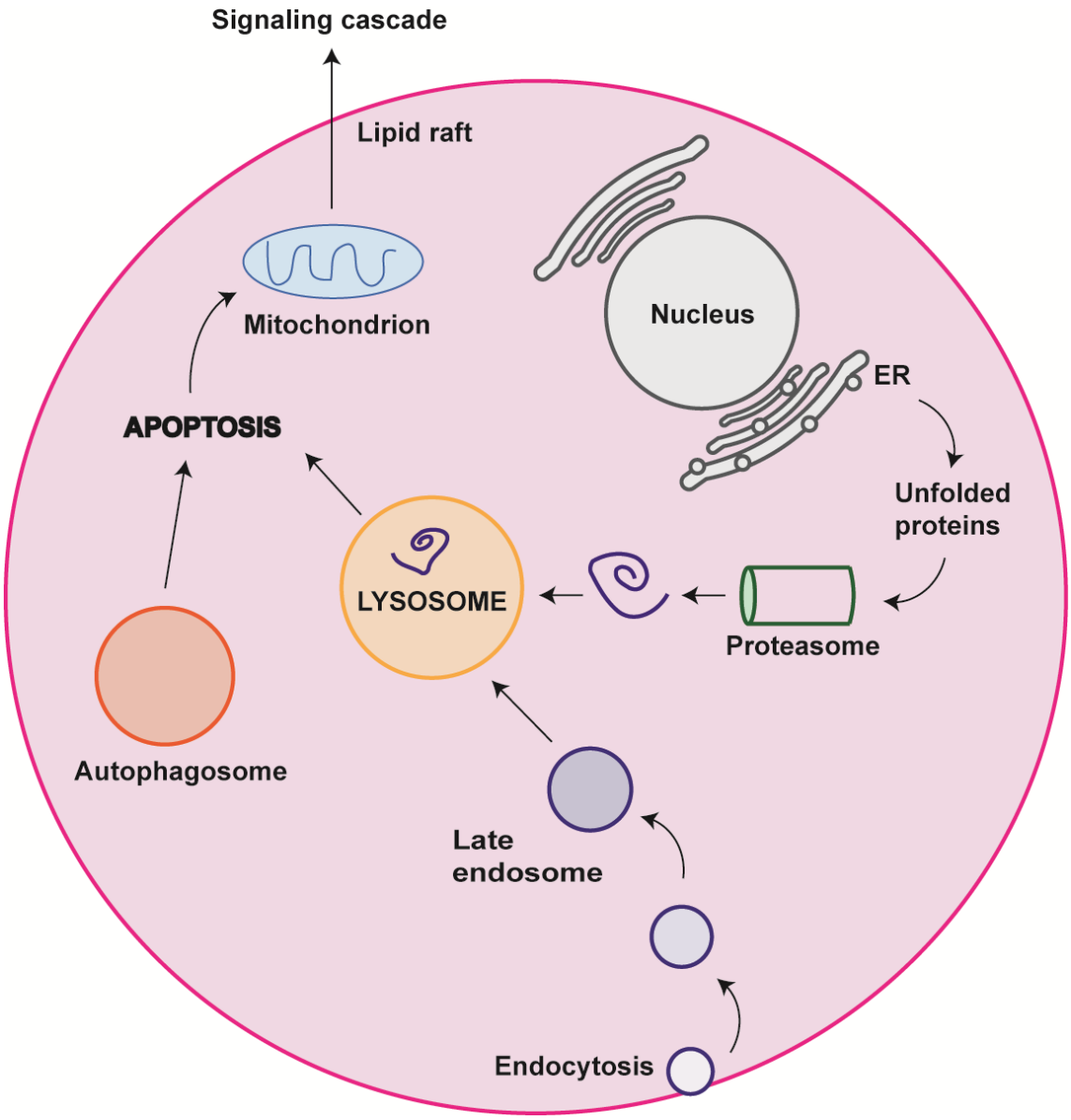

Figure 1 - Cellular mechanisms affected in lysosomal storage disorders.

Schematic representation of the cellular functions of the lysosome. Many cellular compartments and organelles are disrupted in lysosomal storage diseases. Dysfunctions in the endosomal/lysosomal compartment lead to dysregulation of autophagy and cell death. Lipid raft and cellular signalling are also impaired. The endoplasmic reticulum (ER) and calcium homeostasis are affected.

Endoplasmic reticulum (ER) functionality is also impaired in some lysosomal storage disorders. In Gaucher disease the accumulation of glucosylceramide (GlcCer) within neurons causes supraphysiological release of calcium from the ER to the cytosol, inducing the activation of the calcium channel ryanodine receptor and consequent increased response of glutamate in affected neurons (Lloyd-Evans et al., 2003). On the contrary, in Sandhoff and Tay-Sach diseases the reuptake of calcium into the ER via the sarco/endoplasmic reticulum ATPase (SERCA) is inhibited (Pelled et al., 2003). The depletion of calcium within the endoplasmic reticulum affects the correct folding of proteins. It has been reported that a continued unfolded protein response (UPR) is induced by the accumulation of storage material in GM1-gangliosidosis, causing apoptosis through the caspase-12 pathway (Tessitore et al., 2004). As a result of alteration of calcium homeostasis neurotoxicity is promoted, ultimately leading to neuronal loss.

1.1.2. Visceral manifestations

Although the nature of the biologic material that accumulates in different lysosomal storage disorders varies, many of these pathologies share common clinical features. Typically, these disorders have multi-organ presentations. The onset of the phenotypes varies and even though lysosomal storage disorders are usually not congenital, in most acute cases the manifestations can be present at birth. In many diseases, like Gaucher, Niemann-Pick, MPSs, and other sphingolipidoses, one of the first pathological manifestations is hepatosplenomegaly, often already present at birth (Staretz-Chacham et al., 2009). Cardiomyopathies, including cardiomegaly, heart failure and deposition of glycogen in the heart valves are associated with many lysosomal storage disorders and can be present in newborns, like in infantile Pompe disease, or have a later onset as in several shpingolipidoses (Guertl et al., 2000). Severe respiratory manifestations have been described in Pompe disease patients, where muscular hypotonicity causes reduction in lung volume (Disease et al., 2006); as well as in NPC-2 (Morisot et al., 2005) and Farber disease patients (Devi et al., 2006). Haematological and endocrine manifestations are also typical of lysosomal storage disorders: anaemia and thrombocytopenia are haematological features characteristic of Gaucher disease (Roth et al., 2005), while osteopenia and enlargement of endocrine glands are present in other

lysosomal storage disorders, especially in MPSs patients (Polgreen et al., 2008). As secondary manifestation of haematological disorders and organomegaly, many lysosomal storage disease patients, including MPS, GM1-gangliosidosis, NP-C, Gaucher and Farber disease, present with hydrops fetalis (Stone and Sidransky, 1999). Abnormal bone formation, joint contractures and swelling usually develop later in Gaucher, Farber, MPS and GM1-gangliosidosis patients, although bone disease has been occasionally described in neonates (Staretz-Chacham et al., 2009). Various cutaneous manifestations, such as ichtchyosis, skin lesions and an increase in body hair are typical of Gaucher (Sidransky et al., 1996), MPSs and Fabry disease (Boustany, 2013). New born patients can also present dysmorphic features, as coarse facies, depressed or absent nasal septum and unusual facial appearances (Boustany, 2007).

1.1.3. Neuropathology

The central and peripheral nervous systems are affected in many forms of lysosomal storage diseases, causing a variety of symptoms, including neurocognitive impairment, movement disorders, seizures, optical manifestations and deafness, which usually lead to premature death (Walkley, 2009). Even though many lysosomal storage disorders share common neurological phenotypes, the pathological mechanisms underlying neurodegeneration can be various. Clearly, the accumulation of different substrates and their effects on neurons depend on the specific cell type, morphology and distribution: in fact, the storage can be widespread throughout the brain or affect just a restricted more vulnerable cell population. In Fabry disease deposits of primary substrate globotriaosylceramide have been found in a limited number of neurons in specific brain regions, such as the brain stem, hypothalamus, amygdala, and in the spinal cord (deVeber et al., 1992).

It has been shown that the accumulation of sphingolipids, such as ceramide and glucosylceramide plays a significant role in the neuroinflammatory response in lysosomal storage diseases (Nixon, 2009). Whether primary neuronal damage triggers the activation of glial cells or neurodegeneration and neuronal death are caused by metabolic dysfunctions within microglia has not yet been clarified (Bosch and Kielian, 2015). It is evident that chronic inflammation and neurodegeneration are tightly

correlated; however the neuropathology in lysosomal storage disorders is not triggered exclusively by primary storage in neurons. For instance, in α-mannosidosis brains are affected by primary accumulation of mannose-rich oligosaccharides, although secondary storage of GM2 and GM3-gangliosides specifically in cortical pyramidal neurons is thought to affect neuronal integrity and contribute to the formation of ectopic dendrites and axonal spheroids (Crawley and Walkley, 2007).

Although severe neuropathology can be already present at birth, in most patients the onset of the first neurological symptoms may range from late infancy to adulthood in less acute chronic cases (Jardim et al., 2010). As for the visceral manifestations, neurological clinical expressions can vary accordingly to the severity of the mutations. The heterogeneity in symptoms and onset can lead to misdiagnosis or delayed diagnosis, in particular for subjects without family history. Therefore, the initial screening requires confirmation through biochemical and\or genetic analysis (Pastores and Maegawa, 2013).

1.1.4. Therapies

Enzyme replacement therapy is today's standard approved treatment for many lysosomal storage disorders, including Gaucher disease type I, Fabry disease, Pompe disease and some MPSs (Desnick and Schuchman, 2012). In the early 1970s, it was already evident that replacing the specific missing or defective enzyme by systemically administering it to the body was sufficient to at least partially correct the intracellular enzymatic activity and consequently clear the stored material. Therefore, regular intravenous infusions of purified recombinant exogenous enzyme resulted in a feasible and effective therapeutic option, particularly successful in milder cases where patients present residual enzymatic activity. In the past two decades researchers have established new strategies to improve the enzyme formulation. The concept of cross-correction developed after the discovery that many lysosomal enzymes are targeted to the lysosomes via the mannose-6-phosphate (M6P) receptor pathway, and the same receptor is also present on the surface of the plasma membrane (Platt and Lachmann, 2009). According to this mechanism the addition of a M6P group to a recombinant enzyme allows the cellular uptake by nearby cells of administered or secreted enzyme and

facilitates its transport to the lysosomes. Thus, the necessity of correcting every cell is overcome and low levels of intracellular enzymatic activity can be sufficient to restore the metabolic defect. It is obvious that the cross-correction principle is limited to soluble enzymes and it is not suitable for disorders involving transmembrane proteins. Although enzyme replacement therapy is safe and usually well tolerated, it presents some disadvantages: patients are subjected to continuous and frequent infusions; the cost of repetitive administrations is significant; often combination therapies, like bone marrow transplantation are required; and more importantly the currently approved products do not show any efficacy in the treatment of central nervous system pathologies (Brady, 2006). In fact, the infused recombinant enzyme is not able to cross the blood-brain barrier, even when administered at high dose. Direct intracerebral or intrathecal administration can be a successful alternative. The U.S. Food and Drug Administration has recently approved a novel enzyme replacement therapy for late infantile CLN2 patients (Brineura©, (Administration, 2017)). The treatment is administered once every other week directly into the cerebrospinal fluid via a reservoir with a ventricular catheter. Although Brineura© has demonstrated to be efficacious in paediatric patients and has received Orphan Drug designation, the nature of the procedure is considered invasive and allows for further consideration of other treatment strategies.

An alternative approach is to use a small molecule drug that reduces the synthesis of the accumulating pathogenic substrate. This is known as substrate reduction therapy. An approved substrate reduction therapy consists of the administration of the imino sugar *N*-butyldeoxynojirimycin (miglustat), a competitive inhibitor of ceramide glucosyltransferase that blocks the biosynthesis of glucosylceramide and glucosylceramide-derived glycosphingolipids (Platt et al., 1994). Although miglustat was first commercialised for Gaucher disease type I, it also has potential for treatment of other lysosomal storage disorders, such as Niemann-Pick type C, Fabry disease, and GM1 and GM2-gangliosidose, where secondary accumulation of glucosylceramide-based glycosphingolipids occurs. Moreover, miglustat has shown the ability to cross the blood-brain barrier and therefore it can be used as a treatment for neurological manifestations (Jeyakumar et al., 2005). The main side effect of miglustat medication is the development of severe gastrointestinal symptoms and occasional peripheral neuropathy and tremor.

Most lysosomal storage disorders are associated with mutations in genes that influence protein conformation, folding and trafficking resulting in unstable and degradable enzymes. Pharmacological chaperones are molecules that, binding to the nascent polypeptides, promote protein stability and inhibit misfolding and protein aggregation (Parenti et al., 2015). Pharmacological chaperone therapy had first been proposed as a treatment for Fabry disease, where 1-deoxygalactonojirimycin (migalastat hydrochloride) binds to the active site of α-galactosidase A, increasing its activity (Young-Gqamana et al., 2013). More recently, Orphan Drug designation was granted to Arimoclomol© (Orphazyme AsP) as a potential treatment for Niemann-Pick type C patients. Arimoclomol© is a co-inducer of the heat-shock response that induces the expression of molecular chaperones like Hsp70, and activates natural cellular repair pathways (Parfitt et al., 2014). The treatment has already shown beneficial effects in pre-clinical studies on animal models of amyotrophic lateral sclerosis, spinal bulbar muscular atrophy and retinitis pigmentosa. The on-going phase 2 study (NCT02612129) is currently investigating the efficacy and safety of the drug on NP-C subjects. Since not all mutations will be responsive to potential chaperone therapy and the effects of the treatment may not always be sufficient, researchers are investigating the possibility of chaperone therapy in combination with other treatments.

Bone marrow transplant for lysosomal storage diseases has been widely performed in the last two decades with the aim of engrafting donor cells of haemapoietic origin to correct enzyme deficiency in the host (Vellodi, 2014). Although this treatment results in amelioration of some disorders, such as Hurler disease, bone marrow transplant is not effective for acute neurodegenerative phenotypes. Although donor-derived cells can be found in the cerebrospinal fluid, the small percentage of corrected microglia cells is not always enough to provide robust enzyme expression and correct the most severe cases of neurodegeneration.

To summarise, although there are some therapeutic options available to treat some specific types of lysosomal storage disorders, others remain only partially treatable or have no therapeutic strategies available at all. This is particularly so in those conditions that also affect the central nervous system. Moreover, the significant financial cost associated to these therapies is a burden that the healthcare system will have to carry for the duration of the patients' lives.

Viral gene therapy represents a suitable candidate for the treatment of lysosomal storage disorders and is a central theme in this thesis. Therefore, it will be further discussed in more detail as a promising potential therapeutic option.

1.2. Gaucher disease

Gaucher disease is the most common lysosomal storage disorder, with an approximate prevalence of 1:100,000 and annual incidence in the general population of 1:60,000 (Belmatoug, 2012). The pathology was named after Philippe Gaucher in 1882, who first described the typical enlarged spleen cells in a 32-year-old woman. At that time, Gaucher incorrectly identified the pathology as splenetic cancer. It was only in 1965 that the condition was defined as an autosomal recessive disease characterized by the inability of the defective lysosomal enzyme β-glucocerebrosidase to efficiently degrade its substrate glucosylceramide (Hruska et al., 2008).

1.2.1. Clinical classification

Classically, Gaucher disease has been broadly classified into three main forms based on the absence (type I) or presence and severity of neurological symptoms (type II and type III). However, the more realistic clinical assessment of patients has shown that Gaucher disease exhibits a continuum of phenotypes with the main distinction of presence or absence of neurological involvement (Sidransky, 2004) (**Figure 2**). Nevertheless, to aid in recognition, this text will refer to the traditional classification.

Type I – Type I is the most frequent form of Gaucher disease and its manifestations do not involve central nervous system impairment. The physical presentation is characterised by a number of visceral symptoms. This includes severe splenomegaly: the size of the spleen can reach 1500-3000 cm^3, compared to the average 50-200 cm^3 in healthy adults (Stone et al., 2000a). Hypersplenism is accompanied by massive distention of the abdomen and consequent pancytopenia (Nagral, 2014). Anaemia, thrombocytopenia and leukopenia can be accompanied by coagulation defects. Although enlargement of the liver is common, it usually does not lead to empathic

failure. Bone disease is present in 70-100% of type I patients: individuals often develop bone crises, pathologic fractures, arthritis, osteonecrosis of the joints and collapse of the vertebrae (Pastores et al., 2000). Pulmonary involvement includes pulmonary hypertension and interstitial lung disease (Mistry et al., 2002). Renal and cardiac complications are less common. Gaucher disease type I has a broad range of onset: first symptoms can appear in early childhood and worsen with time, or they can manifest in adult patients (Mehta, 2006).

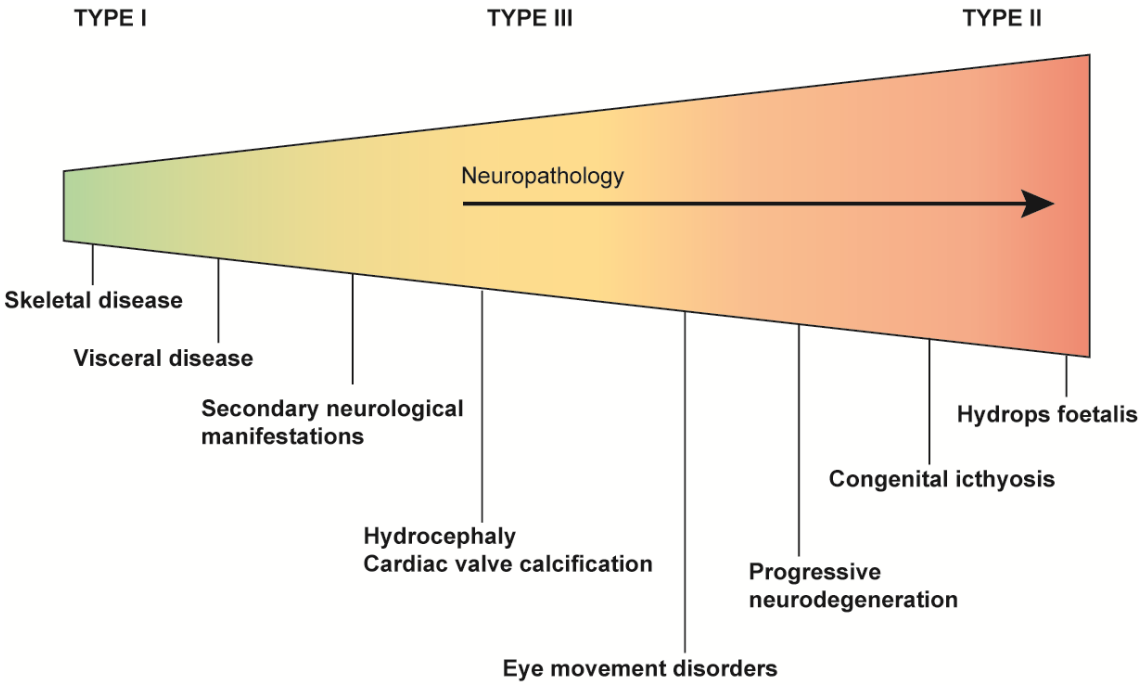

Figure 2 - Wide spectrum of phenotypes in Gaucher disease.

Although Gaucher disease has been classically classified in three distinct types (type I, II and III), it presents with a continuum of manifestations. The primary distinction is now based on the presence or absence of neurological symptoms (Sidransky, 2004).

Type II – Type II is described as the acute neuronopathic form of Gaucher disease. The onset of the disease is in the neonatal period and death occurs by age two to four years (Goker-Alpan et al., 2003). However, some cases of perinatal-lethal Gaucher disease associated with hepatosplenomegaly, skin abnormalities and intrauterine death have been reported (Mignot et al., 2006). Gaucher disease type II presents the same visceral manifestation of type I, with significant hepatosplenomegaly and pulmonary

involvement. Patients develop ichthyosis, ranging from mild skin peeling to the "colloid baby" phenotype (Holleran et al., 2006). The earliest neurological symptoms are strabismus and horizontal gaze palsy (Harris et al., 1999), hypertonic posturing and retroflexion of the head (Pastores and Hughes, 2015). Soon after birth, patients manifest difficulties in swallowing, seizures and progressive epilepsy (Blom and Erikson, 1983). Death usually occurs following apnoea and laryngospasm as a consequence of extensive paralysis (Zimran, 2011).

Type III – Type III is the chronic neuronopathic form of Gaucher disease. Individuals can manifest the first symptoms already in early infancy, however the progression of the disease is slow and lifespan can be prolonged to adulthood. The visceral pathology is extended and present at birth, while the neurological signs can appear before two years of age or manifest later in life (Goker-Alpan et al., 2003). In some cases of chronic neurologic Gaucher disease, dementia and ataxia can be observed in the latest stage of the pathology (Pastores and Hughes, 2015). The clinical course not always depends on age of onset and rate of progression. Furthermore, a subset of patients can manifest an intermediate phenotype between type II and III, characterised by a late onset and rapid progression of acute neurodegeneration (Goker-Alpan et al., 2003).

1.2.2. Genetics and epidemiology

The gene encoding β-glucocerebrosidase (*GBA1*; MIM# 606463) is located on chromosome 1 (1q21) (Barneveld et al., 1983). It consists of 11 exons and 10 introns spanning a total of 7.6kb (Hruska et al., 2008) A pseudogene (*GBAP*) that shares 96% of homology with the functional gene and has similar exonic organization is located 16kb downstream (Horowitz et al., 1989). The *GBA1* gene sequence is highly conserved among different species, in particular between human and different species of mammals (Chenna et al., 2003). On the contrary, the *GBAP* pseudogene is only present in primates (Martinez-Arias et al., 2001). The cDNA sequence for *GBA1* is 1.6kb long. The *GBA1* gene is transcribed into different mRNAs, mainly deriving from alternative splicing events, alternative polyadenylation sites and transcription of the pseudogene (Graves et al., 1988). The levels of mRNA vary in different tissues, and they are not predictive of the enzymatic activity (Reiner and Horowitz, 1988). This is a reflection of

the dissimilarities in the ability to translate the mRNA into a mature protein in different cell populations (Xu et al., 1995).

A

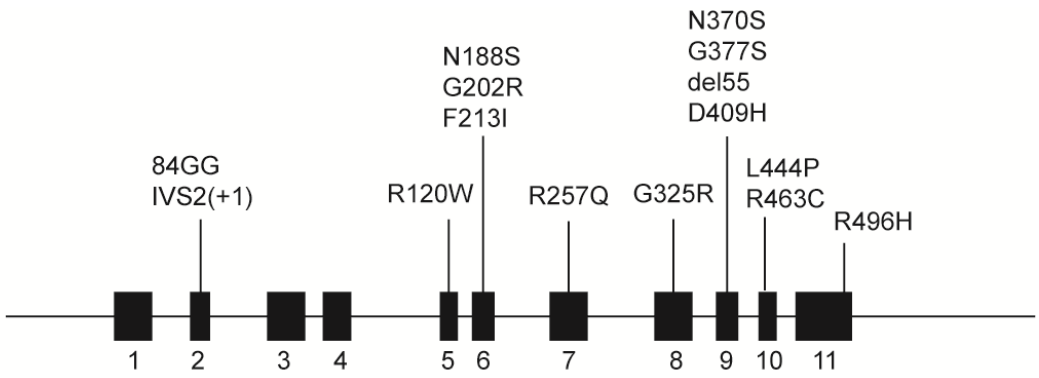

B

GENETIC VARIANT	TYPE	AFFECTED INDIVIDUALS
N370S/N370S	I	29%
N370S/-	I	20%
N370S/L444P	I	16%
N370S/84GG	I	12%
L444P/L444P	II, III	6%
L444P/-	III	3%
N370S/IVS2(+1)	I	3%
Others	I,II, III	11%

Figure 3 - *GBA1* gene.

A Exonic structure of the human *GBA1* gene. The most common mutations described in Gaucher patients are indicated. **B** Proportion of patients carrying the most common mutations and predicted phenotype. Data are based on 1097 subjects in the Gaucher Registry (International Collaborative Gaucher Group, 1999) (Pastores and Hughes, 2015).

Today, approximately 300 mutations in the *GBA1* gene are known (Scholz and Jeon, 2015) (**Figure 3**). The vast majority are missense mutations, but also nonsense mutations, small deletions and insertions, and splice junction mutations have been reported (Hruska et al., 2008). Different recombinant events between *GBA1* and its pseudogene can also lead to pathological alterations (Eyal et al., 1990). Most of the missense pathological mutations found in patients are conserved in those mammalian

species that present high homology with the human gene sequence (Chenna et al., 2003). The most common mutations[1] were first described in 1988 by Tsuji and colleagues (Tsuji et al., 1988): N370S (c.1226A>G) and L444P (c.1448T>C) are the most prevalent mutated alleles found in Gaucher disease patients. The N370S substitution is the most common mutation within Jewish populations and is normally associated with Gaucher disease type I. L444P, F231I (c.754T>A), IVS2(+1) G>A and the 55bp deletion Δ55 (c.1263-1317del) are usually associated with the acute neuropathic form of Gaucher disease (Stone et al., 2000b). As already mentioned, the correlation between genotype and phenotype is not always direct, as the genetic state of the patients and the residual enzymatic activity do not always correspond to the severity of the pathology, resulting in the prediction of disease being challenging. Generally, individuals with at least one N307S allele do not develop neuropathology. In homozygous patients (N370S/N370S), the low residual enzyme activity is sufficient to prevent the central nervous system pathology, however, subjects present a wide range of systemic manifestations from asymptomatic adults to severe organomegaly and bone disease (Koprivica et al., 2000). Patients homozygous for the L444P and F231I mutations develop, in most of the cases, the chronic form of neuropathic Gaucher disease (Stone et al., 2000b). However, when either mutation is in combination with a null allele, patients are more likely to develop the acute type II phenotype. So far, more than 50 mutations have been described for Gaucher disease type II, generally including rare and recombinant alleles. Type III patients with mild neurological manifestation, in addition of the L444P allele, often carry the R463C (c.1504C>T) mutation; while the N188S (c.680A>G) and G377 (c.1246G>A) mutations in combination with a null or recombinant allele are more common in individuals with more severe epileptic phenotype (Koprivica et al., 2000). Patients carrying the D409H (c.1342G>C) mutation manifest a particular form cardiomyopathy consisting in calcification of the cardiac valves (Bohlega et al., 2000). However, when D409H is in *cis* with H255Q (c.882T>G) patients develop severe neuropathology. PCR-based detection techniques are not suitable to discriminate between the gene and the pseudogene, and may not identify recombinant alleles leading to misgenotyping. For this reason, today a combination of

[1] Mutations discussed in the text are indicated with the traditional name of the allele. The cDNA nomenclature is reported in parentheses, as recommended at http://varnomen.hgvs.org, where nucleotide +1 (c.1) is the adenine of the first ATG initiation codon.

genome sequencing and genotyping at polymorphic repeat regions is successfully used to identify recombinant events and possible new *GBA1* mutations

Ethnic origin contributes to the distribution of pathological mutations between different populations. The N370S mutation generally occurs in European, American and Middle East populations, with greater frequency among Ashkenazi Jews, Spanish (46%) and Portuguese (63%), caused by a founder effect (Pastores and Hughes, 2015). In particular, in the Ashkenazi community Gaucher disease type I has a prevalence of almost 1:1,000 and the N370S mutation accounts for 70% of the pathogenic variants. The L444P allele is more common in North Sweden, Egypt and East Asia (Nagral, 2014). The N370S and 84GG (c.84dupG) alleles are not present in Japanese and Chinese populations, while the L444P is more prevalent (41% and 54% respectively) (Wan et al., 2006) The mutation D409H prevails in Palestine (Jenin Arabs), Greece and Albania.

1.2.3. Biochemistry and cellular pathology

The lysosomal enzyme β-glucocerebrosidase (GCase) is responsible for the cleavage of the β-glucosidic linkage of the substrate glucosylceramide (GlcCer) (Grabowski et al., 1990). The first crystal structure of the enzyme was solved in 2003 (Dvir et al., 2003) (**Figure 4A**). The enzyme has a molecular weight of 59kDa and is composed of three domains: domain I (residues 1-27, 383-414) is a three-stranded antiparallel β-sheet containing two disulphide bridges that are essential for the correct folding of the protein; domain II (residues 30-75, 431-497) is an independent immunoglobulin-like domain formed by two β-sheet structures; domain III (residues 76-381, 416-430) has a TIM barrel structure and contains the catalytic site. More recently the structure of one of the mutated form (N370S) of β-glucocerebrosidase was also obtained (Wei et al., 2011). The N370S mutation is located on the longest α-helix of the catalytic domain in the interface between domain II and III, where several other pathogenic mutations have been identified. The N370S mutant results in a correctly folded molecule; however the protein structure is less flexible and the enzyme does not efficiently bind the substrate, resulting in a reduction of its catalytic activity. The L444P mutation causes a conformational change in the hydrophobic core of the protein, altering the folding of

domain II and therefore the stability of the enzyme. β-glucocerebrosidase, unlike most

A

B

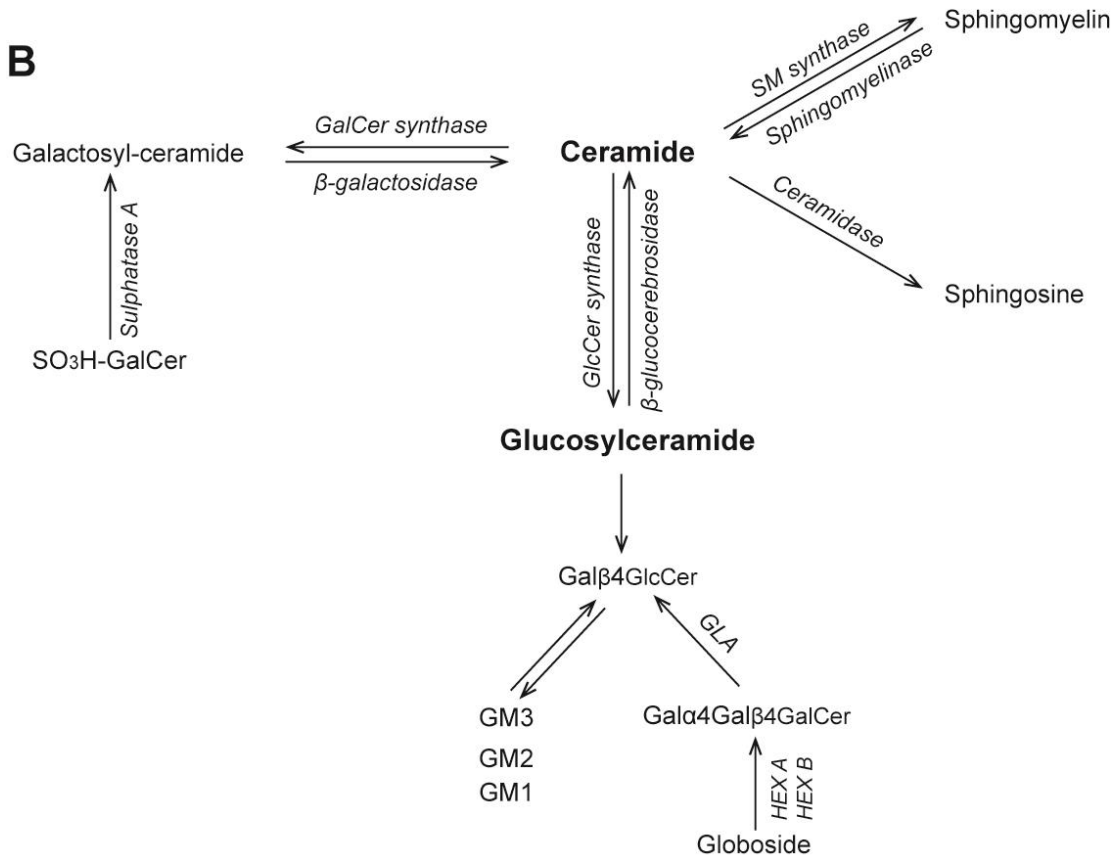

Figure 4 - β-glucocerebrosidase and glycosphingolipids metabolic pathway.

A X-ray structure at 2.0 Å of the β-glucocerebrosidase enzyme (Dvir et al., 2003). Domain I is represented in magenta, domain II is in green and domain III is in blue. Some of the most common mutations discussed in the text are reported. N370S and L444P are highlighted with red circles. **B** Glycosphingolipids biochemical pathway associated with lysosomal storage disorders. The enzymes involved in the most common lysosomal storage disease are indicated by arrows.

of the lysosomal enzymes, is transported via a mannose-6-phosphate independent pathway. In humans, the enzyme binds to the chaperone lysosomal integral membrane protein type 2 (LIMP-2), and the complex is then transported to the lysosomes in a M6P-independent trafficking pathway (Reczek et al., 2007).

Glucosylceramide consists of a glucose molecule esterified to ceramide (C18, C22 or C24 sphingosine). This glucocerebroside is an important intermediate of the glycosphingolipid metabolic pathway (**Figure 4B**) and it is the basic biochemical structure from which most glycosphingolipids originate (Platt, 2014). Glucosylceramide derives from complex glycosphingolipids mainly resulting from the degradation of cellular membranes, in particular senescent blood cells (Sandhoff, 2013).

β-glucocerebrosidase can also hydrolyse glucosylsphingosine, a deacylated form of glucosylceramide (Dekker et al., 2011). This second substrate is cleaved less efficiently than glucosylceramide. Nonetheless, it accumulates in the tissues of Gaucher patients, in particular within the brain of type II patients and contributes to the progression of the pathology. Indeed, glucosylsphingosine has detergent-like properties and damages the cell membrane; inhibits protein kinase C; interferes with signal transduction and cell differentiation processes; and promotes apoptosis (Spiegel and Merrill, 1996). Moreover, glucosylsphingosine is a non-competitive inhibitor of β-glucocerebrosidase, so that its accumulation leads to a negative feedback loop and exacerbates the storage of substrates (Schueler et al., 2003).

Glucosylceramide accumulation also correlates with the levels of saposin C, since this

glycoprotein is a necessary activator for β-glucocerebrosidase (Tamargo et al., 2012). The proposed mechanism suggests that the saposin-enzyme complex is located in the proximity of the phospholipidic membrane, where saposin C can solubilise the membrane so that endogenous glucosylceramide is accessible for hydrolysis. In Gaucher disease, the interaction between saposin C and the N370S mutated form of the enzyme is reduced, contributing to the decrease in the enzymatic activity. Deficiency in saposin C can interfere with the normal β-glucocerebrosidase activity and lead to glucosylceramide accumulation. Few patients with mutations in the gene coding for saposin C have developed phenotypes similar to type I and type III Gaucher disease, despite their β-glucocerebrosidase activity being in the normal range. These findings confirm that deficiency in saposin C in association with mutations in the *GBA1* gene can affect the β-glucocerebrosidase enzymatic activity and contribute to the severity of the pathology.

Lysosomal accumulation of glucosylceramide is more prominent in those organs that present elevated levels of macrophage-lineage cells and cells with myeloid and lymphoid derivation (Grabowski, 2012) . Defects in the β-glucocerebrosidase enzyme result in the build-up of the substrate glucosylceramide in cells of liver, spleen, bone and blood. However, other organs like lungs, skin, heart, kidney and cells of the nervous system can be affected. With the development of organomegaly the accumulation process occurs at higher rate, further increasing the production of new antigen-presenting cells, such as macrophages, dendritic cells, thymic T cells and osteoblasts (Mistry et al., 2010). These cells turn to an activated state and consequently release a series of cytokines and chemokines, contributing to inflammation and progression of the disease (Pandey et al., 2012). Activated macrophages become engorged with lysosomes containing the stored substrate. These swollen cells are the so-called ‘Gaucher cells’, a hallmark of disease progression (Bitton et al., 2004). Gaucher cells can reach 100μm in diameter and present morphological anomalies, such as small eccentric nuclei and abnormal cytoplasmic striations (Jmoudiak and Futerman, 2005). In addition, activated macrophages in inflammatory conditions produce high levels of chitotriosidase. Serum levels of this enzyme are used as diagnostic biomarker in the screening and monitoring of Gaucher patients (Hollak et al., 1994). The mechanisms through which the accumulation of glucosylceramide leads to organomegaly are not fully elucidated (Grabowski, 2010) and even if the storage of the substrate is consistent, it does not fully

explain the massive enlargement of spleen and liver in Gaucher patients (Cox, 2001). Thus, dysfunctions in other metabolic pathways and the involvement of different organelles and cell types should be taken into consideration when investigating the causes of organomegaly in Gaucher disease. The involvement of other cell types in the storage of glucosylceramide is demonstrated by the fact that the knock out of the β-glucocerebrosidase enzyme in macrophage-lineage cells only leads to a late development of visceral pathology in Gaucher mouse model, while the complete depletion of the enzyme in all tissues result in premature death (Xu et al., 2008).

1.2.4. Neuropathology

Neuronopathic forms of Gaucher disease are characterised by perivascular and parenchymal accumulation of Gaucher cells, with pronounced neuronal loss, neuronal atrophy and necrosis (Wong et al., 2004). In particular, the acute infantile form is characterised by a severe, widespread and rapid neurodegeneration. Neuronal loss is prominent in cortex, hippocampus, hypothalamus, nuclei of the midbrain, cerebellum and brain stem. Affected brains also show extensive astrogliosis, microglia activation and non-specific grey matter gliosis (Adachi et al., 1967).

The most affected areas of the cortex are the calcarine cortical layer IV, cerebral cortex of the temporal and posterior parietal lobe, entorhinal cortex, cingulate gyrus, and occipital lobe of layer V (Wong et al., 2004). Layer III is also affected but the neuropathology is less extensive. These regions are characterised by acute astrogliosis and neuronal loss. In type II patients, neurodegeneration is strictly confined within the layer IVb of the cortex. CA2, CA3 and CA4 hippocampal regions have acute pyramidal cell neuronal loss and severe astrogliosis (Wong et al., 2004). In these localised areas astrocytes have intricate glial fibrillary acidic protein (GFAP) positive filaments branching from the cell body (fibrillary astrogliosis) and also accumulate GFAP filaments in the soma (gemistocytic astrogliosis). There is no neuronal loss and increase in astrogliosis in CA1. Pryamidal neurons in CA2-4 hippocampal regions are rich in excitatory glutaminergic mossy fibres and work in concert with inhibitory GABA-ergic interneurons to maintain a finely controlled balance. Thus, minor disequilibrium in sensitivity caused by cytotoxic effects of accumulation glucosylceramide can lead to a

pathological hypersensitive state, resulting in diffuse seizures.

Intense microglia activation is present in the reticular thalamic nucleus and in the ventral posterior nucleus, with extensive neuronal loss and Gaucher cell accumulation in the parenchyma (Wong et al., 2004).

Pons, medulla, and dentate nuclei in the brain stem show neuronal loss and gliosis in proximity of foci of Gaucher cells. Neurons are swollen and contain floccular filaments (Conradi et al., 1984).

Neuroinflammation is thought to further contribute to neuronal loss in severe cases of type II, which is mirrored in a murine model of neuronopathic Gaucher disease (Vitner et al., 2010). In particular, a chronic and sustained inflammatory state leads to cell death, contributing to neuropathology (Bosch and Kielian, 2015). Activated microglia in affected brains produce a series of cytokines and chemokines that recruit immune cells and activate surrounding cells. Reactive astrocytes are also involved in the pathogenesis, releasing chemokines and other cytotoxic molecules. In neuronopathic Gaucher disease brains it is possible to detect elevated levels of proinflammatory cytokines, like IL-1α, TNFα and reactive oxygen species (Vitner and Futerman, 2013). The accumulation of glucosylceramide in inflammatory cells impairs cell migration and antigen presentation, contributing to a persistent neuroinflammatory state. It is still not clear whether neuroinflammation is a triggering event or a response to neurodegeneration. However, it has been shown that neuroinflammation can be detected before neuronal loss in a mouse model of neuronopathic Gaucher disease (Farfel-Becker et al., 2011b). In this model, astrocytosis and microglia activation occur in those brain regions that are characterised by intense neuronal loss, possibly preceding the onset of neuronal death events. Enquist and colleagues created a Gaucher mouse model where microglia cells (of hematopoietic origin) express physiological levels of β-glucocerebrosidase but neural and glial progenitor cells lack the enzyme (Enquist et al., 2007). The study proposes that when the glucosylceramide storage exceeds pathological levels in neurons, astrocytes and oligodendrocytes, a microglial proinflammatory response is activated, suggesting that neuronal loss is a cell-autonomous reaction (Vitner et al., 2012).

More recently, a study from Vitner and colleagues on two different mouse models of neuronopathic Gaucher disease demonstrated that neuronal loss is not triggered by caspase-dependent apoptosis, but by a regulated cell death mechanism named necroptosis (Vitner et al., 2014). Necroptosis can be promoted by tumour necrosis factors, Toll-like receptors and various extracellular stimuli, which activate the receptor-interacting kinases 1 and 3 (RIPK1 and RIPK3) signalling cascade, resulting in the disruption of the cell membrane and consequent cell death. The study showed that RIPK1 and 3 are upregulated in Gaucher disease, not only in the affected mice but also in the brain from a type II human patient. The involvement of the necroptotic mechanism in neuronal death was further corroborated in an additional mouse model of Krabbe disease. Since necroptosis is thought to be involved in several neurodegenerative diseases (Zhang et al., 2017), targeting the RIPK family could be a promising therapeutic strategy. However the currently known RIPK3 inhibitors are not suitable to treat neurodegenerative disorders, as they do not cross the blood-brain barrier or have an unfeasibly short half-life.

Glucosylsphingosine, a second substrate for β-glucocerebrosidase, is an additional neurotoxic substance that promotes neuroapoptosis and is found in elevated levels in brains from type II and III patients (Nilsson and Svennerholm, 1982). It has been shown that the accumulation of glucosylsphingosine alters neuronal morphology, disrupting the plasma membrane and leads to neuronal death (Schueler et al., 2003). High levels of glucosylsphingosine appear during development and drastically increase throughout gestation in type II patients, confirming that the neurotoxic effect may already be present before birth (Orvisky et al., 2000).

In recent years, many studies have demonstrated that mutations in the *GBA1* gene are linked to parkinsonism (Neumann et al., 2009), and they are now considered an important risk factor for developing Parkinson's disease (Sidransky and Lopez, 2012). Parkinson's patients with mutations to the β-glucocerebrosidase enzyme present accumulation of glucosylceramide in the majority of Lewy bodies (Goker-Alpan et al., 2010). It has been suggested that dysfunction in the lysosomal system might contribute to the build-up of α-synuclein, and this accumulation can inhibit β-glucocerebrosidase activity establishing a loop mechanism that regulates the link between synucleinopathy and Gaucher disease (Mazzulli et al., 2011). The accumulation of misfolded β-

glucocerebrosidase proteins can either interfere with the clearance of α-synuclein or increase its aggregation. The exact mechanisms through which the mutated enzyme could affect α-synuclein aggregation are still not fully understood. Since various lysosomal storage disorders have been linked to Parkinson's disease (Shachar et al., 2011), it is plausible that this gain-of-function effect is not specific for β-glucocerebrosidase only. A contrasting hypothesis based on a loss-of-function mechanism has been proposed (Futerman and Hardy, 2016). In fact, mice completely deficient for β-glucocerebrosidase do not produce the misfolded protein but can still develop α-synuclein aggregates. It is evident that, since most Gaucher patients do not develop parkinsonism, mutations in the *GBA1* gene are not a separate risk element, but they rather augment more complex pathological modifiers like ageing and environmental factors. Different *GBA1* mutations influence risk and onset of Parkinson's disease: carriers of severe mutations, like L444P, have a higher risk to develop parkinsonism with earlier onset, compared to those carrying milder mutation, as N370S (Gan-Or et al., 2015).

α-synuclein inclusions similar to Lewy bodies have been found in the cortex, hippocampus and brain stem of Gaucher patients that also develop milder parkinsonian symptoms (Goker-Alpan et al., 2008). These patients present profound neuronal loss and extended gliosis the in substantia nigra. The age of onset of Parkinson's is typically earlier than in the sporadic patients and in carriers of a single mutated *GBA1* allele.

1.2.5. Therapies

Currently, there are different treatment options available for the non-neurological Gaucher disease type I. Enzyme replacement therapy and substrate reduction therapy are administered in combination with other standard treatments for lysosomal storage disorders, such as splenectomy, transfusions, and analgesic treatments (Pastores and Hughes, 2015).

Aglucerase was the first recombinant human enzyme successfully used in clinical trials and became available in 1991for the treatement of Gaucher disease (Barton et al., 1991). A few years later, more efficient molecules engineered from Chinese hamster ovary

cells (imiglucerase, Cerezyme®; Genzyme) and human fibrosarcoma cell line (velaglucerase alfa; Shire HGT) became the gold standard treatment for Gaucher disease (Deegan and Cox, 2012). Taliglucerase alfa (Elelyso®; Pfizer) is derived form a carrot cell line and is commercially available in the USA since 2012. These drugs show a significant dose-response effect, reducing the systemic manifestations in viscera, bones and blood of Gaucher patients, with mild and occasional adverse effects. Imiglucerase is administered via intravenous infusions every two weeks for the duration of the patient's life. Due to the cost of production and the prolonged time of administration, enzyme replacement treatment is expensive, with an annual cost of approximately $300,000 per patient in USA (Sinha, 2014), up to £187,800 in UK (https://www.gaucher.org.uk). Although the cost-effectiveness balance abundantly exceeds the normal threshold, imiglucerase has been approved as an Orphan Drug (Belmatoug, 2012).

The first molecule used for substrate reduction therapy in Gaucher disease was the imminosugar miglustat (Zavesca®) (Cox et al., 2000). The drug is administered orally three times a day. Substrate reduction therapy is effective in reducing the organomegaly and the chitotriosidase activity, and ameliorating the skeletal diseases. However, it does not have major effects on the hematopathology and its administration is accompanied by persistent gastrointestinal adverse effects. Although miglustat crosses the blood-brain barrier, no beneficial effects on the neuropathology have been reported when administered to type III patients (Marshall et al., 2016). An alternative molecule used in substrate reduction therapy is eliglustat (Genzyme) (Lukina et al., 2010). The treatment demonstrates reversal of organomegaly, amelioration of anaemia and thrombocytopenia, and improvement in bone disease. However, since it does not cross the blood-brain barrier, eliglustat is not suitable for type II and type III patients.

A more recent therapeutic strategy for treating the neuropathology of Gaucher patients relies on the use of pharmacological chaperones (Parenti et al., 2014). These small molecules help maintaining a mutated protein into a stable conformation and therefore prevent their degradation by the endoplasmic reticulum quality control system. Since pharmacological chaperones are thought to cross the blood-brain barrier, they could be suitable for the treatment of neuronopathic forms of Gaucher disease. A 2016 pilot study showed that the administration of high-dose ambroxol was well tolerated and

resulted in improvements in neuro-ophthalmologic parameters and seizure frequency in type III patients (Narita et al., 2016).

1.2.6. Gaucher type II mouse models

A number of mouse models have been generated to mimic the acute neuronopathic form of type II Gaucher diseases, the primary focus of this study. This has been achieved through genetic manipulation or chemical induction, and has helped shed light on the pathological pathways leading to neurodegeneration.

K14-lnl/lnl model – A murine model of acute neuronopathic Gaucher disease was developed at Lund University by Prof. Karlsson's group using Cre-lox technology (Enquist et al., 2007). In the first attempt to create a Gaucher type II mouse model, a loxP-neo-loxP cassette enclosing the neomycin gene was inserted into intron 8, causing abnormal splicing of the *Gba1* mRNA (lnl allele). However, β-glucocerebrosidase-deficient mice die at birth because of skin dehydration. In fact, glucosylceramide is one of the major component of the skin lipids, forming lamellar bodies in the stratum corneum of the epidermis, and plays an important role in maintaining the water permeability of the skin (Coderch et al., 2003). To prevent the mice from dying from skin phenotype, the *Gba1* knock-out mice were bred with a K14-Cre strain, which expresses the enzyme Cre recombinase under control of the human keratine promoter K14 (

Figure 5). Therefore, K14-lnl/lnl animals are knocked-out for *Gba1* in all organs and tissues except epidermis, where they express the wild-type allele (wt). These mice present a minimal residual β-glucocerebrosidase activity, although the enzyme levels are severely reduced in brain (<10% of controls), spleen (<2%) and liver (<8%) compared to the wild-type levels. Heterozygote animals (K14-lnl/wt) do not show any pathological phenotype.

This K14-lnl/lnl mouse model recapitulates the symptoms described for human Gaucher disease type II patients. The animals develop both the visceral disease and the acute neuropathology. The major disease's visceral symptoms are enlarged spleen and liver,

thrombocytopenia and lungs impairments. The brain pathology is severe and manifests with intense neuronal loss affecting particularly cortex, hippocampus, thalamus and cerebellum, extended microglia activation, volume brain reduction and massive accumulation of glucosylceramide in enlarged vacuoles. After an asymptomatic period of about 10 days, mice start to develop the neurological symptoms, with tremor, seizures, motor dysfunction and clasping phenotype. The neurodegeneration progresses rapidly and the animals die of end-stage paralysis at 12-14 days of age. Unlike other models, in the K14-lnl/lnl mice both neurons and microglia are defective for *Gba1*. This results in high levels of activated microglia throughout the entire brain (Vardi et al., 2016) and leads to severe neurodegeneration and premature death.

This is the first genetically modified animal model that recapitulates the pathology of Gaucher type II and therefore provides a useful tool for studying the neuropathology progression, as well as the systemic diseases. The K14-lnl/lnl model has been previously used in a pre-clinical study on neonatal intracerebroventricular administration of recombinant human β-glucocerebrosidase for the possible treatment of neuronopathic Gaucher patients (Cabrera-Salazar et al., 2012). The therapy doubled the life span of the treated animals and reduced the accumulation of substrate in the brain; however mice developed severe neurodegeneration and died at 23 days of age. The study demonstrated that the acute neuropathology of the K14-lnl/lnl mouse model, and Gaucher patients, requires a substantial and more sustained treatment.

Nestin-flox/flox model – Enquist and colleagues developed a second mouse model in which neuronal and glial precursor cells are *Gba1* deficient whereas microglia maintain normal enzymatic activity (Enquist et al., 2007). Nestin-Cre mice (Tronche et al., 1999), in which Cre recombinase is expressed in neuron and glia precursor cells in the central nervous system, were bred with the $gba^{flox/flox}$ strain. Resulting Nestin-flox/flox mice develop the Gaucher neurological symptoms, although the pathology has later onset and slower progression, demonstrating that *Gba1* deficiency in microglia is not a primary cause of neurodegeneration. The use of this model suggested that the restoration of enzyme levels in microglia following bone marrow transplantation has a minor effect on the fatal neurodegeneration and therefore will not be sufficient to cure the devastating neuropathology occurring in type II patients. The Nestin-flox/flox mice manifest first symptoms in 2-3 weeks and reach the end-stage of paralysis 7-10 days after. The

neuropathology is characterised by extensive and severe neuronal loss, astrocytosis and microglial activation, similarly to the K14-lnl/lnl mice. Because the Nestin-flox/flox mice survive longer than the K14-lnl/lnl ones, it was possible to monitor the progression of the neuropathology over time and in particular elucidate the correlations between neuroinflammation and neuronal loss (Farfel-Becker et al., 2011b). In the Nestin-flox/flox mice neuroinflammation is detectable in the brain of pre-symptomatic animals and occurs in the same brain regions characterised by neuronal cell death.

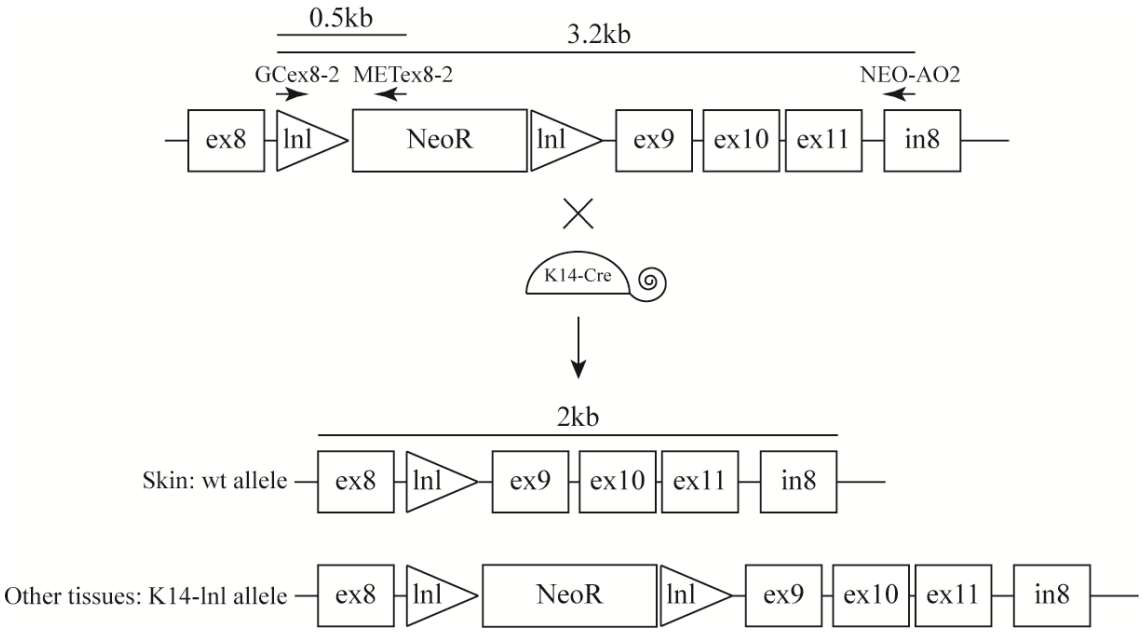

Figure 5 - Neuronopathic Gaucher disease mouse model.

Schematic representation of the generation of the knock-out mouse model (Enquist et al., 2007). Intron 8 is interrupted by a neomycin cassette flanked by loxP sites. The Cre recombinase is under control of the K14 promoter and reverts the mutation in the epidermis cells, so that mice have the wild-type allele in the skin. All other tissues are knocked-out for the *Gba1* gene. Neonate mice affected by skin dehydration die soon after birth, while K14-lnl/lnl mice express the wild-type *Gba1* alleles in skin cells and die at 12-14 days because of severe neurodegeneration.

CBE induced model – Conduritol-β-epoxide (CBE) is a glucocerebrosidase inhibitor. Daily intraperitoneal injections of CBE for 3 weeks result in drastic reduction (>90%) of enzymatic activity in the brain, liver and spleen (Stephens et al., 1978). The cessation of the administration reverts the disease progression in the viscera; however, early

depletion of β-glucocerebrosidase in the brain is not reversible. In fact, when neonatal mice receive high dose of CBE (8-9 daily injections) the neuropathology is not restored upon cessation of administration and animals die from severe neurodegeneration 7-12 days after last injection (Xu et al., 2008). The use of this chemically induced model for the study of the neuropathology was questioned, due to the fact that the blood-brain barrier could prevent the complete penetration of CBE into the brain, especially when administered to older animals. It has been demonstrated that mice injected during the neonatal period develop a neuropathological pattern similar to the Nestin-flox/flox animals, in a dose-dependent fashion (Vardi et al., 2016). However later injections result in less severe neurodegeneration, showing that administration of CBE to older mice is less effective in penetrating the brain and suggesting that the central nervous system might be less sensitive to glucosylceramide accumulation in older animals. Furthermore, Vardi and colleagues demonstrated that astrogliosis and microglia activation precede neuronal loss. Nonetheless, the brain pathology caused by CBE administration is less severe than in the acute K14-lnl/lnl model.

Models based on point mutations – Mice carrying the L444P/L444P and L444P/A456P mutations have been generated using insertion mutagenesis (Liu et al., 1998). The L444P/A456P (or RecNciI) mice show very reduced (>90%) glucosylceramide levels in brain and visceral organs, while the L444P/L444P animals present a 20% residual enzymatic activity. Both strains die soon after birth because of skin dehydration rather than neuropathology.

1.3. Gene therapy

Gene therapy can be defined as the introduction of genetic material to the cells of patients for therapeutic benefit (NIH, 2017). This includes the delivery of a functional version of a gene to compensate for an inherited defective disease-causing copy. In 2012 alipogene tiparvovec (Glybera®; uniQure) was the first gene therapy product to be approved in the Western world for the treatment of lipoprotein lipase deficiency (Melchiorri et al., 2013). Many successful clinical studies followed focusing not only on inherited genetic disorders, like factor IX deficiency in haemophilia B (Nathwani et al., 2014), but also on several types of cancer (Husain et al., 2015). Different strategies

have been employed, ranging from *ex vivo* gene therapy on hematopoietic stem cells, T-cell immunotherapy, and *in vivo* gene delivery using viral vectors to the latest CRISPR/Cas9 gene editing system (Naldini, 2015).

Despite the significant and rapid advancements, the gene therapy field still needs to address some major problematic issues. Although gene therapy is a promising technique for the treatment of genetic disorders, it has become clear over the years that delivering genes into the cell and to a specific cell population is a very challenging process (Naldini, 2015). The cells of the body are composed of numerous physical (e.g. cell membrane, nuclear envelope, cytoplasm, etc.) and biochemical (e.g. nucleases, acidic compartments, etc.) barriers. Therefore, an essential component of gene therapy is the development and availability of gene delivery technology that can efficiently transport genetic material into cells. Yet, once cells are corrected they must be able to persist in the organism long enough to sustain the therapeutic effect, providing robust and constant gene expression and avoiding immunological responses. The safety issue has been one of the main concerns over gene therapy technology. However, the increasing number of successful clinical trials in recent years is providing evidence that gene therapy can be an efficient and safe treatment option. The cost of these therapies remains a major challenge. Although the price of Glybera® at over €1 million ($1 million) (Morrison, 2015) per patient seems to be excessive, one needs to take into consideration that the initial cost of pre-clinical studies and manufacturing conforming to the Good Manufacturing Practice (Administration, 2016) are extremely high. Nonetheless the production costs will be more likely to pay off in the long term as a single long-lasting administration could result cheaper than the dispensation of standard treatments for the time of a patient's life. However, of note, uniQure who manufactures Glybera® have now terminated post-marketing studies which are required for prolonging the market approval from the European Medicine Agency.

The most successful gene therapy clinical trials and applications are based on the use of viral vectors. Different virus families have been employed, according to their packaging size, cell tropism, integration properties and transduction efficiency. These viral vectors have been extensively engineered with the intent of replacing the genomic regions responsible for viral replication and toxicity with the transgene or therapeutic gene of interest. Thus, the virus retains the sequences that are necessary for packaging and

synthesis of structural proteins, yet removing pathogenic features.

Hereafter, the attention will be focused on viral vectors as a therapeutic tool in the development of gene therapy approaches for lysosomal storage disorders, in particular on the potential use of adeno-associated viruses for the treatment of neuronopathic Gaucher disease.

1.3.1. Adeno-associated virus

Adeno-associated viruses (AAV) belong to the family *Parvoviridae*, specifically the *Dependovirus* genus, as they are not able to replicate autonomously (Siegl et al., 1985). A successful replicative cycle of an adeno-associated virus requires the presence of a lytic helper virus (adenovirus or herpesvirus) that provides those genes necessary for replication and productive infection of the cell. When the helper virus is not present the AAV particle remains latent. Adeno-associated viruses are small (20-26nm in diameter), non-enveloped, and contain a linear single-stranded DNA genome (ssAAV) (Berns and Giraud, 1996). Although most of the adult population is seropositive, adeno-associated viruses are not pathogenic in humans or any other species (Daya and Berns, 2008). Several serotypes are known in nature: because the capsid serotype determines the tissue specificity of the virus, the capsid proteins can be engineered in order to alter the cellular tropism and create more efficient pseudotypes. All these characteristics, together with the ability to produce high titre of the vector, make adeno-associated viruses an excellent candidate as a gene therapy vector.

The most studied adeno-associated virus serotype is AAV2 (Srivastava et al., 1983). The AAV2 genome is linear single-stranded DNA of 4.7kb in size. Both sense and antisense strands are packaged into the capsid with the same frequency. The genome is organised into two open reading frames, flanked by two inverted terminal repeats (ITRs) of 145bp each. These form a hairpin structure and play a fundamental role in the replication. These sequences are also the origins of replication for the synthesis of the second strand of DNA. The two open reading frames encode for the genes *rep* and *cap*. *rep* is expressed from two promoters in four different transcripts: Rep78, Rep68, Rep52 and Rep40. Rep proteins are involved in DNA replication, binding to the ITR hairpins,

regulating AAV gene expression and in virion assembly (Pereira et al., 1997). *cap* encodes three capsid proteins (VP1, VP2 and VP3). The gene is transcribed in two mRNAs: the unspliced transcript produces the biggest protein VP1 (87kDa), while the second transcript is spliced and originates VP2 (72kDa) and VP3 (62kDa). 60 capsid proteins combine and arrange in an icosahedral capsid outer shell, in a 1:1:10 molar ratio of VP1, VP2 and VP3 respectively (Daya and Berns, 2008).

AAV2 alone is not able to replicate and it is maintained in a lysogenic state. When the virus is latent its gene expression is repressed, and it can either exist in the episomal state, or stably integrate in the human chromosome 19q13.4 upstream of the transcription starting site of the myosin binding subunit 85 gene (*MBS85*) with a frequency of 0.1% (Kotin et al., 1990). If the helper virus is present, it will provide all those elements necessary for the replication, like DNA polymerase and helicase, and allows the release of the AAV2 particles from the infected cell (Daya and Berns, 2008). Adeno-associated virus binds to the heparan-sulphate proteoglycan receptors on the cell surface and through the interaction with a series of co-receptors, like integrins and growth factor receptors, is internalised through the endocytic pathway (Summerford and Samulski, 1998). Once internalised, the viral particle escapes the late endosomal vesicles probably through the interaction of the phospholipase A_2 motif present at the N-terminus of the VP1 protein (Girod et al., 2002). The mechanism through which the particle is then translocated into the nucleus is still unclear. In the nucleus the capsid proteins are disassembled, the single-stranded DNA is released, the complementary strand is synthesised and transcription of the viral genome begins.

So far, 12 natural serotypes in both human and non-human primates have been described in literature (Schmidt et al., 2008, Saraiva et al., 2016). Despite the high homology in the capsid amino acid sequences (50-90%) (Lisowski et al., 2014), different serotypes have distinct cellular tropism (**Table 2**). Neutralising anti capsid antibodies are widespread in the human population (AAV2: 72%, AAV1: 67%, AAV9: 47%, AAV4: 46%, AAV5: 40% and AAV8: 38%) (Boutin et al., 2010). In addition to neutralising antibodies resulting from natural exposition to the virus, the capsid epitopes can be cross-presented on major histocompatibility complexes class I (MHC I) after cellular transduction, triggering an adaptive immune reaction.

TISSUE TROPISM	SEROTYPE
CNS	AAV1, AAV2, AAV4, AAV5, AAV8, AAV9
Liver	AAV7, AAV8, AAV9
Heart	AAV1, AAV8, AAV9
Lung	AAV4, AAV5, AAV6, AVV9
Kidney	AAV2, AAV9
Pancreas	AAV8
Skeletal muscle	AAV1, AAV6, AAV7, AAV8, AAV9
Photoreceptors	AAV2, AAV5, AAV8

Table 2 - Cellular tropism of AAV 1-9 serotypes.

The table summarises the cellular tropism of the main natural occurring AAV serotypes (Naso et al., 2017).

1.3.2. Adeno-associated virus as a gene delivery vector

The lack of pathogenicity, the ability to infect both dividing and non-diving cells, broad tropism and a variety of naturally occurring serotypes available has meant that development of gene delivery vectors based on adeno-associated virus has been the focus of much research in the gene therapy community. However, some obstacles like the small packaging capacity, tissue tropism and the host immune response needed to be circumnavigated in order to produce efficient vectors for the clinical use. In recent years, significant advances in adeno-associated virus engineering have been achieved, resulting in the design and production of more effective adeno-associated vectors (Snyder et al., 2011).

Recombinant vectors (rAAV) are generally based on the well characterised AAV2 genome and have been manipulated, so that the reading frames of *rep* and *cap* can be substituted with the expression cassette of interest. The inverted terminal repeat sequences contain the *cis*-acting elements necessary during replication and packaging, while the genes required for replication and assembly are provided in *trans* (**Figure 6**). The resulting vectors remain as extrachromosomal elements. (Daya and Berns, 2008).

The efficiency of gene expression is limited among other factors by the synthesis of the complementary DNA strand after the translocation to the nucleus (Ferrari et al., 1996). The generation of self-complementary vectors (scAAV) can circumvent this (McCarty, 2008). These vectors can reanneal into a double-stranded DNA molecule and therefore bypass the rate-limiting process. However, the improvement in efficiency comes at the price of reduced packaging capacity: the size of the expression cassette is in fact halved (2.4kb), although the packaging capacity of scAAVs can be stretched up to 3.3kb without affecting transduction efficiency (Wu et al., 2007).

As an alternative to the use of self-complementary vectors, the transgene expression of ssAAV can be improved by the presence of enhancer sequences, like the woodchuck hepatitis virus regulatory element (WPRE). When the WPRE element is provided in *cis* with the transgene in recombinant vectors, the efficacy of gene expression is increased (Loeb et al., 1999). Gene expression mediated by a scAAV9 vector lacking WPRE and a ssAAV9 with the WPRE sequence has previously been compared (Mattar et al., 2015). The study revealed that following systemic administration to foetal and neonatal mice, transgene expression was higher in those animals injected with the single-stranded version of the vector carrying the WPRE sequence, compared to the WPRE-less scAAV counterpart.

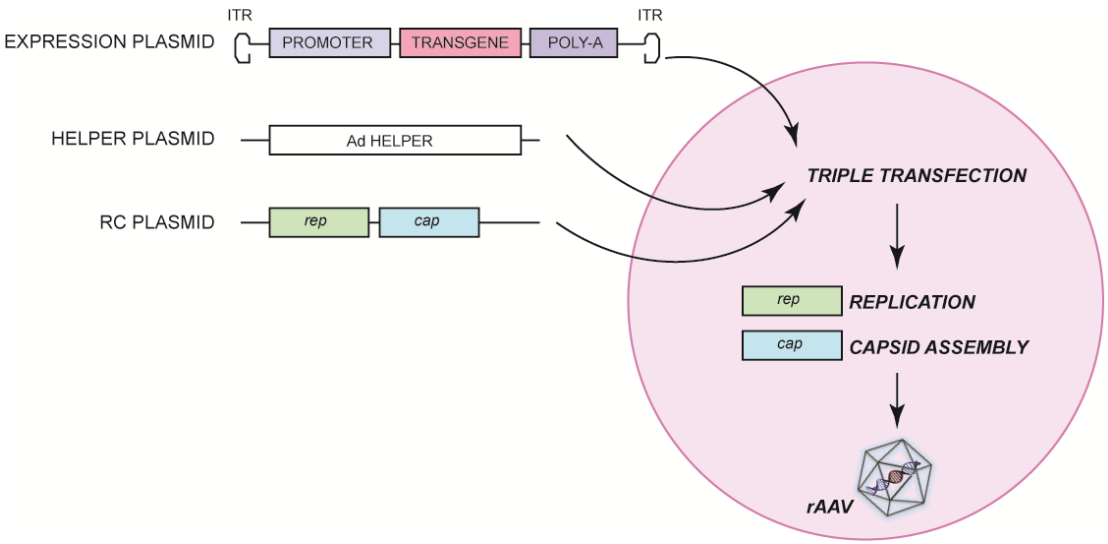

Figure 6 - Generation of recombinant AAV vectors.

Cells are co-transfected with three plasmids: the expression plasmid contains the transgene expression cassette, the helper plasmid carries the adenoviral sequences responsible for viral replication, and the RC plasmid contains the *rep* and *cap* genes for replication and capsid assembly (Saraiva et al., 2016).

Although adeno-associated viruses show a broad tissue tropism, some cell types are not efficiently transduced by naturally available serotypes. Therefore, different capsid engineering approaches have been developed in order to create libraries of novel viral particles (Kotterman and Schaffer, 2014). The capsid genes can be modified through the insertion of point mutations and casual peptide sequences, or form random chimeras of *cap* open reading frames following DNA shuffling. These novel engineered variants are then screened in *in vitro* and *in vivo* systems and finally selected for the desired characteristics.

Despite the significant progress in the development of novel adeno-associated vectors, host immune response remains one of the most challenging aspects of using AAV in therapeutic gene delivery. Previous exposure of the virus triggers the humoral immune response accompanied by the harbouring of neutralising antibodies against the capsid proteins (Halbert et al., 2006). The immune reaction against adeno-associated virus is thought to be T-cell dependent and is associated with the loss of viral gene expression.

This phenomenon was first observed in the phase I/II clinical trial for the treatment of haemophilia B, where cell-mediated immunity against the AAV vector caused gradual decline in Factor IX gene expression and induced transaminitis in liver of treated patients (Manno et al., 2006). The absence of pre-existing antibodies is therefore a strict criterion for inclusion of patients participating in AAV-based gene therapy clinical trials.

Although adeno-associated viruses are defined as non-integrating vectors, an increased risk of insertional mutagenesis has first been reported in a preclinical study on carcinoma hepatocytes in mouse (Donsante et al., 2007). These findings were confirmed by several following studies, which in addition highlighted the correlation between hepatocarcinoma and administration of the vector during the neonatal period (Chandler et al., 2015). Interestingly, recent studies have reported that similar integration events of the wild-type AAV2 genome have been observed in human patients with hepatocellular carcinoma (Nault et al., 2015). Therefore, although clinical trials using recombinant adeno-associated viral vectors have not shown any major safety complications, the possibility of the development of genotoxicity following AAV administration in clinical application should be taken in serious consideration (Chandler et al., 2017).

Despite the existing limitations, AAV-based gene therapy is one of the most promising gene transfer technology platforms, as demonstrated by the increasing number of preclinical studies and clinical trials in recent years (Naldini, 2015). The gene therapy clinical trial for the treatment of haemophilia B is perhaps one of the best example examples of a successful AAV-mediated gene therapy study (Nathwani et al., 2011, Nathwani et al., 2014). A previous separate study attempted gene therapy for severe haemophilia B by delivering an adeno-associated viral vector carrying the Factor IX therapeutic gene through intramuscular injections first to a canine model and consequently to human patients (Manno et al., 2003). However, levels of factor IX in the serum did not increase in treated patients. Nathwani and colleagues used a different approach with the intravenous administration of a rAAV2/8 vector carrying the therapeutic gene through the hepatic artery. Patients that had received the treatment achieved long-term expression of the defective factor IX, reaching 3%-11% of physiological levels. This was enough to drastically reduce the clinical manifestations from severe to a milder form of haemophilia.

1.3.3. Adeno-associated virus mediated gene delivery to the central nervous system

Targeting the central nervous system can be challenging, because of the unique features that characterise the brain. Firstly, the skull represents a physical barrier in its own right, encapsulating the brain. Then the blood-brain barrier plays an essential role in protecting the brain and limiting the access to the CNS. Recombinant adeno-associated viral vectors are currently considered a valuable gene delivery system for combining efficient and widespread central nervous system transduction. The ability to transduce post-mitotic cells leads to stable and persisted gene expression, for at least 15 years in non-human primates (Sehara et al., 2017) and 10 years in the human brain (Leone et al., 2012). Different AAV serotypes have been used to efficiently transduce the central nervous system in several animal models (Bradbury et al., 2015, Davidson et al., 2000, Watakabe et al., 2015). Moreover, some serotypes (AAV1, 8 and 9) have shown the ability to transduce brain regions distal from the injection site, through both anterograde and retrograde axonal transport (Castle et al., 2014). Overall, CNS transduction following AAV-mediated gene delivery results in widespread and highly efficient expression in many brain regions, like cortex, hippocampus, thalamus, striatum and cerebellum (Cearley and Wolfe, 2006). Due to their characteristics adeno-associated viruses are suitable vectors for gene therapy of neurological disorders. Several studies have demonstrated that AAV9-based virus is the preferred vector for CNS gene delivery, due to its extraordinary ability to cross the blood-brain barrier compared to other serotypes in different species like mice, rats and cats (Dayton et al., 2012, Foust et al., 2009, Duque et al., 2009). These studies demonstrated how the use of adeno-associated viral vectors, particularly AAV9, to target neurons in the central nervous system is not limited to intracranial topical administration but can be extended to other less invasive delivery routes, such as systemic injections.

Focal gene delivery is successfully achieved with stereotactic intracranial injections (IC) of the vector into the brain parenchyma. Target-site gene expression is suitable for the treatment of those diseases in which only a circumscribed area of the brain is affected, like the substantia nigra in Parkinson's disease (Bartus et al., 2014). However, this route of administration is less likely to be effective in those neurological conditions where the

neuropathology is substantial and larger areas of the brain are affected. In order to achieve the widespread transduction required to treat sufficiently large areas of the brain, multiple parenchymal injection sites might be necessary to achieve therapeutic effects (Worgall et al., 2008, Tardieu et al., 2014). Yet this procedure is highly invasive and can lead to serious complications.

A less invasive administration route is the injection into the cerebrospinal fluid through intracerebroventricular (ICV) or intrathecal (IT) infusions. Extensive gene expression has been achieved when an adeno-associated viral vector is injected into the ventricles of the brain or via intrathecal administration through the spine: the transduction spreads throughout the brain due to the continual movement of the cerebrospinal fluid (Liu et al., 2005). The vector distributes to both hemispheres allowing a more global delivery to both grey and white matter, transducing not only neurons but also other surrounding cell types. Interestingly, more efficient penetration of the vector has been reported when injecting neonatal animals compared to adults (Passini et al., 2003). This phenomenon is thought to be due to the incomplete maturation of ependymal cells that line the luminal surface of the ventricles in new-born mice, allowing the virus to diffuse from the ventricle to the brain parenchyma.

While the intraparenchymal and intraventricular administrations of gene delivery vectors hold great promise for treating a range of neurological diseases, they are invasive techniques that require significant neurosurgical skills and discomfort to the patient. The ideal administration route would be to deliver the vector directly into the bloodstream of the patient via intravenous infusion, which is minimally invasive and uses the brain vasculature, to allow for maximal spread of the vector throughout the brain. Historically, intravenous drug administration for the treatment of the central nervous system has been challenging, due to the selective properties of the blood-brain barrier (Zhang et al., 2011). However, it has now been shown that AAV9 vectors can efficiently cross the blood-brain barrier through an active transport mechanism and effectively deliver genes to cells throughout the brain and spinal cord (Manfredsson et al., 2009). Intravenous administration of AAV9 leads to a differential transduction pattern depending on the age of administration (Foust et al., 2009). Injections into neonatal mice result in neuron specific targeting, while the administration into adult animals is followed by predominant transduction of astrocytes. It has been hypothesised

that once the virus escapes the vases of the blood-brain barrier it preferentially transduces astrocytes in the proximity of the capillary endothelial cells; although the precise molecular mechanism is still under investigation. Moreover, neurons are more abundant in number than glia in neonatal brains. Similar results have been achieved in a neonatal rat model, where the administration of a single-stranded AAV9 vector resulted in efficient transduction of motor neurons, dorsal root ganglion and Purkinje neurons (Wang et al., 2010). Consistent outcomes have been reported in neonatal and adult non-human primates injected with AAV9 (Dayton et al., 2012). A summary of the most relevant studies comparing different times of injections in several animal models is described in **Table 3** (Saraiva et al., 2016). These findings clearly bring to light the potential use of intravenously administered gene therapy for the treatment of paediatric neurological disorders. While intravenous administration of AAV9 leads to efficient transduction of the brain, other organs of the body will also receive a significant dose of vector. Different studies have demonstrated that a wide variety of visceral organs and tissues are also transduced by AAV9 leading to significant gene delivery and expression in foetal and neonatal mice (Rahim et al., 2011) and non-human primates (Mattar et al., 2013). Hence, systemic gene delivery is potentially highly advantageous in treating those neurological diseases that also have additional significant visceral components like many lysosomal storage diseases. On the downside, the elevated vector dose that is needed to achieve effective transduction in the central nervous system following systemic administration raises the problem of developing more efficient vectors. In addition, the intravenous administration route could be more challenging for disorders caused by defects of integral proteins, where cross-correction mechanism is not applicable and the largest number of neurons must be transduced.

ANIMAL MODEL	STUDY	TIME OF INJECTION	VIRUS	TITER	ASSESMENT POST-INJECTION	OUTCOME
Neonatal rodents						
Mouse	Foust et al., 2009	P1	scAAV9.CBA.*GFP*	4 x 10^11 vg/animal	10-21 days	Neuronal expression in striatum, cingulate gyrus, anterior commissure, internal capsule, corpus callosum, hippocampus, dentate gyrus, midbrain, cerebellum.
Mouse	Rahim et al., 2011	P1	ss and scAAV2/9.CMV.*GFP*	4 x 10^11 vg/animal	1 month	Neuronal expression in CNS (bain, spinal cord, retina) and PNS (myenteric plexus and innervating nerves).
Mouse	Miyake at al., 2011	P1, P5, P14	ssAAV1, 8, 9, 10. CAG.*GFP*	1.5 x 10^11-12 vg/animal	1 month	Expression in neurons and/or astrocytes in cortex, cerebellum olfactory bulbs, brain stem, spinal cord. Transduction efficiency decreases over time.
Rat	Wang et al., 2010	P1	ssAAV9.CAG.*GFP*	2 x 10^12 vg/animal	1-3 months	Neuronal expression in cortex, olfactory nuclei, cingulate cortex, lateral septum, striatum, hippocampus, thalamus, midbrain, cerebellum, brain stem, spinal cord.
Adult rodents						
Mouse	Foust et al., 2009	10 weeks	scAAV9.CBA.*GFP*	4 x 10^11-12 vg/animal	2-7 weeks	Astrocytic transduction.
Mouse	Duque et al., 2009	6 weeks	scAAV9.CMV.*GFP*	3 x 10^11 - 2 x 10^12 vg/animal	2-4 weeks	Motor neurons and glia in spinal cord.
Mouse	Gray et al., 2011	8-12 weeks	scAAV9.CBA.*GFP*	2.5 x 10^10 - 1.6 x 10^12 vg/animal	4 weeks	Astrocytic expression in cortex; neuronal expression in hippocampus, striatum, spinal cord. Dose-dependent transgene expression.
Felines						
Cat	Duque et al., 2009	P2	scAAV9.CMV.*GFP*	1.5 x 10^12 vg/animal	15 days	High transduction efficiency im cervical and lumbar motor neurons.
Cat	Duque et al., 2009	7 weeks	scAAV9.CMV.*GFP*	1.2 x 10^12 vg/animal	15 days	Lower motor neurons.
Non-human primates						
Cynomolgus macaque	Foust et al., 2010	P1	scAAV9.CBA.*GFP*	1 x 10^14 vg/kg	21 days	Extensive motor neuron transduction.
Cynomolgus macaque	Bevan et al., 2011	P1-P90	scAAV9.CBA.*GFP*	1-3 x 10^14 vg/kg	21-24 days	Cortex, thalamus, putamen, hippocampus.
Cynomolgus macaque	Bevan et al., 2011	3 years	scAAV9.CBA.*GFP*	2.7 x 10^13 vg/kg	21-24 days	Predominantly astrocytes and microglia. Cortex, thalamus, putamen, hippocampus, cranial nerves.
Rehsus macaque	Gray et al., 2011	3-4 years	scAAV9.CBA.*GFP*	1 x 10^13 vg/kg	4 weeks	Neuronal and glial transduction in cortex, hippocampus, cerebelum, spinal cord.
Rehsus macaque	Dehay et al., 2012	P1	scAAV9.CMV.*GFP*	10^12 - 10^15 vg/kg	2 months	Neuronal expression in layer II/III/IV, striatum, globus pallidus, thalamus, substantia nigra, hippocmpus, cerebellum.

Table 3 - Summary of preclinical studies on intravenous administration of AAV9 vectors targeting the central nervous system.

The table summarises the most relevant studies comparing different times of administration in rodent, feline and non-human primate animal models (Saraiva et al., 2016). Abbreviations: CBA: chicken-β-actin promoter; CMV: cytomegalovirus promoter; *GFP*: green fluorescent protein; P: postnatal day; vg: viral genome.

The promising results of AAV-mediated gene delivery to the central nervous system opened the way to clinical application of gene therapy for neurological disorders. An AAV9 vector has been used to target motor neurons in a clinical trial for spinal muscular atrophy type I (NCT02122952). This phase I study involves an intravenous delivery of the AAV9 carrying the therapeutic *SMN* gene to affected infants. While this study is on-going, preliminary results have shown remarkable improvement in neck strength, breathing, swallowing abilities and sitting (Mendell, 2016b). AAV2 vectors are used in phase I/II current studies for the treatment of neurodegenerative disorders like Alzheimer's disease (NCT00876863) and Parkinson's disease (NCT01973543), in which the virus has been stereotactically injected into the brain parenchyma into the basal forebrain and striatum, respectively. Due to its cellular tropism, AAV2 has been extensively used in phase I/II trials for the treatment of eye disorders, like neurovascular age-related macular degeneration (NTC01024998) and Tübingen choroideremia (NCT02671539). Efficacy phase III studies are on going for Leber congenital amaurosis (NCT00999609) and Leber's hereditary optic neuropathy (NCT02652767).

1.3.4. Gene therapy for lysosomal storage disorders

Lysosomal storage disorders possess optimal characteristics that render these pathologies an appropriate target for viral gene therapy (Rastall and Amalfitano, 2015). The pathological mechanisms underlying most lysosomal storage diseases are well established, and because of their monogenic nature the administration of a vector carrying a single therapeutic gene could reverse the genetic defects. Moreover, it has been shown that reaching wild-type enzyme levels might not always be necessary, since a modest increase in the enzymatic activity can restore the pathology in milder cases. Averagely, patients with a mild form of lysosomal disease with adult onset exhibit a higher residual enzymatic activity (<10% of wild-type), compared to the infantile acute cases (<1%). Thus, even reduced transfection efficiency leading to a moderate increase in the defective enzyme levels could have significant beneficial effects. These results can be further improved taking in account the already mentioned cross-correction mechanism, according to which a functional soluble enzyme can be taken up from other neighbouring untransfected cells and trafficked to the lysosomes (**Figure 7**). The same approach is exploited by enzyme replacement therapy approaches, where the circulating

enzyme can reach distal organs through the bloodstream. However, a gene therapy based administration of the enzyme can strategically target individual cell populations, so that a specific organ becomes a factory for the production and release of the therapeutic protein. This concept has been demonstrated in liver-targeted gene therapy studies, in which the use of an adeno-associated virus vector carrying a specific liver promoter resulted in amelioration of systemic manifestations in MPS IIIA (Sorrentino et al., 2013), Fabry disease (Ziegler et al., 2007) and Pompe disease animal models (Franco et al., 2005). Finally, the availability of many animal models allows the development of preclinical studies, providing significant advances on pathogenesis and therapeutic effects of the treatment.

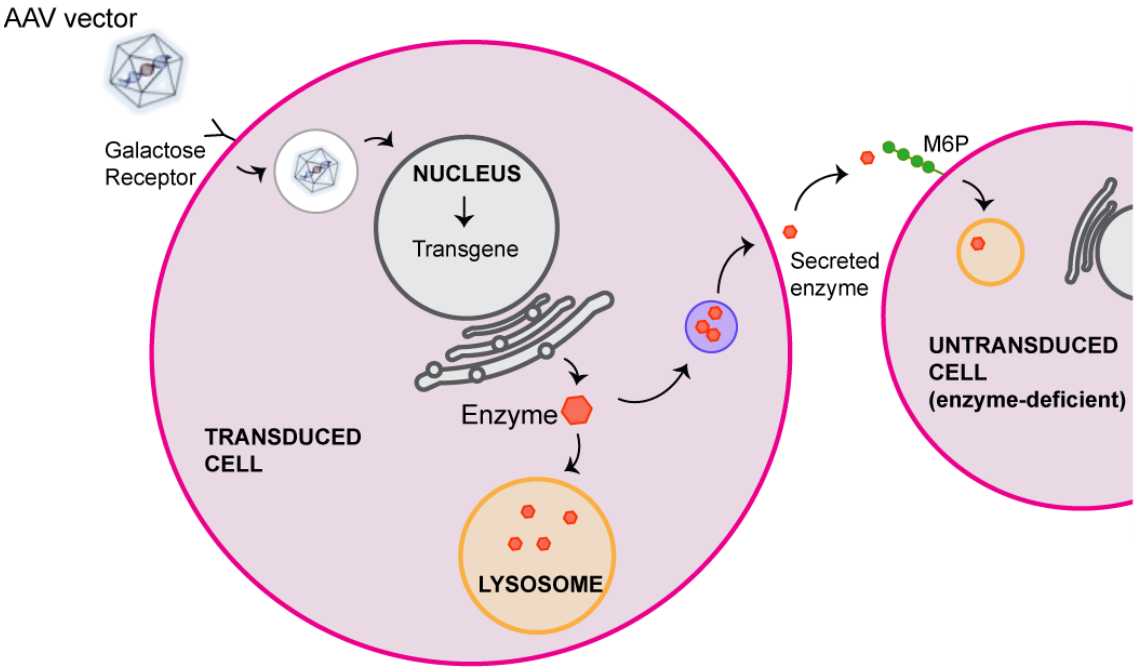

Figure 7 - Cross-correction events following viral transfection.

Once the vector successfully transfects the target cell, the transgene is translated and the functional protein is produced. The soluble therapeutic enzyme is either translocated to the lysosomes, or secreted. The surrounding cells can up-take the secreted molecule via the mannose-6-phosphate receptors or alternative M6P-independent pathways and translocate the enzyme to the lysosomal compartment.

The increased number of gene therapy clinical trials has highlighted the potential benefits of the use of adeno-associated virus as a gene delivery system in the treatment of lysosomal storage disorders. Some of the phase I and II on going and completed trials (https://clinicaltrials.gov, http://www.isrctn.com) on lysosomal storage diseases are reported in Table 4. The ability of adeno-associated viral vectors to successfully transduce neurons has provided significant evidence to justify the use of AAVs as therapeutic option for lysosomal storage disorders with neurological manifestations. Indeed more than 50% of lysosomal storage disorders present neurological involvement (Futerman and van Meer, 2004) and currently there are no treatments for many of these diseases. Therefore, it is not surprising that most of the clinical studies focused on gene delivery to the central nervous system.

Several gene therapy based strategies for the treatment of Gaucher disease have been attempted in preclinical studies. Initial experiments on the feasibility of gene therapy for Gaucher disease were performed on *in vitro* systems, using retroviral vectors to express the *GBA1* gene in cultured bone marrow cells derived from patients (Fink et al., 1990). A decade later, the advent of adeno-associated virus technology lead to the development of *in vivo* strategies, where the intravenous administration of a recombinant AAV vector carrying the *GBA1* gene under control of the human elongation factor 1-alpha promoter to wild-type mice resulted in sustained expression of β-glucocerebrosidase for weeks after injection (Hong et al., 2004). More recently, gene therapy has been applied to a mouse model of Gaucher disease type I using an AAV8 vector expressing the human *GBA1* gene under control of a hepatocyte-specific promoter (McEachern et al., 2006). The treatment was administered to juvenile (4 weeks old) and adult mice (6 months old) carrying the D409V mutation, in which the visceral pathology was already established. These mice presented Gaucher cells accumulation with high levels of glucosylceramide in the liver, spleen, lungs and bone marrow. The treatment successfully rescued the β-glucocerebrosidase deficiency to therapeutic levels and cleared the accumulation of substrate in liver and spleen, with only minimal effects on the lung pathology. Rescue of the established phenotype in old type I mice was also achieved through *ex vivo* transfection of bone marrow cells and consequent transplantation (Enquist et al., 2006, Dahl et al., 2015, Enquist et al., 2009). This *ex vivo* approach was previously employed in a first clinical attempt utilising early retroviral vectors; however the transduction efficiency of hematopoietic stem cells was not sufficient to trigger a therapeutic affect

on treated patients (Cox, 2010).

DISEASE	STUDY ID	PHASE	VECTOR	ROUTE OF ADMINISTRATION
Batten				
	NCT00151216	I	AAV2.Cuh.*CLN2*	Intracerebral
	NCT01414985	I/II	AAVrh.10CU.*CLN2*	Intracerebral
	NCT02725580	I/II	scAVV9.CB.*CLN6*	Intrathecal
Metachromatic leukodystrophy				
	NCT01801709	I/II	AAVrh.10cu.*ARSA*	Intracerebral
MPS IIIA				
	NCT02716246	I/II	scAAV9.U1a.*hSGSH*	Intravenous
	NCT02053064	I/II	AAVrh10.*hSGSH*, *SUMF1*	Intracerebral
MPS IIIB				
	ISRCTN19853672	I/II	AAV5.*NAGLU*	Intracerebral
Pompe				
	NCT02240407	I	rAAV9.DES.*hGAA*	Intramuscular

Table 4 - Summary of clinical trials for lysosomal storage disorders.

The table reports some of the on going clinical trials for lysosomal storage diseases. The vector used and the route of administration are also described.

These reports, regardless of their successful results, targeted only the visceral pathology while the therapeutic intervention on the neuropathology of type II and III was not addressed. The present study describes the attempt to treat both the neurological and

visceral manifestations of neuronopathic Gaucher disease, intravenously administering two different AAV9 vectors carrying the therapeutic copy of the human *GBA1* gene to a type II mouse model.

1.4. Rationale

There is currently no effective clinical treatment for the lethal neurological manifestations of the neurodegenerative forms of Gaucher disease. Ideally, a treatment would primarily address the lethal neurological involvement, but also the visceral manifestations. The ability of AAV9 to cross the blood-brain barrier following intravenous administration provides a potential systemic therapy that could achieve this ideal therapeutic result.

The aim of this project is to evaluate the efficacy of the intravenous administration of gene therapy for the treatment of neuronopathic Gaucher disease using adeno-associated viral vectors. The overarching hypothesis of the study is demonstrating that systemic delivery of gene therapy will result in increase in lifespan, amelioration of neuropathology and improvement of visceral pathology in a neuronopathic Gaucher disease mouse model. In order to achieve these objectives, two suitable gene delivery vectors were produced and administered to neonatal knock-out mice, following evaluation of their transduction efficiency.

The first part of the current study provided evidence of efficient systemic transduction of the brain and the viscera following intravenous administration of the scAAV2/9.GUSB.*GFP*.bGHpA vector in a reporter gene analysis.

The second part aimed to treat the acute K14-lnl/lnl mouse model of type II Gaucher disease with a single intravenous administration of the therapeutic scAAV2/9.GUSB.*hGBA1*.bGHpA vector to neonatal animals. Survival, body weight, splenomegaly and a series of behavioural motor function parameters were assessed in treated animals. The β-glucocerebrosidase enzymatic activity was measured in different organs and a blood analysis was performed. Finally, post-mortem neuropathology and

histopathology analysis provided indication of amelioration of the pathology in the brain and viscera. Intracerebroventricular treated mice were used as age-matched controls in the analysis of the visceral pathology.

The third part focused on the use of an alternative single-stranded vector, in which the *GBA1* expression is driven by a strong neuronal promoter (ssAAV2/9.hSyn1.*hGBA1*.WPRE.hGHpA), as an attempt to increase the therapeutic efficacy in the central nervous system yet maintaining a beneficial systemic effect following intravenous administration. A preliminary reporter gene study demonstrated the widespread transgene expression, not only in the brain but also in some of the visceral organs. The viral vector carrying the human *GBA1* gene was administered intravenously to neonatal K14-lnl/lnl mice and the pathological parameters were assessed.

2. Materials and methods

2.1. Primer sequences

Primer sequences were designed using the MacVector v15.0 software (MacVector Inc., Apex NC, USA) and purchased from Sigma-Aldrich (St. Louis MI, USA).

The sequences of the primers used in this study are shown in **Table 5**.

PRIMER NAME	SEQUENCE
GCex8-2	5'-GTACGTTCATGGCATTGCTGTTCACT-3'
METex8-2	5'-ATTCCAGCTGTCCCTCGTCTCC-3'
NEO-AO2	5'-AAGACAGAATAAAACGCACGGGTGTTGG-3'
Cre 134_f	5'-AATGCTTCTGTCCGTTTGCCGGTC-3'
Cre 365_r	5'-GATCCGTCGCATGACCAGTGAAAC-3'
GBA_BspEI_f	5'-CACATCCGGAGCCACCATGGAGTTTTCAA-3'
GBA_EcoRI_r	5'-CAATGAATTCTCACTGGCGACGC-3'
Seq-1	5'-CTGCCTCAGTCTGCGGTG-3'

Table 5 – Primers.

Names and sequences (5'-3') of the primers used in the study (Sigma-Aldrich).

2.2. Antibodies

A description of the antibodies used in the study is presented in **Table 6**.

ANTIBODY	HOST	DILUTION USED
Primary antibodies		
Anti e*GFP* (ab290, Abcam, Cambridge, UK)	Rabbit	1:1,000
Anti C-terminal Gcase (G4171, Sigma-Aldrich)	Rabbit	1:1,000
Anti CD68 (MCA1957, AbD Serotech, Kidlington, UK)	Rat	1:2,000
Anti GFAP (MAB3402, Millipore, Burlington MA, USA)	Mouse	1:1,000
Anti LAMP1 (ab24170, Abcam)	Rabbit	1:2,000
Anti Calbindin (CB38, Swant, Marly, Switzerland)	Rabbit	1:10,000
Anti NeuN (MAB377, Millipore)	Rabbit	1:500
Secondary antibodies		
Biotinylated anti mouse IgG (BA-9200, Vector Lb Inc., Burlingame CA, USA)	Goat	1:1,000
Biotinylated anti rabbit IgG (BA-1000, Vector Lb Inc.)	Goat	1:1,000
Biotinylated anti rat IgG (BA-9400, Vector Lb Inc.)	Goat	1:1,000
Fluorescence secondary antibody		
Alexa Fluor 488 (A11008, Life Technology, Carlsbad CA, USA)	Goat	1:200
Alexa Fluor 568 (A11034, Life Technology)	Goat	1:200

Table 6 - List of antibodies used in the study.

2.3. Cloning

2.3.1. Transformation of plasmid DNA

Plasmid DNA was amplified into *E. coli* bacterial cells (SURE competent cells, Agilent Technologies, Santa Clara CA, USA) following manufacturer's protocol. The transformed culture was grown on lysogenic broth agar (Fisher Scientific, Loughborough, UK) plates containing 100µg/ml of ampicillin antibiotic (Sigma-Aldrich) at 37°C overnight. Positive colonies were used to inoculate 5ml of lysogenic broth as starter cultures (Sigma-Aldrich) with 100µg/ml of ampicillin at 37°C overnight and constant shaking at 225rpm.

2.3.2. Amplification of plasmid DNA

Plasmid DNA was purified using the QIAprep Spin Miniprep kit (QIAGEN, Hilden, Germany) according to manufacturer's instructions. The DNA was eluted into 50µl of dH_2O and the concentration was determined by spectrophotometry (NanoDrop 1000, Thermo Scientific, Waltham MA, USA). Absorbance of the sample was measured at 260nm, and the ratio of absorbance at 260nm and 280nm (~1.8) was used to assess the purity of the DNA sample.

For large-scale plasmid DNA preparations, 500µl of bacterial culture was incubated with 500ml of lysogenic broth with 100µg/ml of ampicillin at 37°C overnight and constant shaking at 225rpm. The plasmid DNA was purified using the Plasmid Maxi kit (QIAGEN) according manufacturer's instructions. The plasmid was resuspended in 500µl of dH_2O and the concentration was assessed (NanoDrop 1000, Thermo Scientific).

2.3.3. Digest

DNA sequences were analysed with the MacVector v15.0 software (MacVector Inc.) and the appropriate restriction cut sites were selected. 1µg of DNA was digested with

the defined restriction enzymes (New England Biolab, Ipswich MA, USA) according to manufacturer's specifications.

The reaction mix was assembled as following:

1µg DNA

2.5µl 10X Restriction buffer (New England Biolab)

1u (unit) Restriction enzyme

dH_2O to final volume of 25µl

2.3.4. Gel electrophoresis

50X Tris Acetate-EDTA TAE buffer: 242g Trizma (Sigma-Aldrich), 57.1ml Glacial acetic acid (Fisher Scientific), 100ml 0.5M Ethylenediaminetetraacetic acid EDTA (Sigma-Aldrich), dH_2O to total volume of 1l.

1X Orange G loading buffer (Sigma-Aldrich) was added to the samples and DNA fragments were separated on an agarose gel (1% agarose in 1X TAE buffer for optimal resolution of 500-10,000 bp DNA; Invitrogen, Carlsbad CA, USA) with 1:10,000 Safeview nucleic acid stain (Applied Biological Materials, Richmond, Canada) in 1X TAE buffer for DNA visualisation. 1Kb plus molecular weight marker (Invitrogen) was used to determine the DNA sample size. Gels were run at 110V (PowerPac Basic, Biorad, Hercules CA, USA) for a minimum of 30 minutes depending on the expected band size. The results were visualised using a UV transilluminator and images were captured with the attached CCD digital camera (InGenius, Syngene, Cambridge, UK).

2.3.5. Extraction of DNA fragments from agarose gel

DNA fragment of interest were excised from the agarose gel under limited exposure of UV light and processed using the QIAquick Gel Extraction kit (QIAGEN) following the manufacturer's instructions. The purified plasmid DNA was eluted in dH_2O to a final volume of 30µl.

2.3.6. Ligation of DNA fragments

The molar ratios of 1:1 or 1:2 of vector:insert DNA were used when cloning a DNA fragment into a plasmid vector.

The ligation reaction was assembled as followed:

100ng Vector DNA

100-200ng Insert DNA

1µl 10X Ligase buffer (Promega, Madison WI, USA)

1u (unit) T4 DNA Ligase (Promega)

dH_2O to final volume of 10µl

The reaction was incubated at 4°C overnight.

2.3.7. Sequencing

Automated Sanger sequencing (**Table 5** 'Seq-1') of the plasmids was outsourced to SourceBioscience (www.lifesciences.sourcebioscience.com, UK). The resulting sequences were aligned to the original consensus and analysed with the MacVector v15.0 software.

2.4. Tissue culture

2.4.1. Cell lines

HEK-293T cells were used for *in vitro* testing of gene expression from the plasmids. HEK-293T AAV pro cells (Clonetech, Mountain View CA, USA) were used for virus production. Cells were grown in Dulbecco's Modified Eagle Medium DMEM GlutaMax™ (ThermoFisher Scientific) in standard conditions of 37°C and 5% CO_2.

When specified, 10% heat-inactivated Fetal Bovine Serum FBS (Gibco, ThermoFisher Scientific) (56°C for 30 minutes) and/or 1% Pen/Strep antibiotic (Gibco) were added to standard DMEM GlutaMax™. Cells were passaged with trypsin (trypsin-EDTA 0.05%, Gibco) when 70% confluent, with a standard ratio of 1:10 every 48 hours.

2.4.2. Cell transfection

HEK-293T cells were grown in DMEM GlutaMax™ (ThermoFisher Scientific) with 10% FBS (Gibco) and 1% antibiotics (Pen/Strep Penicillin 5,000 unit/ml, Streptomycin 5,000 µg/ml, Gibco). 250,000 cells/well were seeded onto 6-well plates and transfected 24 hours later. The transfection mix per sample was the following: 500µl of Opti-MEM (Gibco), 2µg of DNA plasmid and 2.5µl of polyethylenimine PEI (Polyscience, Niles IL, USA). The solution was vortexed and left at room temperature for 20 minutes to allow the formation of DNA-PEI complexes. The transfection mix was then added to the cells. 48 hours post-transfection the cells were harvested. Cells and supernatant were processed separately. The medium was transferred into microcentrifuge tubes and centrifuged at 12,000 x g at 4°C for 5 minutes. The supernatant was placed into fresh tubes and kept at -20°C for future use. The cells were washed with 400µl of phosphate buffered saline PBS (Gibco). 250µl of ice-cold RIPA Lysis buffer (ThermoFisher Scientific) supplemented with 1X of protease inhibitor cocktail (ThermoFisher Scientific) were added. The plate was kept on ice for 5 minutes. The cells were then scraped and transferred to centrifuge tubes. The samples were centrifuged at 14,000 x g at 4°C for 15 minutes. The supernatant was transferred into fresh tubes and stored at -20°C for future use.

2.5. AAV9 production

1X Lysis Buffer: 140mM NaCl (Sigma-Aldrich), 5mM KCl (Sigma-Aldrich), 0.7mM K_2HPO_4 (Sigma-Aldrich), 3.5mM $MgCl_2$ (Sigma-Aldrich), 25mM Trizma. pH 7.5. The solution was filter sterilized and autoclaved.

PBS-MK: 1X PBS 2.5mM KCl, 1mM $MgCl_2$. The final solution was filter sterilized

(0.22µm filter, Millipore).

5X TD buffer: 5X PBS (Sigma-Aldrich), 5mM $MgCl_2$, 12.5 mM KCl.

2.5.1. Seeding

A 10 layer cell factory (Corning, NY, USA) was seeded with $5x10^8$ HEK-293T AAV pro cells in 1 litre of DMEM GlutaMax™ (ThermoFisher Scientific) with 10% FBS (Gibco) and 1% Pen/Strep (Gibco), ensuring equal distribution of the media in each layer of the cell factory. Cells were incubated at 37°C in 5% CO_2 for 24 hours.

2.5.2. Transfection

The transfection mixes were prepared as following: the transgene plasmid, the packaging plasmid *pDG9*, and the helper plasmid *pHGTI* were added to 50ml of DMEM GlutaMax™ (ThermoFisher Scientific) in a 1:1:3 proportion; 2.8ml of PEI (Polyscience) were added to 50ml of DMEM GlutaMax™ to a final ratio of 5 PEI : 1 DNA. Both solutions were well mixed and incubated at room temperature for 15 minutes. The transfection solutions were added to 1l of DMEM GlutaMax™ with 10% FBS and 1% Pen/Strep and mixed thoroughly. The media was removed from the cell factory and replaced with the transfection mix ensuring that the solution was distributed evenly across the cell factory. Cells were incubated at 37°C in 5% CO_2 for 72 hours.

2.5.3. Harvesting

The media was poured out from the cell factory and collected into 250ml centrifuge tubes. The solution was centrifuged at 1,800 x g for 10 minutes. Afterwards, the supernatant was collected in a clean bottle and the cellular pellet was kept for subsequent use.

The cell factory was washed with 500ml of PBS. The solution was poured into the 250ml tubes containing the previously collected cell pellet. Cells were centrifuged at

1,800 x g for 10 minute. The supernatant was then discarded and 50ml of medium was added to each tube. 500ml of PBS with 50ml of Trypsin-EDTA X10 (Gibco) were added to the cell factory. The cell factory was gently shaken to help the cells detach and was incubated at 37°C for 15 minutes. The solution was collected in the 250ml tubes containing the medium and centrifuged at 1,800 x g for 5 minutes. The cell factory was washed one final time with 500ml of PBS. The solution was poured into the same tubes and centrifuged at 1,800 x g for 5 minutes. The final cell pellets were thoroughly resuspended in 25ml of 1X Lysis Buffer.

2.5.4. Benzonase treatment

The cell lysate obtained from the previous step was frozen at -80°C and then thawed at 37°C in a water bath. When defrosted, the solution was vortexed for 10 minutes. The process was repeated 3 times. 31.3g of $(NH_4)_2SO_4$ (Sigma-Aldrich) per 100ml were added to the previously collected supernatant. The solution was shaken until dissolved, incubated on ice for 30 minutes and centrifuged at 8,300 x g for 30 minutes. The pellet was then resuspended in 25ml of 1X Lysis Buffer.

1mM $MgCl_2$ was added to the lysing mix of both the cell pellet and the supernatant. 5000 units of Benzonase (Sigma-Aldrich) were added respectively to the cell pellet and the supernatant. The solutions were mixed thoroughly, incubated at 37°C for 1 hour and centrifuged at 4,200 x g at 4°C for 30 minutes. The supernatants were transferred and combined into the same tube and stored at -80°C for the following purification.

2.5.5. Purification

Iodixanol gradients buffers were prepared as followed:

15% Iodixanol: 7.5ml Optipep (Sigma-Aldrich), 6ml 5M NaCl, 6ml 5X TD buffer, 10.5ml dH_2O.

25% Iodixanol: 8.33ml Optipep, 4ml 5X TD buffer, 7.7ml dH_2O, 50µl Phenol Red

(Sigma-Aldrich).

40% Iodixanol: 10.2ml Optipep, 3ml 5X TD buffer, 1.8ml dH_2O.

60% Iodixanol: 15ml Optipep, 37.5µl Phenol Red.

The gradient was prepared in ultracentrifuge tubes (Beckman Coulter, Brea CA USA) carefully overlaying 1.55ml of 60% Iodixanol, 1.55ml of 40% Iodixanol, 1.88ml of 25% Iodixanol, 2.8ml of 15% Iodixanol, and 5ml of lysate. The tubes were placed into SW40-Ti swing-out buckets, balanced to within 0.001g and centrifuged at 200,000 x g (Beckman Coulter; acceleration fast, deceleration slow) at 18°C for 3 hours.

When the centrifugation was completed, the ultracentrifuge tubes were carefully extracted from the buckets. Using a 5ml syringe with a 19G11/2 needle (BD Microlance) the 1ml layer below the 60-40% interface containing the virus was aspirated. The extract was diluted in PBS-MK to a total volume of 50ml, filter sterilised (EMD Millipore™ Steritop™ sterile vacuum bottle-top filter 0.22µm, Fisher Scientific) and stored at 4°C.

2.5.6. Concentration

A sterile concentrator (Vivaspin 20, 100KDa cut off, Sartorius Stedim Biotech, Göttingen, Germany) was washed with 5ml of PBS-MK, and equilibrated with additional 10ml of PBS-MK. The column was centrifuged at 2,000 x g for 5 minutes. The solution was discarded from the collector bucket and residual PBS in the concentrator was aspirated. 20ml of sample was added to the column and centrifuged at 2,000 x g to bring the volume down to 1ml. The process was repeated adding the rest of the sample to the concentrator. The column was filled one last time with PBS-MK and concentrated to a final volume of 500µl. The virus was aliquoted and stored at -80°C.

2.5.7. Titration

6X Loading buffer: 0.8g sodium dodecyl sulfate SDS (Sigma-Aldrich), 5ml Trizma pH 6.8, 5ml glycerol (Sigma-Aldrich), 4mg bromophenol blue (Sigma-Aldrich). Add 5% beta-mercaptoethanol (Sigma-Aldrich) before use.

5X Tris-glycine running buffer: 15.1g Trizma, 94g glycine (Sigma-Aldrich), 50ml SDS 10% in 1l dH_2O.

Gel fix solution: 50ml methanol, 7ml acetic acid, 43ml dH_2O.

Gel wash solution: 10ml methanol, 7ml acetic acid, 83ml dH_2O.

50X Alkaline running buffer: 2.5M NaOH (Sigma-Aldrich), 50mM EDTA (Sigma-Aldrich).

4X Alkaline loading buffer: 20% glycerol, 4X alkaline running buffer, 1.2% SDS, 1mg xylene cyanol.

Sodium dodecyl sulphate polyacrylamide gel electrophoresis SDS-PAGE (viral protein quantification) - The virus samples and bovine serum albumin BSA (Sigma-Aldrich) standards of known concentration (250ng, 500ng, 750ng, 1000ng) were diluted in 3µl of 6X Loading buffer and heated at 95°C for 5 minutes. The samples were loaded on a NuPAGE Bis-Tris 4-12% polyacrylamide gel (Life Technologies) and the electrophoresis was run at 120V for 2 hours (PowerPac Bio-Rad, Hemel Hampstead, UK). The gel was then incubated twice in gel fix solution for 30 minutes and stained with Sypro Ruby (Invitrogen) overnight. The gel was washed in gel wash solution for 3 minutes, and rinsed in dH_2O before imaging with UV transilluminator (InGenius, Syngene). Quantification of the bands was performed (ImageJ, USA) and VP3 protein concentration (ng/ml) was calculated.

Alkaline gel electrophoresis (viral genome quantification) - A 0.8% alkaline agarose gel was prepared in 980ml of dH_2O and 20ml of 50X alkaline running buffer. 25µl of virus sample was diluted in 8.5µl of 4X alkaline loading buffer, cooled down to 4°C and loaded into the gel. The electrophoresis was performed at 20V at 4°C overnight. The

next day, the gel was washed in 0.1M Trizma pH 8.0 for 1 hour and stained with 4X GelRed (Biotium, Fremont CA, USA) in 0.1M NaCl for 2 hours. Afterwards, the gel was rinsed with water and imaged with a UV transilluminator (InGenius, Syngene). The band quantification of samples and HyperLadder 1kb standard (Bioline Reagents, London, UK) was performed and the genomic concentration (ng/ml) of the AAV sample was calculated.

2.6. *In Vivo* animal studies

2.6.1. Maintenance of transgenic and wild-type mice

K14-Cre $gba^{lnl/lnl}$ knock-out mice (K14-lnl/lnl) were used as a model of acute neuronopatic Gaucher Disease (Enquist et al., 2007) (**Figure 8A**). Heterozygote mice (K14-lnl/wt) were mated to generate knock-out, heterozygotes and wild-type (K14-wt/wt) animals which were used as controls.

Wild-type CD1 strain mice were used in the scAAV2/9.GUSB.*GFP*.bGHpA gene reporter study and in the ssAAV2/9.hSynI.*hGBA1*.WPRE.hHGpA vector toxicity study.

Animals were maintained in the Biological Services Unit at UCL Bloomsbury Campus, London, UK on a 12h light/dark cycle, with free access to water and food. Animals were group-housed into individually ventilated cages (IVCs) with appropriate litter and nesting material, and environmental enrichment elements. No more than two females aged from 6 to 15 weeks per stud male were weekly timed mated.

All listed procedures were conducted under Dr. Waddington's project licence (PPL N 70/8030) and have been approved by the UK Home Office for the conduct of regulated procedures under license (Animal Scientific Procedures Act, 1986), and by the ethical review committees of University College London. The Animal Research Reporting of *In Vivo* Experiments (ARRIVE) guidelines were followed.

Mice were weighed weekly and were sacrificed if a loss of more than 15% of the total

body mass was observed as a comprehensive humane endpoint. The animals were routinely monitored and culled if the humane endpoint was reached (mouse presents with paralysis, spasticity, neck hypertension or unconsciousness for more than 4 hours).

2.6.2. Genotyping

DNA extraction from earclips

DNA Extraction Solution 1, pH 12: 1g NaOH, 74.4mg EDTA in 1l of dH_2O.

DNA Extraction Solution 2, pH 5: 40mM Trizma-HCl.

Tissue samples (2-3mm ear clips) were placed in microcentrifuge tubes. 75µl of DNA Extraction Solution 1 was added to each tube and mixed making sure that tissue is submerged. Samples were incubated at 95°C for 10-30 minutes. Once the solutions cooled to room temperature, 75µl of DNA Extraction Solution 2 was added. Samples were stored at -20°C if not used immediately.

DNA extraction from liver samples

Liver samples were extracted from culled mice, being careful to avoid any contact or contamination from the skin. DNeasy Blood & Tissue Kit (QIAGEN) was used to extract DNA from liver tissues as per manufacturer's protocol.

Polymerase Chain Reaction (PCR)

DNA extracted from liver tissues was used for PCR genotyping (**Figure 8B**) to confirm the phenotyping results obtained from the dried blood spot assay.

Uninjected mice were earclipped at 21 days of age and genotyped through PCR.

The reaction mix was assembled as follows:

2µl Buffer 10X (Promega)

2µl 10mM dNTPs (VWR, Lutterworth, UK)

1µl each 50µM primers (GCex8-2, METex8-2, NEO-AO2)

0.1µl *Pfu* DNA polymerase (Promega)

4µl DNA

dH_2O to final volume of 20µl

The cycle conditions were set up as follows:

Initial denaturation 94°C for 5 min

Denaturation 94°C for 30 sec

Annealing 61°C for 30 sec

Extension 72°C for 5 min

Final extension 72°C for 8 min

(35 cycles of denaturation, annealing and extension)

Uninjected animals were also screened for Cre recombinase expression within the skin.

The reaction mix was assembled as follows:

2µl Buffer 10X (Invitrogen)

2µl 10mM dNTPs (VWR)

0.6µl 50mM $MgCl_2$ (Invitrogen)

1µl each 50µM primers (Cre 134_f, Cre 365_r)

0.1µl Taq DNA polymerase (Invitrogen)

4µl DNA

dH_2O to final volume of 20µl

The cycle conditions were the following:

Initial denaturation 94°C for 4 min

Denaturation 94°C for 30 sec

Annealing 60°C for 30 sec

Extension 72°C for 1 min

Final extension 72°C for 7 min

(35 cycles of denaturation, annealing and extension)

DNA amplicates were run on an agarose gel via electrophoresis and the results were visualised with a UV transilluminator (InGenius, Syngene).

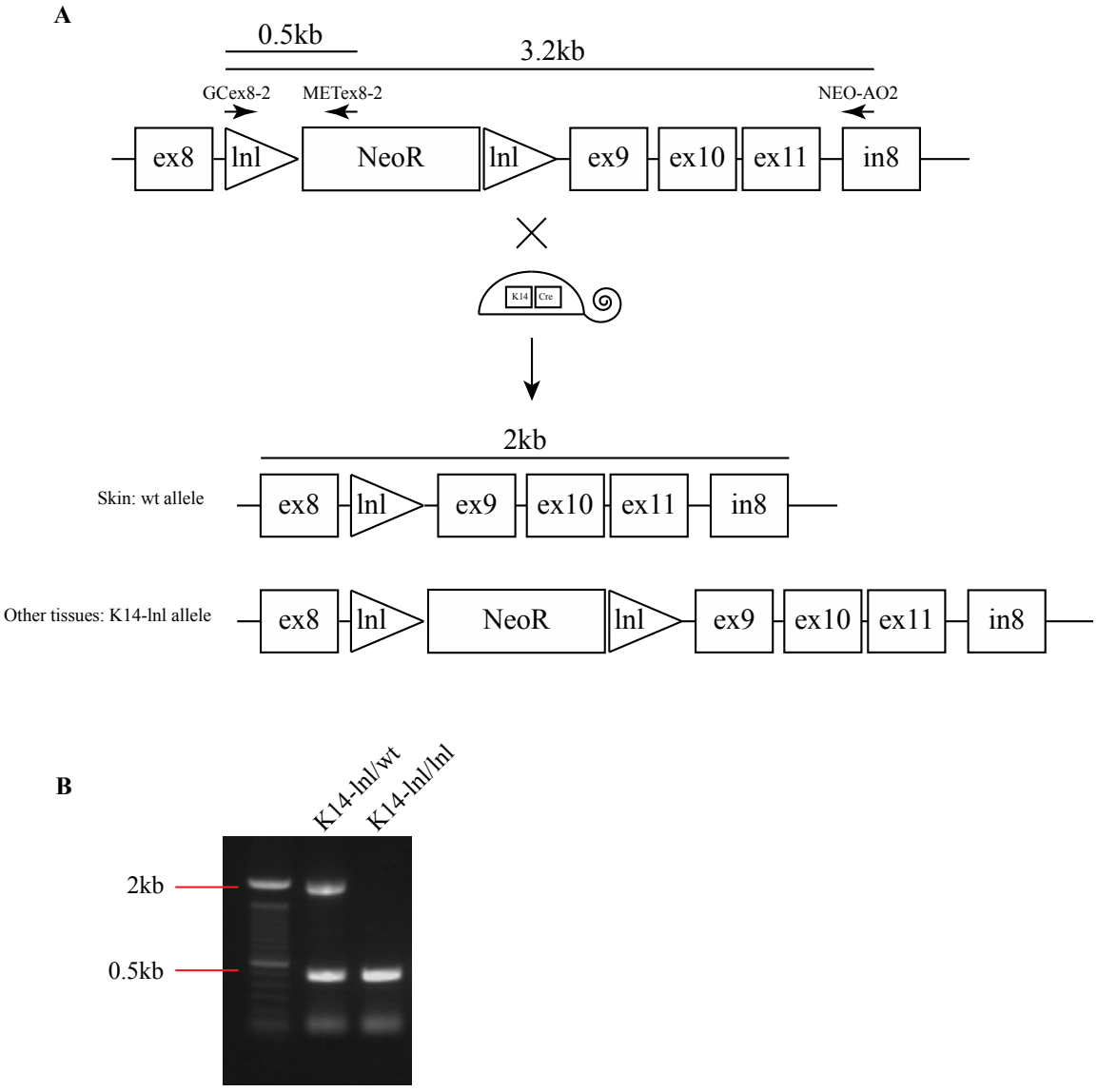

Figure 8 - K14-lnl/lnl mouse model.

A Schematic representation of the genetics of the K14-lnl/lnl mouse. The *Gba1* gene is disrupted by a neomycin cassette (NeoR), flanked by two loxP sites. The Cre recombinase is expressed in keratinocytes, so that mice carry a wild-type allele in the skin. The primers used for genotyping and the length of the fragments are reported. **B** Example of genotyping gel of a heterozygote mouse (K14-lnl/wt) expressing the Cre recombinase in the skin, and a knock-out mouse (K14-lnl/lnl).

2.6.3. Identification

Animals were identified through permanent paw tattooing performed at day of birth (Castelhano-Carlos et al., 2010). 2µl of tattoo ink (Harvard Apparatus, Holliston MA, USA. Dilution 1:3 in PBS) were injected subcutaneously into pups' palms using a 33-gauge needle (Hamilton, Cole-Parmer, London, UK). The needle was slowly removed from the paw 2-3 seconds after the injection and the excess of ink was removed. A 4-feet numbering system was used to identify different animals when house-grouped.

2.6.4. Virus administration

Injections were performed by Dr. Waddington, UCL Institute for Women's Health, UK. At postnatal day 0-1 pups were anesthetised on ice for 30-60 seconds and intravenous injections were performed via the superficial temporal vein with 40µl of vector using a 33-gauge needle (Hamilton) (Gombash Lampe et al., 2014). Once the needle was slowly removed, gentle pressure was applied to the injection site. When the pup fully recovered it was returned to the dam.

The bilateral intracerebroventricular injections were directed to the anterior horn of the lateral ventricle. The injection site was identified at 2/5 of the distance from the lambda suture to each eye (Kim et al., 2014). P0-1 mice were anesthetised on ice for 30-60 seconds. The needle was inserted perpendicularly at the injection site to a depth of 3mm and 5µl of vector was slowly administered. Following a brief pause to allow vector distribution, the contralateral ventricle was injected with the same volume of vector. The pup was allowed to recover and placed back into the cage.

Adult mice (P30) were injected into the lateral tail vein using a 33-gauge needle (Hamilton) (Walter et al., 1996). Animals were administered with 40µl of vector.

2.6.5. Behavioural assessment of mice

Animals were moved to the test room 20 minutes before the assessment. All tests were

filmed and results recorded.

***Rotarod test* -** Mice were trained for three days before performing the tests. The rotarod (Panlab LE8200, Cornella, Spain) was set with a start speed of 4 rpm and 20 rpm/min acceleration (Deacon, 2013). The animal was placed on the rotating rod. After having ensured that the animal was able to grip the rod and walk forward, the acceleration started. When a mouse fell off the time and speed was noted, up to four times per experiment. If the mouse fell within the first 5 seconds due to poor placing, the experiments would not be recorded. The speed of the rotarod and the time of each fall were recorded.

***Open field test* -** The mouse was placed in the centre of a square transparent Plexiglas chamber measuring 27cm x 27cm and allowed to freely explore the chamber (Bailey, 2009). Animals were filmed from the top of the chamber. The duration of each session was 4 minutes. The analysis of the tests was carried out using ANY-maze Behaviour Tracking Software v. 4.99 (Stoelting, Dublin, Ireland), assessing distance, average speed, mobility and immobility time of each animal.

***Tail suspension test* -** The mouse was suspended by the end of its tail approximately 20cm from the bench, ensuring that the animal cannot grasp its tail (Can et al., 2012). The test was recorded for 1 minute with a camera facing towards the abdomen of the mouse. Limb clasping phenotype was assessed. Wild-type mice extend out all limbs, while mice with motor deficiency would clasp their limbs towards the abdomen when suspended by the tail (**Figure 9**). The clasping phenotype was scored as following:

- All limbs extended out from the body all the time = 0
- Hind limbs are extended out most of the time; one hind limb is retracted in a clasping position less than 50% of the time = 1
- Both hind limbs are partially retracted for more than 50% of the time = 2
- Both hind limbs exhibit a clear clasping phenotype touching the abdomen for more than 50% of the time = 3

Righting reflex test - The mouse was placed in a supine position on a flat surface and rapidly released (Brooks and Dunnett, 2009). The ability of the mouse to right itself (four paws on the ground) was assessed. Wild-type healthy animals show fast latency to return to prone position (< 1 second, score=1), while animals with impairments in motor coordination functions exhibit slow latency to right their selves (>10 seconds, score=0) or completely fail the test. The time each mouse spent to return in supine position was recorded.

Figure 9 - Tail suspension test.

A Wild-type mouse extends out all limbs when suspended by the tail. **B** Affected mouse showing the clasping phenotype.

Foot fault test - The mouse was placed on a metal mesh surface (mesh gap size 1.3cm) elevated 20cm from the bench. The animal was allowed to cross the device and the run was recorded over one minute. The number of total steps for fore limbs and hind limbs was counted (Shelton et al., 2008). The number of paw misplacements was also recorded.

Footprint pattern test - The paws of the mouse were painted with different coloured non-toxic dyes (fore paws: blue; hind paws: red). The animal was then allowed to walk along a corridor, leaving a trail of footprints on a paper sheet. The stride length and base width were measured (Brooks and Dunnett, 2009).

2.7. Collection and analysis of blood samples

2.7.1. Blood analysis

Large volume samples of up to 1ml were collected through ventricular cardiac puncture at terminal stages of the study while animals were in terminal anaesthesia.

Samples were stored in tubes with EDTA at 4°C and analysed on the same day. Blood samples were processed through fluorescence-activated cell sorting (FACS) by Central Diagnostic Service at the Queen's Vet School Hospital, Cambridge, UK.

2.7.2. Dried blood spots collection

Blood samples were taken from the temporal vein of P0 mice. The vein was punctured with a 25g needle (BD Microlance) and a drop of blood was collected with a pipette. A maximum of 10% of the total blood volume was collected. Gentle pressure was applied to the sampling site in order to stop the bleeding. The pup was allowed to recover and consequently placed back into the home cage.

10µl of blood was blotted on filter paper (Whatman 903 paper, CDC 5-spot card, 100/pk, GE Healthcare, USA). If not immediately processed, the samples were placed in plastic bags with a dessicant sachet and kept at -20°C, or at -80°C for longer periods.

2.7.3. Genotyping through GCase enzymatic assay on dried blood spot samples

All stock solutions were stored protected from light, and placed in bags with dessicant sachets.

0.2M Citrate Buffer: 46.5ml of 0.15M citric acid (Sigma-Aldrich), 53.5ml of 0.3M Na_3PO_4 (Sigma-Aldrich).

GAUCHER EXTRACTION BUFFER: Triton X-100 was made by adding 5ml of Triton X-100 to 45ml of 0.2M Citrate Buffer. 5ml of 10% Triton X-100 (Sigma-Aldrich) were added to the bottle containing 1g of sodium taurodeoxycholate (Sigma-Aldrich) and the solution was transferred to a cylinder. 5ml of 10% Triton X-100 were added again to wash the bottle and transferred to the cylinder two more times. 0.2M Citrate Buffer was added up to 100ml ad the pH was adjusted to 5.2. The solution was aliquoted and stored at 4°C.

GAUCHER SUBSTRATE BUFFER (4-MUβGlu): 2.3ml of DMSO (Sigma-Aldrich) were added to 778.11mg of 4-methylumbelliferyl-β-D-glucopyranoside (Sigma-Aldrich). The solution was mixed and aliquots were stored at -20°C.

GAUCHER WORKING SOLUTION (GWS): 75µl of 4-MUβGlu were dissolved in 5.925ml of dH_2O. The solution was prepared fresh on the day.

CBE SOLUTION: 5mg of 0.26M Conduritol B epoxide (Sigma-Aldrich) were dissolved in 120.5µl of DMSO. The solution was aliquoted and stored at -20°C.

GAUCHER INHIBITING SOLUTION (GIS): 5.6µl of CBE solution were added to 3ml of GWS. The solution was prepared fresh on the day.

GAUCHER STOP SOLUTION: 0.5M EDTA pH 11.3-12. The solution was filtered using 0.22µm filter.

GAUCHER STANDARD SOLUTION (6μM 4-MU): 0.011g of 4-methylumbelliferone (Sigma-Aldrich) was dissolved in 10ml of methanol. 1μl of the solution was then diluted in 99μl of dH_2O.

Since all mice carried the wild-type allele in the skin, it was not possible to genotype neonatal animals using the standard DNA extraction from ear or tail clips. Therefore, knock-out mice were identified through detection of β-glucosicerebrosidase enzymatic activity in blood samples. This assay allowed the identification of *Gba1* knock-out animals; however, it was not suitable to differentiate with certainty between heterozygote and wild-type mice.

A 6mm disk was punched from the centre of a blood spot directly into a 1.5ml tube and 400μl of Gaucher extraction buffer were added. When the punch was not completely in contact with the buffer, the tube was quickly vortexed allowing the liquid to entirely cover the paper. The tube was mixed for 1 hour at 4°C. The paper disk was removed and the tube was centrifuged for 30 minutes at RT at 10,000 x g. The sample was returned immediately onto ice and the supernatant was moved to a fresh tube. 40μl of sample were incubated with 80μl of Gaucher working solution in 96-well black bottom plates (Corning, USA). Each sample was tested in duplicate. Columns 11 and 12 were left empty for following use. The plate was sealed and incubated at 37°C for a minimum of 6 hours to a maximum of 24 hours. After the incubation period, the adhesive film was removed from the plate. 100μl of dH_2O were added to all wells in column 11. 100μl of the Gaucher standard solution (6μM 4-MU) were added to wells A11. The following serial dilutions of the Gaucher standard solution were created transferring 100μl of the solution from each well to the following one, starting from wells A11 to B11, from B11 to C11, from C11 to D11 and so on: 0.3125nM (A11), 0.1563nM (B11), 0.0781nM (C11), 0.039nM (D11), 0.098nM (E11), 0.0049nM (F11), 0.000nM (G11). Well G11 contained only 100μl of dH_2O. The serial dilutions described above were repeated for column 12, starting from well A12. 100μl of the Gaucher Stop Solution were added in each well. Fluorescence was red from the top of the plate using the following parameters: excitation wavelength: 360nm; emission wavelength: 450nm (FluoStar Optima Plate Reader, BMG Labtech, Aylesbury, UK).

2.8. Harvesting and tissue preparation

Mice were euthanised by transcardial perfusion using PBS while under terminal isofluorane anaestehsia and organs were subsequently harvested.

One hemisphere of the brain was fixed in 4% PFA (Sigma-Aldrich) for 48 hours, transferred to a cryopreserving solution of 30% sucrose (w/v) (Sigma-Aldrich) in PBS and stored at 4°C. The other hemisphere was frozen and stored at -20°C.

Visceral organs were cut in two parts and placed in separate tubes. One half was preserved in 4% PFA at 4°C for 48 hours, then moved to 30% sucrose in PBS and stored at 4°C; the parts intended for enzymatic assay and protein extraction were frozen and stored at -20°C.

2.9. Histological analysis of tissues

2.9.1. Cryosectioning of murine tissue samples

1X Tris Buffered Saline TBS: 6.04g Trizma, 8.5g NaCl, 3.2ml 1M HCl (Sigma-Aldrich), dH_2O to final volume of 1l.

TBS with anti-freeze (TBSAF): 350ml of TBSA (1X TBS, 0.05% sodium azide (VWR)), 150ml of ethylene glycol (VWR), 30% sucrose solution.

Fixed organs were embedded with specimen matrix (Thermo Scientific), frozen and cut at 40µm in thickness at constant temperature of -20°C with a Cryostat Leica CM3050 (Leica Biosystems, Milton Keynes, UK). Coronal brain sections were sliced starting from the front of the olfactory bulbs to the cerebellum and brain stem. Slices were stored at 4°C in TBSAF in 96-well plates.

2.9.2. Preparation of chrome-gelatine coated slides

2.5g of gelatin (VWR) and 0.25g of chromium (III) potassium sulphate 12-hydrate (VWR) were dissolved in 500ml of dH_2O preheated to 45°C. The slides (75 x 25 x 1.2 mm, VWR) were immersed in the gelatine solution for a few seconds and left to dry at 56°C overnight. The process was repeated on the next day.

2.9.3. Immunohistochemical staining on free-floating tissue sections

TBS with Triton X-100 (TBS-T): 1X TBS, 0.3% Triton X-100.

A series of representative sections was collected in six-well plates and washed three times with 3ml of TBS with 5 minutes between each wash on a rocking table. Endogenous peroxidase activity was blocked with 1% H_2O_2 in 1X TBS for 30-60 minutes under constant gentle agitation. Slices were rinsed three times in 1X TBS and the non-specific binding was blocked in 15% normal serum (Sigma-Aldrich) in 1X TBS-T for 30 minutes on a rocking table. Sections were washed three times with 1X TBS and the primary antibody diluted with 10% normal serum in TBS-T was added. The plate was incubated at 4°C overnight on a rocking table. The following day, slices were washed three times with 1X TBS and incubated for 2 hours at room temperature with the secondary antibody diluted with 10% normal serum in TBS-T. Afterwards, sections were rinsed three times in 1X TBS and incubated for 2 hours with 1:1000 avidine-biotin reagent (Vectastain Elite ABC kit, Vector Labs, UK). Sections were then washed three times in 1X TBS and immunoreaction was detected by adding 0.45µm filtered 0.05% 3,3'-diaminobenzidine tetrahydrochloride (Sigma-Aldrich) and 0.001% H_2O_2 in 1X TBS (one DAB tablet in 20ml of TBS). The plate was covered with foil and kept under agitation for a few minutes. The reaction was stopped by adding ice-cold 1X TBS. After three washes in 1X TBS, sections were mounted on chrome-gelatine coated slides and left to air-dry overnight. Slides were dehydrated in 100% ethanol, cleared in Histo-clear (National Diagnostic, Atlanta GA, USA) for 30 minutes and cover slipped with DPX mountant (Fisher Scientific).

2.9.4. Immunofluorescent staining of tissue sections

DAPI working solution: 1mg/ml (aq) 4',6-diamidino-2-phenylindole (DAPI, Sigma-Aldrich) diluted 1:1,000 in 1X TBS.

Sections were initially stained as described in **Section 2.9.3**. Following incubation with secondary antibodies with Alexa Fluor conjugates, the sections were washed three times in 1X TBS and incubated with DAPI working solution for 5 minutes protected from light.

Sections were rinsed three times in 1X TBS and mounted on chrome-gelatine coated slides. When the sections were dried, the slides were coverslipped with Fluoromount G (SouthernBiotech, Birmingham AL, USA) and kept at 4°C protected from light.

2.9.5. Nissl staining of brain sections

0.05% Cresyl Violet Working Solution: 0.5ml of 10% (aq) acetic acid per 100ml of 0.5% (aq) cresyl fast violet (VWR).

Brain sections were mounted on chrome-gelatine coated slides and air-dried overnight. Slides were stained in 0.05% Cresyl Violet Working Solution at 60°C for 30-45 minutes. Slides were then rinsed twice in fresh dH_2O and dehydrated in IMS and Histo-clear as follows:

- 70% IMS, 5 min
- 80% IMS, 2 min
- 90% IMS, 2 min
- 95% IMS, 2 min
- 100% IMS, 2 min
- 100% IMS, 2 min
- 50% Histo-clear in IMS, 2 min
- 100% Histo-clear, 2 min

When the background staining disappeared, the slides were incubated in fresh Histo-clear for 30 minutes and consequently coverslipped with DPX mountant medium.

2.9.6. Hematoxylin and Eosin (H&E) staining

0.5% Eosin: 1.5g of Eosin (Sigma-Aldrich) in 300ml of 95% ethanol.

Tissue sections were mounted on chrome-gelatine coated slides and air dried overnight. The sections were stained protected from light with filtered 0.1% Mayer Hematoxylin (Sigma-Aldrich) for 10 minutes. The slides were rinsed in dH_2O for 5 minutes and consequently dipped 12 times in 0.5% Eosin solution. The sections were quickly washed in dH_2O and subsequently dehydrated for 30 seconds in rising concentrations of ethanol (50%, 70%, 95%, 100%). The slides were finally incubated in Histo-clear for 30 minutes and coverslipped with DPX mountant medium.

2.9.7. Microscope imaging

Light bright-field images were taken with a Nikon DS-Fi1 camera (Nikon, Tokyo, Japan) attached to a Nikon Eclipse E600 microscope. Representative images of the full brain section were taken with a 1X. Higher magnification pictures of discrete areas of the sections were taken with 10X/0.25 and 40X/0.65 objectives (CFI Achromat, Nikon). Specific brain regions were identified according to the Paxinos and Franklin's Mouse Brain Atlas (Paxinos, 2012). Antero-posterior coordinates from bregma for each region are reported in **Table 7**.

Immunofluorescent stained sections were analysed with Zeiss LSM 710 laser scanning confocal microscope (Carl Zeiss AG, Oberkochen, Germany).

BRAIN REGION	BREGMA (mm)
Prefrontal cortex	From +3 to +2
Lateral ventricles	From +1 to 0
Cortex	From -1 to -2
Hippocampus	From -1.5 to -2
Thalamus	From -1.5 to -2
Midbrain	From -2.5 to -3
Cerebellum	From -5.5 to -6.5
Brain stem	From -5.5 to -6.5

Table 7 - Coordinates from bregma.

Brain regions analysed in the study and relative antero-posterior coordinates from bregma are reported.

2.9.8. Staining quantification

The region of interest on a section was first identified at low magnification. The objective was then changed to 40X and the optimal focus and light intensity were adjusted. 10 consecutive non-overlapped images per distinct area were taken. The light intensity was kept constant throughout the imaging process of each region of all brains and visceral organs stained against the same antibody.

The evaluation of the immunoreactivity of stained sections was performed using the Image-Pro Premier analysis system (Media Cybernetics, Rockville MD, USA). The minimum threshold value of stained pixel intensity was assigned. All the images of sections stained with the same antibody were processed simultaneously. The extent of staining, defined as level of intensity above the assigned threshold for each stained pixel, and expressed as percentage of the total area of the image was measured. Results were presented as the percentage of average value of immunoreactivity of 10 consecutive images for each distinct region.

2.9.9. Neuronal counts in discrete brain regions using stereology

Neuron counting and cortical thickness measurements were estimated with Stereo

Investigator software (MBF Bioscience, Williston VE, USA) on Nissl stained sections with a Nikon Optihot light microscope (Nikon) attached to a Q-Imagin camera (MBF 2000R-CLR-12, Bioscience). The user was blinded to the experimental slides being analysed by another person covering the slide labels with tape.

Neurons were counted with the Optical Fractionator probe using the 40X objective. The grid size and the counting frame used for analysing different brain regions were the following: S1BF 150 x 150 μm, 50 x 50 μm; VPM/VPL 175 x 175 μm, 50 x 50 μm; Gi 100 x 100 μm, 50 x 50 μm. Cells were counted using a 100X objective. Efficient sampling was estimated by a coefficient of error between 0.05 and 0.1 (Gundersen et al., 1999). 3 to 4 sections for each brain were analysed and the average values of cell counting were used in the calculations.

The mean thickness of the S1BF cortical region was estimated by using the Cavalieri vertical sections principle (Baddeley et al., 1986). The length of 10 parallel consecutive lines intersecting perpendicularly the cerebral cortex, traced from the somatosensory barrel cortical layer 1 to the corpus callosum, was measured. 3 sections of the midbrain region per each brain were analysed and the average values were reported.

2.10. Protein analysis

2.10.1. Protein concentration measurements from tissue and transfected cell samples

The total protein concentration of tissue homogenates and transfected cell extracts was estimated using the Pierce BCA Protein Assay Kit (Thermo Scientific) accordingly to the manufacturer's instructions.

2.10.2. Glucocerebosidase enzymatic activity assay on frozen tissue

1M Glycine buffer: 7.5g glycine, 5.8g NaCl in 100ml dH_2O. Add 5.6ml of solution to

4.4ml of 1M NaOH solution. pH 10.4.

Frozen tissue samples were homogenised with dH_2O on ice. The total protein concentration was measured.

The same reagents described for the dried blood spot assay (**Section 2.7.3**) were used. A 96-well plate was divided into rows of 4 wells per each sample. 3µl of sample and 30µl of 4.8mM 4-MUβGlu in Gaucher Extraction Buffer were added in duplicate into the first and second wells of each row. The plate was incubated at 37°C for 2 hours. 1ml of 1M Glycine buffer pH 10.4 was added to wells 1 and 2 to stop the reaction. For each sample a standard and a standard blank were set up as following: 200µl of 1nM 4-methylumbelliferone, 950µl of 1M Glycine buffer and 15µl of sample were added to well 3; 200µl of dH_2O, 950µl of 1M Glycine buffer and 15µl of sample were added to the last well. Fluorescence was read (FluoStar Optima Plate Reader. Excitation wavelength: 360nm; emission wavelength: 450nm; fluorescent top reading; gain: 750).

The enzymatic activity (nmol/hr/µg) was calculated using the following equations.

For each sample:

Standard – Standard blank = fluorescence of 1nmol of 4-methylumbelliferone

$$\frac{Fluorescence\ sample}{Fluorescence\ standard} * \frac{60(\text{minutes})}{120(\text{minutes})} * \frac{1000(\mu l)}{15(\mu l)} * \frac{1(\mu g)}{sample\ concentration\ (\frac{\mu g}{\mu l})}$$

2.10.3. Protein analysis using Western blot

1X SDS Running buffer: 50ml 20X NuPAGEMES (Invitrogen, USA), 950ml dH_2O. On the day, add 250µl of anti-oxidant (Invitrogen) per 100ml of buffer.

TBS-Tween: 1X TBS, 0.1% Tween (Sigma-Aldrich).

Transfected cells were processed as described in **Section 2.4.2**. Protein concentrations from cell samples were normalised to 1µg/µl. 1X LDS Sample buffer (Life Technologies) and 1X Reducing agent (Life Technologies) were added to each sample. The samples were boiled at 95°C for 5 minutes to denaturate the proteins. 20-40µg of protein sample and 10µl of molecular weight marker (RPN800E, GE Healthcare) were loaded into NuPAGE Bis-Tris 4-12% polyacrylamide gel (Novex, Life Technologies) with 1X SDS Running buffer. The gel was run at 90V for 2 hours (PowerPac, Bio-Rad). PDVF membrane (Millipore) was incubated in methanol for 1-2 minutes. Afterwards, the membrane and the gel were equilibrated in ice-cold Transfer buffer for 5 minutes. A sandwich of filter paper/PVDF membrane/gel/filter paper wetted in Transfer buffer was placed into the transfer apparatus (Trans-Blot SD, Bio-Rad). The transfer was performed at 400mA for 1 hour. The membrane was washed in TBS-Tween buffer and blocked in 5% BSA in TBS-Tween at 4°C for 1 hour with agitation. The membrane was then incubated with the primary antibody diluted in TBS-Tween with 3% BSA at 4°C overnight with agitation. The membrane was then washed 3 times in TBS-Tween buffer while agitating, 5 minutes per wash. The membrane was incubated with the secondary HRP-conjugated antibody (Abcam) diluted in TBS-Tween with 3% BSA at room temperature for 1 hour with agitation, and finally washed 3 times in TBS-Tween.

The membrane was developed using SuperSignal West Pico kit (Thermo Fisher) accordingly to manufacturer's instructions. The imaging of the membrane was performed with GeneGnome Imager (Syngene).

2.10.4. Enzyme-linked immunosorbent assay (ELISA)

The ELISA test was carried out by Dr. Buckley, UCL Institute for Women's Health, London, UK in order to obtain a quantitative measurement of GFP protein in the visceral organs for mice injected with the scAAV2/9.GUSB.*GFP*.bGHpA vector.

A 96-well plate was incubated with the primary anti GFP antibody (ab1218, Abcam) diluted 1:10,000 in bicarbonate buffer overnight at 4°C. The wells were washed three times with a Tween20-PBS solution (1:2,000) and incubated with a blocking solution (1% BSA in PBS) at 37°C for 1 hour. Tissues were homogenised in lysis buffer and

protein concentration was measured. 100µl/well of sample and serial dilutions of the standards (1µg/ml GFP in wash buffer) were added. The plate was then incubated at 37°C for 1 hour. After three washes, 1:5,000 secondary polyclonal antibody (ab6658, Abcam) in blocking solution was added. The plate was incubated at 37°C for an additional hour. The samples were washed and a streptavidin-HRP substrate solution (1:20,000 in blocking solution) was added. The plate was incubated at 37°C for 1 hour. 100µl/well of tetramethylbenzidine were added and the plate was incubated at room temperature for 10 minutes. 100µl/well of 2.5 H_2SO_4 were added and the fluorescence was immediately read at 450nm (FluoStar Optima Plate Reader).

2.11. Statistical analysis

The statistical analysis was performed with GraphPad Prism Software (v. 6.0e). Data are presented as average values (mean) $\pm$ standard deviation (SD). t-test, one-way ANOVA and two-way ANOVA tests were performed where appropriate. The survival data were analysed with Kaplan-Meier estimate. Tukey's and Mantel-Cox's honest significance ad-hoc tests were used for multiple comparison analysis. Non-statistical significance (ns) was assumed for $p > 0.05$.

3. Evaluation of intravenous AAV9 administration to neonatal and juvenile mice

The current study provides pre-clinical evidence on the beneficial effects of AAV-based gene therapy as a possible treatment for Gaucher disease. The results of this work are articulated in three major sections: (i) the preliminary gene reporter analysis confirms the widespread transduction following intravenous administration to neonatal wild-type mice; (ii) the administration of an AAV vector carrying the functional therapeutic gene rescues the lethal neurodegeneration of an acute Gaucher type II mouse model (Enquist et al., 2007); (iii) the administration of a novel vector with strong neuronal tropism results in recovery of the neuropathology in the mouse model.

3.1. Introduction

Previous studies have shown that the intravenous administration of an AAV9 vector to neonatal mice leads to efficient widespread transduction of neurons, while the administration to adult animals result in a more predominant astrocytic transduction (Foust et al., 2009). Efficient neuronal transduction is necessary to ameliorate the severe neuropathology that characterises Gaucher disease type II. The acute neurodegeneration is already present in the early neonatal period (Goker-Alpan et al., 2003), therefore an early intervention is necessary to prevent further development of neurological impairment. Although Foust and colleagues already demonstrated that the intravascular administration of a scAAV9 vector to neonatal mice results in neuronal transduction, there are no previous data on the use of the β-glucuronidase promoter employed in this study. This chapter will examine the importance of therapeutic intervention in early developmental stages to achieve an efficient and widespread neuronal transduction using an AAV9 vector configuration and promoter that would be suitable as part of a

preclinical study.

In this preliminary reporter gene study, a scAAV2/9 vector carrying the green fluorescent protein (*GFP*) gene was administered intravenously to wild-type mice at two different time points and brain transduction was assessed. The transgene expression was under control of the ubiquitous β-glucuronidase (GUSB) promoter. Although GUSB has been used in other preclinical studies (Husain et al., 2009), relatively little is known on whether it can mediate gene expression in neural cells following systemic administration. The present study aimed to confirm that central nervous system transduction was achievable following intravenous administration of the vector into neonatal mice and any potential advantages this has over administration into older juvenile mice. The immune response against the virus or transgene expression in the central nervous system was also evaluated. In order to evaluate the efficiency of the vector to transduce different cell types, the distribution of the transgene expression in the viscera was assessed.

3.2. scAAV2/9.GUSB.*GFP*.bGHpA vector

The construct was kindly provided by Dr. Seng H. Cheng (Sanofi Genzyme). The green fluorescent protein gene was cloned into a shuttle plasmid containing the inverted terminal repeat (ITR) sequences derived from a scAAV2 vector and the β-glucuronidase (GUSB) promoter, followed by a short bovine growth hormone poly-adenylation signal (bGHpA). The recombinant scAAV2/9.GUSB.*GFP*.bGHpA vector (**Figure 10**) was generated by standard triple plasmid transfection. The titre of the supplied viral stock was $1x10^{13}$ gc/ml.

Figure 10 - Schematic of the scAAV2/9.GUSB.*GFP*.bGHpA final expression cassette.

The reporter gene *GFP* was cloned into the scAAV2/9 vector backbone downstream the β-glucuronidase promoter (GUSB). The viral inverted terminal repeats (ITRs) are derived from a scAAV2 vector.

3.3. Analysis of GFP expression in the brain following intravenous administration of the scAAV2/9.GUSB.*GFP*.bGHpA vector to neonatal and juvenile mice

Wild-type outbred CD1 mice were intravenously injected via the superficial temporal vein at the day of birth (from now referred to as 'neonatal administered') with 4 x 10^{11} gc of scAAV2/9.GUSB.*GFP*.bGHpA in a total volume of 40µl (n=5). Young adult mice (referred to as 'juvenile administered') were injected at 30 days of age (n=4). Uninjected CD1 mice were used as controls (n=3). The animals were sacrificed one month after virus administration and the brains were harvested, sectioned and examined for GFP expression using immunoperoxidase staining.

The brains from neonatally injected mice showed widespread rostro-caudal transduction in both hemispheres, including the pre-frontal cortex, hippocampus, thalamus, midbrain, cerebellum and brain stem (**Figure 11**). In comparison the transgene expression in brains from juvenile administered mice was limited to fewer areas and staining for GFP was less intense. Highly efficient transduction was detected in distinct regions of the brain stem, however the GFP expression in the anterior part of the brain was reduced compared to the neonatal administered mice. Some scattered GFP positive cells could

be detected in the midbrain.

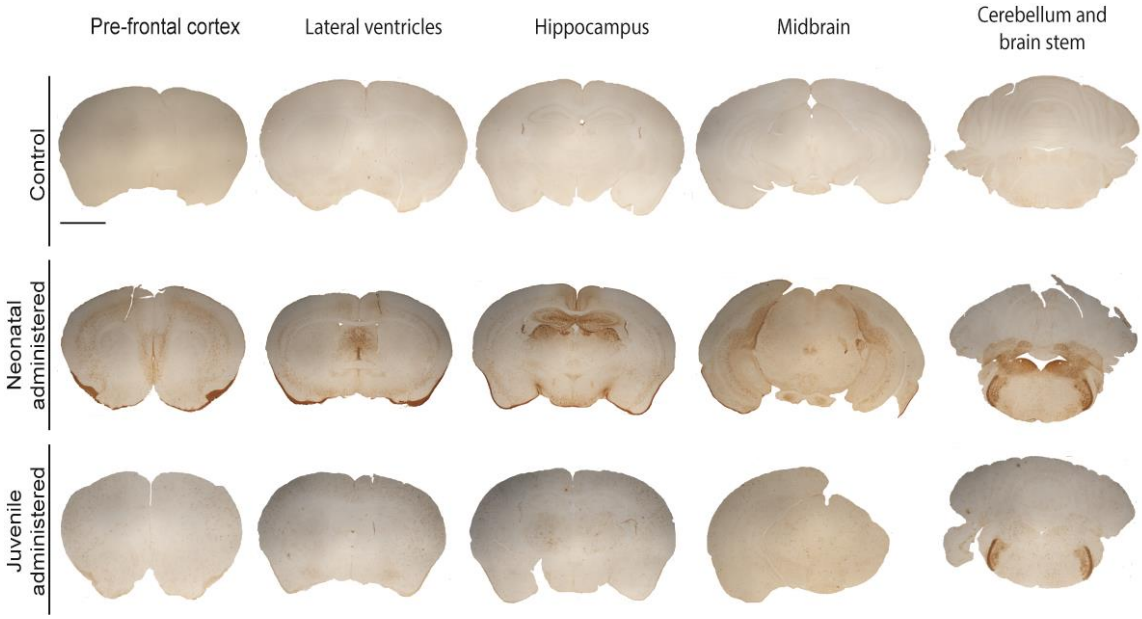

Figure 11 - Immunoperoxidase detection for GFP protein in brain sections from mice administered with 4 x 10^{11} gc scAAV2/9.GUSB.*GFP*.bGHpA following intravenous injection into neonatal administered and juvenile administered mice.

When injected into neonates, the scAAV2/9.GUSB.*GFP*.bGHpA vector efficiently transduced the cortex, hippocampus, thalamus, hypothalamus, cerebellum and brain stem. The brains from mice injected at P30 (juvenile administered) showed reduced transduction limited to fewer areas of the brain stem. Uninjected mice were used as control (Scale bar: 1mm).

Quantification of the immunoreactivity (**Figure 12**) was performed using thresholding image analysis to estimate the transgene expression in five discrete brain regions, including: somato-barrel field cortex (S1BF), cornu annuli 1 and 2 of the hippocampus (CA1/CA2), ventral post-medial and post-lateral nuclei of the thalamus (VPM/VPL), central lobule 2 of the cerebellum (CENT2) and the gigantocellular region of the brain stem (Gi). Statistical analysis confirmed that the GFP expression in neonatal administered brains was elevated in all regions compared to uninjected controls. Although the staining for GFP was predominantly more intense in the brain of neonatal administered mice compared to the juvenile administered ones, GFP expression was significantly higher in the hippocampus ($p<0.0001$) and in the cerebellum ($p=0.003$) of

neonatal administered mice compared to juvenile administered mice.

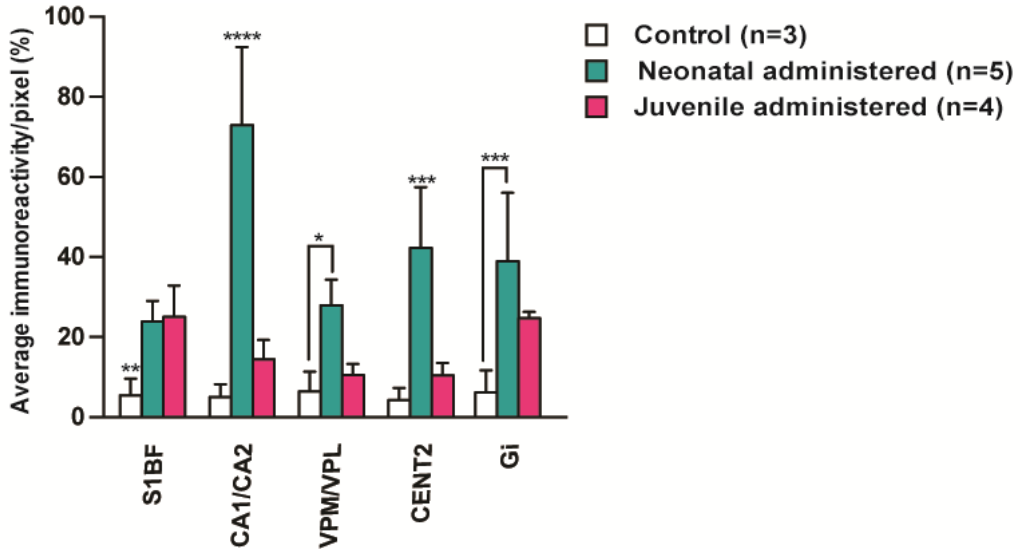

Figure 12 - Quantification of GFP immunostaining.

Analysis of immunostaining of uninjected controls (n=3), neonatal administered (n=5) and juvenile administered (n=4) brains. The average immunoreactivity of each brain region has been reported. The areas taken into consideration were: cortex (S1BF), hippocampus (CA1/CA2), thalamus (VPM/VPL), cerebellum (CENT2), and brain stem (Gi). Brains from neonatal administered mice showed elevated and widespread GFP expression. Significant difference in immunoreactivity was observed in the juvenile administered brains compared to uninjected controls (Data presented as average $\pm$ SD. Statistical analysis: two-wayANOVA, Tukey's multiple comparisons test; * $p \leq 0.05$, ** $p \leq 0.01$, *** $p \leq 0.0001$, **** $p < 0.0001$).

Using light microscopy, a semi-quantitative analysis of GFP expression in more detailed regions of the brain was carried out (**Figure 13**). Overall, higher levels of GFP expression were visible in the brains from mice that received intravenous neonatal administration of scAAV2/9.GUSB.*GFP*.bGHpA compared to those that received injections at P30.

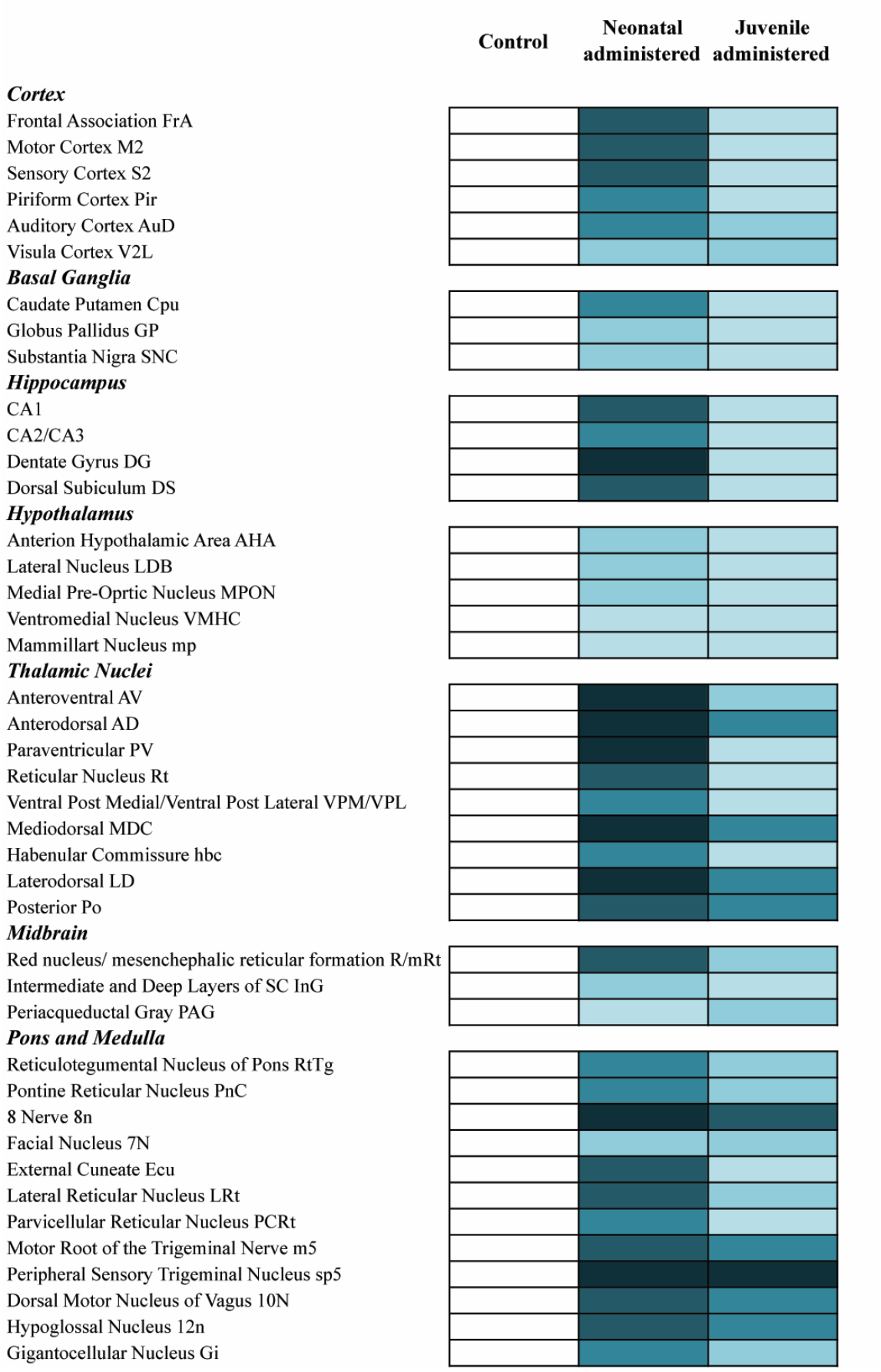
Control
Neonatal administered
Juvenile administered
Cortex
Frontal Association FrA
Motor Cortex M2
Sensory Cortex S2
Piriform Cortex Pir
Auditory Cortex AuD
Visula Cortex V2L
Basal Ganglia
Caudate Putamen Cpu
Globus Pallidus GP
Substantia Nigra SNC
Hippocampus
CA1
CA2/CA3
Dentate Gyrus DG
Dorsal Subiculum DS
Hypothalamus
Anterion Hypothalamic Area AHA
Lateral Nucleus LDB
Medial Pre-Oprtic Nucleus MPON
Ventromedial Nucleus VMHC
Mammillart Nucleus mp
Thalamic Nuclei
Anteroventral AV
Anterodorsal AD
Paraventricular PV
Reticular Nucleus Rt
Ventral Post Medial/Ventral Post Lateral VPM/VPL
Mediodorsal MDC
Habenular Commissure hbc
Laterodorsal LD
Posterior Po
Midbrain
Red nucleus/ mesenchephalic reticular formation R/mRt
Intermediate and Deep Layers of SC InG
Periacqueductal Gray PAG
Pons and Medulla
Reticulotegumental Nucleus of Pons RtTg
Pontine Reticular Nucleus PnC
8 Nerve 8n
Facial Nucleus 7N
External Cuneate Ecu
Lateral Reticular Nucleus LRt
Parvicellular Reticular Nucleus PCRt
Motor Root of the Trigeminal Nerve m5
Peripheral Sensory Trigeminal Nucleus sp5
Dorsal Motor Nucleus of Vagus 10N
Hypoglossal Nucleus 12n
Gigantocellular Nucleus Gi

Figure 13 - Distribution of GFP-positive cells in different brain regions.

The colour indicates the density of GFP positive cells. The absence of transduced cells is represented by a white square, while the highest GFP expression is represented by a dark square. Neonatal injections of scAAV2/9.GUSB.*GFP*.bGHpA resulted in higher and widespread transduction compared to juvenile administered brains.

Higher magnification light microscopy pictures showed in detail the differences in transgene expression between neonatal and juvenile administered mice within discrete regions of the brain (**Figure 14**). From the images it was possible to appreciate that the expression in the neonatal administered mice appeared to be predominantly in cells of neuronal morphology, whereas in the juvenile administered brains transduced cells appeared to be a more heterogeneous population of astrocytes and neurons. In particular, within the cortex, the hippocampus and partially in the thalamus of juvenile administered brains the tropism of the vector is mainly astrocytic.

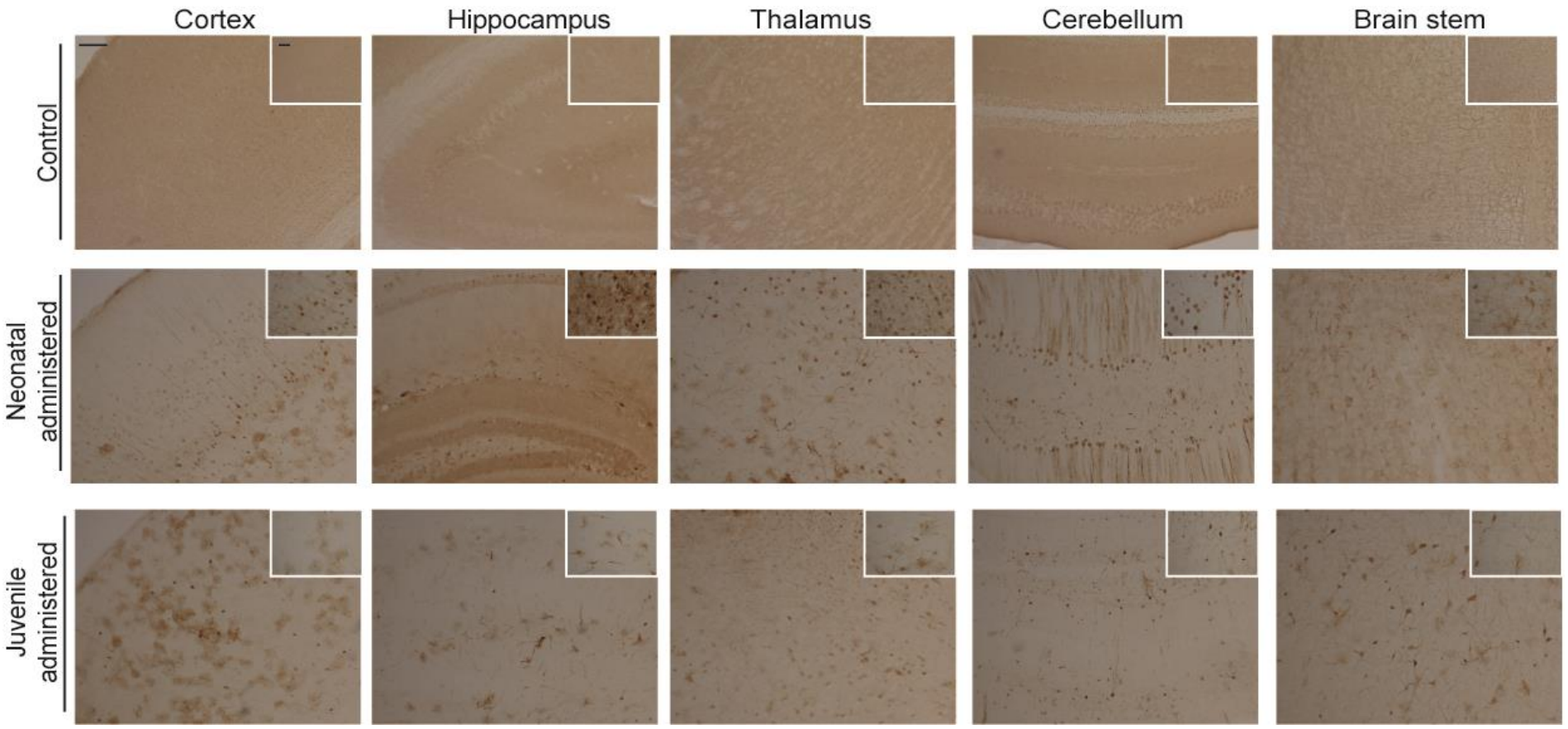
Cortex
Hippocampus
Thalamus
Cerebellum
Brain stem
Control
Neonatal administered
Juvenile administered

Figure 14 - *GFP* transduction in neonatal and juvenile administered brains following intravenous injection of scAAV2/9.GUSB.*GFP*.bGHpA.

Brain sections from mice administered neonatally showed widespread transduction in the cortical region cortical S1BF, hippocampal CA1/CA2, thalamic nuclei VPM/VPL, cerebellar lobi and brain stem. The later administration of the vector to juvenile mice resulted in moderate GFP expression (Scale bars: low magnification 100μm; high magnification 60μm).

3.4. An evaluation of immune response following intravenous administration of scAAV2/9.GUSB.*GFP*.bGHpA

In order to assess if the systemic administration of the scAAV2/9.GUSB.*GFP*.bGHpA vector harbored an immune response in the brains of injected mice, immunohistochemistry was performed on tissue sections using antibodies against the macrophage/microglial protein cluster of differentiation 68 (CD68). This lipoprotein is usually found in the cytoplasmic granules of macrophage-lineage cells and can be utilised as a useful marker for detecting microglia associated with brain injury and neuroinflammation (Graeber et al., 1990). Untreated K14-lnl/lnl mice were used as positive control for microglia activation. The quantification of the immunoreactivity (**Figure 15**) confirmed that the administration of the vector did not cause immune response in the brain of injected mice. In fact here was no indication of increased microglial staining in brains from mice that received neonatal and juvenile administration of scAAV2/9.GUSB.*GFP*.bGHpA when brain sections were examined by light microscopy (**Figure 15A**). Quantification by threshold image analysis confirmed that there was no significant difference between controls uninjected mice and any of the AAV9 administered animals (**Figure 15B**).

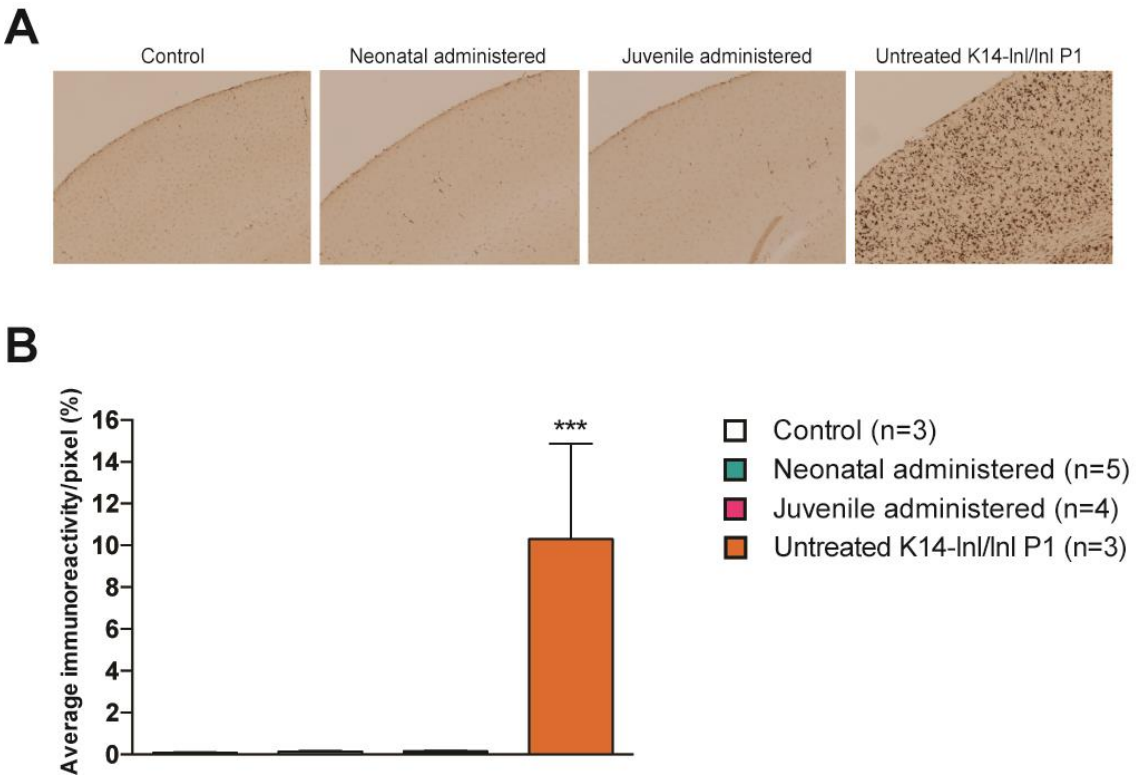

Figure 15 - Immune response in brains from mice administered with scAAV2/9.GUSB.*GFP*.bGHpA.

A Brain sections were assessed for microglia activation. Brains from mice administered neonatally (n=5) and as juveniles (n=4) did not showed staining for the microglia marker CD68 following administration of the vector. Untreated K14-lnl/lnl mice were used as positive controls. **B** Quantification of the staining for CD68 confirmed that the administration of the vector did not cause microglia activation in the brains of injected mice (Data presented as average ± SD. Statistical analysis: one-wayANOVA, Tukey's multiple comparisons test; *** $p \leq 0.001$).

3.5. Vector distribution in the visceral organs

The aim of this study is to gain an insight into systemic gene delivery of a scAAV2/9 vector expressing *GFP* under control of the GUSB promoter in neonatal mice. Intravenous administration of the vector would also mean that systemic delivery may also be possible. This would be advantageous for the treatment of the Gaucher disease type II mouse model since, although the primary cause of death is neurodegeneration,

the mice also suffer from symptoms in the visceral organs (Enquist et al., 2007). Therefore the distribution of viral transduction in visceral organs following the injection was analysed. GFP expression in different tissues was evaluated by ELISA analysis (**Figure 16**). Overall, GFP detection was robust in mice injected at day of birth. In particular, the analysis of the lungs revealed a highly significant increase (p=0.0005) in GFP levels in the mice administered neonatally when compared to the mice administered as juveniles. High levels of GFP protein were identified in the liver of both neonatal administered mice and mice administered as juveniles. The presence of GFP protein in the liver of control animals can be attributed to the high background signal of the assay.

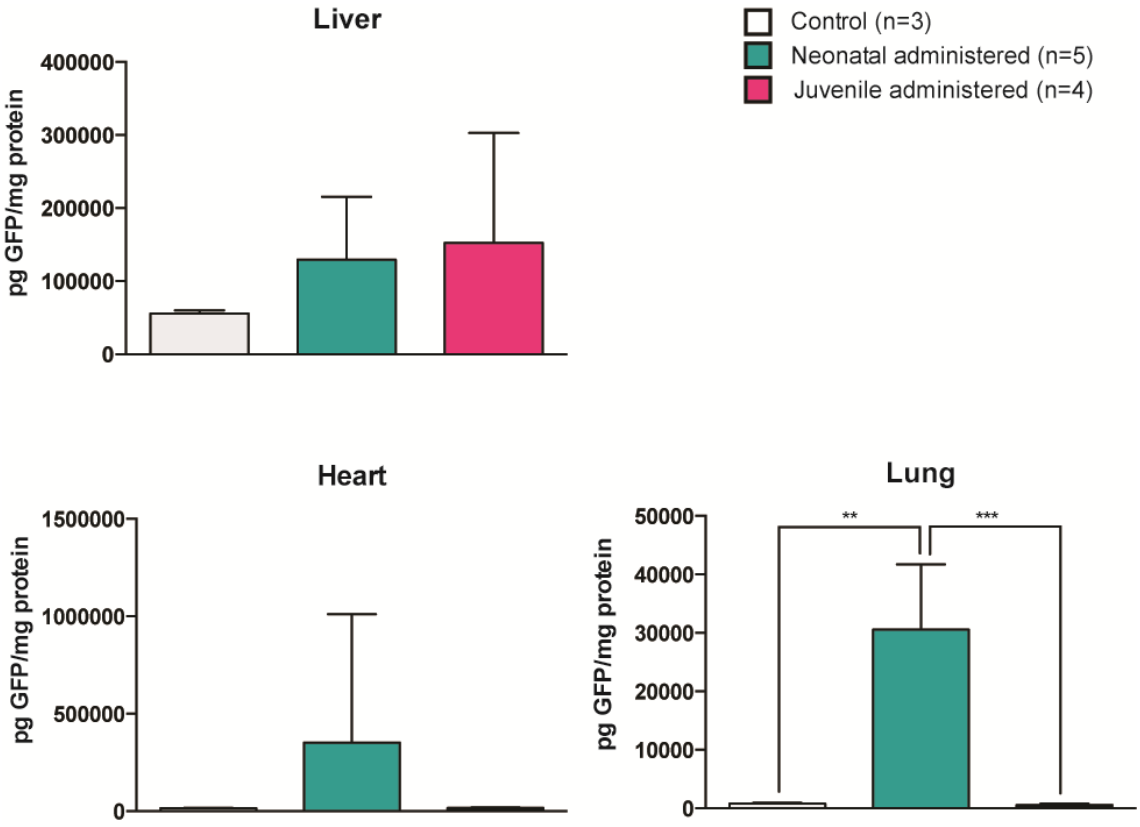

Figure 16 - GFP ELISA assay on visceral organ samples from neonatal and juvenile administered mice injected with scAAV2/9.GUSB.*GFP*.bGHpA.

Levels of GFP protein in the liver, lung and heart of treated mice neonatal administered (n=5), juvenile administered (n=4) and controls (n=3) were determined by ELISA assay. High levels of GFP protein were detected in the organs harvested from the neonatal administered mice (Data

presented as average ± SD. Statistical analysis: one-way ANOVA, Tukey's multiple comparisons test; ** $p \leq 0.01$, *** $p \leq 0.001$).

3.6. Conclusions

The aim of the preliminary reporter gene study was to evaluate the feasibility of an adeno-associated viral vector to efficiently transduce the central nervous system and the viscera following a single systemic administration. The result of the study confirmed that a scAAV2/9 vector carrying the GUSB promoter is able to efficiently transduce cells of both the viscera and central nervous system following a single intravenous administration in neonatal mice.

The scAAV2/9.GUSB.*GFP*.bGHpA vector was injected into neonatal and young adult wild-type mice and the efficiency of gene delivery was assessed one month after administration. The early administration of the vector led to a more extensive central nervous system transduction in neonatal administered mice compared to juvenile administered animals. The analysis of some areas (cortex, hippocampus, thalamus, cerebellum and brain stem) revealed that the scAAV2/9.GUSB.*GFP*.bGHpA vector seems to preferentially transduce cells with neuronal morphology following neonatal administration, whereas its cellular tropism appears more astrocytic in juvenile administered brains. These results confirmed the possible use of an AAV9-based vector for effective gene delivery to the central nervous system using a transgene that is driven by the GUSB promoter. In particular, the ability of the virus to transduce preferentially neuronal cells when administered at early age (Foust et al., 2009) confirmed that an early intervention can be beneficial for the treatment of the severe neurodegeneration, as characterised by acute neuronopathic Gaucher disease.

In order to establish whether the administration of the vector provoked an immune response in the brain of treated mice, the levels of microglia activation were analysed. No increase in CD68-positive cells was detected in brains of treated mice, confirming that adeno-associated viruses are non-pathogenic and the administration to animals that have not previously been exposed to the virus does not harbour immune response.

Finally, the distribution of the vector in the viscera was evaluated. The GFP ELISA analysis revealed that the transgene is efficiently expressed in the liver, heart and lungs of treated mice. The early administration to neonatal mice resulted in elevated levels of GFP protein in the heart and in the lungs, compared to the juvenile administered animals. The GFP expression levels in the liver of neonatal administered mice were similar in both groups. Adeno-associated virus serotype 9 is known to transduce the liver, lung and heart well (Grimm and Kay, 2003); however in the context of the ubiquitous β-glucuronidase promoter its tropism required confirmation.

Overall, the reporter gene study showed that the administration of the scAAV2/9.GUSB.*GFP*.bGHpA vector resulted in widespread transduction of the brain and the visceral organs of wild-type mice when injected intravenously to neonatal animals. This study validated the use this vector configuration and switching the *GFP* marker gene for the therapeutic human *GBA1* gene for extensive neonatal gene delivery to a Gaucher type II mouse model.

4. Intravenous AAV9-mediated gene therapy rescues a neonatal lethal mouse model of neuronopathic Gaucher disease

4.1. Introduction

The reporter gene study confirmed that the self-complementary AAV2/9 vector was able to transduce neurons in the brain and a variety of visceral organs. Therefore, a vector with the same configuration of the scAAV2/9.GUSB.*GFP*.bGHpA carrying the human *GBA1* gene was provided, in order to conduct a gene therapy rescue study on the acute lethal mouse model of Gaucher disease type II. The K14-lnl/lnl knock-out mouse is deficient in *Gba1* and develops severe neurodegeneration and visceral pathology, resulting in premature death at two weeks of age (Enquist et al., 2007). Hence this mouse strain is a valuable model for studying the effects of gene therapy on both the neuropathology and the systemic diseases.

In this study an AAV9 vector carrying the functional *GBA1* gene was intravenously administered to neonatal K14-lnl/lnl mice and the effect on lifespan, amelioration of the neuropathology and the therapeutic outcome on the viscera were assessed. The health of the mice was constantly monitored and a series of behavioral tests were performed in order to evaluate changes in the neurological symptoms of treated animals. The neuropathology was extensively studied performing a wide range of immunohistochemical and stereological analysis. The visceral organs were examined for the presence of Gaucher cells, and the β-glucocerebrosidase enzymatic activity was measured. Finally, a long-term study was conducted to assess any extension in lifespan.

4.2. scAAV2/9.GUSB.*hGBA1*.bGHpA gene therapy vector

The scAAV2/9.GUSB.*hGBA1*.bGHpA vector (**Figure 17**) was produced by Dr. Seng H. Cheng (Sanofi Genzyme). The virus maintains the same configuration as the scAAV2/9.GUSB.*GFP*.bGHpA vector used in the reporter gene study (**Chapter 3**). The human β-glucocerebrosidase gene (*hGBA1*) was cloned into the AAV9 construct, downstream of the GUSB promoter and followed by the bHGpA poly-adenylation signal sequence. The human and murine *GBA1* gene sequences are 86% homologous (O'Neill et al., 1989) and all the amino acids essential for the correct enzymatic activity of the protein are conserved between mouse and man. Taking into account any potential future perspective of clinical application, the human sequence was chosen. The expression cassette was flanked by two ITRs driving from a scAAV vector. The titre of the supplied viral vector was $1x10^{13}$ gc/ml.

Figure 17 - Schematic of the scAAV2/9.GUSB.*hGBA1*.bGHpA expression cassette.

The human *hGBA1* gene was cloned into the scAAV2/9.GUSB backbone.

4.3. Development of a blood spot assay for the identification of homozygous *Gba1* deficient mice at day of birth

Mouse models of neuronopathic Gaucher disease in which the *Gba1* activity is completely deficient die shortly after birth due to dehydration and loss of fluid through the skin. The mouse model used in this study is genetically engineered so that the *Gba1*

gene is knocked-out in all the tissues apart from the skin using Cre-lox technology. As a consequence, the affected mouse dies from neurological symptoms associated to Gaucher disease rather than dehydration (Enquist et al., 2007). However, because the *Gba1* gene is reconstituted in the skin, the conventional genotyping from ear or tail clipping is not suitable to determine the genotype of the animals. An alternative, accurate and rapid method was required to identify homozygous *Gba1* knockout mice at birth. In collaboration with Prof. Simon Heales and Mr. Derek Burke (UCL Institute of Child Health, London, UK) an alternative phenotyping strategy based on GCase enzyme activity was developed. The enzymatic assay was based on dried blood spots and allowed the detection of β-glucocerebrosidase activity in the samples, enabling the recognition of *Gba1* deficient mice on the day of birth. Blood spots were collected from mice at birth and a fluorescence-based assay for GCase activity was conducted using a synthetic version of the beta-galactoside substrate that is cleaved by the enzyme. Minimal enzymatic activity indicated that the animal was homozygote (K14-lnl/lnl) for the *Gba1* mutation (**Figure 18A**). The results were confirmed by PCR on DNA extracted from liver samples (**Figure 18B**), demonstrating that the blood spot assay was a reliable alternative method to genotype the animals at day of birth.

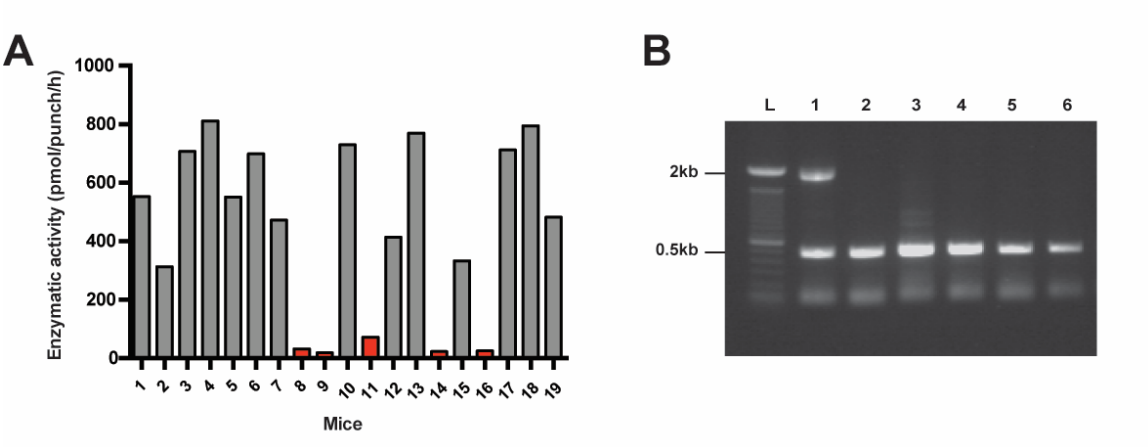

Figure 18 - Identification of knock-out mice at day of birth.

A The graph shows the GCase enzymatic activity in blood samples from newborn mice from a K14-lnl/wt x K14-lnl/wt breeding pair. 5 (red) out of 19 mice showed reduced levels of enzymatic activity in the blood samples (samples 8, 9, 11, 14 and 16). The remaining littermates (grey) were either wild-type (K14-wt/wt) or heterozygotes (K14-lnl/wt) for the *Gba1* mutation.

B Confirmation of the genotyping by PCR. L: ladder; lane 1: sample 1 (K14-lnl/wt); lanes 2-6: samples 8, 9, 11, 14, 16 (K14-lnl/lnl).

4.4. Increased life span of K14-lnl/lnl treated animals following neonatal intravenous administration of scAAV2/9.GUSB.*hGBA1*.bGHpA

The blood spot assay allowed the phenotyping of *Gba1* knock-out mice on the day of birth. Eleven K14-lnl/lnl mice were identified, of which five animals were intravenously injected at P0 into the temporal vein with 4 x 10^{11} gc of scAAV2/9.GUSB.*hGBA1*.bGHpA in a total volume of 40µl (IV treated K14-lnl/lnl); three were administered with 1 x 10^{11} gc of the same vector via bilateral intracerebroventricular injection (ICV treated K14-lnl/lnl); three remained untreated and were used as controls (Untreated K14-lnl/lnl), together with three wild-type littermates (K14-wt/wt).

The animals were continually monitored for neurological symptoms and sacrificed if the humane end point (greater than 15% body weight loss; severe and prolonged paralysis or unconsciousness) stipulated on the UK Home Office Project Licence was reached. Consistent with the study from Enquist and colleagues, untreated *Gba1* knock-out mice started developing observable and progressive neurological symptoms at 10 days after birth and by 12-14 days of age they had seizures, tremor, motor dysfunction and paralysis, and required sacrificing in accordance with the humane end point. Both the IV and the ICV treated mice survived beyond the critical point of 14 days (**Figure 19A**). Since the animals did not show any abnormal behaviour or develop any evident pathological symptoms, the treated mice and the wild-type controls were sacrificed at 55 days of age in order to conduct a short-term analysis. This promising result demonstrated that the treated K14-lnl/lnl mice were rescued from premature death associated with neurodegeneration and a single administration of the scAAV2/9.GUB.*hGBA1*.bGHpA vector resulted in approximately a 4-fold increase in the life span of the animals.

Treated animals were weighted regularly in order to keep track of any significant loss of body weight. IV and ICV treated K14-lnl/lnl mice did not show any significant difference in their body weight at any of the time points compared to the wild-type controls (**Figure 19B**).

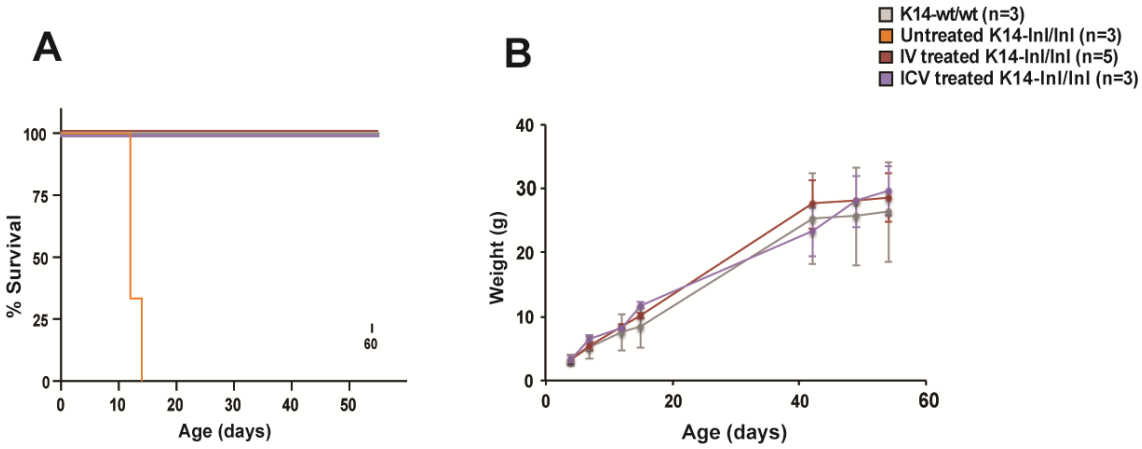

Figure 19 - Increase in life span and weight analysis of K14-lnl/lnl treated mice.

A Kaplan-Meier survival curve. IV treated K14-lnl/lnl (n=5) and ICV treated K14-lnl/lnl (n=3) survived the critical time point of 14 days after birth. All untreated knock-out mice (n=3) died before two weeks of age. Treated animals and wild-type (K14-lnl/lnl) controls were sacrificed at 55 days of age. Life span of treated animals was significantly extended following viral vector administration (Statistical analysis: log rank (Mantel-Cox) test; $p \leq 0.001$). **B** Body weight of IV and ICV treated animals and wild-type controls. No significant differences were observed between treated animals and wild-type controls (Data presented as average $\pm$ SD. Statistical analysis: two-wayANOVA, Tukey's multiple comparisons test; ns $p > 0.05$).

4.5. Assessment of neurological functions in intravenously Treated K14-lnl/lnl mice

Treated K14-lnl/lnl, untreated K14-lnl/lnl and wild-type K14-wt/wt animals were assessed for motor coordination impairment at P10. At this time point, the untreated mice started to exhibit neurological phenotype. The onset of neurological manifestations was confirmed by the results of the righting reflex test (**Figure 20A**). Untreated K14-

lnl/lnl mice were not able to return to prone position when placed on their back. In comparison IV treated K14-lnl/lnl mice showed a fast latency to right themselves, with no significant difference from wild-type controls ($p>0.9999$). Since untreated K14-lnl/lnl mice did not survive two weeks of age, conducting further behavioural analysis on this cohort of the experiment was not feasible as the animals were too young for more complex tests.

The rotarod test was conducted to assess the motor coordination of the IV treated K14-lnl/lnl mice compared to age-matched wild-type animals (**Figure 20B**). At 50 days of age IV treated mice did not show any significant difference in motor co-ordination compared to the wild-type littermates. Although locomotor function was not impaired in the injected mice, the IV treated K14-lnl/lnl animals showed a moderate hind limb clasping phenotype (**Figure 20C**). Four animals did retract both limbs for more than 50% of the test time, while only one adopted the clasping position for less than 50% of the time (average score: 1.8). Wild-type mice did not display pronounced clasping phenotype (average score: 0.3).

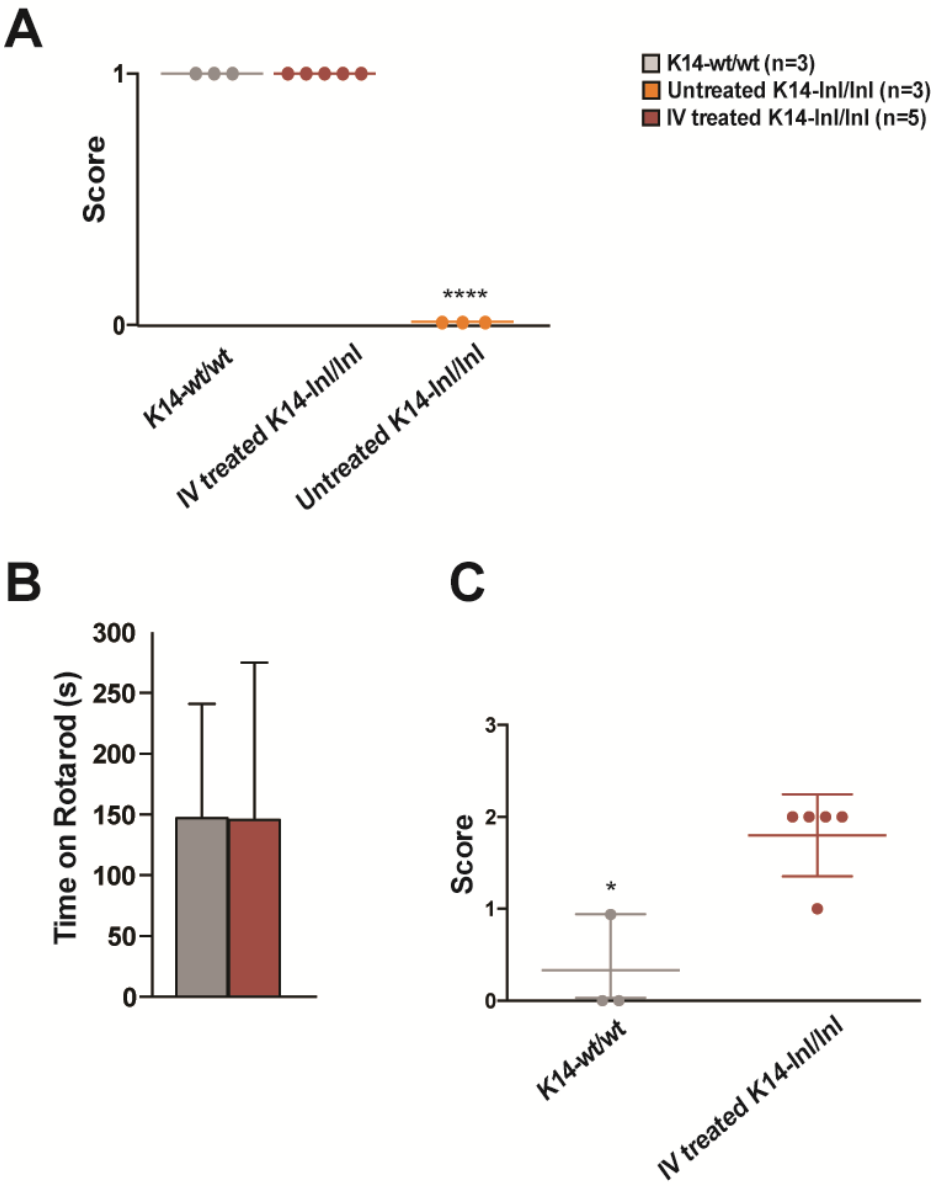

Figure 20 - Behavioural analysis of IV treated mice.

A Righting reflex test. IV treated K14-lnl/lnl mice, wild-type controls and untreated K14-lnl/lnl animals were tested for motor coordination at P10. Untreated animals failed the test, showing slow latency to right themselves (score=0), while treated K14-lnl/lnl mice exhibited the same phenotype as healthy wild-type controls (score=1) (Statistical analysis: one-wayANOVA, Holm-Sidak's multiple comparisons test; ns $p>0.9999$, **** $p<0.0001$). **B** Rotarod test at P50. The speed of the first four falls was reported. Treated mice did not show any behavioral difference compared to the controls when placed on the rotarod (Data presented as average $\pm$ SD. Statistical analysis: unpaired t-test, Welch's correction; ns $p>0.05$). **C** Tail suspension test at P50. IV treated K14-lnl/lnl animals displayed moderate clasping phenotype compared to wild-type littermates (Statistical analysis: unpaired t-test, Welch's correction; * $p<0.01$).

4.6. Analysis of neuropathology in IV treated K14-lnl/lnl mice

In order to further study the effects of intravenously administered gene therapy on the rescued K14-lnl/lnl mice, a wide range of immunoperoxidase based experiments were performed on brain sections to assess the following parameters: the expression of the human GCase protein, astrogliosis, microglial cell activation and the presence of enlarged lysosomes. A quantitative evaluation of the staining was performed in the regions of the brain known to be most affected in neuronopathic Gaucher disease. Finally, a stereological analysis determined the effects of the treatment on the neurodegeneration by counting the number of neurons within a region and any atrophy by measuring cortical thickness.

4.6.1. Widespread overexpression of β-glucocerebrosidase following intravenous administration of scAAV2/9.GUSB.*hGBA1*.bGHpA to neonatal *Gba1* knock-out mice

Immunostaining of brains from K14-wt/wt controls, age-matched IV treated K14-lnl/lnl and untreated knock-out mice at their end-stage at P14 showed that the administration of the vector resulted in a strong and widespread expression of the GCase protein (**Figure 21A**). In particular, the cortical region S1BF ($p=0.0006$), the cerebellar lobe CENT2 ($p=0.02$) and the brain stem ($p=0.014$) showed a significant increase in *GBA1* expression compared to end-stage knockouts and age-matched wild-type mice (**Figure 21B**). Although no statistical difference between the IV treated mice and the age-matched wild-types groups was measured in the hippocampus (CA1/CA2) and the thalamic region VPM/VPL, *GBA1* expression was more elevated in treated brains compared to untreated K14-lnl/lnl mice. Unexpectedly, GCase-positive cells were detected at low levels in the tissue of untreated K14-lnl/lnl mice, particularly in the thalamic region. However, high magnification light microscopy revealed that the background of the immunoperoxidase signal was elevated, as most of GCase-positive elements were blood vessels and not discrete neural cells.

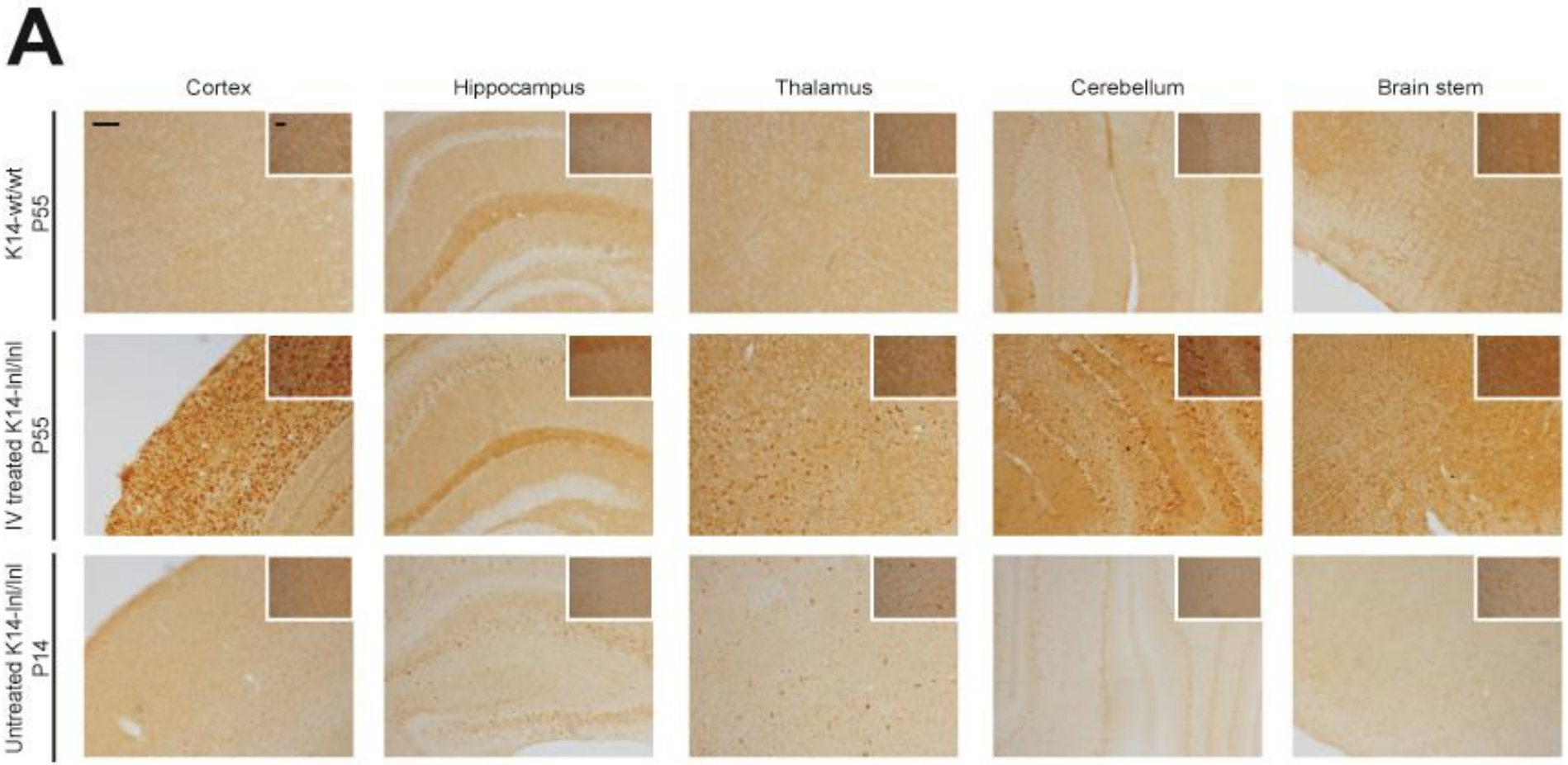
A
Cortex
Hippocampus
Thalamus
Cerebellum
Brain stem
K14-wt/wt P55
IV treated K14-Inl/Inl P55
Untreated K14-Inl/Inl P14

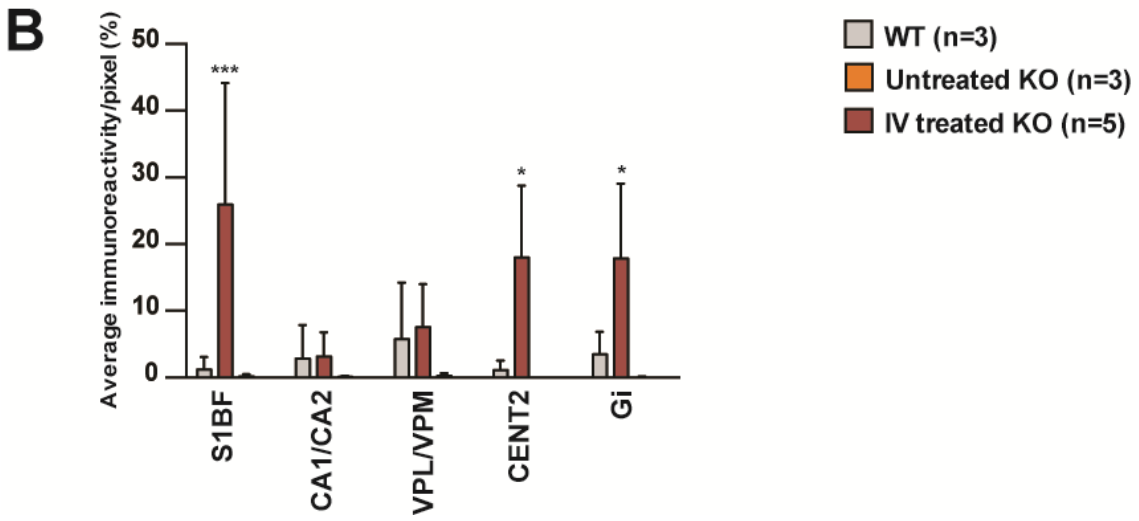

Figure 21 - β-glucocerebrosidase expression following vector administration.

A Brains from wild-type controls, IV treated knock-out mice and untreated knock-outs were stained for GCase. Intravenous administration of the scAAv2/9.GUSB.*GBA1*.bGHpA vector resulted in widespread overexpression of β-glucocerebrosidase in treated brains of knockout K14-lnl/lnl mice (Scale bars: low magnification 100μm; high magnification 60μm). **B** S1BF cortex; CA1/CA2 hippocampus; VPL/VPM thalamus, CENT2 cerebellum; Gi brain stem. Cortex, cerebellum and brain stem of IV treated K14-lnl/lnl mice showed a significant increase in GCase-positive cells compared to both the wild-type animals and the untreated controls (Data presented as average $\pm$ SD. Statistical analysis: two-way ANOVA, Tukey's multiple comparisons test; * $p \leq 0.05$, *** $p \leq 0.001$).

4.6.2. An assessment of lysosomes in the brain of IV treated K14-lnl/lnl mice

The lysosome-associated membrane glycoprotein 1 (LAMP1) was used as a marker to detect enlarged lysosome resulting from the build-up of glucosylceramide in the brain (**Figure 22A**). Tissue from the untreated end-stage K14-lnl/lnl mice showed extensive staining throughout the brain, as most of the brain regions were affected by lysosomal accumulation. The IV treated K14-lnl/lnl mice showed a heterogeneous pattern of LAMP1 staining intensities in various regions of the brain. While some areas, like cortex, thalamus and cerebellum, expressed high levels of LAMP1 marker, other

regions in the hippocampus and brain stem showed consistent reduction in the staining intensity, indicative of normal cellular lysosomal content comparable to wild-type levels. The quantification of the immunoreactivity (**Figure 22B**) confirmed a significant decrease ($p=0.0013$) in LAMP1 staining in the gigantocellular nuclei region in the brain stem of IV treated K14-lnl/lnl mice compared to untreated *Gba1* knock-out animals and was comparable to that of age-matched wild-type mice. However, in the somato-barrel field cortical region LAMP1 expression was significantly increased in IV treated K14-lnl/lnl ($p=0.02$) and the lysosomal protein levels in the treated brains were comparable to the untreated end-stage knock-out mice. Other than the cortex, there was no statistically significant difference between wild-type animals and IV treated knock-out mice.

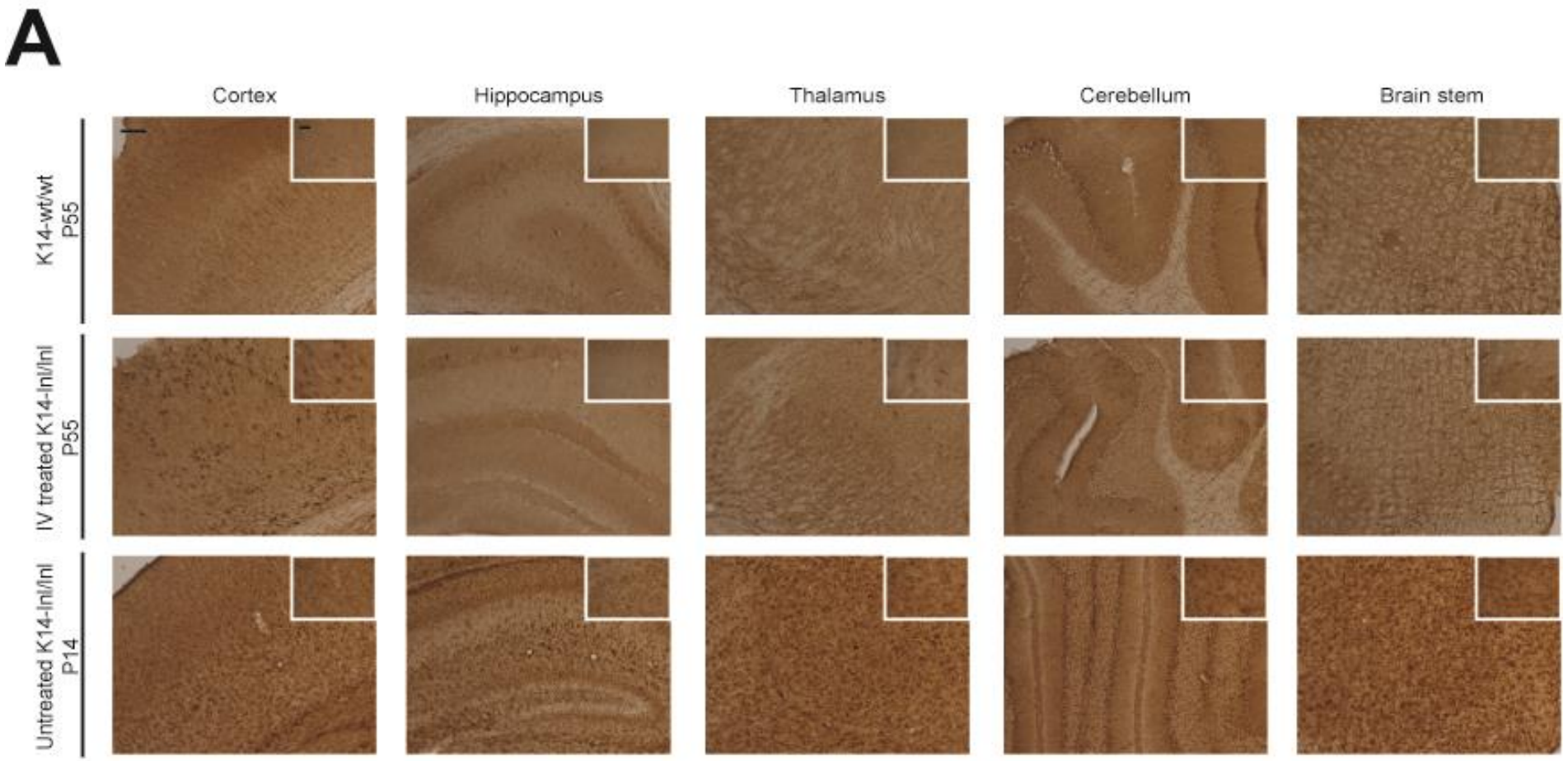
A
Cortex
Hippocampus
Thalamus
Cerebellum
Brain stem
K14-wt/wt P55
IV treated K14-Inl/Inl P55
Untreated K14-Inl/Inl P14

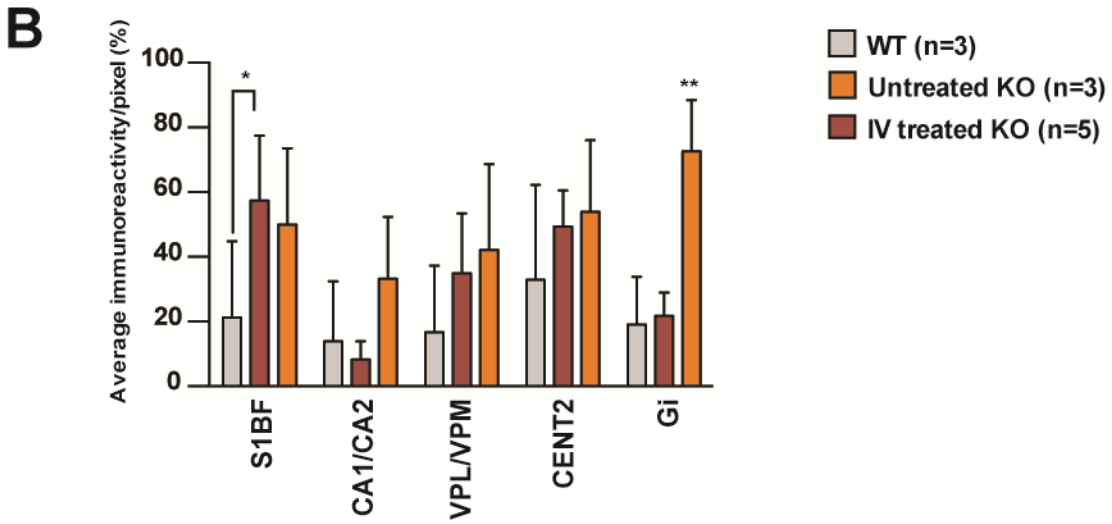

Figure 22 - Anti-LAMP1 lysosomal staining.

A Representative images of brain sections stained for the lysosomal marker LAMP1. Diffuse lysosomal staining was detected in the untreated knock-out brains. The IV treated K14-lnl/lnl samples showed elevated levels of LAMP1 in the cortical regions. However, the rest of the brain was less affected by lysosomal accumulation (Scale bars: low magnification 100µm; high magnification 60µm). **B** S1BF cortex; CA1/CA2 hippocampus; VPL/VPM thalamus, CENT2 cerebellum; Gi brain stem. Untreated end-stage knock-out mice showed a significant increase in the lysosomal marker in the brain stem (Gi) compared to age-matched wild-type controls and treated mice. In the cortical region S1BF the immunoreactivity of IV treated K14-lnl/lnl was significantly higher than the wild-type controls (Data presented as average $\pm$ SD. Statistical analysis: two-wayANOVA, Tukey's multiple comparisons test; * $p \leq 0.05$, ** $p \leq 0.01$).

4.6.3. An assessment of astrogliosis in the brain of IV treated K14-lnl/lnl mice

The glial fibrillary acidic protein GFAP was used to detect activated astrocytes as a readout of neuroinflammation. As previously reported, the K14-lnl/lnl mice developed acute astrogliosis with activated GFAP positive cells observed throughout the whole brain (Enquist et al., 2007). Brains from IV treated K14-lnl/lnl mice showed diffuse glial cell activation in the cortex, hippocampus, thalamus and cerebellum when compared to the wild-type animals (**Figure 23A**). The Gi region of the brain stem did not develop severe astrogliosis in the treated mice, although it was still possible to

identify a few diffuse positive cells. However, quantification of the staining and statistical analysis (**Figure 23B**) did not reveal significant differences in GFAP staining intensity in hippocampus, thalamus and brain stem of IV treated *Gba1* knock-out mice, untreated K14-lnl/lnl and wild-type controls. A significant increase in astrogliosis marker was present in the somato-barrel field cortex ($p=0.03$) and cerebellar lobe ($p=0.02$) of treated mice when compared to K14-wt/wt animals.

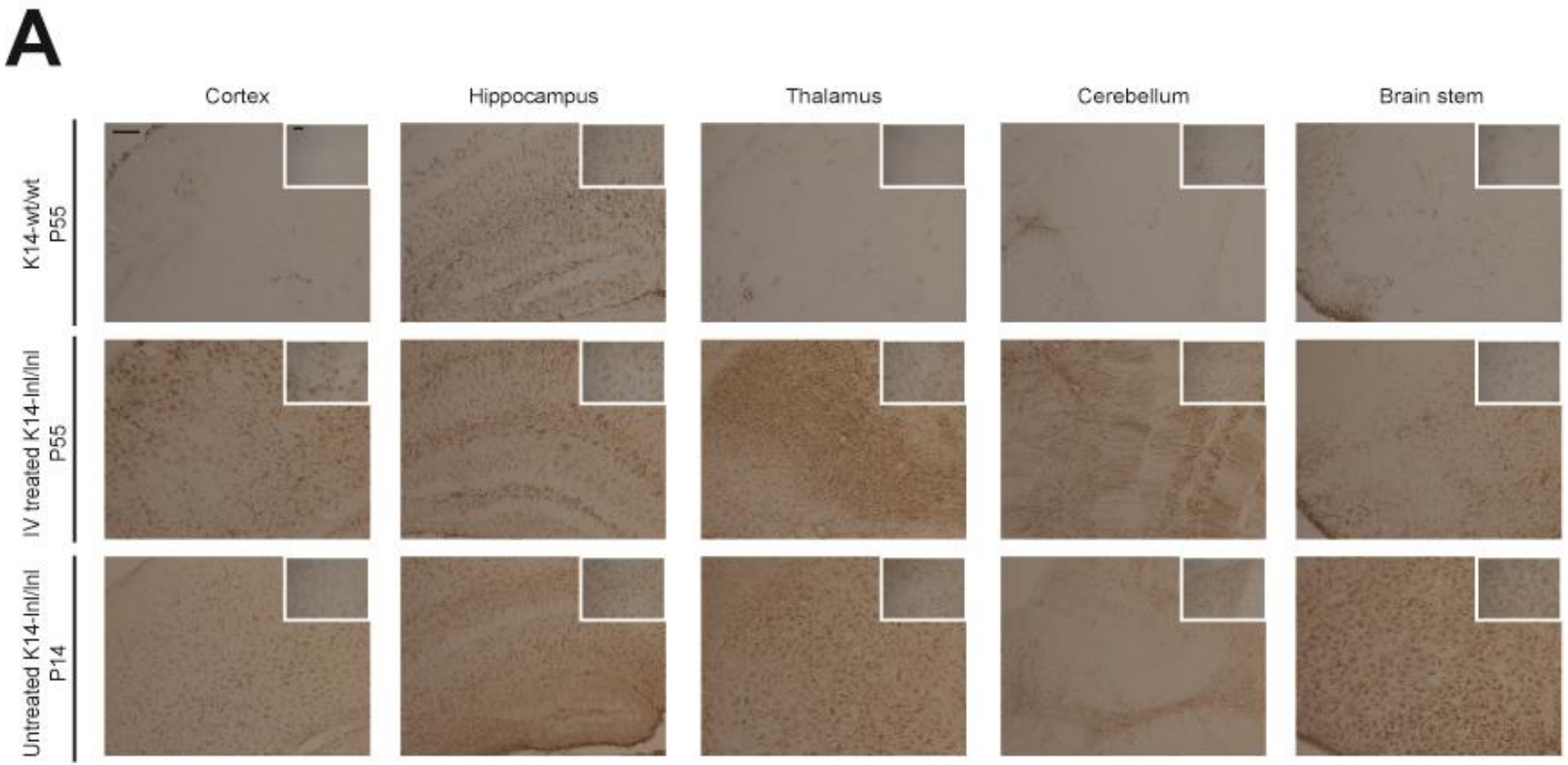
A
Cortex
Hippocampus
Thalamus
Cerebellum
Brain stem
K14-wt/wt P55
IV treated K14-Inl/Inl P55
Untreated K14-Inl/Inl P14

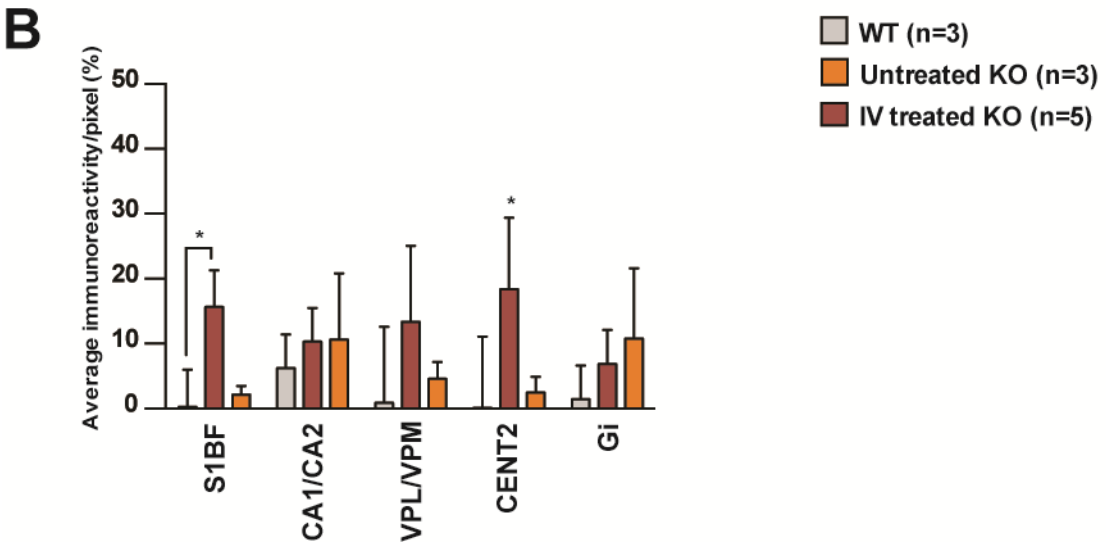

Figure 23 - Astrocyte activation in K14-ln/lnl treated mice.

A Immunoperoxidase staining for the astrocytic marker GFAP. IV treated mice developed widespread neuroinflammation compared to age-matched wild-type controls. Activated astrocytes were diffuse in the untreated brains (Scale bars: low magnification 100μm; high magnification 60μm). **B** S1BF cortex; CA1/CA2 hippocampus; VPL/VPM thalamus, CENT2 cerebellum; Gi brain stem. Quantification of the immunoreactivity. IV treated K14-lnln/lnl mice showed an increase in GFAP-positive cells in the cortex (S1BF) and cerebellum (CENT2) compared to the wild-type controls. Activated astrocytes were not detected in the brain stem (Gi) of IV treated brains (Data presented as average ± SD. Statistical analysis: two-wayANOVA, Tukey's multiple comparisons test; * $p \leq 0.05$).

4.6.4. An assessment of microglia activation in the brain of IV treated K14-lnl/lnl mice

K14-lnl/lnl mice developed extensive microglia activation. Staining for the microglial CD68 marker showed intense proliferation of microglial cells, in the cortex, hippocampus, thalamus, cerebellum and brain stem of untreated mice (**Figure 24A**). However, brain tissue from IV treated K14-lnl/lnl mice revealed a general amelioration of microglial activation, with a heterogeneous staining pattern throughout the brain. As for the neuroinflammatory marker GFAP, intense CD68 expression was present in the cortical regions of treated brains. Scattered CD68-positive cells were found in the

midbrain and cerebellum, while the brain stem showed the most dramatic amelioration in CD68 staining for microglia when compared to the end-stage untreated mice. An elevated accumulation of activated microglia was found in the CA2 layer of the hippocampus of IV treated brains. Quantification of immunoreactivity (**Figure 24B**) confirmed that there was no statistical difference between treated mice and wild-type controls in the CA1/CA2 layers of the hippocampus, the thalamic nuclei, the central lobule 2 of the cerebellum and the brain stem. However, the increase in CD68-positive cells in the somato-barrel cortical field in IV treated K14-lnl/lnl mice were significantly higher than both the physiological levels in the wild-type controls ($p<0.0001$) and in the affected K14-lnl/lnl mice ($p=0.0005$).

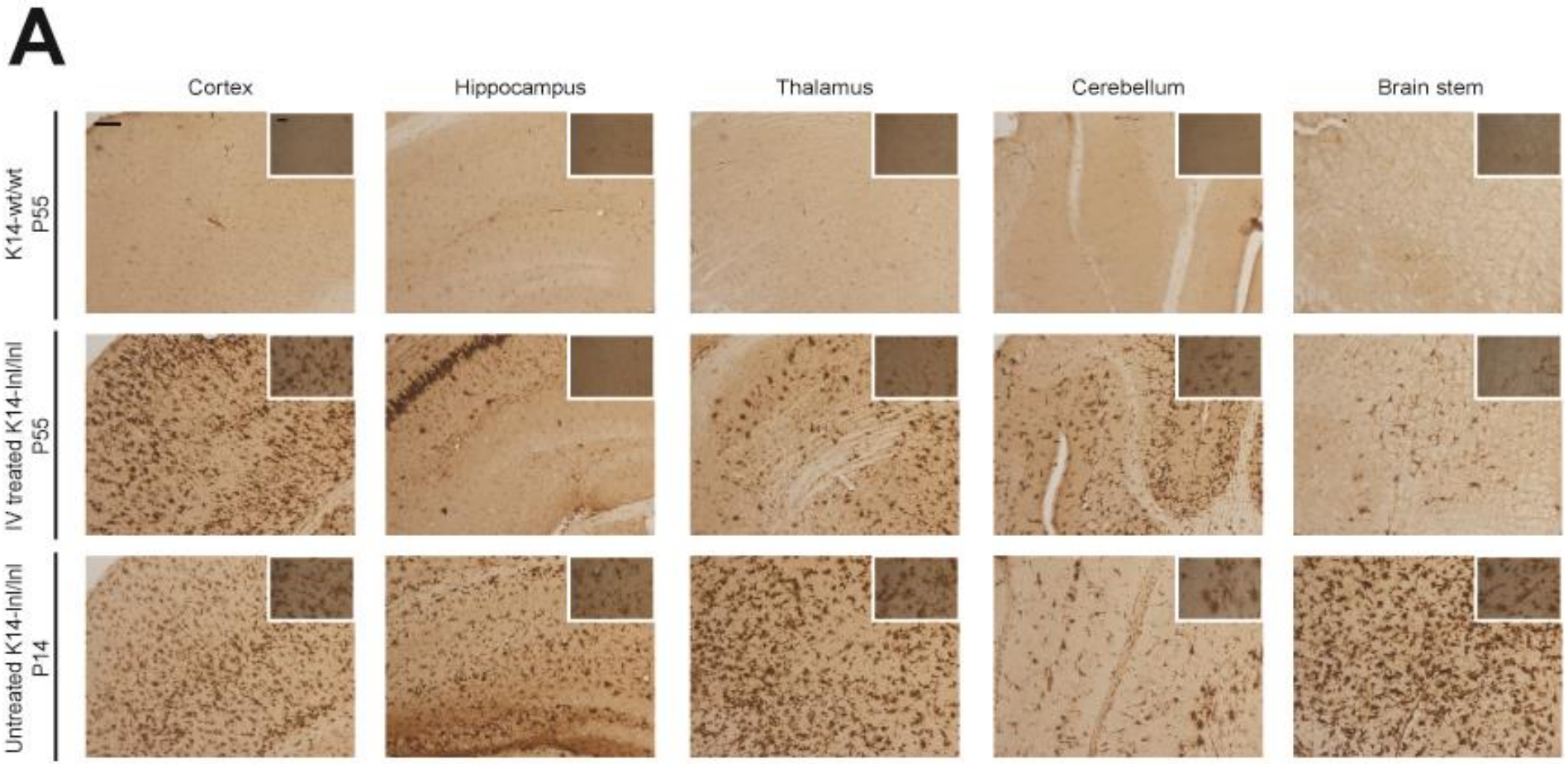
A
Cortex
Hippocampus
Thalamus
Cerebellum
Brain stem
K14-wt/wt P55
IV treated K14-Inl/Inl P55
Untreated K14-Inl/Inl P14

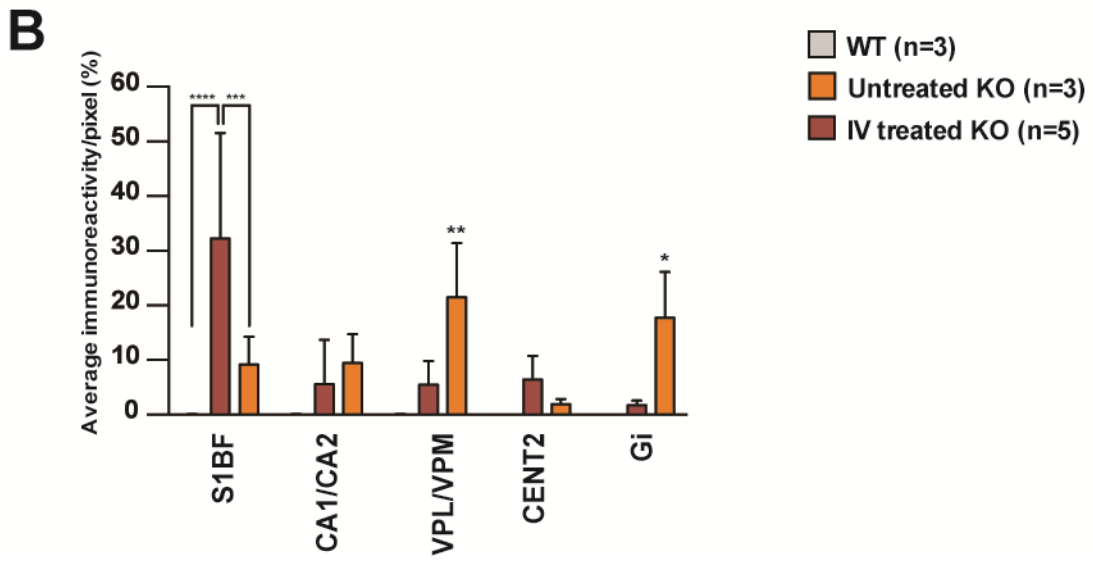

Figure 24 - Amelioration of microglia activation in IV treated mice.

A Representative brain sections stained for the microglial marker CD68. IV treated K14-lnl/lnl mice showed intense CD68 staining in the cortex, while the presence of CD68-positive cells was reduced in the hippocampus, thalamus and cerebellum compared to untreated end-stage K14-lnl/lnl mice. Very few CD68-positive cells were detected in the brain stem of treated animals (Scale bars: low magnification 100µm; high magnification 60µm). **B** S1BF cortex; CA1/CA2 hippocampus; VPL/VPM thalamus, CENT2 cerebellum; Gi brain stem. The results of the immunostaining were supported by the quantification of immunoreactivity where IV treated mice showed a significant increase in the CD68-positive cells in the cortex and thalamus compared to the controls. Extensive CD68 expression was detected in the thalamic nuclei and in the brain stem of untreated K14-lnl/lnl mice (Data presented as average $\pm$ SD. Statistical analysis: two-wayANOVA, Tukey's multiple comparisons test; * $p \leq 0.05$, ** $p \leq 0.01$, *** $p \leq 0.001$, **** $p < 0.0001$).

4.6.5. An analysis of neuronal loss and cortical thickness in IV treated K14-lnl/lnl mice

Nissl staining is a widely used method to study anatomy, tissue architecture and pathology of the brain. The cresyl violet dye binds to the RNA present in the ER and ribosomes of cells. The characteristic cytoplasm of a neuron is rich in endoplasmic reticulum and ribosomes compared to other CNS cell populations, therefore it can be

specifically stained with the Nissl method allowing the distinction between neurons and other glial cells (Scott and Willett, 1966).

The Nissl stained brain sections were analysed with the Stereo Investigator software. The stereological technique provides a quantitative and unbiased estimation of the number of neurons, thickness and volume of specific brain regions through the combination of an optical dissector and an optical fractionator (West et al., 1991). The optical dissector is a three-dimensional probe that creates a 3D model of the tissue sample from a series of two-dimensional measurements. This allows the accurate estimation of the number of neurons in the total volume of the analysed brain region. The optical fractionator relies on a systematic and random sampling scheme, so that each portion of the analysed brain region has the same probability of being sampled. The Cavalieri estimator is used to measure the dimension and volume of a specific brain region (Gundersen et al., 1999).

The stereological analysis compared brains from IV treated K14-lnl/lnl animals and wild-type controls. The brain developmental stage of the younger end-stage P14 untreated K14-lnl/lnl mice did not allow a direct age-related comparison with the older P55 animals, as different maturation time points are characterised by specific features, like brain size and number of neurons (Pressler and Auvin, 2013).

It has been reported that affected brains of the K14-lnl/lnl mice are characterised by cerebral atrophy, particularly in the somatosensory regions (Farfel-Becker et al., 2011b). Decrease in the thickness of the cortical layer in treated mice was observed (**Figure 25A**). The use of the Stereo Investigator software to determine the cortical thickness demonstrated that the atrophy in treated brains was significant ($p<0.0001$) compared to age-matched wild-type controls (**Figure 25B**). Furthermore, the lateral ventricles appeared enlarged (**Figure 25A**). Ventriculomegaly has been described in different types of lysosomal storage disorders (Wang et al., 2011) as a symptom of the progression of the neuropathology and accompanies cortical thinning.

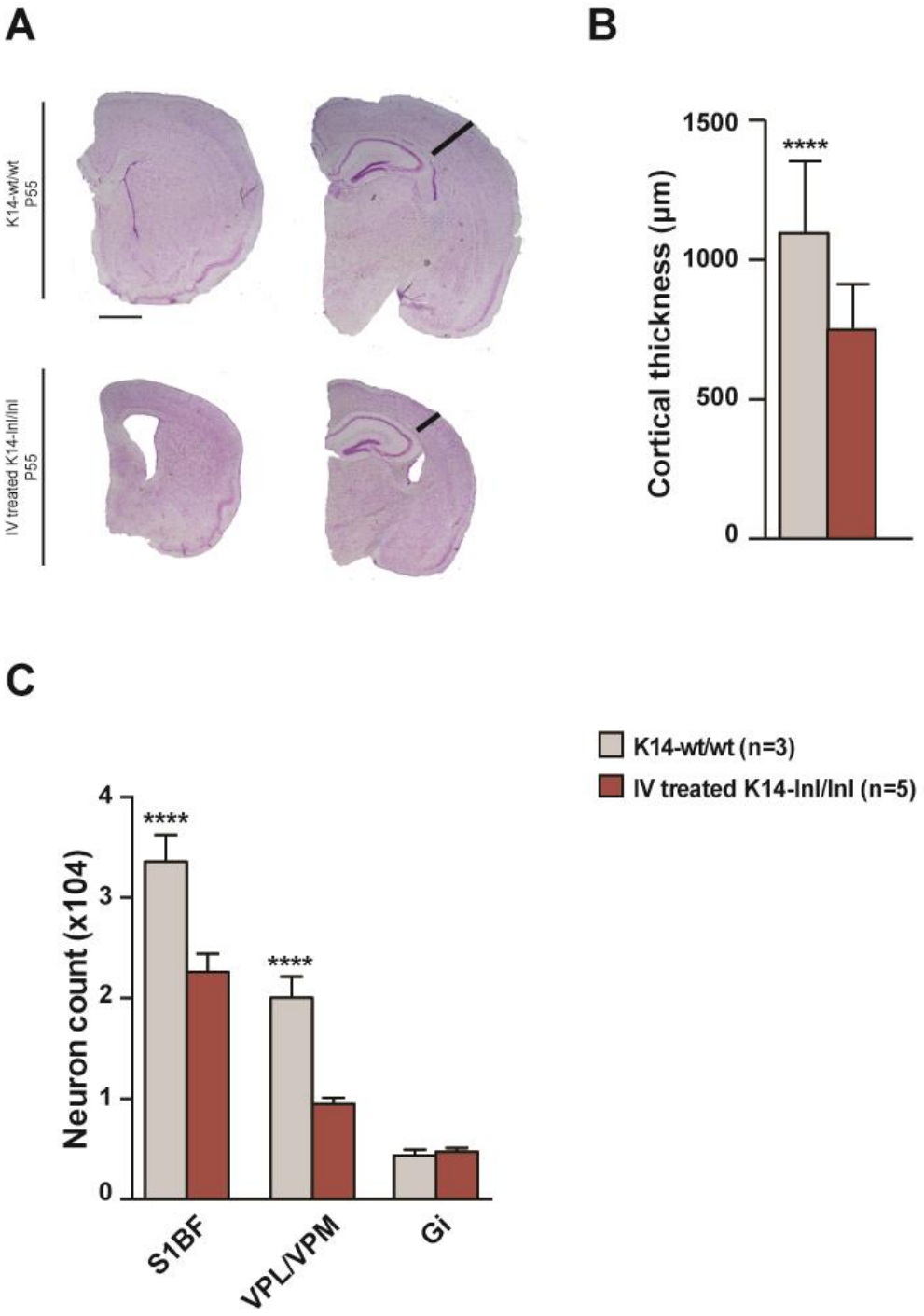

Figure 25 - Nissl staining and stereology analysis.

A Brain sections from wild-type controls and treated K14-lnl/lnl mice stained with the Nissl method. Treated brains were smaller, with enlarged ventricles and atrophic cortex (Scale bar: 1mm). **B** Cortical thickness measurements in wild-type and IV treated knock-out mice. Treated K14-lnl/lnl mice showed significant cortical atrophy (Data presented as average ± SD. Statistical analysis: unpaired t test, Welch's correction; **** $p<0.0001$). **C** Neuron counts in cortex (S1BF), thalamus (VPM/VPL) and brain stem (Gi). IV treated K14-lnl/lnl mice showed a

significant reduction in the number of neurons compared to wild-type controls. No significant neuronal loss was identified in the brain stem compared to control wild-type mice (Data presented as average ± SD. Statistical analysis: two-wayANOVA, Tukey's multiple comparisons test; **** $p<0.0001$).

Gaucher disease type II is characterised by acute and widespread neuronal loss (Farfel-Becker et al., 2014). The cortical area S1BF in treated brains was the most affected region, characterised by astrogliosis, intense microglial activation and atrophy. Stereological counts by optical fractionation revealed that the number of neurons in the cortical region of treated mice was significantly reduced ($p<0.0001$) compared to the wild-type controls (**Figure 25C**). Although the neuropathology was less accentuated in the thalamic nuclei, a significant neuronal loss was measured in the VPM/VPL region in IV treated K14-lnl/lnl brains ($p<0.0001$) compared to the wild-type controls. However, complete neuroprotection of the neuronal cells in the treated brain stem was measured with no significant difference in neuron counts compared to the wild-type control brain sections.

4.7. An amelioration of visceral pathology in treated K14-lnl/lnl mice

Although Gaucher disease type II is mainly characterised by severe neuropathology patients develop extensive visceral pathology, affecting particularly the spleen, liver and lungs (Stirnemann et al., 2017). One of the aims of this study was to demonstrate whether the intravenous administration of the scAAV2/9.GUSB.*hGBA1*.bGHpA vector resulted in not only a therapeutic effect in the brain but also a widespread systemic delivery of the therapeutic *GBA1* gene to the visceral organs. To assess the efficacy of the visceral therapy, organs harvested from P55 IV treated K14-lnl/lnl mice were compared to age-matched wild-type controls and P55 ICV treated knock-out mice. Spleen weight, presence of Gaucher cells and tissue architecture of spleen, liver and lung were analysed. The glucocerebrosidase enzymatic activity was measured in different visceral organs. Finally, a blood analysis was performed in order to evaluate the possible effects on anaemia and thrombocytopenia.

4.7.1. Normalisation of spleen weight and reduction of macrophage activation in IV treated K14-lnl/lnl mice

K14-lnl/lnl mice that received intracerebroventricular administration of the scAAv2/9.GUSB.*hGBA1*.bGHpA vector developed splenomegaly. However, the systemic injection of the vector resulted in the reduction of spleen size (**Figure 26A**). While the spleen weight of ICV treated K14-lnl/lnl mice were observably increased compared to the age-matched wild-type controls (p=0.049), there was no statistically significant difference between ICV and IV treated mice (**Figure 26B**). However, the weight of the spleen in IV treated knock-out mice was comparable to the controls.

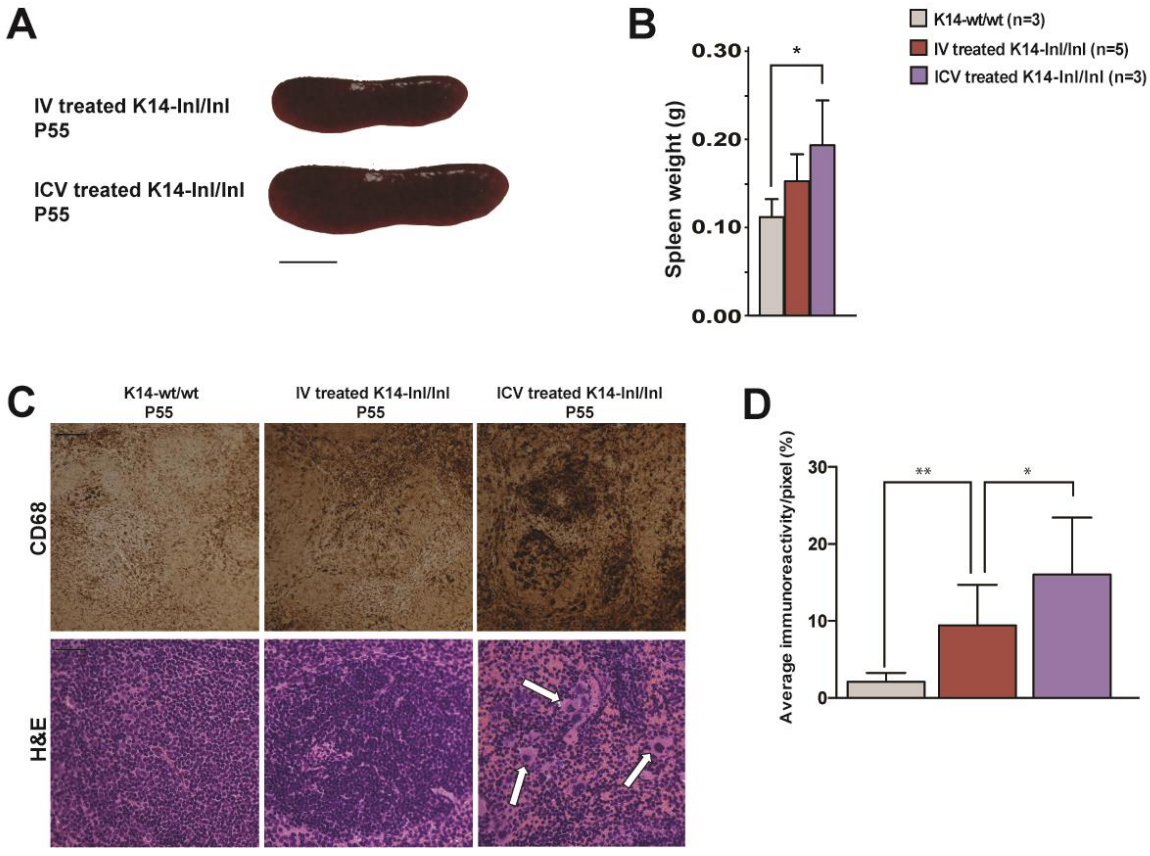

Figure 26 - Amelioration of spleen pathology following systemic administration of the scAAv2/9.GUSB.*hGBA1*.bGHpA vector.

A Spleens harvested from a IV treated K14-lnl/lnl mouse (P55) and an age-matched ICV treated animal (Scale bar: 0.5cm). **B** ICV treated knock-out mice developed splenomegaly, while IV treated animals did not show significant enlargement of the spleen, compared to the age-

matched controls (Data presented as average ± SD. Statistical analysis: one-wayANOVA, Tukey's multiple comparions test; * $p<0.05$). **C** Images of spleen from wild-type, IV treated and ICV treated animals. Top panel: Immunoperoxidase using antibodies against CD68 showed increased macrophage activation in sections of spleen taken from ICV treated mice. Bottom panel: Hematoxylin and Eosin staining revealed the presence of Gaucher cells (indicated by white arrows) in spleen from ICV treated K14-lnl/lnl, while the intravenous administration resulted in correction of the pathology (Scale bar: 200μm). **D** Quantification of immunostaining against the CD68 macrophagic marker (Data presented as average ± SD. Statistical analysis: one-wayANOVA, Tukey's multiple comparisons test; * $p\leq0.05$, ** $p\leq0.01$).

The immunostaining for CD68 on spleen sections to detect the accumulation of engorged macrophages showed that the pathology in the IV treated K14-lnl/lnl mice was reduced compared to the age-matched ICV treated animals, particularly in the white pulp regions (**Figure 26C, top panel**).

The sections from the same organs were stained with Haematoxylin and Eosin (H&E) and the histological analysis was carried out (**Figure 26C, bottom panel**). H&E staining is widely used in histopathology, in order to assess cellular morphology and tissue architecture (Fischer et al., 2008). This staining technique labels the nucleic acids in the nucleus with a blue colour and the cytoplasmic proteins with a pink dye. The analysis of spleen section stained with H&E confirmed the previous findings: the tissue structure of the white pulp in the ICV treated mice was disrupted. The stain highlighted the presence of numerous enlarged Gaucher cells (indicated by white arrows), interfering with the physiological cell distribution. In the spleen from age-matched IV treated K14-lnl/lnl mice, the tissue architecture was better maintained similarly to the wild-type controls, and very few or no enlarged cells were detected.

These results were corroborated by the quantification of the anti-CD68 immunohistochemistry experiment. The analysis revealed that the activation of macrophages was substantial in the spleen of ICV treated K14-lnl/lnl mice compared to both the IV treated knock-out animals higher ($p=0.015$) and the K14-wt/wt controls ($p<0.0001$) (**Figure 26D**). However, an increase ($p=0.005$) in the levels of activated macrophages in spleens harvested from IV treated knock-out mice and wild-type

controls was also reported.

4.7.2. Systemic administration of scAAV2/9.GUSB.*hGBA1*.bGHpA ameliorates pathology in the liver of treated *Gba1* knock-out mice

The analysis of the CD68 marker for macrophage activation in liver sections revealed that the IV treated K14-lnl/lnl mice did not develop pathology and the macrophage levels were comparable to the age-matched wild-type controls (**Figure 27A**). The activation of macrophages was more extensive in the livers of age-matched ICV treated animals, where numerous enlarged CD68-positive cells were identified by immunoperoxidase staining. In addition, the H&E stain demonstrated that the integrity of the tissue was profoundly disrupted in the ICV treated mice. However, the liver tissue from IV treated K14-lnl/lnl mice was observably improved in integrity of the architecture and only a few scattered Gaucher cells were detected.

Quantification of the staining of the macrophagic marker CD68 (**Figure 27B**) confirmed that the K14-lnl/lnl mice that received ICV injections of the virus had significantly higher levels of CD68-positive cells compared to the age-matched IV treated knock-out mice ($p=0.0007$) and the wild-type control livers ($p=0.003$). Systemic administration of the vector resulted in drastic reduction of activated macrophages to physiological levels.

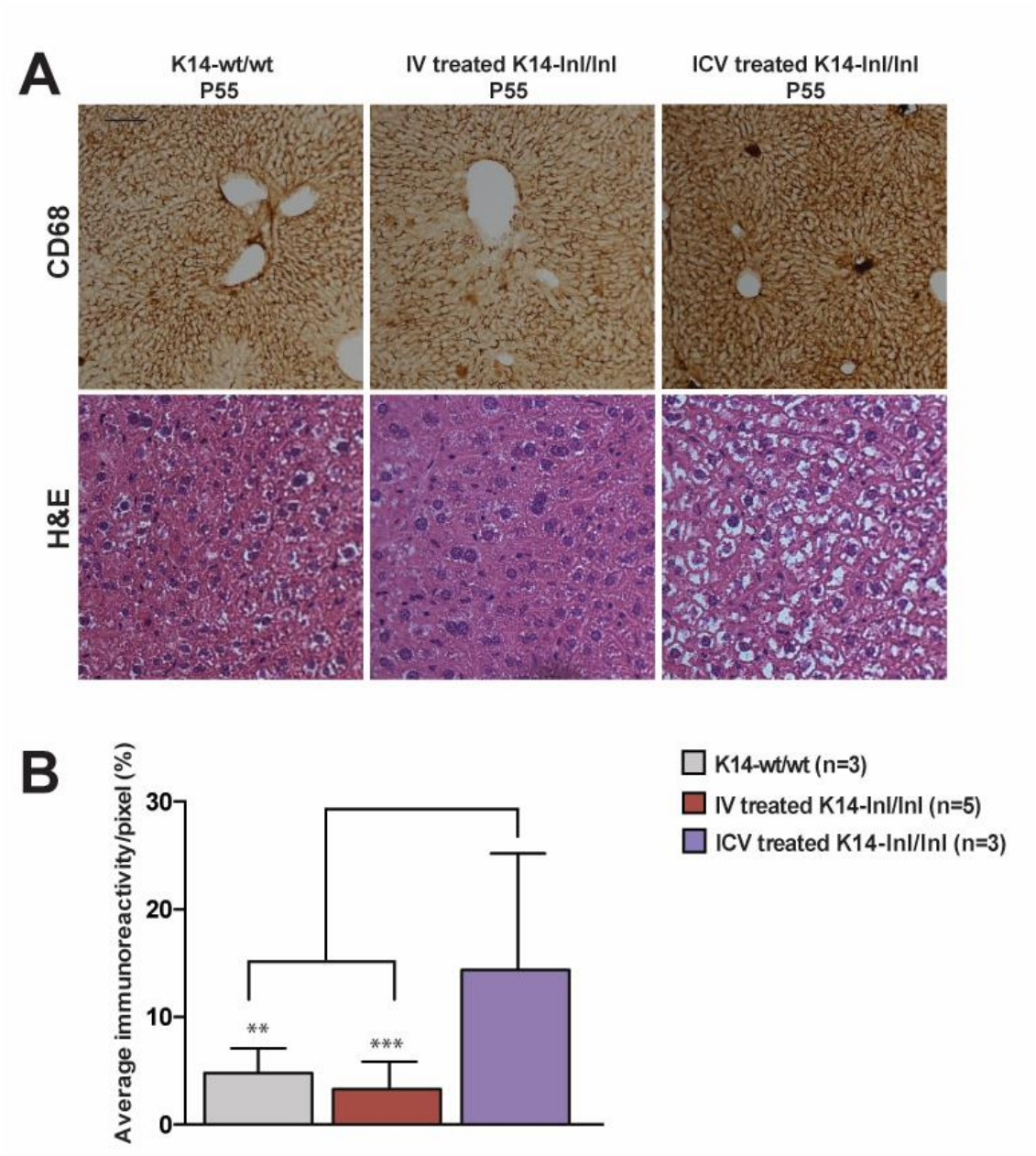

Figure 27 - Correction of the liver pathology in IV treated K14-lnl/lnl mice.

A Immunostaining to the macrophagic marker CD68. IV treated *Gba1* knock-out mice did not develop liver pathology, while ICV treated K14-lnl/lnl mice showed high macrophagic activation and disruption of the tissue architecture (Scale bar: 200μm). **B** The quantification of the immunoreactivity confirmed the profound macrophage activation in tissue from ICV treated animals. No statistically significant difference was found between wild-type controls and IV treated K14-lnl/lnl mice (Data presented as average $\pm$ SD. Statistical analysis: one-wayANOVA, Tukey's multiple comparisons test; ** $p \leq 0.01$, *** $p \leq 0.001$).

4.7.3. Amelioration of lung pathology resulting from intravenous administration of scAAV2/9.GUSB.*hGBA1*.bGHp

The analysis of macrophage activation and infiltration in lung tissue samples revealed a significant increase in CD68-positive cells in ICV treated K14-lnl/lnl mice (**Figure 28A**). Although the extent of activated macrophages in *Gba1* knock-out mice that received systemic injection of the viral vector was clearly reduced to normal physiological level, few scattered CD68-positive enlarged cells could be detected.

H&E histological analysis revealed that the architecture of the tissue from ICV treated mice was extremely compromised: the alveoli's structure was disrupted and numerous engorged macrophages could be observed. The lung tissue from IV treated K14-lnl/lnl mice showed a regular tissue organisation, with open air sacs structures and the presence of only a few Gaucher cells. Overall, the sections from intravenously treated mice highly resembled the wild-type tissue.

The thresholding of the immunoreactivity (**Figure 28B**) confirmed that the intracerebroventricular administration of the vector did not have a therapeutic effect on the lung pathology, as the ICV treated mice showed increased macrophage infiltration compared to both wild-type controls ($p=0.0005$) and IV treated K14-lnl/lnl mice ($p<0.0001$). In comparison the systemic administration of the scAAV2/9.GUSB.*hGBA1*.bGHp vector significantly reduced the accumulation of CD68-positive cells.

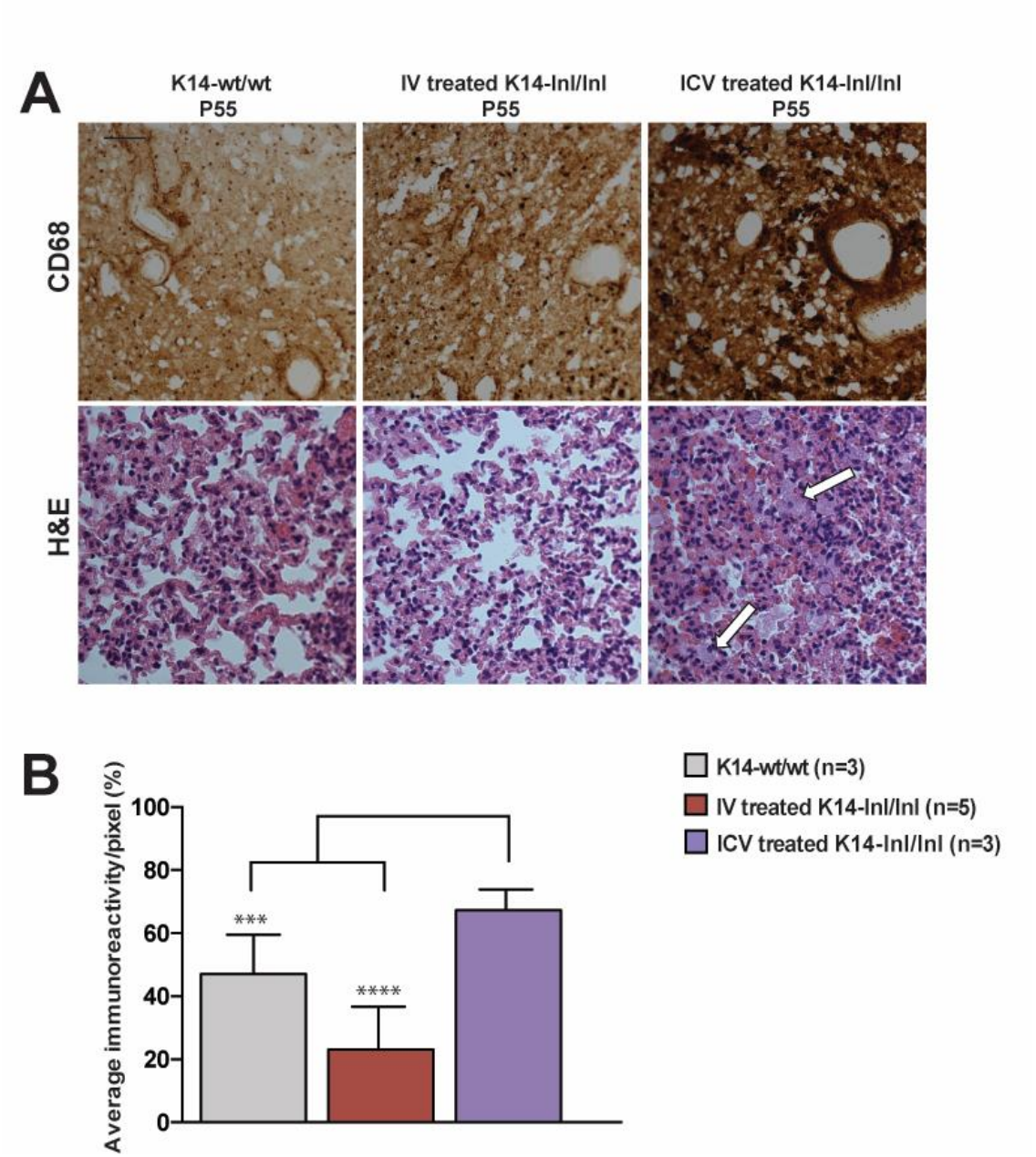

Figure 28 - Histological analysis of lung tissue from IV treated K14-lnl/lnl mice.

A Accumulation of activated macrophages was present in the tissues from ICV treated *Gba1* knock-out mice, while only few CD68-positive cells were detected in the lung tissue from IV treated K14-lnl/lnl mice. In the tissue from ICV treated mice it was possible to identify numerous Gaucher cells (indicated with white arrows). The tissue samples from IV treated knock-out mice samples appeared healthy, and only a limited number of Gaucher cells was detected (Scale bar: 200μm). **B** The quantification of the immunoreactivity confirmed that IV treated mice had a significant decrease in macrophage activation and infiltration in the lungs (Data presented as average $\pm$ SD. Statistical analysis: one-wayANOVA, Tukey's multiple comparisons test; *** $p \leq 0.001$, **** $p < 0.0001$).

4.7.4. Blood parameters in *Gba1* knock-out mice treated following systemic injection of scAAV2/9.GUSB.*hGBA1*.bGHp

Anaemia, thrombocytopenia and leukopenia are characteristic of Gaucher disease (Nagral, 2014). This condition is mirrored in some of the murine models (Farfel-Becker et al., 2011a, Mistry et al., 2010), although in the literature there is no evidence of blood abnormalities in the K14-lnl/lnl model. The untreated knock-out mice die within the first two weeks of life, therefore might not be sufficiently old to develop severe anaemia. In order to establish whether adult 55 day-old treated animals developed blood pathology, samples from IV treated knock-out and age-matched wild-type mice were analysed (**Figure 29**). The results demonstrated that the number of erythrocytes, haemoglobin levels, platelet count and number of white blood cells in samples from IV treated K14-lnln/lnl were comparable to the wild-type physiological range.

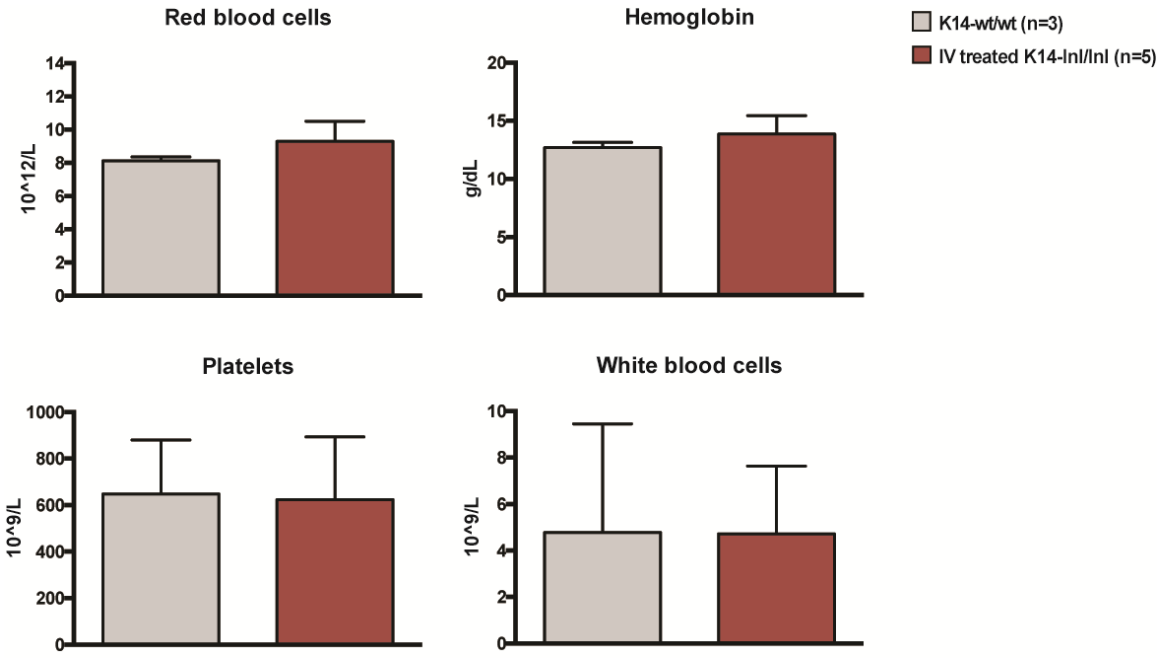

Figure 29 - Blood analysis.

Blood samples from IV treated K14-lnl/lnl mice and age-matched wild-type controls were analysed. Red blood cells count, hemoglobin, platelets and leukocytes concentration were measured (Data presented as average ± SD. Statistical analysis: unpaired t test, Welch's correction; ns $p \geq 0.05$).

4.7.5. Intravenous administration of scAAV2/9.GUSB.*hGBA1*.bGHp resulted in the increase of the β-glucocerebrosidase activity in some organs

Although the *Gba1* gene is knocked-out in the K14-lnl/lnl mouse model, low levels of mRNA are still produced (Enquist et al., 2007). This results in minimal β-glucocerebrosidase activity in liver (ca. 10%) and spleen (ca. 2%). However, the residual enzymatic activity is not sufficient to clear the elevated glucosylceramide that accumulates in the organs.

The analysis of enzymatic activity investigated whether the intravenous administration of the viral vector carrying the functional *hGBA1* gene resulted in the production of active β-glucocerebrosidase enzyme in the visceral organs and if the physiological enzyme levels could be restored in treated mice. The enzymatic activity in tissues from IV treated K14-lnl/lnl mice was compared with samples from wild-type animals, ICV treated *Gba1* knock-out mice, and untreated K14-lnl/lnl mice (**Figure 30**).

The β-glucocerebrosidase activity in the spleen of both IV and ICV treated mice was decreased (ca. 42%) compared to the normal physiological level; however, the difference was not statistically significant. The enzyme levels in the liver tissue harvested from untreated K14-lnl/lnl were significantly reduced ($p=0.018$) compared to wild-type levels, confirming the results from Enquist's study. Physiological enzyme levels in the spleen were very low and although the intravenous administration almost doubled (ca. 196%) the β-glucocerebrosidase activity compared to untreated mice, the overall difference was not significant.

The response to the treatment in the lungs was encouraging: the intravenous administration of the vector resulted in the increase of the enzymatic activity compared to both untreated K14-lnl/lnl and ICV injected mice. In tissues from IV treated knock-out mice the β-glucocerebrosidase residual activity raised to ca. 54% of the

physiological levels. However, there was no statistically significant difference between the two routes of administration.

The systemic injection of the scAAV2/9.GUSB.*hGBA1*.bGHp caused a drastic increase (ca. 728%) of the enzymatic activity in the heart compared to wild-type levels ($p<0.0001$). The β-glucocerebrosidase residual activity in cardiac tissue from ICV treated mice was comparable to the normal physiological levels (ca. 67%).

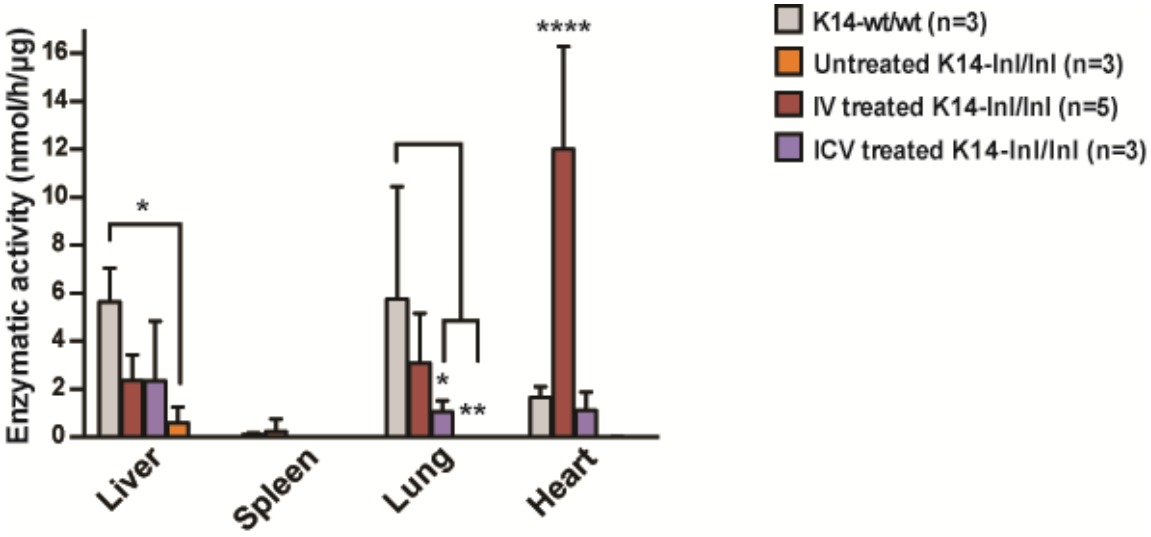

Figure 30 - Enzymatic activity in different visceral organs.

The systemic injection of the scAAV2/9.GUSB.*hGBA1*.bGHp resulted in a general increase in the β-glucocerebrosidase residual activity in liver, spleen, lung and heart tissues. The enzymatic activity in organs from the intravenous administered mice was compared to the β-glucocerebrosidase activity in organs from wild-type controls, ICV treated knock-out animals and untreated K14-lnl/lnl mice (Data presented as average $\pm$ SD. Statistical analysis: two-wayANOVA, Tukey's multiple comparisons test; * $p\leq0.05$, ** $p\leq0.01$, **** $p<0.0001$).

4.8. Long-term study

The intravenous administration of the scAAV2/9.GUSB.*hGBA1*.bGHp vector resulted in the extension of the lifespan, partial amelioration of the neuropathology and improvement in the visceral pathology K14-lnl/lnl mice at 55 days of age. The effects of gene therapy on lifespan over a longer period of time were investigated.

Following neonatal injection of the viral vector, all treated mice (IV treated K14-lnl/lnl n=5; ICV treated K14-lnl/lnl n=9) were rescued from neonatal neurodegeneration-associated death and survived up to at least 180 days of age (**Figure 31A**). At this point the animals were sacrificed.

The therapeutic effect of the systemic treatment on the long-term survival mice was assessed. Since the most evident symptom of Gaucher disease in the viscera is the enlargement of the spleen, their weight was measured (**Figure 31B**). Encouragingly, there was no significant difference between the intravenously treated knock-out and the wild-type control samples. Whereas, the spleen size of the ICV treated K14-lnl/lnl animals was significantly higher ($p=0.009$) than the wild-type controls. Although the spleen size of the IV treated animals was reduced compared to the age-matched ICV treated mice, the difference was not statistically significant.

The aforementioned results were supported by the analysis of immunostaining of spleen sections with the macrophagic marker CD68 (**Figure 31C**). In the samples obtained from ICV treated mice it was possible to detect intense macrophage activation, characterised by clusters of enlarged affected macrophages within the white pulp. However, the number of CD68-positive cells in the spleen form IV treated K14-lnl/lnl mice was significantly reduced, almost comparable to the wild-type controls.

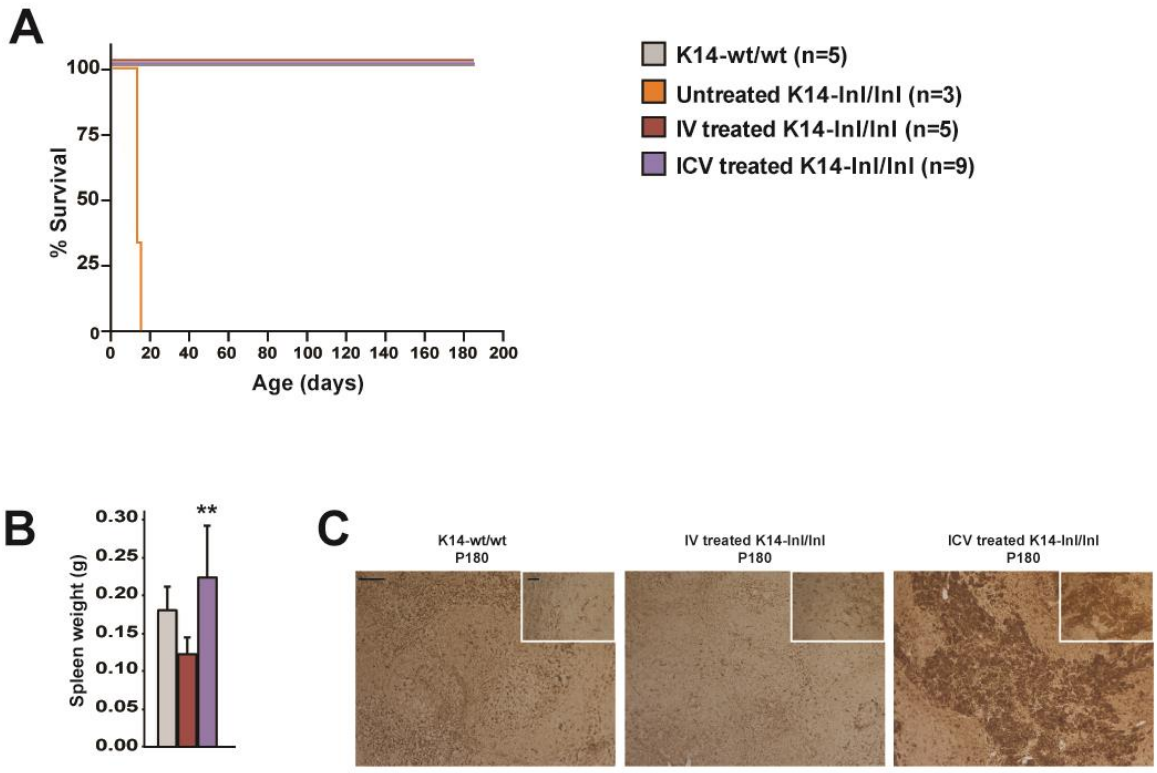

Figure 31 - Effects of the intravenous administration of gene therapy in K14-lnl/lnl in a long-term study.

A *Gba1* knock-out mice usually die at 14 days of age, whereas K14-lnl/lnl mice treated with systemic gene therapy at day of birth lived for at least six months. Wild-type and ICV treated mice were used as controls (Statistical analysis: log rank (Mantel-Cox) test; $p \leq 0.001$). **B** Average spleen weight. Statistical analysis revealed that the size of the spleen from ICV treated mice was significantly higher than wild-type controls. The spleen weight was reduced in K14-lnl/lnl mice that received intravenous injection of the vector (Data presented as average $\pm$ SD. Statistical analysis: one-wayANOVA, Tukey's multiple comparisons test; ** $p \leq 0.01$). **C** Anti-CD68 staining on spleen sections. Aged ICV treated mice showed numerous enlarged Gaucher cells in the white pulp of the spleen. Spleens derived from IV treated knock-out mice did not develop macrophage activation (Scale bars: low magnification 100µm; high magnification 60µm).

4.9. Conclusions

This study demonstrated that a single intravenous injection of the scAAV2/9.GUSB.*hGBA1*.bGHpA vector resulted in a significant extension of the lifespan of *Gba1* knock-out animals. For the duration of their life, the animals were monitored for pathological manifestations, however they did not develop significant neurological symptoms. Moreover, the body weight was maintained within the normal range. The mice were sacrificed at 55 days of age and an extensive neuropathological analysis was conducted. In general, the effect of the gene therapy on neuropathology was heterogeneous and varied from region to region. While the administration of the vector caused widespread overexpression of the β-glucocerebrosidase protein, some brain regions continued to present neuropathology. Extensive astrogliosis and microglial activation was detected in the cortical region S1BF. Whereas other areas, such as the brain stem, resulted in the prevention of activated astrocytes and microglia cells. Intense lysosome accumulation was found in the same cortical regions characterised by severe neuroinflammation. The somato-barrel field region was subjected to atrophy and neuronal loss. On the contrary, the Gi region in the brain stem was not affected by neuronal death, with neuron numbers comparable to healthy controls.

Although the intravenous administration of the vector only partially ameliorated the neuropathology, treated mice were rescued up to at least 6 months of age with no observable neurological symptoms.

In terms of the effect of gene therapy on the visceral organs, treated mice exhibited amelioration in macrophage activation in the liver, spleen and lungs, where only a limited number of Gaucher cells were identified. Moreover, the tissue architecture was preserved, as it highly resembled the cellular organisation of wild-type age-matched mouse samples. The positive effects of the treatment were confirmed by the analysis of the β-glucocerebrosidase activity in different organ samples. Overall, tissues derived from IV treated K14-lnl/lnl showed increased residual enzymatic activity compared to untreated knock-out mice. Even though the wild-type levels were not achieved in all considered tissues, the residual β-glucocerebrosidase activity was sufficient to

considerably ameliorate the visceral pathology in treated mice. This phenomenon has been already observed in the study on gene therapy for haemophilia, where a modest increase in the enzymatic levels led to a therapeutic effect (Nathwani et al., 2014). The blood analysis revealed that IV treated K14-lnl/lnl mice did not develop hematologic conditions typical of Gaucher disease.

While gene therapy targeted to the brain via ICV administration did provide long-term rescue of the treated K14-lnl/lnl mice, they did develop the systemic visceral manifestations of Gaucher disease. The last part of the present study confirmed that the intravenous administration of the viral vector to neonatal *Gba1* knock-out mice also allowed to extend the lifespan of treated animals up to six months. In addition, the animals did not develop splenomegaly. The histological analysis of the tissue confirmed that macrophage activation was not present in the samples derived from IV treated mice.

Together these results provided evidence that the intravenous administration of scAAV2/9.GUSB.*hGBA1*.bGHpA at the day of birth led to amelioration of the neurodegeneration and visceral pathology in *Gba1* knock-out mice. The lifespan of treated animals was extended from 14 days to at least 180 days.

5. AAV9-mediated expression targeted to neurons enhances therapeutic efficacy in the brain of a neuronopathic Gaucher disease mouse model

5.1. Introduction

The administration of scAAV2/9.GUSB.*hGBA1*.bGHpA resulted in significant long-term extension of the lifespan of K14-lnl/lnl knock-out mice. However, the neuropathology of treated animals was only partially ameliorated. This was thought to be caused by the low efficiency of the vector, particularly due to the expression driven by a relatively weak promoter. In the following chapter, the creation and testing of a new and improved vector is described. In comparison to the initial vector, the genome conformation of the second viral vector was single-stranded. This allowed the manipulation of the expression cassette and the insertion of transcription and transduction enhancing elements. Moreover, a strong neuron-specific promoter was used in order to improve transgene expression in the central nervous system following systemic administration.

The first part of this chapter describes the design and production of the new viral vector carrying the *eGFP* reporter gene, and the subsequent study of vector specificity and distribution following intravenous administration of the vector to neonatal wild-type mice. Subsequently, a vector carrying the therapeutic *GBA1* gene was designed and produced, and a safety analysis was conducted on wild-type mice injected with the vector at day of birth. Finally, this *GBA1* vector was systemically administered to

neonatal *Gba1* knock-out mice and the extension in lifespan was evaluated together with behavioural studies. The animals were also assessed for pathological manifestations. Once the mice were sacrificed, neuropathological analysis was conducted, where β-glucocerebrosidase overexpression, neuroinflammation, microglia activation and lysosome accumulation in the central nervous system was evaluated. A stereological study was also performed, investigating neuronal loss and brain atrophy. Finally the effect of gene therapy on the visceral pathology of treated mice was assessed. This included the evaluation of splenomegaly, the presence of activated macrophages and Gaucher cells, and β-glucocerebrosidase enzymatic activity measurement within the liver, spleen, lung and heart of treated mice.

5.2. Reporter gene study

5.2.1. ssAAV2/9.hSynI.*eGFP*.WPRE.hGHpA vector

The AAV9 plasmid vector carrying the *eGFP* gene (**Figure 32**) was previously engineered in Dr. Rahim's laboratory. Previous results showed that, although the intravenous administration of scAAV2/9.GUSB.*hGBA1*.bGHpA resulted in considerable extension of treated mice, the vector only partially ameliorated the neuropathology of the *Gba1* knock-out mice. Therefore a series of steps were taken in order to enhance transgene expression, particularly within the central nervous system. The human synapsin promoter hSynI (Schoch et al., 1996) was cloned into the expression cassette, upstream of the *eGFP* reporter gene. In previous studies, it has been shown that synapsin I is a strong promoter that leads to neuron-specific *eGFP* transduction in the central nervous system of mice injected in the brain with an AAV9 vector (McLean et al., 2014) and also following systemic administration (Jackson et al., 2016). The new vector had a single-stranded conformation: the extra space in the expression cassette allowed for the insertion of additional expression enhancing sequences. The translation enhancing Kozak consensus sequence (Kozak, 2005) was added at the 5' of the *eGFP* gene, while the WPRE element (Loeb et al., 1999) was cloned downstream the reporter gene. The polyA sequence was derived from the human growth hormone polyadenylation signal. Furthermore, previous studies have shown that

a single-stranded AAV9 vector that includes a WPRE sequence has an enhanced expression profile in various organs when compared to a self-complementary vector configuration that lacks a WPRE enhancing sequence (Mattar et al., 2015).

Figure 32 - ssAAV2/9.hSynI.*eGFP*.WPRE.hGHpA vector.

In the single-stranded AAV2/9 vector, *eGFP* expression was driven by the human synapsin I promoter. The Kozak sequence was added at the 5' of the transgene and the enhancer viral element WPRE was cloned immediately downstream.

The vector was produced following the triple transfection of HEK-293T cells and purification was completed by iodixanol gradient ultracentrifugation. The final viral titer was measured via both SDS-PAGE and alkaline gel electrophoresis, and subsequent densitometric analysis. The quantification of viral capsid protein VP3 (**Figure 33A**) against bovine serum albumin standards of known concentrations resulted in a titer of 8.04 x 10^{12} viral particles per ml. From the analysis of genome content (**Figure 33B**), the resulting titre of the virus was 2.47 x 10^{12} viral genome copies per ml. Since the result obtained by the analysis of the alkaline gel was slightly lower than the quantification of the viral particles, an average value of 5.2 x 10^{12} vp/ml was assumed as the final titer of the ssAAV2/9.hSynI.*eGFP*.WPRE.hGHpA vector.

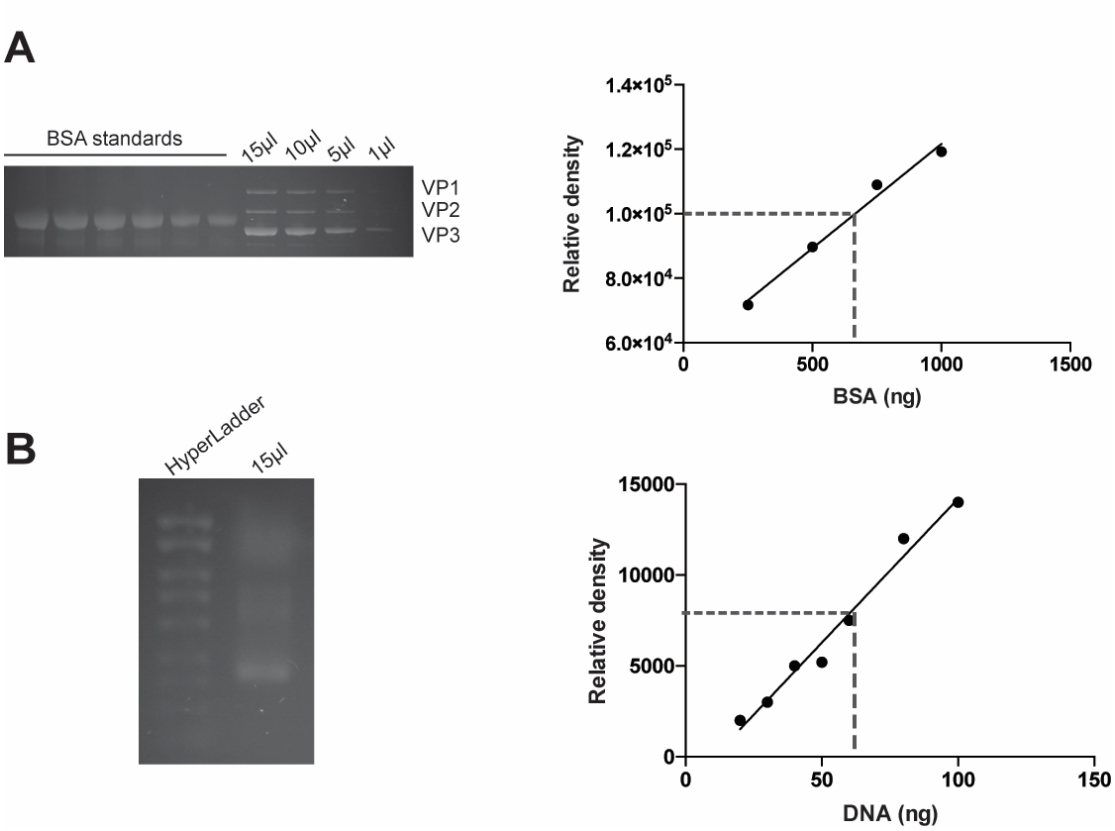

Figure 33 - Titration of ssAAV2/9.hSynI.*eGFP*.WPRE.hGHpA.

A Capsid protein analysis by SDS-PAGE. Different dilution of the virus (15µl, 10µl, 5µl, 1µl) and BSA standard (250ng, 500ng, 750ng, 1000ng) were loaded in a polyacrylamide gel. Assuming that each viral particle contains 4.987 x 10^9 ng of VP3, the resulting titer of the virus was 8.04 x 10^{12} vp/ml. **B** Genome content analysis by alkaline gel electrophoresis. The DNA concentration of 15µl of the virus was measured against the HyperLadder. Assuming that the mass of one copy of vector is 2.916 x 10^9 ng, the resulting titer was determined to be 2.47 x 10^{12} vg/ml.

5.2.2. eGFP neuronal expression profile following intravenous administration of the ssAAV2/9.hSynI.*eGFP*.WPRE.hGHpA vector to neonatal mice

Three wild-type CD1 mice were intravenously injected into the temporal vein on the day of birth with 40µl of the ssAAV2/9.hSynI.*eGFP*.WPRE.hGHpA vector, resulting in a total dose of 2 x 10^{11} vp. The animals were sacrificed at one month of age and eGFP

expression analysis was carried out.

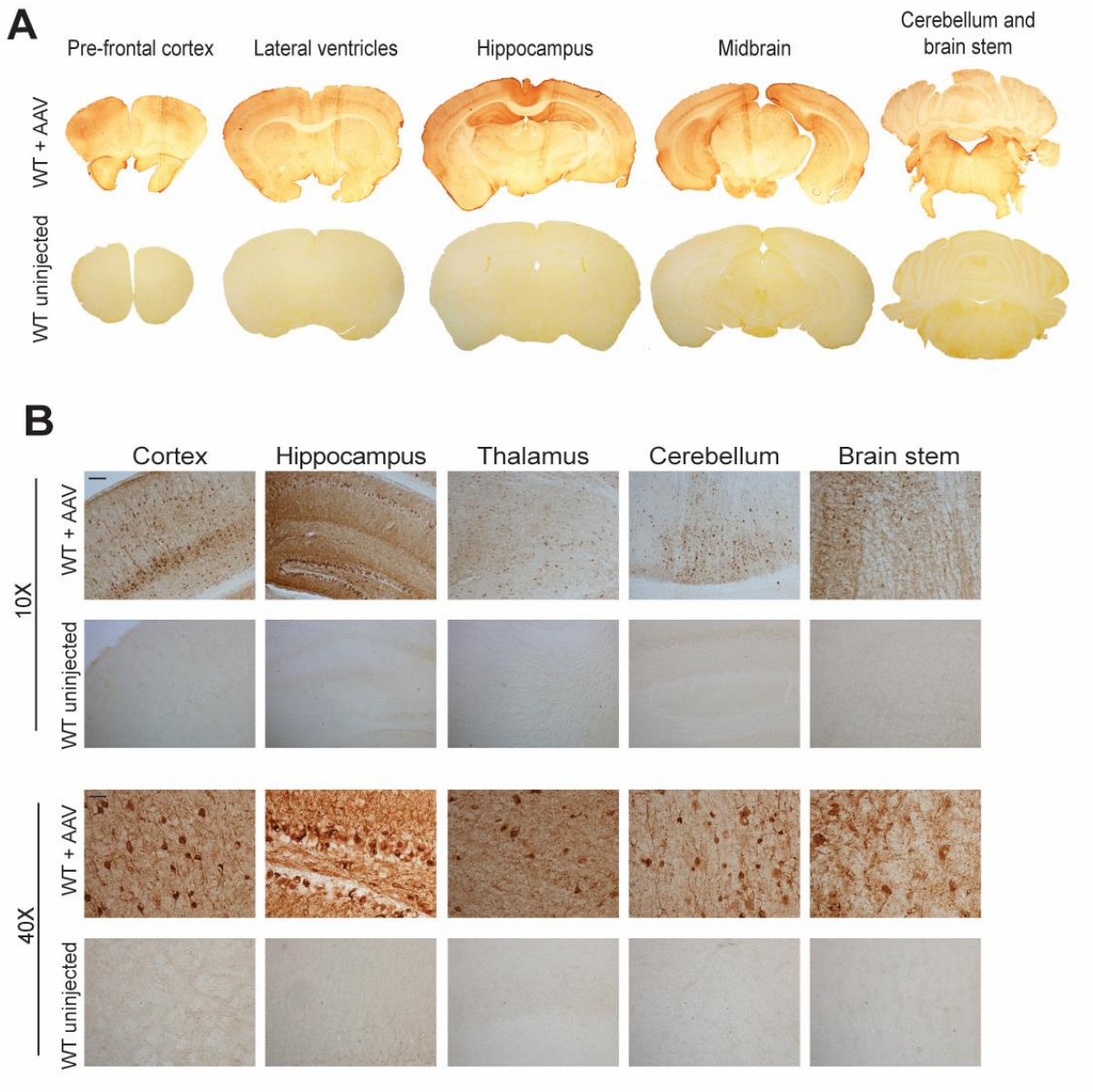

Figure 34 - Widespread neuronal expression following intravenous administration of ssAAV2/9.hSynI.*eGFP*.WPRE.hGHpA.

A eGFP expression in brains from injected mice was assessed following immunohistochemical staining. Intravenous administration of the vector resulted in extensive and substantial rostro-caudal eGFP expression in the brains of injected mice (WT + AAV) compared to controls (WT uninjected). **B** Light microscopy images of discrete brain regions. On the basis of cell morphology, the transgene expression appeared neuron-specific throughout the whole brain (Scale bars: low magnification 100µm; high magnification 60µm).

The systemic administration of the vector resulted in intense and widespread eGFP expression throughout the whole brain (**Figure 34A**). Light microscopy analysis revealed that high transduction was being achieved in the cortex, with particular efficiency in layer V of the cortex, in the CA1/CA2 region and the dentate gyrus of the hippocampus, in the thalamic nuclei, in the Purkinje cells of the cerebellum, and in the gigantocellular nuclei in the brain stem (**Figure 34B**). At higher magnification it was possible to appreciate that transduced cells had distinct neuronal morphology.

In order to confirm that *eGFP* expression driven by the synapsin promoter was neuron-specific, immunofluorescence was conducted using cell-specific antibodies together with imaging using confocal microscopy. Brain sections from injected mice and uninjected controls were co-stained with fluorescent antibodies against the eGFP protein and the neuronal marker NeuN or the astrocytic marker GFAP. The nucleic acid marker DAPI was used in order to identify cellular nuclei. In the brain of injected mice it was possible to identify cells positive for the neuronal marker NeuN which also showed positive eGFP protein expression (**Figure 35A**). In comparison, eGFP could not be detected in cells positively stained for the astrocytic marker GFAP (**Figure 35B**). These images demonstrated that the synapsin promoter resulted in transgene expression specifically in neurons and not in other macroglial cells within the central nervous system.

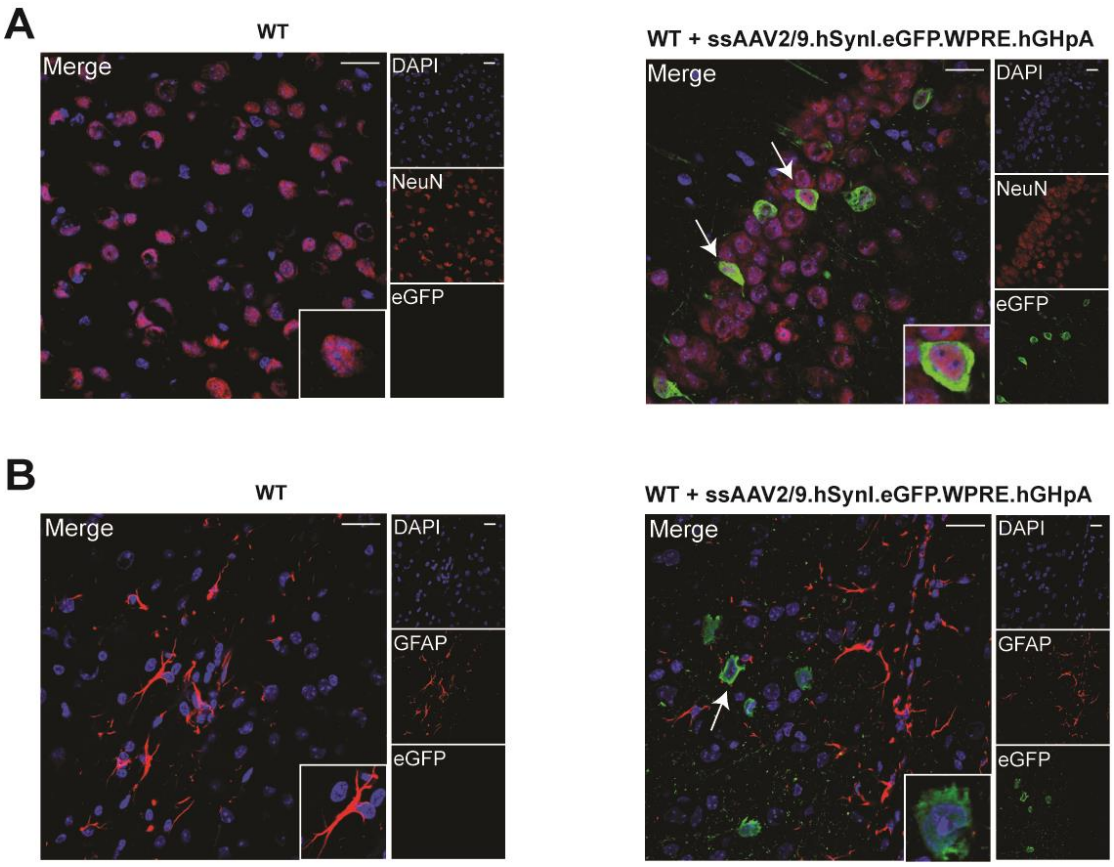

Figure 35 - Confocal microscopy imaging demonstrated neuronal-specific tropism of the vector.

A Brain sections of injected mice (WT + ssAAV2/9.hSynI.*eGFP*.WPRE.hGHp) were co-stained for the neuronal marker NeuN and the GFP reporter. eGFP expression in cells transduced by the virus showed specifically neuronal morphology (white arrows). Uninjected wild-type mice (WT) were used as control. Single channel pictures and merged images are shown (Scale bars: 20µm). **B** In order to confirm that the transgene expression was strictly limited to neurons, brain sections were stained for the astrocytic marker GFAP. Cells expressing eGFP did not co-localised with GFAP labelled cells (white arrow).

5.2.3. Transduction of the visceral organs

The use of neuron specific promoter did bring into a question its ability to mediate a systemic therapeutic effect for the treatment of Gaucher disease type II in the visceral organs. However, although hSynI is a neuron-specific promoter, it has been demonstrated that synapsin I protein is expressed in the trans-Golgi compartment of

epithelial cells in the liver of mice (Bustos et al., 2001). Therefore, a more detailed analysis of the visceral organs was performed to determine if the hSynI promoter was actually able to express eGFP in other non-neuronal cell types in the viscera. The liver tissue harvested from injected mice was analysed for eGFP expression (**Figure 36**). The administration of the vector resulted in transduction of liver cells in injected mice. Consequently the transduction efficiency in other cell types was assessed. Evidence of vector-mediated gene expression was found in the spleen, lung and heart.

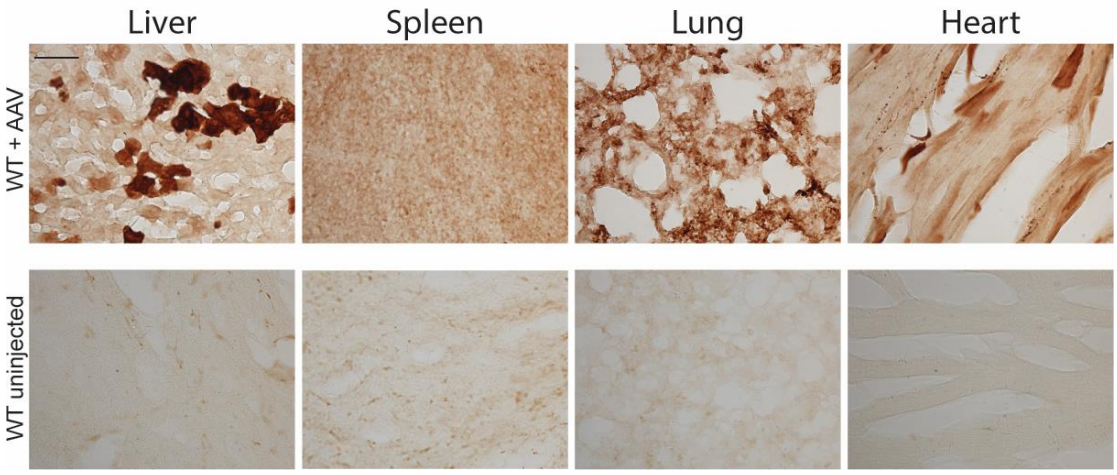

Figure 36 - Transduction of visceral organs following administration of the ssAAV2/9.hSynI.*eGFP*.WPRE.hGHpA vector.

Strong transgene expression was found in the liver of injected mice. Scattered eGFP-positive cells were found in spleen, lung and heart (Scale bar: 100μm).

5.3. ssAAV2/9.hSynI.*hGBA1*.WPRE.hGHpA vector

The reporter gene study demonstrated that the use of a strong neuronal promoter resulted in extensive brain transduction following intravenous administration to neonatal mice, with evidence of transgene expression within visceral organs. However, for the purpose of systemic gene delivery of the soluble protein β-glucocerebrosidase, the higher transduction observed in the liver and lower levels in the spleen, heart and lung could be sufficient for the synthesis and consequent uptake of the enzyme in other tissues through the cross-correction mechanism.

For these reasons, a *GBA1* version of the viral vector carrying the functional human gene was manufactured. First, the plasmid expressing the human *GBA1* gene was produced and tested *in vitro*. Consequently the viral vector was produced and administered to neonatal wild-type mice, in order to (i) evaluate whether the *GBA1* transgene expression was comparable to the results obtained with the *eGFP* construct, and (ii) assess any possible neuroinflammatory reaction following overexpression of the β-glucocerebrosidase protein in the brain.

5.3.1. Cloning of the *hGBA1* gene and *in vitro* testing

The *GBA1* gene was amplified via PCR, using the GBA_BspEI_f and the GBA_EcoRI_r primers. Two restriction site sequences corresponding to the *BspEI* and *EcoRI* enzymes were introduced at the 5' and 3' of the gene, respectively. The *eGFP* gene was removed from the original *pAAV.hSynI.eGFP.WPRE.hGHpA* plasmid through restriction enzyme digest with the aforementioned enzymes and replaced with the *hGBA1* sequence via ligation reaction (**Figure 37A**). Automated Sanger sequencing of the plasmid confirmed the successful introduction of the human *GBA1* gene into the AAV construct.

In order to verify whether the β-glucocerebrosidase protein was efficiently produced, HEK-293T cells were transfected with the *pAAV.hSynI.hGBA1.WPRE.hGHpA* plasmid. The amount of GCase protein produced in transfected cells and untreated control cells after 48 hours was measured through Western blot analysis (**Figure 37B**). The membrane stained with the antibody against β-glucocerebrosidase revealed that the transfection with the plasmid produced the correct size protein (59kDa). The quantification of the relative protein expression showed that transfection with the *pAAV.hSynI.hGBA1.WPRE.hGHpA* plasmid resulted in a significant 16-fold increase ($p=0.04$) in β-glucocerebrosidase expression compared to untransfected control cells (**Figure 37C**). This was despite using the neuron specific hSynI promoter and suggesting that it has the ability to express in non-neuronal cells such the kidney derived HEK-293T cells. These results demonstrated that the β-glucocerebrosidase protein was being efficiently produced and the transfection with the *pAAV.hSynI.hGBA1.WPRE.hGHpA* plasmid resulted in overexpression of the GCase

enzyme. To determine if the β-glucocerebrosidase produced following transfection was functional, the enzymatic activity of the protein was assessed. The enzyme was extracted from the cell lysate (**Figure 37D**) of transfected and control cells. Following incubation with the substrate 4-methylumbelliferyl-β-D-glucopyranoside, quantification of the enzymatic activity was carried out. Results confirmed that β-glucocerebrosidase was enzymatically active. The increase in the enzymatic activity (p=0.04) in treated samples reflected the overexpression of the protein following transfection. The β-glucocerebrosidase enzymatic activity was also tested in the supernatant of transfected and control cells (**Figure 37E**), in order to establish whether the protein was correctly secreted. The quantification revealed that the secreted protein was enzymatically functional and displayed a catalytic activity similar to the control samples.

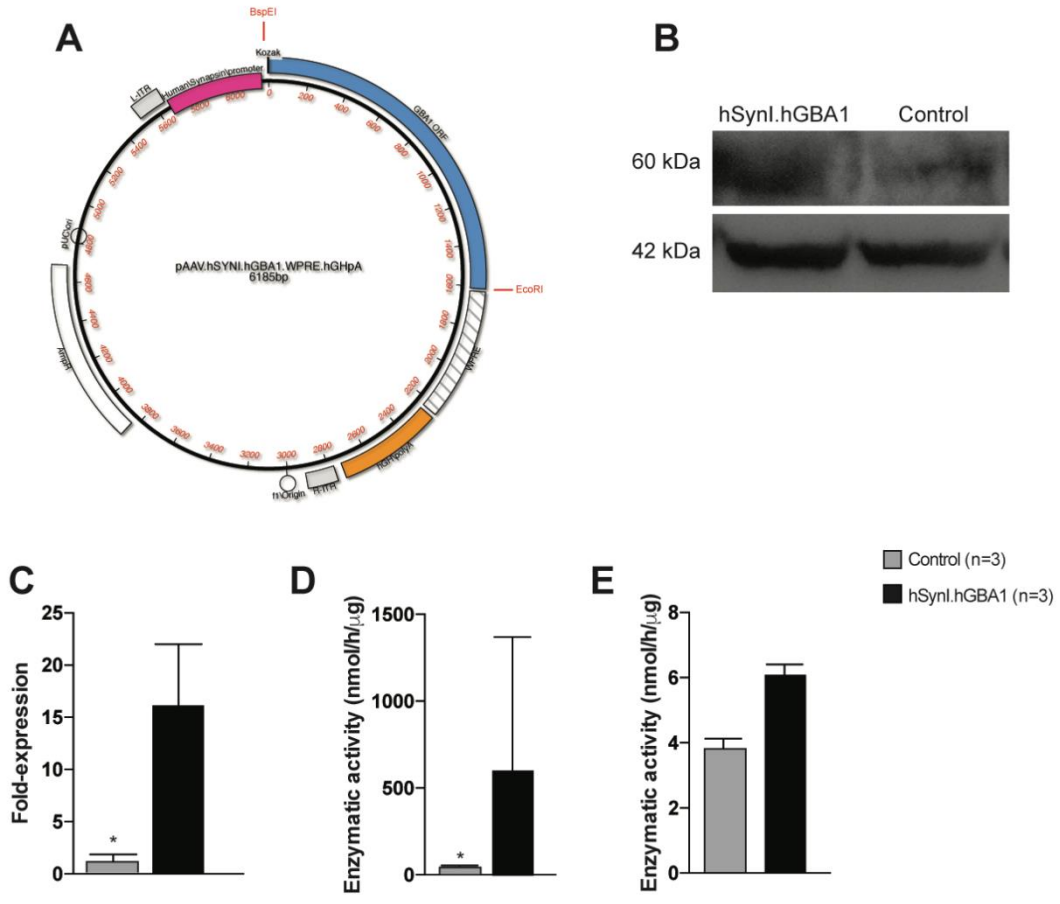

Figure 37 - Cloning and *in vitro* testing of the *pAAV.hSynI.eGFP.WPRE.hGHpA* plasmid.

A Map of the plasmid, showing the main elements of the expression cassette and the *BspEI* and EcoRI restriction enzyme sites. **B** Western blot result. HEK-293T cells transfected with the

pAAV.hSynI.eGFP.WPRE.hGHpA plasmid (hSynI.hGBA1) produced the GCase protein (59kDa). In transfected cells the protein levels were significantly higher than in the control (Loading control: β-actin). **C** Quantification of the Western blot analysis. Expression in transfected cells was 16-fold higher than control levels. **D** Enzymatic assay on cell lysate and **E** supernatant demonstrated that the β-glucocerebrosidase protein was enzymatically functional (Data presented as average ± SD. Statistical analysis: unpaired t test, Welch's correction; * $p \leq 0.05$).

5.3.2. Codon optimisation of the *GBA1* sequence

In order to further improve the expression of the human *GBA1* gene, the sequence of the wild-type gene underwent codon-optimisation processing. The principle underlying codon-optimisation is based on the degenerative properties of the genetic code: optimal codon usage can contribute to increase translation rate and specificity, resulting in higher gene expression (Karlin and Mrazek, 1996). The OptimumGene™ algorithm (GenScript) was used to modify the *GBA1* nucleotide sequence yet maintaining the same amino acid sequence (*GBA1_CO*). The Kozak sequence and the *BspEI* restriction enzyme site were synthesised upstream of the *GBA1_CO* sequence, while the *EcoRI* site was incorporated at the 3' end, so that it was possible to clone the optimised sequence into the *pAAV.hSynI.hGBA1.WPRE.hGHpA* plasmid replacing the wild-type gene. The resulting *pAAV.hSynI.GBA1_CO.WPRE.hGHpA* plasmid was used to transfect HEK-293T cells and the β-glucocerebrosidase protein expression was measured by Western blot analysis. The densitometric quantification of the GCase protein (**Figure 38**) showed that the transfection with the plasmid expressing the codon-optimized sequence resulted in an increase ($p=0.019$) of β-glucocerebrosidase protein expression compared to the untransfected control. Although there was no statistically significant difference between the two sets of samples, the transfection with the wild-type sequence produced higher levels of protein. For this reason, the original *pAAV.hSynI.hGBA1.WPRE.hGHpA* plasmid carrying the wild-type *GBA1* sequence was chosen and consequently used to produce the viral vector.

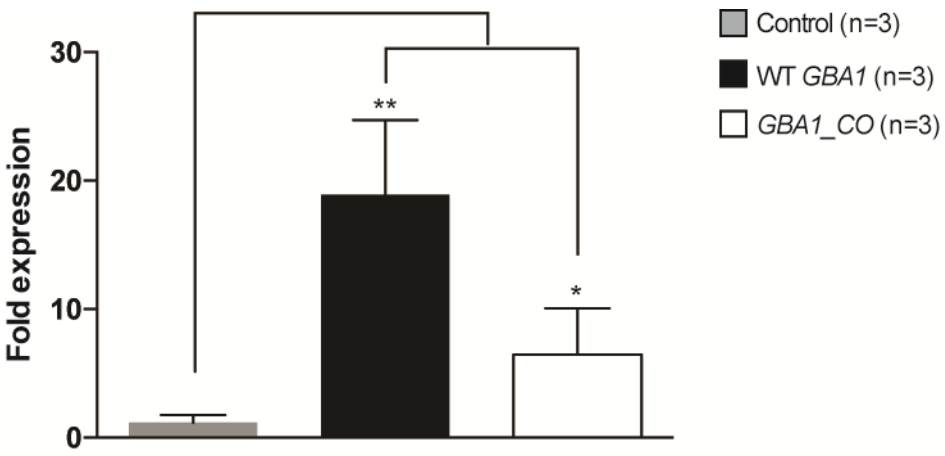

Figure 38 - Codon optimisation of the *GBA1* gene.

Quantification of Western blot analysis. The use of the codon-optimized sequence (*GBA1_CO*) did not improve the β-glucocerebrosidase protein expression in transfected cells, compared to the wild-type sequence (*WT GBA1*) (Data presented as average ± SD. Statistical analysis: unpaired t test, Welch's correction; * $p \leq 0.05$, ** $p \leq 0.01$).

5.3.3. ssAAV2/9.hSynI.*hGBA1*.WPRE.hGHpA viral vector production

The *pAAV.hSynI.hGBA1.WPRE.hGHpA* plasmid was used to produce the ssAAV2/9.hSynI.*hGBA1*.WPRE.hGHpA viral vector (**Figure 39A**). The same triple transfection process employed to produce the *eGFP* version of the vector was carried out. The titer of the virus was measured by SDS-PAGE (**Figure 39B**) and consequent densitometric analysis (**Figure 39C**). The analysis of polyacrylamide gel showed that the virus was efficiently produced and the amount of VP3 protein was consequently determined. The average titer of the preparation was quantified to be 6×10^{13} vp/ml.

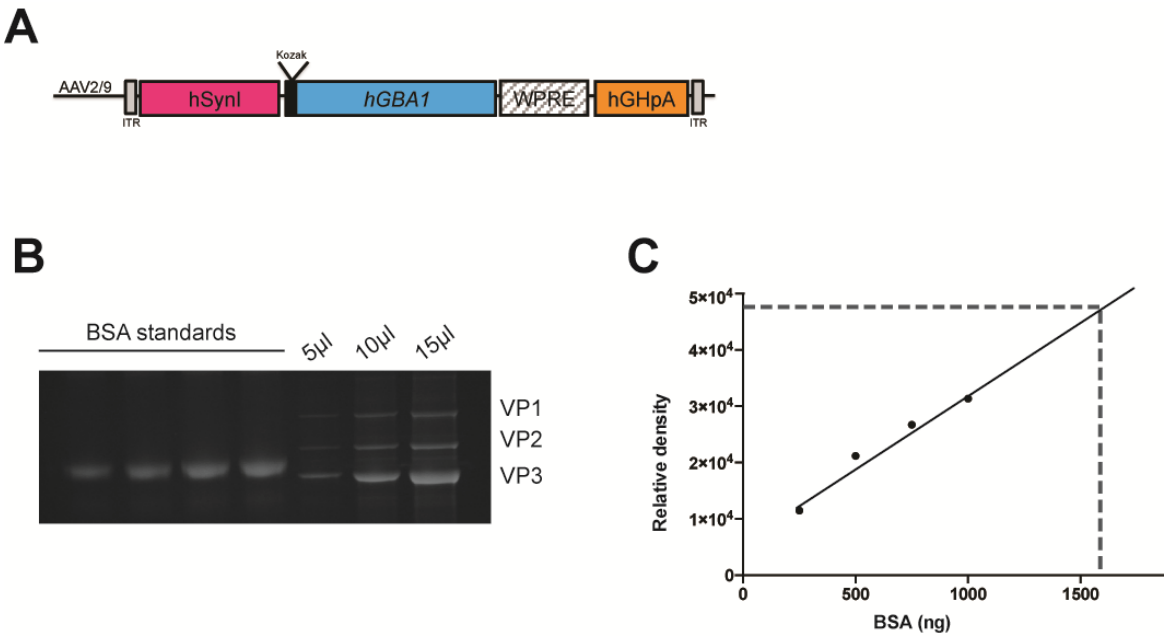

Figure 39 - ssAAV2/9.hSynI.*hGBA1*.WPRE.hGHpA virus production.

A Schematic of the expression cassette. The human *GBA1* gene was under control of the synapsin I promoter. **B** SDS-PAGE gel. 5µl, 10µl and 15µl of the viral preparation were loaded and the amount of VP3 capsid protein was measured. **C** Titration of the preparation. The viral vector was produced with an average titer of 6 x 10^{13} vp/ml.

5.3.4. Assessment of neuroinflammatory response

In order to evaluate whether the injection of a high dose of the viral vector could result in toxicity within the central nervous system, the inflammatory response following administration was assessed. A total dose of 2.4 x 10^{12} vp was intravenously administered to three neonatal wild-type mice. The animals were sacrificed at one month of age and the brain was harvested and processed. The neuroinflammatory response following administration of the vector was assessed. Brain sections from injected mice and untreated controls were stained for the astrocytic marker GFAP (**Figure 40A**). Activated astrocytes were not visible in the tissue and the staining intensity levels throughout the whole brain of injected mice were comparable to the controls. Quantification of GFAP immunoreactivity in the cortical region S1BF, in the hippocampus and in the thalamic nuclei confirmed that mice injected with the vector did

not develop astrocytosis in any of these brain regions (**Figure 40B**). Hence it was concluded that the administration of the vector did not cause an astroglial-mediated inflammatory response in the brain of injected mice.

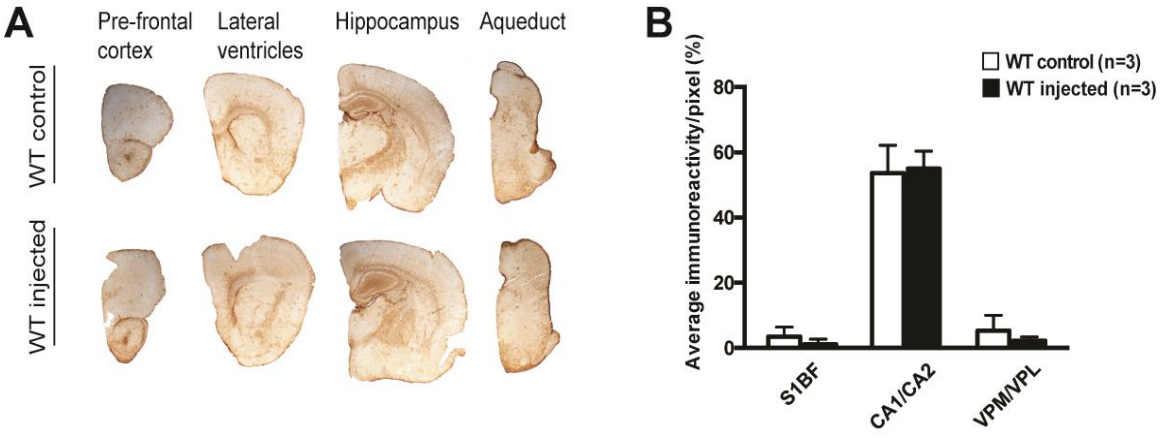

Figure 40 - Analysis of neuroinflammation following administration of the vector to wild-type mice.

A Immunohistochemical staining for the marker GFAP did not show increase in astrocytosis in brains from injected mice (WT injected) compared to untreated controls (WT controls). **B** S1BF cortex; CA1/CA2 hippocampus; VPL/VPM thalamus. Quantification of the GFAP intensity confirmed normal levels of astrocytes in injected brains (Data presented as average $\pm$ SD. Statistical analysis: two-wayANOVA, Tukey's multiple comparisons test; ns $p>0.05$).

5.4. Gene therapy in the mouse model for neuronopathic Gaucher disease

Since the toxicological study carried out on wild-type mice did not show adverse effect following administration of the vector and the β-glucocerebrosidase expression was elevated in the brain of injected mice, the ssAAV2/9.hSynI.*hGBA1*.WPRE.hGHpA viral vector was utilised to administer gene therapy to the Gaucher mouse model. Five K14-lnl/lnl mice were intravenously injected on the day of birth via the temporal vein with 40µl of the vector, resulting in a total dose of of 2.4 x 10^{12} viral particles. The animals were monitored for weight loss and neurological symptoms. Due to an undesired eye

infection spread in the animal facility, the mice were sacrificed at nine weeks of age and the neuropathological analysis was performed. Immunohistochemistry on brain sections was carried out, and possible neuronal loss was measured. The effects of gene therapy on the visceral organs were also evaluated through the analysis of macrophage accumulation and β-glucocerebrosidase enzymatic activity.

5.4.1. Extension of lifespan and health monitoring

While the untreated K14-lnl/lnl mice were collected at the humane endpoint at two weeks of age, the administration of gene therapy resulted in significant extension of the lifespan of the treated animals (**Figure 41A**). *Gba1* knock-out mice that received intravenous injection of the ssAAV2/9.hSynI.*hGBA1*.WPRE.hGHpA vector on the day of birth survived up to at least nine weeks of age. At that point, both treated animals and age-matched wild-type controls were sacrificed, as required from the UCL Home Office Veterinary because of an infection unrelated to the treatment. The body weight of the animals was constantly monitored. Treated animals did not show any significant difference in weight compared to wild-type littermates (**Figure 41B**).

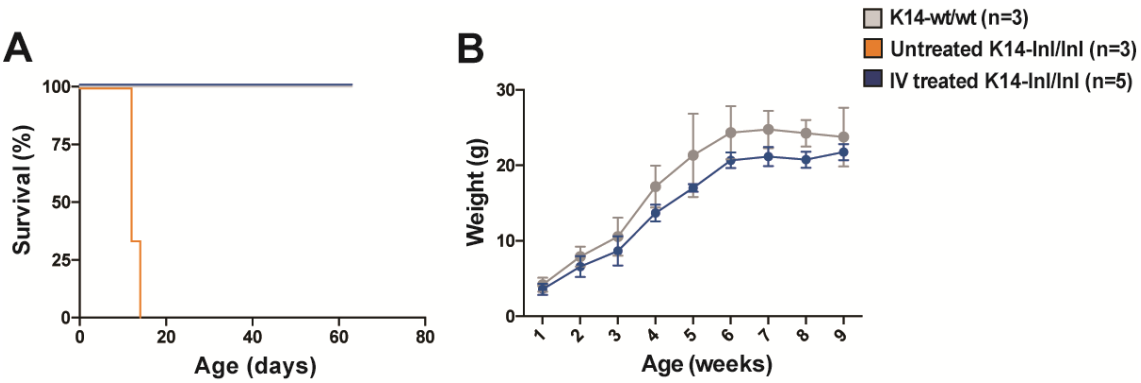

Figure 41 - Prolonged lifespan of treated K14-lnl/lnl animals.

A Kaplan-Meier survival curve. Intravenous administration of the vector resulted in extended life of treated animals (IV treated K14-lnln/lnl) (Statistical analysis: log rank (Mantel-Cox) test; $p \leq 0.001$). **B** Treated mice maintained body weight comparable to controls (Statistical analysis: two-way ANOVA, Tukey's multiple comparisons test; ns $p \geq 0.05$).

5.4.2. Assessment of neurological manifestations

A series of behavioural tests were conducted in order to evaluate neurological symptoms in treated mice. As the untreated K14-lnl/lnl mice were not old enough to be trained and tested before being sacrificed at the humane end-point at P14, most of the analysis was carried out on treated animals and wild-type age-matched controls. Data shown in **Figure 42** show the results of tests conducted on 60-day-old mice; except for the righting reflex test (**Figure 42A**), which was conducted on 14 day-old mice.

K14-lnl/lnl mice rapidly developed neurological manifestations at two weeks of age. At the end-stage the animals were not able to right themselves when place in a supine position. Untreated *Gba1* knock-out animals completely failed the righting reflex test (score 0), whereas all IV treated mice and wild-type controls returned to prone position in less than 1 second (score 1) at P14 (**Figure 42A**).

IV treated K14-lnl/lnl and K14-wt/wt were tested for locomotor dysfunction on the rotarod apparatus (**Figure 42B**). The time at fall from the rod was recorded. Treated mice performed similarly to the controls, falling at an average time of 36.5s, compared to wild-type animals at 49.5s. Although the time achieved by treated knock-out mice on the rotarod was slightly shorter than duration of the controls the difference was not statistically significant.

Similar results were obtained from the open field test, where mice were placed into a transparent chamber and movement was recorded for 4 minutes (**Figure 42C**). Several different parameters were analysed: distance travelled, average speed, time the animal was in motion and time it remained immobile. IV treated mice performed equally to the controls in all the examined tasks. Examples of resulting movement traces are also shown in **Figure 42C**. All animals showed exploratory behaviour. IV treated mice did not walk preferentially on the edge of the field, but crossed the centre of the chamber several times comparably to their wild-type littermate controls.

Mice were also assessed for a clasping phenotype to evaluate eventual cerebellar ataxia (**Figure 42D**). IV treated K14-lnl/lnl displayed dissimilar phenotypes. Three of the five

animals showed a mild clasping behaviour, occasionally retracting one leg for less than 30s (score 1). One animal exhibited a more severe phenotype, retracting both hind limbs for more than 50% of the experimental time (score 2). The last mouse did not show any pathological manifestation, extending all libs out from the body like wild-type controls (score 0).

Motor coordination was measured by placing animals on a grid for 1 minute and counting the paw misplacements over the total number of steps (**Figure 42E**). Both IV treated K14-lnl/lnl and K14-wt/wt animals faulted a comparable number of front paw placements. However, treated mice performed worse than controls when specifically the back paw misplacements were measured ($p=0.0039$).

Finally, an indicative gait evaluation was performed measuring stride length and base width (**Figure 42F**). The footprint analysis revealed that IV treated mice did not show overt motor deficits, maintaining a good coordination and balance similar to the wild-type controls.

Combined these behavioural analyses indicated that K14-lnl/lnl mice that received gene therapy on the day of birth did not develop severe neurological symptoms nine weeks after the administration. One isolate animal showed moderate clasping phenotype. Overall, however IV treated mice showed higher back paw misplacement in the foot faults test, treated mice performed similarly to the wild-type controls in all the tests, demonstrating that motor coordination deficits were largely prevented following the treatment.

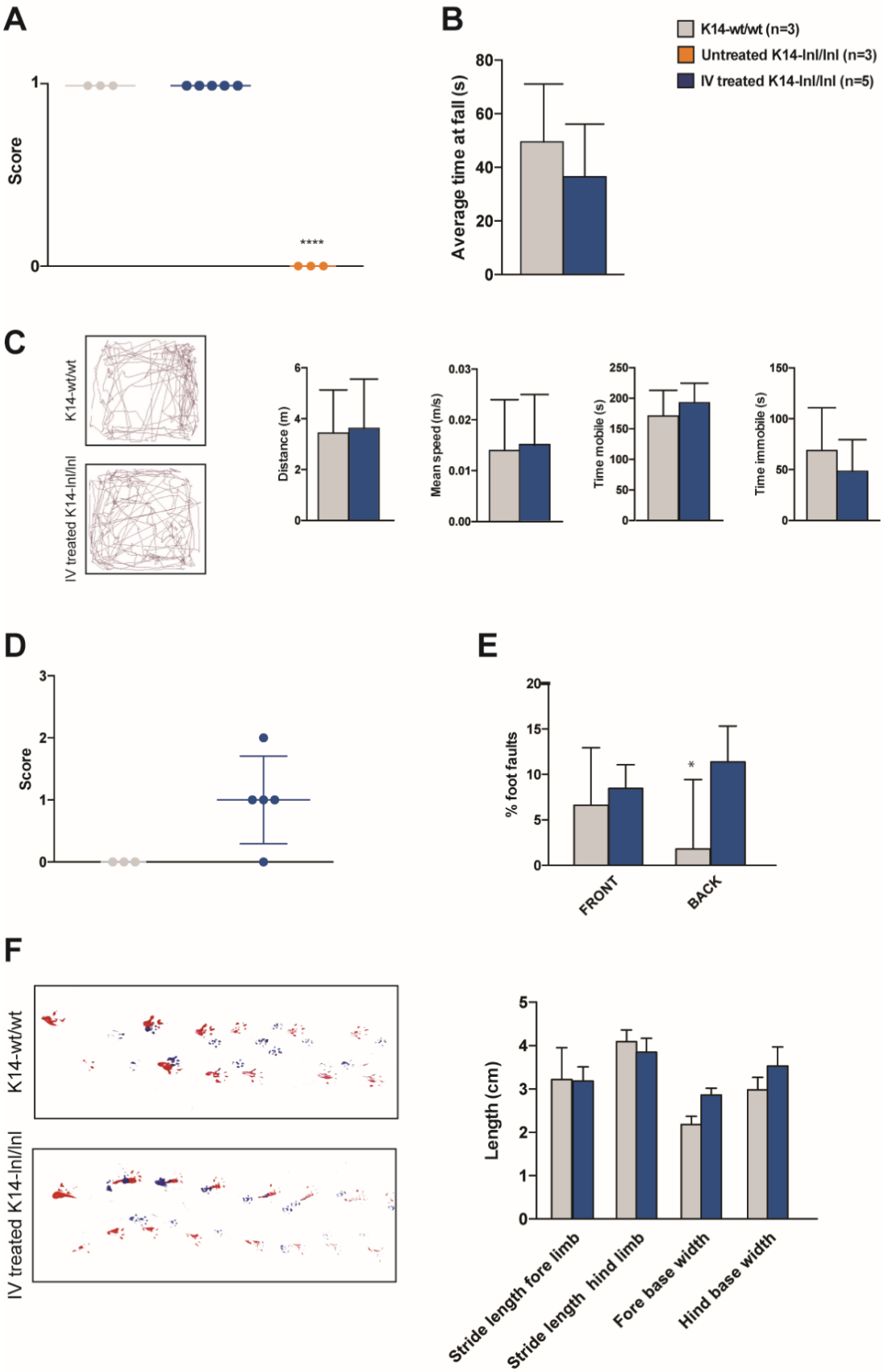
A
Score
1
0
****
B
K14-wt/wt (n=3)
Untreated K14-Inl/Inl (n=3)
IV treated K14-Inl/Inl (n=5)
Average time at fall (s)
80
60
40
20
0
C
K14-wt/wt
IV treated K14-Inl/Inl
Distance (m)
Mean speed (m/s)
Time mobile (s)
Time immobile (s)
D
Score
E
% foot faults
FRONT
BACK
F
K14-wt/wt
IV treated K14-Inl/Inl
Length (cm)
Stride length fore limb
Stride length hind limb
Fore base width
Hind base width

Figure 42 - Behavioural assessment of treated mice.

A Righting reflex test. Untreated K14-lnl/lnl mice were unable to right themselves when place in supine position (score=0), while treated mice showed fast latency to turn (score=1) (Statistical analysis: one-way ANOVA, Holm-Sidak's multiple comparisons test; **** $p<0.0001$). **B** Rotarod. Treated mice did not show loco-motor impairments when positioned on the rotarod (Data presented as average $\pm$ SD. Statistical analysis: unpaired t test, Welch's correction; ns $p>0.05$). **C** Open field test (traces and data analysis). Mice were assessed for distance walked, speed, time of mobility and immobility when placed into the open field box. Overall, treated animals performed as the wild-type controls (Data presented as average $\pm$ SD. Statistical analysis: unpaired t test, Welch's correction; ns $p>0.05$). **D** Tail suspension. Treated mice showed different phenotypes, from moderate clasping (score=2) to normal behavior (score=0) (Statistical analysis: unpaired t-test, Welch's correction; ns $p>0.05$). **E** Foot faults test. Paw misplacement was counted over the total number of steps. Treated mice showed increased back foot misplacement compared to controls (Data presented as average $\pm$ SD. Statistical analysis: two-way ANOVA, Tukey's multiple comparisons test; * $p\leq0.05$). **F** Footprint test (Traces and data analysis). Stride length and base width of the steps were analysed. Treated knock-out mice maintained good coordination skills and performed similarly to wild-type controls (Data presented as average $\pm$ SD. Statistical analysis: two-way ANOVA, Tukey's multiple comparisons test; ns $p\geq0.05$).

5.4.3. Widespread overexpression of β-glucocerebrosidase in the brain of treated K14-lnl/lnl mice

Untreated K14-lnl/lnl, IV treated K14-lnl/lnl and wild-type mice were sacrificed and an extensive histological analysis of the brain was performed.

The intravenous injection of the ssAAV2/9.hSynI.*hGBA1*.WPRE.hGHpA vector to neonatal wild-type mice resulted in intense and widespread overexpression of β-glucocerebrosidase in the brain. In order to evaluate whether the administration of the vector to *Gba1* knock-out animals caused an increase in the expression of the protein, brain sections of treated mice underwent immunohistochemical staining against the GCase protein (**Figure 43A**) and the most affected brain regions observed in Gaucher patients were analysed. The systemic administration of the vector resulted in widespread

β-glucocerebrosidase expression. Exceptionally high transduction was observed in the thalamic nuclei of treated brains. In other regions the concentration of GCase-positive neurons was lower; nevertheless in the cortex, hippocampus, cerebellum and brain stem it was still possible to detect many stained cells. The quantification of the immunoreactivity (**Figure 43B**) confirmed the significant β-glucocerebrosidase overexpression in treated brains compared to the wild-type controls, while untreated K14-lnl/lnl mice expressed minimal amount of protein.

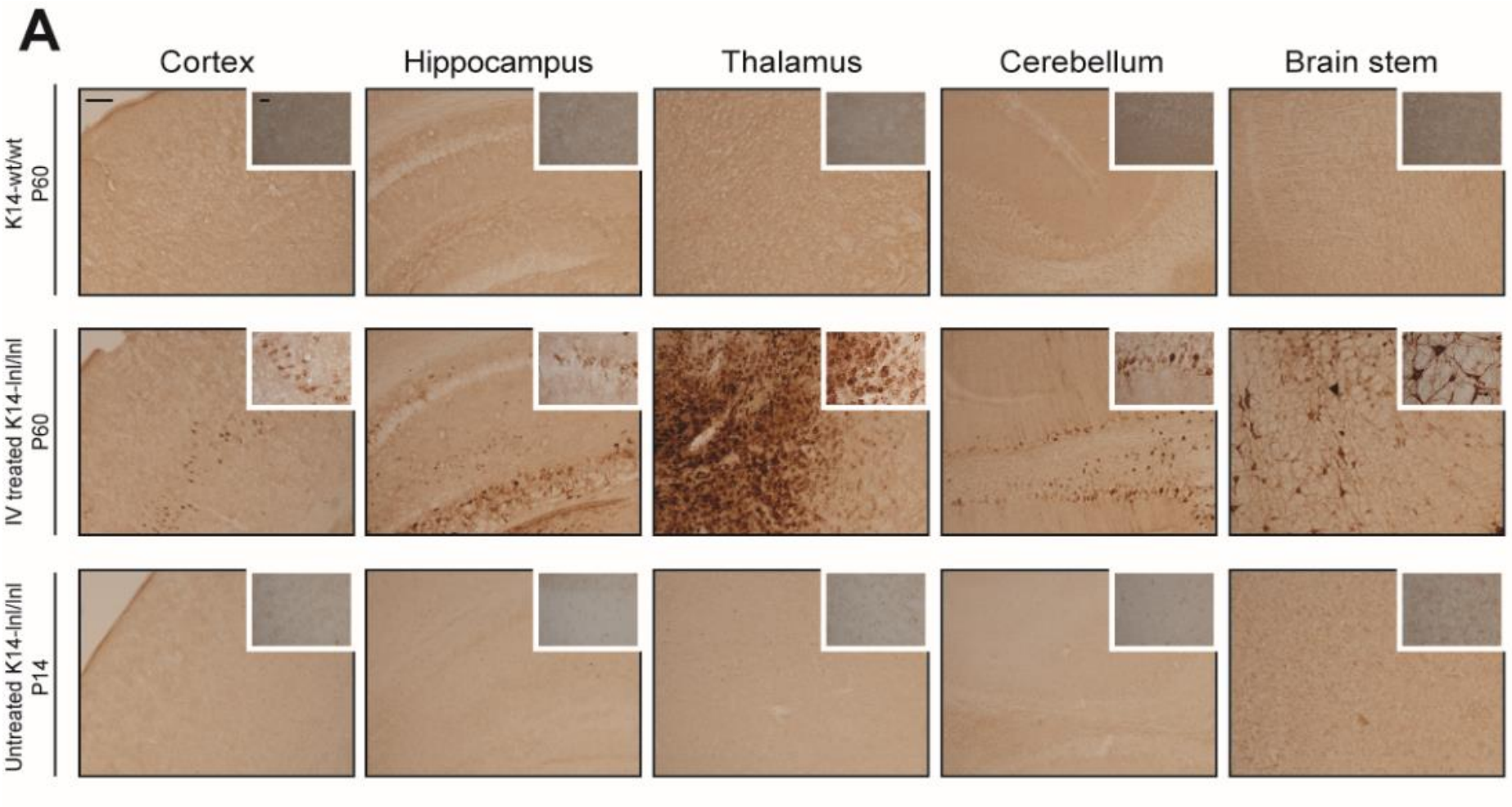
A
Cortex
Hippocampus
Thalamus
Cerebellum
Brain stem
K14-wt/wt P60
IV treated K14-Inl/Inl P60
Untreated K14-Inl/Inl P14

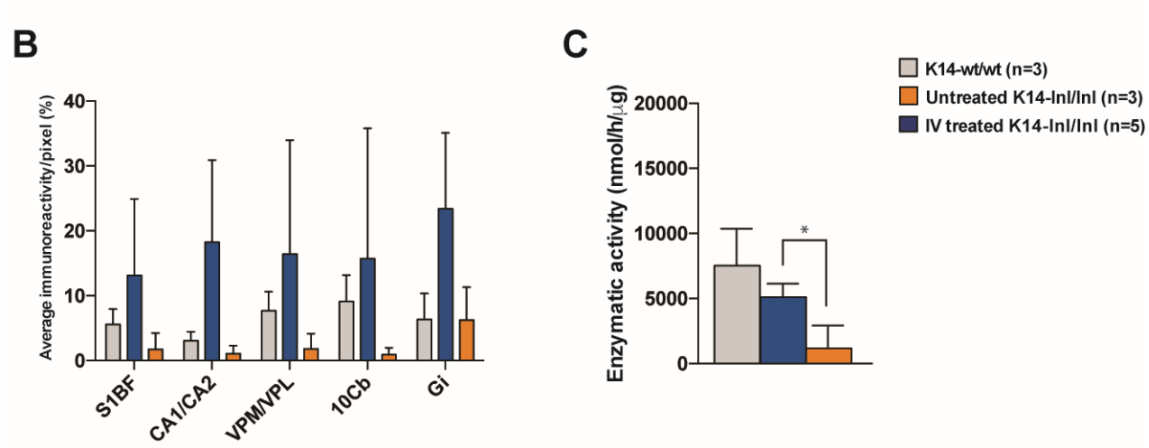

Figure 43 - Overexpression of β-glucocerebrosidase in treated brains.

A Brain sections from wild-type, treated K14-lnl/lnl mice and untreated K14-lnl/lnl mice were stained for β-glucocerebrosidase. Intense neuronal staining was observed throughout the whole brain of treated mice (Scale bars: low magnification 100μm; high magnification 60μm). **B** S1BF cortex; CA1/CA2 hippocampus; VPM/VPL thalamus, 10Cb cerebellum; Gi brain stem. Quantification of immunoreactivity confirmed the widespread overexpression of *GBA1* in different regions of the brain (Data presented as average ± SD. Statistical analysis: two-way ANOVA, Tukey's multiple comparisons test; ns $p>0.05$). **C** Enzymatic assay. Administration of the vector resulted in increase of the enzymatic activity in the brain of treated mice (Data presented as average ± SD. Statistical analysis: one-way ANOVA, Tukey's multiple comparisons test; * $p\leq0.05$).

To determine whether transduced cells produced enzymatically functional β-glucocerebrosidase, frozen brain samples were homogenised and the catalytic activity of the enzyme was measured (**Figure 43C**). Results showed that the overexpression of the *GBA1* gene normalized the β-glucocerebrosidase enzymatic activity into wild-type levels. GCase residual activity in treated brains was 68% that of the normal range, while the untreated *Gba1* knock-out brains maintained only minimal reduced ($p=0.04$) enzymatic activity. No significant difference was found between control and treated samples.

5.4.4. Reduction of neuroinflammation in *Gba1* knock-out mice following vector administration

The presence of numerous and diffuse activated astrocytes in many brain regions, particularly within cortical areas is characteristic of *Gba1* knock-out mice. Brain sections form untreated *Gba1* knock-out (14 day-old), treated mice (60 day-old), and age-matched wild-type controls (60 day-old) were stained for the GFAP marker. The administration of the ssAAV2/9.hSynI.*hGBA1*.WPRE.hGHpA cleared the presence of activated astrocytes within the cortical layers and the thalamic nuclei of treated mice compared to the untreated animals (**Figure 44A**). A notable amelioration in neuroinflammation was observed in the brain stem and cerebellum, although the GFAP intensity was still not comparable to the wild-type control levels. The quantification of the anti-GFAP staining (**Figure 44B**) demonstrated that neuroinflammation levels were completely normalised in the somato-barrel field region S1BF and the thalamic nuclei VPM/VPL in treated brains. GFAP-positive cells were found in the CA1/CA2 layers of the hippocampus and in the cerebellum, however the difference with wild-type control was not statistically significant. In the gigantocellular nuclei region of the cerebellum the immunoreactivity was markedly elevated ($p=0.017$) in treated brains compared to controls. However, GFAP levels in brains harvested from IV treated K14-lnl/lnl mice were lower ($p=0.0005$) than the average astrocytic activation in the untreated *Gba1* knock-out samples.

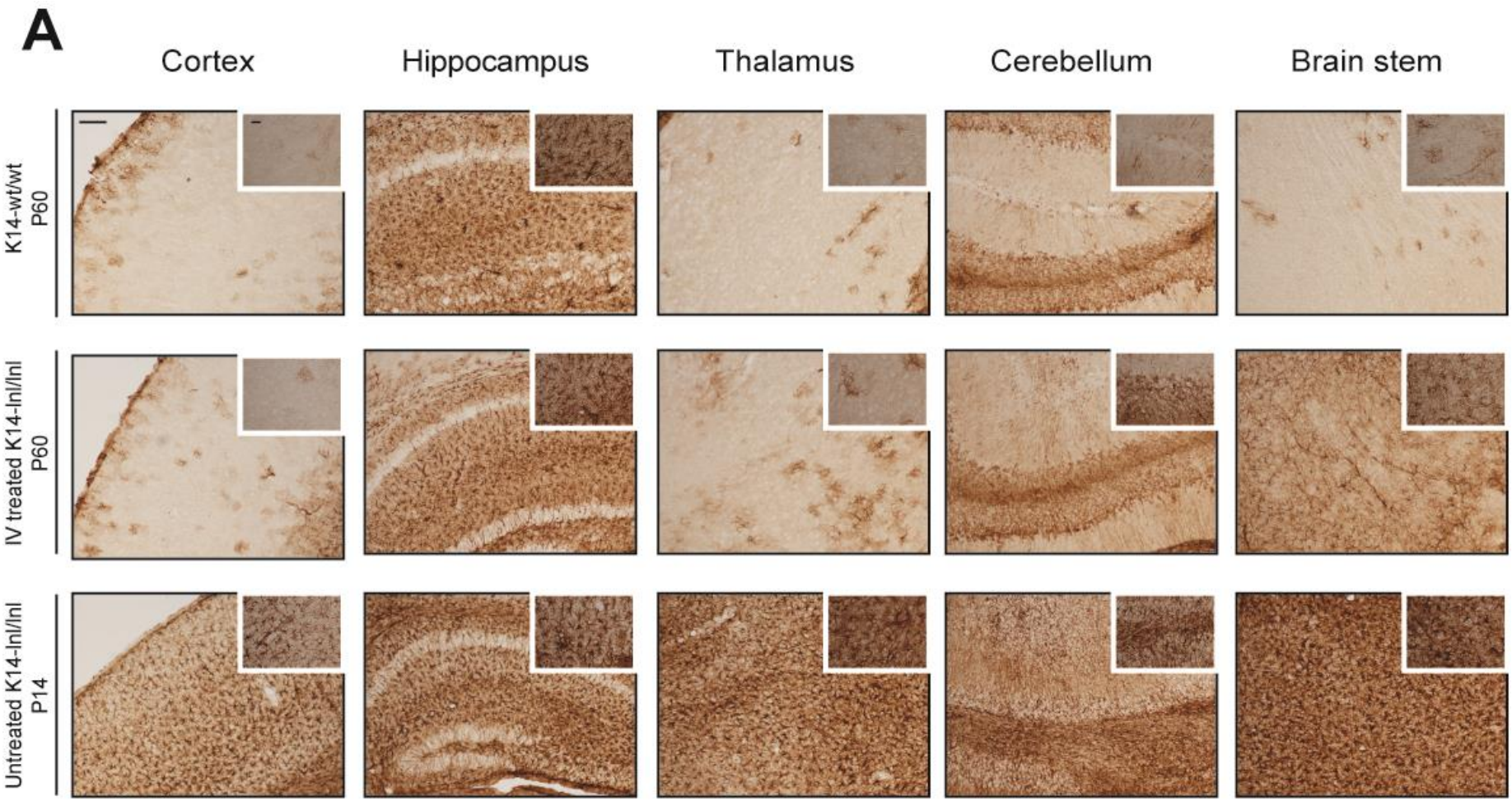
A
Cortex
Hippocampus
Thalamus
Cerebellum
Brain stem
K14-wt/wt P60
IV treated K14-Inl/Inl P60
Untreated K14-Inl/Inl P14

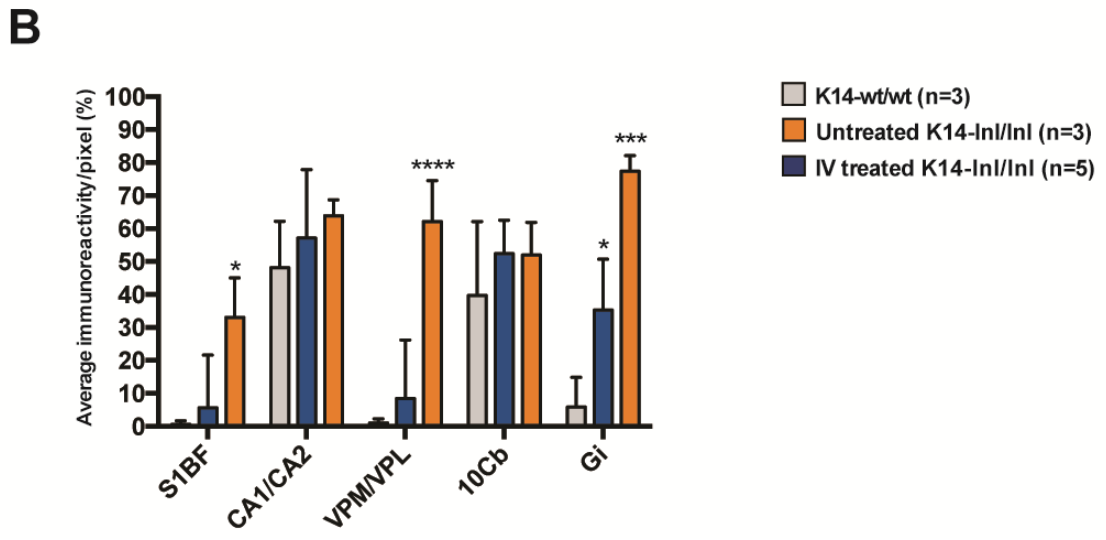

Figure 44 - Reduction of astrocytosis in treated mice.

A Light microscopy imaging of immunohistochemical staining for the astrocytic marker GFAP. Neuroinflammation was normalised in the cortex, thalamus and cerebellum of treated K14-lnl/lnl mice (Scale bars: low magnification 100µm; high magnification 60µm). **B** S1BF cortex; CA1/CA2 hippocampus; VPM/VPL thalamus, 10Cb cerebellum; Gi brain stem. Significant reduction in astrocytosis was observed in the S1BF cortical region, the thalamic nuclei and brain stem of treated mice, while untreated knock-out animals developed intense and extensive astrocytic activation (Data presented as average ± SD. Statistical analysis: two-wayANOVA, Tukey's multiple comparisons test; * $p \leq 0.05$, *** $p \leq 0.001$, **** $p < 0.0001$).

5.4.5. Normalisation of microglia activation in treated K14-lnl/lnl mice

The previous chapter demonstrated that the administration of the scAAV2/9.GUSB.*hGBA1*.bGHpA vector resulted in only partial amelioration of microglial activation in treated brains, limited to restricted regions. Intense CD68-positive staining was detected in the cortex and in the hippocampus of the previously treated mice. However, the treatment with ssAAV2/9.hSynI.*hGBA1*.WPRE.hGHpA provided more promising results. Brains from mice treated with this second vector did not develop microglia activation (**Figure 45A**). The brain sections stained for the microglial marker CD68 resulted in the complete clearance of positive cells, comparable to wild-type samples. This result was confirmed by quantification of the

immunoreactivity (**Figure 45B**). In all analysed regions it was not possible to identify enlarged CD68-positive cells in brain sections from both IV treated and wild-type control mice. Immunohistochemistry on untreated K14-lnl/lnl brains showed diffuse and intense microglia activation throughout the whole brain, demonstrating the beneficial effect of gene therapy on treated mice.

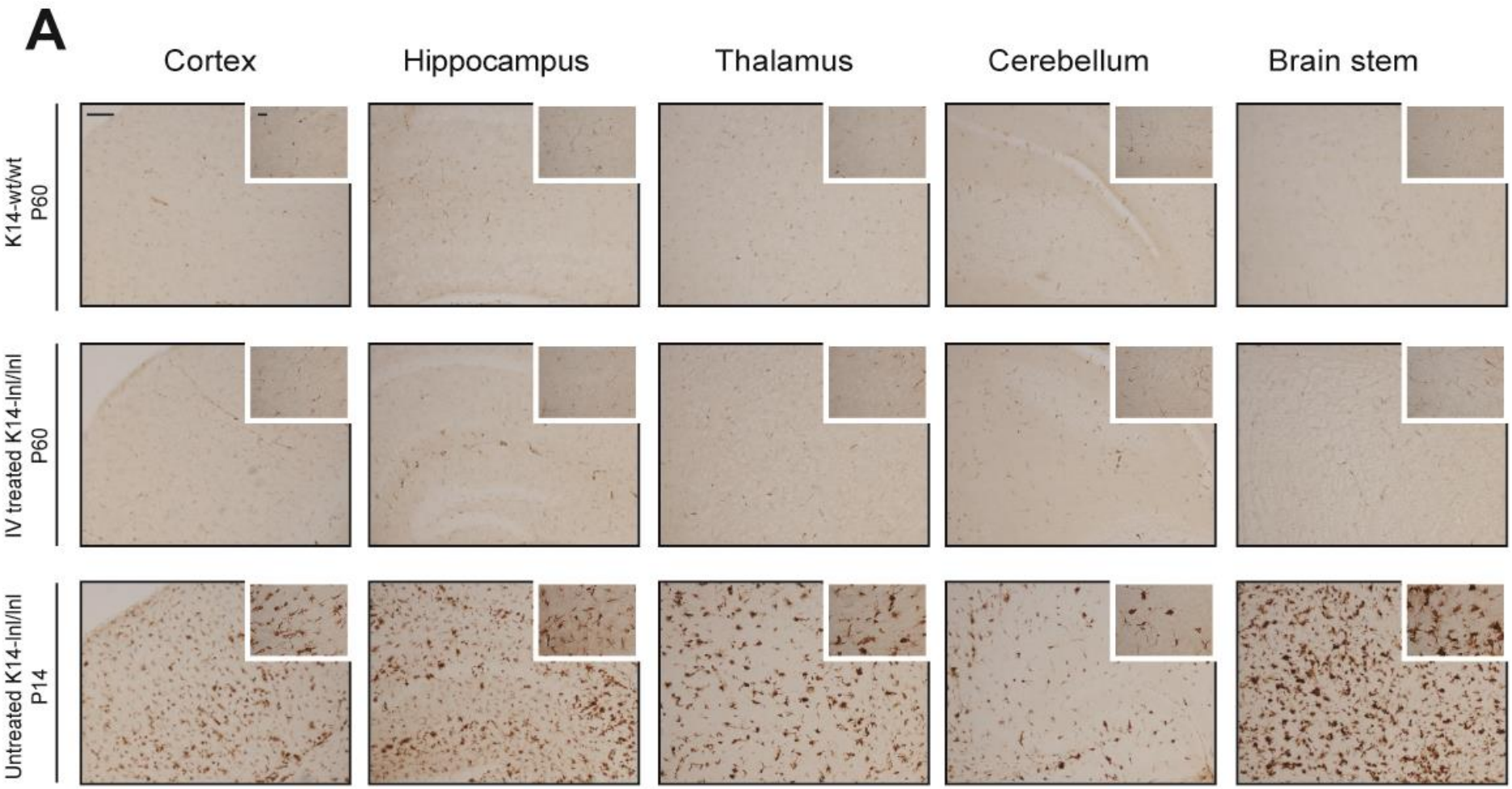
A
Cortex
Hippocampus
Thalamus
Cerebellum
Brain stem
K14-wt/wt P60
IV treated K14-Inl/Inl P60
Untreated K14-Inl/Inl P14

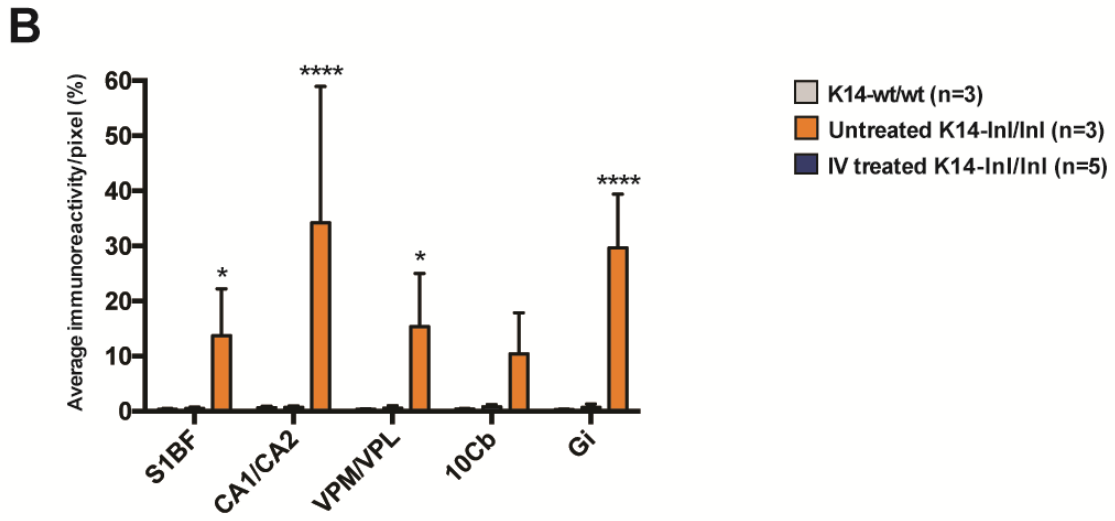

Figure 45 - Reduction of microglia activation in treated K14-lnl/lnl mice.

A Brain sections stained for the microglial marker CD68. Samples from treated mice resulted in the complete clearance of CD68-positive cells (Scale bars: low magnification 100µm; high magnification 60µm). **B** S1BF cortex; CA1/CA2 hippocampus; VPM/VPL thalamus, 10Cb cerebellum; Gi brain stem. Quantification of immunoreactivity confirmed that gene therapy normalised microglia activation levels in treated brains (Data presented as average ± SD. Statistical analysis: two-way ANOVA, Tukey's multiple comparisons test; * $p \leq 0.05$, **** $p < 0.0001$).

5.4.6. Administration of the ssAAV2/9.hSynI.*hGBA1*.WPRE.hGHpA vector prevented accumulation of lysosomes in the brain

In order to determine if the systemic treatment with the ssAAV2/9.hSynI.*hGBA1*.WPRE.hGHpA vector ameliorated the accumulation of disrupted lysosomes within the brain of affected mice, brain sections were incubated with anti-LAMP1 antibody (**Figure 46A)**. The analysis of the lysosomal marker distribution showed that the build-up in treated brains was reduced compared to untreated K14-lnl/lnl sections. The improvement was confirmed by quantification of the average immunoreactivity (**Figure 46B**). Lysosome marker levels were normalised to control levels in all the analysed brain areas in tissue from IV treated animals. Thus, it was demonstrated that the overexpression of β-glucocerebrosidase in the brain

prevented the accumulation of lysosomes in the brain of treated mice.

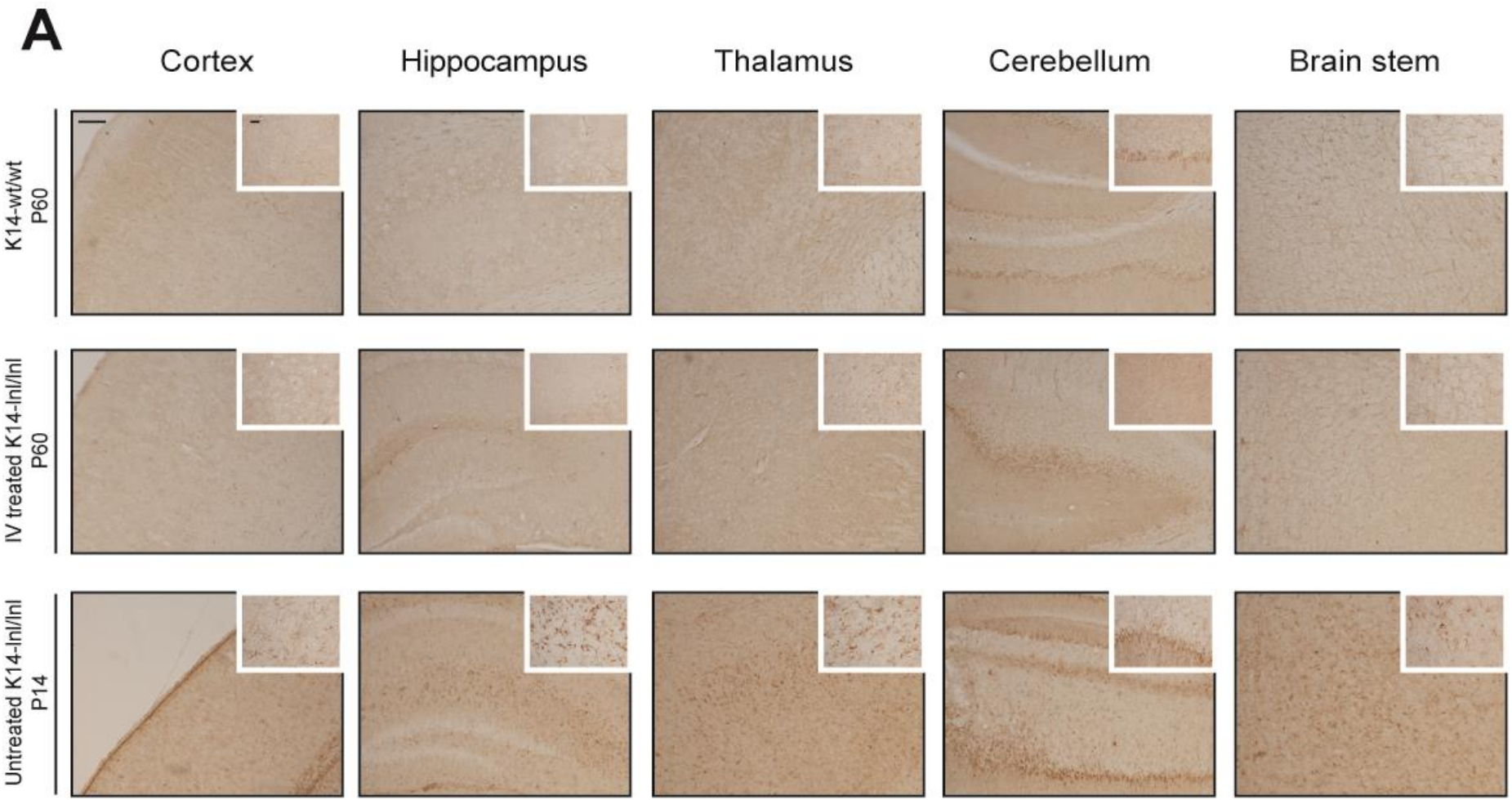
A
Cortex
Hippocampus
Thalamus
Cerebellum
Brain stem
K14-wt/wt P60
IV treated K14-Inl/Inl P60
Untreated K14-Inl/Inl P14

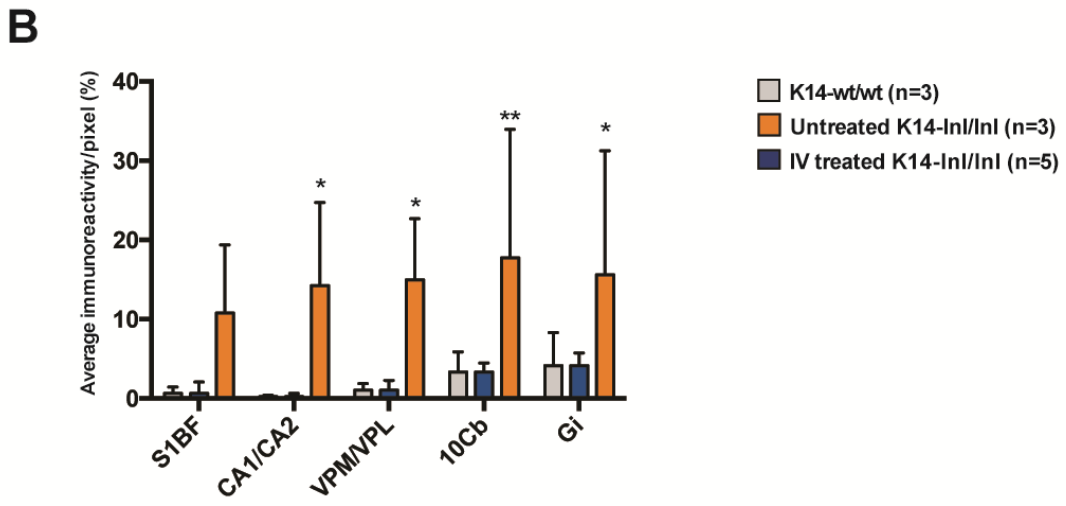

Figure 46 - Normalisation of lysosome accumulation levels following gene therapy administration.

A Reduction of lysosome accumulation in treated brains compared to untreated *Gba1* knock-out samples (Scale bars: low magnification 100µm; high magnification 60µm). **B** S1BF cortex; CA1/CA2 hippocampus; VPM/VPL thalamus, 10Cb cerebellum; Gi brain stem. The administration of the vector resulted in complete normalisation of lysosomal marker LAMP1 in all the analysed regions of treated brains (Data presented as average ± SD. Statistical analysis: two-wayANOVA, Tukey's multiple comparisons test; * $p \leq 0.05$, ** $p \leq 0.01$).

5.4.7. Gene therapy prevents neuronal loss

Brain tissue from IV treated mice and age-matched wild-type controls were stained with cresyl violet Nissl and an analysis of neuronal counts was performed using stereology software. Previous results showed that although the intravenous administration of scAAV2/9.GUSB.*hGBA1*.bGHpA extended the lifespan of treated K14-lnl/lnl, the mice developed widespread neuropathology characterised by neuronal loss, ventriculomegaly and brain atrophy. In order to establish whether the treatment with ssAAV2/9.hSynI.*hGBA1*.WPRE.hGHpA ameliorated the neuropathology, cortical thickness measurements were carried out (**Figure 47B**). Statistical analysis revealed that, although the difference was minimal, the cortex of IV treated mice brain had reduced cortical thickness ($p=0.0013$) compared to the wild-type controls. Despite the shrinkage of the cortical regions, the anatomy of the brains harvested from treated mice

was not disrupted, and there was no sign of pathological enlargement of the lateral ventricles (**Figure 47A**).

The number of neurons in the somato-barrel field cortical region, the thalamic nuclei and the Gi region in the brain stem was evaluated (**Figure 47C**). In all analysed areas, the neuron count in treated samples was comparable to the age-matched wild type controls. The systemic administration of the ssAAV2/9.hSynI.*hGBA1*.WPRE.hGHpA vector resulted in efficient neuron-specific transduction and prevented neurodegeneration and cell loss in 9 weeks old treated mice.

A non-quantitative analysis on neuron loss in the cerebellum was also performed. Calbindin is an established marker specific for Purkinje cells (Kim et al., 2009). Cerebellar sections of brains from wild-type controls, IV treated K14-lnl/lnl mice and P14 untreated *Gba1* knock-out animals were stained for calbindin and light microscopy images were taken (**Figure 47D**). The pictures showed that while wild-type brain was characterized by ordered elongating Purkinje cells, in the treated brain neurons displayed a more arborising phenotype. There was no evident loss of neuron loss in cerebellar tissue form treated animals, however only few dispersed Purkinje cells were identified in the brain of untreated mice.

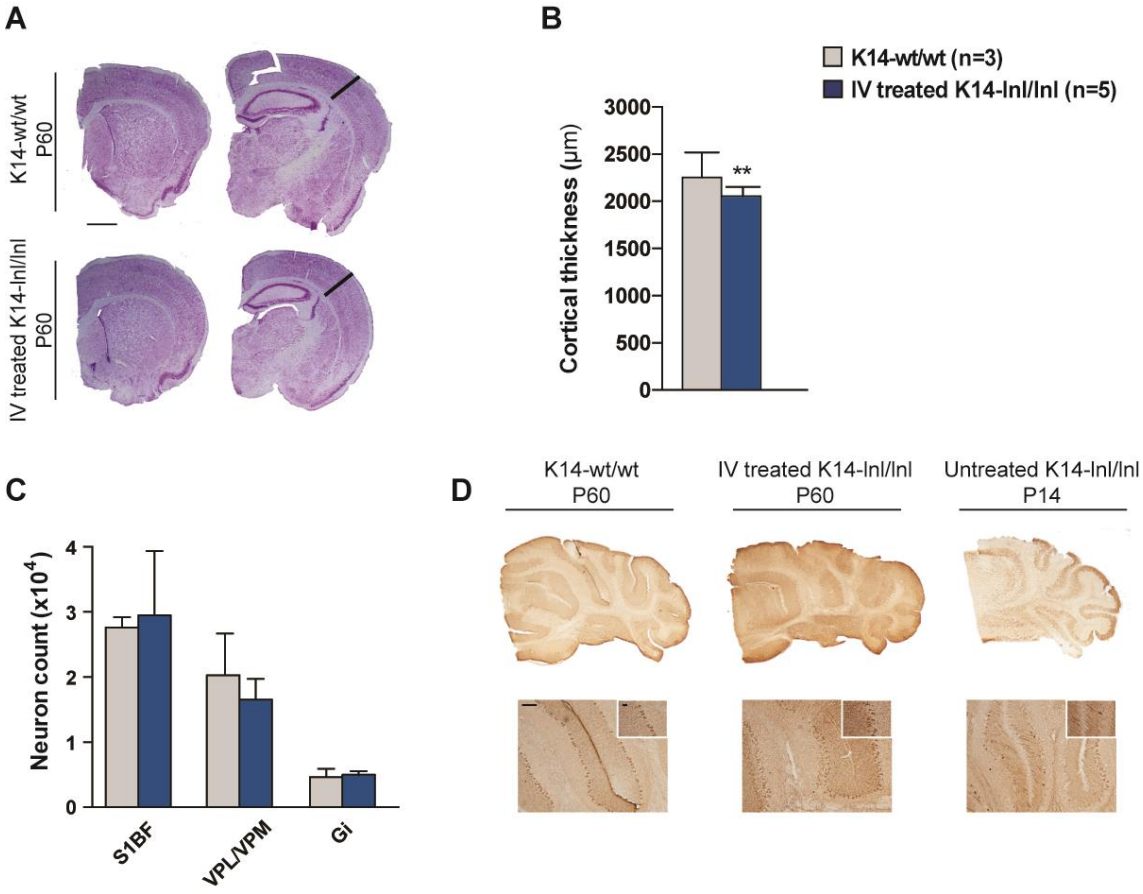

Figure 47 - Analysis of neurodegeneration following gene therapy.

A Brain sections from wild-type controls and treated K14-lnl/lnl mice stained with the Nissl method. Treated brains did not display ventriculomegaly (Scale bar: 1mm). **B** Cortical thickness measurements in wild-type and IV treated knock-out mice. Treated K14-lnl/lnl mice showed mild, although significant cortical atrophy compared to controls (Data presented as average $\pm$ SD. Statistical analysis: unpaired t test, Welch's correction; ** $p \leq 0.01$). **C** Neuron count showed that K14-lnl/lnl treated mice did not develop significant neurodegeneration. The number of neurons in cortex, thalamus and brain stem demonstrated that treated brains were not subject to neuronal loss (Data presented as average $\pm$ SD. Statistical analysis: two-wayANOVA, Tukey's multiple comparisons test; ns $p > 0.05$). **D** Calbindin staining of cerebellar sections. In IV treated brains there was no significant Purkinje neuron loss, as opposed to samples form untreated K14-lnl/lnl (Scale bars: low magnification 100µm; high magnification 60µm).

5.4.8. Effects of gene therapy on the visceral pathology

The results of the reported gene study on visceral transduction following administration of the ssAAV2/9.hSynI.*eGFP*.WPRE.hGHpA vector showed that the transgene expression under control of a neuron-specific promoter is not extremely efficient. Although many transduced cells were identified in the liver of injected mice, much lower levels were detected in the heart, spleen and lungs. In order to evaluate if the visceral pathology in K14-lnl/lnl mice was ameliorated, possibly through the cross-correction mechanism, liver, spleen, lung and heart tissues were examined.

As splenomegaly is one of the first and most common systemic manifestations, the size of the spleen of nine weeks old treated mice was measured (**Figure 48A**). The animals that received gene therapy did not develop organomegaly, as the average weight of the spleens from treated mice was comparable to the spleen size of wild-type controls.

The administration of the ssAAV2/9.hSynI.*hGBA1*.WPRE.hGHpA vector to neonatal mice improved both the spleen and the liver pathology. The immunohistochemical staining of the macrophagic marker CD68 (**Figure 48C**) showed that tissues from IV treated K14-lnl/lnl mice were not characterised by the accumulation of enlarged macrophages. The amelioration of the pathology in spleen and liver of treated mice was more evident when tissue from nine-weeks-old treated animals where compared to young P14 *Gba1* knock-out mice: in fact, samples from untreated K14-lnl/lnl mice were characterised by extensive infiltration of activated macrophages. Gaucher cells were widely present in heart sections from knock-out mice. Administration of the vector resulted in partial amelioration of macrophage activation: few enlarged macrophages were observed in the heart from IV treated K14-lnl/lnl mice. Unfortunately, gene therapy did not have substantial beneficial effect on the lungs of treated mice, as many CD68 positive cells were identified in the tissue sections.

The improvement of the visceral pathology in treated mice was then confirmed by quantitative threshold imaging of the CD68 staining on serial sections of the organs (**Figure 48B**). The reduction of CD68-positive cells in treated liver ($p=0.02$) and spleen ($p=0.0002$) tissues was significant compared to younger untreated *Gba1* knock-out

samples. Although the difference in macrophagic activation in the lung was not statistically significant when comparing wild-type controls and treated mice, an increase in CD68 staining was observed under the light microscope in treated tissue (**Figure 48C**). Finally, statistical evaluation did not highlight any significant difference in the analysis of heart tissue.

Tissue integrity and architecture was assessed on tissue sections stained with hematoxilyn and eosin dye (**Figure 48D**). While liver tissue from wild-type controls and IV treated K14-lnl/lnl mice appeared very similar, liver sections from untreated knock-out mice were characterised by extensive infiltration of Gaucher cells. These enlarged cells presented expanded cytoplasmic compartment and interfere with tissue structure. Although the staining of CD68 underlined the presence of many activated macrophages in the spleen of untreated mice, H&E staining did not reveal the presence of engorged Gaucher cells. On the contrary, enlarged macrophages were identified in lung sections from IV treated *Gba1* knock-out mice. This result confirmed the previous finding, demonstrating that the administration of the vector resulted in insufficient transduction of lung tissue. Heart sections did not appear to be characterised by Gaucher cells.

Finally, the enzymatic activity of β-glucocerebrosidase in the viscera following administration of the ssAAV2/9.hSynI.*hGBA1*.WPRE.hGHpA vector was measured (**Figure 48E**). Although the enzymatic activity was not normalised to the wild-type levels, β-glucocerebrosidase activity increased in treated mice compared to untreated *Gba1* knock-out animals. GCase residual activity remained significantly lower ($p<0.0001$) than the normal range in livers of treated mice (8%), while β-glucocerebrosidase activity in spleen samples was 43% of the wild-type level. Inefficient transduction of lung and heart following administration of the vector resulted in low residual enzymatic activity (7%) in organs harvested from treated mice.

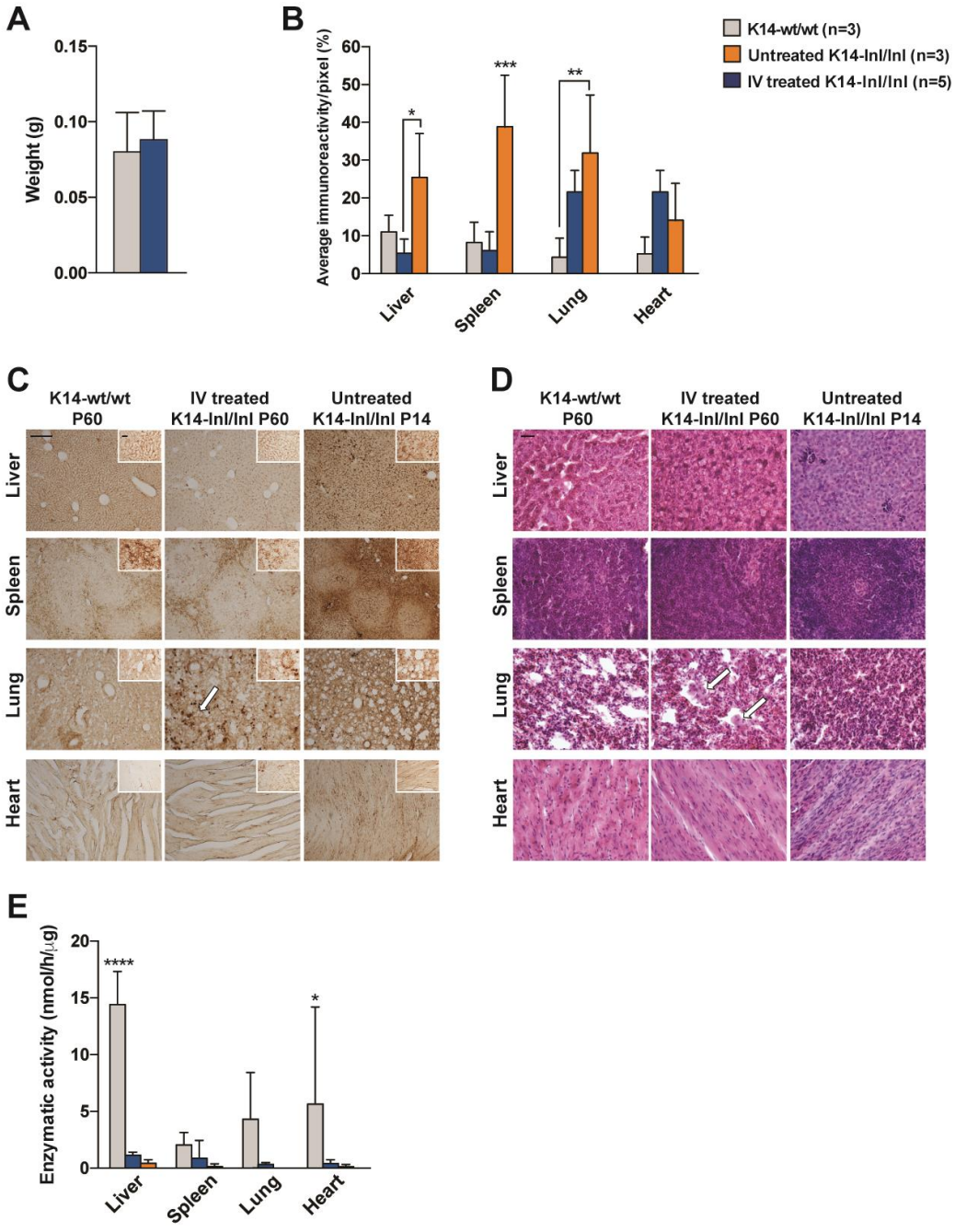

Figure 48 - Analysis of visceral pathology following gene therapy administration.

A Spleen weight. IV treated mice did not develop splenomegaly at 9 weeks of age (Data presented as average ± SD. Statistical analysis: unpaired t test, Welch's correction; ns $p>0.05$). **B** Quantification of immunohistochemical staining for the macrophagic marker CD68. Tissues from treated mice were not characterized by infiltration of activated macrophages. No significant difference between treated and untreated K14-lnl/lnl mice was found in heart tissue (Data presented as average ± SD. Statistical analysis: two-wayANOVA, Tukey's multiple comparisons test; * $p\leq0.05$, ** $p\leq0.01$, *** $p\leq0.001$). **C** CD68 staining of tissue sections. Lung

samples from treated mice presented numerous activated macrophages (indicated by white arrow), while spleen and liver samples resulted in the clearance from engorged macrophages (Scale bar: 200μm). **D** H&E staining. Gaucher cells were found in lung tissue harvested from treated mice. The other tissues were not characterized by Gaucher cells infiltration (Scale bar: 200μm). **E** GCase enzymatic activity was measured in tissue samples. Although β-glucocerebrosidase activity in treated animals was increased compared to untreated K14-lnl/lnl mice, the residual enzymatic levels were not restored to physiological values (Data presented as average $\pm$ SD. Statistical analysis: two-wayANOVA, Tukey's multiple comparisons test; * $p \leq 0.05$, **** $p < 0.0001$).

5.5. Conclusions

The work presented in this chapter described the design, testing and administration of a novel adeno-associated viral vector suitable for the treatment of neuronopatic Gaucher disease.

First, a novel single-stranded vector was designed and a reporter gene study was conducted. In the expression cassette the *eGFP* gene was cloned downstream the human synapsin I promoter sequence. The Kozak sequence was incorporated at the 5' end of the gene, while the viral enhancer element WPRE was cloned at the 3' end in order to amplify the efficiency of transgene expression in *in vivo* studies. The ssAAV2/9.hSynI.*eGFP*.WPRE.hGHpA vector was successfully produced at a titre of 5.2×10^{12} vp/ml. Consequently, the vector was intravenously administered at a dose of 2×10^{11} vp to neonatal wild-type mice. The animals were sacrificed one month after in order to study the transgene expression in the central nervous system and the visceral organs. The administration of the viral vector resulted in widespread and intense expression of the eGFP protein throughout the whole brain. In addition, confocal images demonstrated that synapsin is a strong neuron-specific promoter. The systemic administration of the ssAAV2/9.hSynI.*eGFP*.WPRE.hGHpA vector provided transduction of hepatocytes and transgene expression in the spleen, lung and heart of injected mice, albeit at much lower levels.

The results of the reporter gene study were sufficient to confirm the potential use of the

viral vector for the treatment of Gaucher disease. Therefore the human *GBA1* gene was cloned into the cassette and the expression plasmid was tested *in vitro* with the aim of determine whether (i) the synapsin promoter could efficiently drive the expression of the β-glucocerebrosidase gene and (ii) the resulting protein was catalytically active. Cell transfection with the plasmid resulted in considerable overexpression of the enzymatically active β-glucocerebrosidase protein. In order to further increase the transgene expression, the codon optimised version of the *GBA1* gene was cloned into the vector plasmid and the efficiency of expression was tested *in vitro*. Western blot analysis showed that the use of the codon optimised sequence did not improve gene expression in transfected cells. Therefore the initial expression plasmid carrying the wild-type sequence of the *GBA1* gene was used to produce the ssAAV2/9.hSynI.*hGBA1*.WPRE.hGHpA adeno-associated viral vector. The virus was injected intravenously into wild-type mice at day of birth and any toxic effect of β-glucocerebrosidase overexpression in the brain was assessed. One month after injection the animals were sacrificed and the brain was analysed for pathology. The widespread overexpression of β-glucocerebrosidase did not cause a neuroinflammatory response in injected mice.

At this point the ssAAV2/9.hSynI.*hGBA1*.WPRE.hGHpA vector was demonstrated to be efficient and safe, therefore a high dose of 2.4 x 10^{12} viral particles was administered to neonatal K14-lnl/lnl *Gba1* knock-out mice. Gene therapy resulted in a significant extension in the lifespan of treated animals, normalisation of body weight and amelioration of most of the locomotor and behavioural indexes. The mice were sacrificed at 63 days of age, for reasons unrelated to the treatment. Consequently, the brain was extensively analysed. The administration of the vector caused widespread overexpression of β-glucocerebrosidase in neurons of treated mice. This resulted in complete prevention of a microglia-mediated inflammatory response. Lysosomal accumulation was also normalised. In addition, significant reduction of astrocyte-mediated inflammatory response was observed in the cortex and thalamus, while the cerebellum and brain stem showed only a partial amelioration in astrocyte activation. The overall positive effect of gene therapy in the brain of treated mice was evident when the neuron count was measured. In fact, the number of neurons in the cortical region S1BF, the thalamic nuclei area and the brain stem were comparable to those numbers measured in age-matched wild-type control mice. Moreover, no evident

reduction in the number of Purkinje neurons in the cerebellum of treated mice was observed. However, atrophy of the cortical layer was detected.

Finally, the effects of the systemic administration of gene therapy on the viscera were assessed. As expected, the pathology was reverted in liver and spleen. The tissues did not present enlarged Gaucher cells and the levels of activated macrophages were reduced to the wild-type levels. Also, treated mice did not develop splenomegaly. However, lung tissue was characterised by the presence of many activated macrophages. These results were supported by the analysis of the β-glucocerebrosidase activity in the homogenised tissues. High levels of residual enzymatic activity were found in the spleen of treated mice. In the liver samples the β-glucocerebrosidase activity was 8% of the wild-type normal level; however, this minimal residual activity was sufficient to improve the pathology in the organs of treated *Gba1* knock-out mice. Although enzyme levels in lung and heart tissue were relatively low, the enzymatic activity in tissue from treated animals was still greater than the untreated knock-out controls.

6. Discussion

6.1. Overview

Loss-of-function mutations in the *GBA1* gene lead to Gaucher disease. The more severe mutations result in the neuronopathic type II and type III forms of the disease. There is currently no treatment for the lethal neurodegeneration observed in these patients. Type II is acute and children may die at any time between the perinatal period to a maximum of 2 years of age. A host of visceral manifestations of the disease are also present, the most prominent being hepatosplenomegaly. There is an overwhelming need to develop a novel therapy that addresses the lethal neurodegeneration and preferably also the visceral symptoms.

The aim of the present work is to develop a comprehensive pre-clinical study on intravenously administered gene therapy for neuronopathic Gaucher disease. The rationale behind the study is based on the hypothesis that a single intravenous administration of a viral vector carrying the functional human *GBA1* gene to a knock-out mouse model can potentially improve both the visceral and neurological pathology.

This study provides proof-of-concept that intravenously administered AAV9 vectors that carry a therapeutic copy of the *GBA1* gene can cross the blood-brain barrier and (i) rescue the mouse model from neonatal lethality, (ii) ameliorate neurolopathology, (iii) provide significant increase in lifespan, from 14 days to at least 180 days old and (iv) improve visceral symptoms and pathology.

6.2. Intravenously administered AAV9 gene therapy can rescue an acute neonatal lethal mouse model of neurodegeneration

The mouse model used in this preclinical study does faithfully recapitulate many of the neurological and visceral manifestations of the disease. The neurological component is lethal and while the administration of the AAV9 vectors used in this study does not represent a 'cure', the therapeutic effect is significant, as there is amelioration of the brain pathology sufficient to provide significant long-term extension on lifespan and indices of quality of life.

The only other therapeutic strategy that has shown effect in this K14-lnl/lnl mouse model has been employed in other studies investigating the effects of the administration of a glusosylceramide synthase inhibitor on survival and neuropathology (Cabrera-Salazar et al., 2012). 12 *Gba1* knock-out mice were injected into the peritoneal cavity daily from P4, and 13 were injected into the lateral ventricles at P1, P2 and P3, in combination with intraperitoneal administration from P4. The treatment resulted in reduction of the substrate accumulation, microglial activation and astrogliosis in the central nervous system of administered mice. However the average lifespan of the treated mice increased only by 4 days when the compound was injected intraperitoneally, and 12 days following combination therapy. Therefore, a minimally invasive intravenously administered gene therapy that extends the lifespan of the mice from 14 days to at least 180 days is a major step forward towards developing a treatment for neuronopathic Gaucher disease.

A further consideration is that the K14-lnl/lnl mouse model is one of the most severe and aggressive viable mouse models of a metabolic neurodegenerative disease. To date, it is the most severe mouse model of any neurodegenerative disease to be treated with gene therapy. Any therapeutic success in this model is significant and does suggest that this approach will be beneficial in any number of less acute neurological conditions.

6.3. Amelioration of neuropathology in the K14-lnl/lnl mouse model following intravenous AAV9-mediated gene therapy

The neuropathological analysis on treated mice confirmed that it was possible to ameliorate the acute neurological symptoms in the brain of K14-lnl/lnl mice. The intravenous administration of the vector resulted in overexpression of the human *GBA1* gene in widespread brain regions. Of particular interest is the significant improvement of the brain stem in the pathological markers considered in the study. This brain region is responsible for the conduction of nerve signals between the spinal cord and the brain. It collects the projections originating from the midbrain and provides the motor and sensory innervation to the body through the cranial nerves (Kandel, 2012). The brain stem, and in particular the gigantocellular nuclei region (Gi), plays a fundamental role in the control of swallowing and breathing reflexes. While amelioration in the pathology in a variety of brain regions may cumulatively contribute to preventing neurodegeneration-associated death, the restoration of the endogenous levels of functional glucocerebrosidase in the Gi and prevention of pathology may play a major role in contributing to the increase in lifespan of the animals. Indeed, while a number of factors may contribute, brainstem degeneration leading to aspiration and subsequent pneumonia is one of the ultimate cause of death in type II Gaucher Disease patients (Gupta et al., 2011).

6.4. A single-stranded AAV9 vector that includes the synapsin promoter and the WPRE element is the preferred construct for treating type II neuronopathic Gaucher disease

The first part of the current work demonstrated that the administration of an adeno-associated virus carrying the functional *GBA1* gene increased lifespan of treated animals and improved the visceral pathology. However, the scAAV2/9.GUSB.*hGBA1*.bGHpA vector did not completely address the widespread and acute neurodegeneration when administered systemically. Therefore, a more efficient vector with specific neuronal tropism was designed in order to improve the transgene expression in the central

nervous system. It is well established that neuronopathic forms of Gaucher disease are characterised by widespread neuronal loss (Wong et al., 2004). The involvement of neurons as cause of brain pathology has been also demonstrated in a Gaucher mouse model (Enquist et al., 2007). For this reason, specific targeting of neuronal cells in the affected brains was thought to be essential to improve the efficiency of the treatment. The human synapsin I promoter has been successfully used in gene delivery studies and it was proven to mediate strong and neuron-specific gene expression (Jackson et al., 2016). The use of a neuronal promoter in combination with the inclusion of enhancing sequences like the Kozak fragment and the WPRE element, made the ssAAV2/9.hSynI.*eGFP*.WPRE.hGHpA the optimal vector for gene delivery to neurons and the central nervous system. Although self-complementary adeno-associated viruses mediate a more rapid transduction than the single-stranded vectors (McCarty et al., 2001), the introduction of enhancing elements compensates for the reduced efficiency of ssAAVs. The WPRE element was already known to enhance transgene expression *in vitro* (Loeb et al., 1999). More recently, it has been demonstrated that the intravenous administration of a single-stranded adeno-associated virus expressing *eGFP* and carrying the WPRE sequence resulted in increase of transgene expression (Mattar et al., 2015).

The systemic administration of the ssAAV2/9.hSynI.*eGFP*.WPRE.hGHpA to neonatal wild-type mice resulted in widespread and intense transduction of the central nervous system, demonstrating that the vector was able to efficiently deliver the transgene to the brain when injected intravenously. The virus tropism was neuron-specific and eGFP expression was detected throughout the whole brain.

The advantage of the systemic route of administration relies on the ability of AAV to cross the blood-brain barrier. Since neuronopathic forms of Gaucher disease are characterised by both brain and visceral pathology, a single intravenous injection could address both manifestations. The administration of ssAAV2/9.hSynI.*eGFP*.WPRE.hGHpA resulted in efficient liver transduction and more moderate transgene expression in the spleen, lung and heart. These results were not surprising, considering the facts that (i) the synapsin I protein is expressed in hepatocytes (Bustos et al., 2001) and (ii) the transgene expression was driven by a neuron-specific sequence and not a ubiquitous promoter. The liver-directed gene

therapy for haemophilia demonstrated that targeting of hepatocytes results in the increase of enzyme levels in the blood stream, since the liver is a crucial organ for the major metabolic pathways. Efficient transduction of liver tissue could therefore be beneficial for increasing β-glucocerebrosidase levels in other visceral organs.

The systemic administration of the ssAAV2/9.hSynI.*hGBA1*.WPRE.hGHpA vector to *Gba1* knock-out mice successfully rescued the ultimately fatal neuropathology, resulting in an extension of lifespan and improvement in behaviour and quality of life in the treated mice. The overexpression of glucocerebrosidase in neurons resulted in the reduction of astrogliosis and the microglia-mediated inflammatory response. This observation might seem to contrast the pathological mechanism proposed by Vardi and colleagues (Vardi et al., 2016). In fact, the study demonstrated that in the chemical-induced Gaucher mouse model neuroinflammation precedes neuronal loss. However, our study shows that the rescue of neurons alone has a therapeutic effect on both astrocytes and microglia. In light of these findings, two hypotheses on the therapeutic mechanism of the gene therapy treatment can be proposed: (i) correcting the genetic defect in neurons could prevent the fatal neurodegeneration and neuronal loss, consequently averting the activation of neuroinflammatory responses; (ii) neighbouring cells can uptake the secreted glucocerebrosidase enzyme following *GBA1* overexpression in neurons through the cross-correction mechanism, and this results in amelioration of neuroinflammation and microglia activation.

The brain-targeted gene therapy only partially ameliorated the visceral manifestations. Although the liver could serve as metabolic factory for the production of glucocerebrosidase following ssAAV2/9.hSynI.*hGBA1*.WPRE.hGHpA administration, the levels of circulating enzyme were not sufficient to appreciate a significant amelioration of the pathology in other organs.

Overall, although the treatment might not completely cure the visceral symptoms, a possible clinical use of the vector should be taken in consideration. There is currently no available therapy for the devastating neurodegeneration in Gaucher patients, while the visceral pathology characteristic of type I is successfully rescued by enzyme replacement therapy. Evidently, further research is needed in order to improve the gene

delivery treatment; nonetheless a combination therapy with ERT or another vector may be extremely beneficial and should be considered.

6.5. Clinical precedent for intravenously administered AAV9 gene therapy for neurological diseases

AAV9 is known to be highly efficient at transducing neurons (Foust et al., 2009). However, the finding that it also has the ability to cross the blood-brain barrier has already had a significant impact on the neurological gene therapy field. Since the original pre-clinical studies of intravenously administered AAV9 to rescue a mouse model of spinal muscular atrophy, a clinical trial has been initiated at the Nationwide Children's Hospital in the USA (NCT02122952). While this study is ongoing, the initial reports have been remarkable with significant improvements in locomotor function in treated children (unpublished work (Mendell, 2016a)).

Like Gaucher disease, CLN3 Batten disease is a neurodegenerative lysosomal storage disorder. A recent pre-clinical study published in 2016 reported partial correction of pathology in a mouse model following intravenous administration of an AAV9 vector (Bosch et al., 2016). Abeona Therapeutics have recently been granted FDA Orphan Drug designation to start a clinical trial for this condition. Therefore, there is clinical precedent for intravenously administered AAV9 in the clinic and this is being pursued by other studies. Gaucher disease is, arguably, an easier target than CLN3 Batten disease. This is on the basis that the CLN3 protein is membrane bound within the cell and so there is no real possibility for cross-correction of surrounding cells and much higher levels of gene delivery efficiency may be required. Glucocerebrosidase is a soluble enzyme that could mediate cross-correction of untransduced neighbouring cells and so amplifying the therapeutic efficacy.

Although the main focus of this study has been on developing an intravenous approach for systemic effect, the data show that a direct intracerebroventricular injection of vector also rescues the Gaucher disease mouse model from neonatal lethality. However, the visceral pathology persists and splenomegaly is observed. While there is a case for

combining intracerebroventricular mediated gene therapy to treat the brain and also administering enzyme replacement therapy for the duration of the patients life to treat the visceral organs, this would be hugely expensive. The cost of intravenous gene therapy will be high, but as a one-time treatment it is very likely to be more economical in the long-term than a lifetime of enzyme replacement therapy.

The two different routes of administration used in this study may have consequences for potential clinical trial design. At present, there is debate in the gene therapy community as to whether IV administration of therapeutic AAV vectors is preferable over direct administration to the CSF in clinical trials for other neurodegenerative lysosomal storage diseases. In those diseases where the defective protein is membrane-bound or structural, and so no cross-correction is available, is the ability of AAV9 to cross the BBB efficient enough in humans to have a significant effect? An example of this is a future clinical trial for neurodegenerative CLN3 Batten disease in which the patients will receive an intravenous administration of an AAV9 vector. In contrast, a clinical trial for neurodegenerative CLN6 Batten disease, that also involves a defective membrane bound protein, the patients will receive the AAV9 vector delivered to the CSF via intrathecal administration (NCT02725580). The case for intravenous administration in any future translation of this gene therapy study for neuronopathic Gaucher disease is stronger due to the added advantage of the soluble nature of the glucocerebrosidase protein, allowing for cross-correction. In addition, the systemic administration can address the more profound visceral diseases that accompanies the neurological pathology.

6.6. Final considerations

The first part of the present work showed that, while improvements to the central nervous system transduction were needed, the intravenous administration of the vector had a clear benefit of targeting both the brain and the visceral organs. The reduction in spleen weight and the substantial amelioration of cytopathology in the spleen, liver and lungs were encouraging results. The improvements in the visceral pathology were further demonstrated in the long-term study, where the systemic disease progressed with time in ICV treated mice, resulting in splenomegaly and severe accumulation of

Gaucher cells in the tissues.

The use of a neuron-specific promoter prevented neurodegeneration and rescued the mice from the deadly neuropathology. Conversely, the effects on the visceral pathology were less evident. Unfortunately, because of the scarce availability of *Gba1* knock-out mice, it was not possible to administer the ssAAV2/9.hSynI.*hGBA1*.WPRE.hGHpA vector into the brain of neonatal mice and perform a comparative analysis. Arguably, the direct injection of the neuronal-specific vector would result in reversion of the neurodegeneration, while simultaneously allowing the progression of the visceral symptoms.

Taken together these data have provided a critical insight on the effects of systemic gene therapy for the treatment of neuronapathic Gaucher disease. The intravenous administration of a vector expressing a strong yet ubiquitous promoter could result in widespread enzyme activity, sufficient to ameliorate both the critical neurodegeneration and the visceral pathology. As already mentioned, the possibility of combination therapy administration should also be considered. This could offer two different therapeutic options. First, an intravenous administration of vector with a neuron specific promoter like synapsin to treat the brain and partially treat the visceral organs but with additional supplementation of reduced doses of ERT. This could partially reduce the cost of enzyme replacement therapy. Second, the possibility of using two different viral vectors can be explored. The systemic administration of one viral vector with wide tropism utilising a ubiquitous promoter could be used to treat the visceral manifestations, while a second strong neuron vector injected into the lateral ventricles can rescue the severe neuropathology. Although the double administration would be simultaneous, a possible host immune response should be taken in consideration.

The positive effects of gene therapy on the visceral pathology may also be beneficial for type I patients. As previously mentioned, the current treatment for Gaucher disease type I patients are a considerable burden. On the contrary, a single injection of the viral vector may result in an efficient and definitive amelioration of the disease. In addition, the ability of the AAV2/9 vector to transduce the bones when administered systemically (Rahim et al., 2011) could improve the mild effects of enzyme replacement therapy on

bone crisis pathology and pain in type I patients (Charrow et al., 2007).

The partial clearance of Gaucher cells in the organs demonstrated the potential beneficial effects of systemic gene therapy in the viscera. However, the histological analysis did not entirely reflect the evaluation of the enzymatic activity. With the iteration of the current protocol, the assay can efficiently detect a significant difference in the GCase activity in the blood of knock-out animals compared to wild-type or heterozygote mice, yet it is not able to differentiate with certainty more subtle dissimilarities. This might be improved with a higher powered study and further optimisation of the assay.

While the pathology presented by the K14-lnl/lnl mice reflects the human symptoms, the premature death of the animals due to the acute and rapid neurodegeneration required an early intervention. Since the time window for treatment was narrow, the administration to neonates was necessary. Although a prenatal diagnosis test to identify autosomal founder mutations has been recently proposed (Zeevi et al., 2015), in the current clinical practise an accurate diagnosis is frequently delayed and subjects might not be identified before the first few months of age (Grabowski, 2008). Therefore, the administration of the treatment at day of birth is currently not reliably feasible in human patients in the absence of a national/international new born screening programme, or unless there is a family history of the disease with an already affected sibling. However, the purpose of this study was to provide proof-of-concept evidence on the viability of systemic gene therapy for the treatment of neuronopathic Gaucher disease. The use of subsequent animal models may be useful to determine whether a later intervention can lead to equally promising outputs. Different mouse models, such as the CBE induced model present the advantage of potentially inducing the disease later and assessing intervention in older animals (Vardi et al., 2016).

6.7. Future perspective

The optimisation of novel vectors would be a main objective of future studies. Different vectors carrying powerful ubiquitous promoters will be produced and their effects on

the neurological and visceral pathology of knock-out mice will be assessed. Two potential candidates are the chicken β-actin promoter which has also being used in clinical trials for Batten Disease (NCT02725580), and the CAG promoter which is used in the spinal muscular atrophy clinical trial (NCT02122952) and is known to mediate high levels and long-term transgene expression (Gray et al., 2011). The synthetic sequence is 1.6kb long and comprises the cytomegalovirus enhancer element, the first part of the chicken β-actin promoter and the 3' splice sequence of the rabbit β-globin gene (Miyazaki et al., 1989).

Recent advances in capsid engineering have allowed the creation of novel viral particles with enhanced tropism to specific cell types. In one prominent example, Deverman and colleagues have developed a cell-type-specific capsid selection technique and thereby identified engineered AAV capsids that transduce the brain and the spinal cord of adult mice following systemic administration with high efficiency (Deverman et al., 2016, Chan et al., 2017). The two AAV-PHP.B and AAV-PHP.eB variants showed high efficiency in transducing the CNS following intravenous injection of low dose vector, resulting in improved CNS tropism and 40-fold increase in gene expression, compare to standard AAV9. The use of these novel vectors will significantly enhance brain transduction while substantially reducing the viral load. It is evident that this could have major impact on the availability of the vector and production costs.

The optimisation of the capsid selection system is based on the transduction efficiency of neurons in adult mice. However, these novel AAV variants have not been tested on non-human primates yet. The prediction of cellular tropism and transduction efficiency in humans based on pre-clinical animal studies has not always met the expectations in the clinical application. An example of this is the use of an AAV8-based vector for the treatment of haemophilia (Lisowski et al., 2015). While AAV8 is able to transduce almost 100% of liver cells when administered to mice and non-human primates, only a small percentage of the human hepatocytes expresses the transgene. Although the low dose of reconstituted enzyme is sufficient to provide a therapeutic effect on treated patients, a more specific human tropism needs to be achieved. Therefore, novel capsid variants require further investigation in other species before being applied to the clinical practice.

6.8. Conclusion

The results reported in this work demonstrated that viral gene delivery is a potential therapeutic option for the treatment of neuronapathic Gaucher disease. The advantage of this approach is that a single systemic injection of the vector can ameliorate both the visceral pathology and the fatal neuropathology of the K14-lnl/lnl mouse model. Two different adeno-associated viral vectors have been tested, the administration of which resulted in significant extension of the lifespan of treated mice. The different design of each vector reflected their distinctive therapeutic characteristics. The scAAV2/9.GUSB.*hGBA1*.bGHpA vector mediated the ubiquitous expression of the *GBA1* gene following intravenous administration to neonatal mice. While the neuropathology was only partially ameliorated, the visceral manifestations noticeably benefited from the treatment. A second vector was produced with the intent of improve the central nervous system transduction following systemic administration, since there is currently no available cure for the devastating neuropathology that characterises Gaucher disease type II. As expected, the administration of the neuron-specific ssAAV2/9.hSynI.*hGBA1*.WPRE.hGHpA vector successfully prevented the neurodegeneration and rescued the mice from premature death.

The present work, together with the significant and recent advances in the field, validated the use of viral gene therapy for the treatment of genetic diseases for which there is currently no cure. Although it is an extremely long and challenging process, the unmet need of a life-saving treatment for rare neurological lysosomal storage disorders has to be addressed. Further enhancement in gene therapy will improve the translation from academic research to clinic application. However, the major obstacles in developing a gene therapy treatment remain the prohibitive cost of the production process and the availability of highly specialised centres. More research needs to be carried out in order to facilitate the development of novel and efficacious therapies. This will possibly result in reduction of the manufacture and commercialisation costs, rendering gene therapy an attractive treatment option for a wider range of diseases.

Bibliography

ADACHI, M., WALLACE, B. J., SCHNECK, L. & VOLK, B. W. 1967. Fine structure of central nervous system in early infantile Gaucher's disease. *Arch Pathol,* 83**,** 513-26.

BADDELEY, A. J., GUNDERSEN, H. J. & CRUZ-ORIVE, L. M. 1986. Estimation of surface area from vertical sections. *J Microsc,* 142**,** 259-76.

BAILEY, K. R. C., J. N. 2009. Anxiety-related behaviors in mice. *In:* JJ, B. (ed.) *Methods of behavior analysis in neuroscience.* Boca Ranton (FL): CRC Press/Taylor & Francis.

BARNEVELD, R. A., KEIJZER, W., TEGELAERS, F. P., GINNS, E. I., GEURTS VAN KESSEL, A., BRADY, R. O., BARRANGER, J. A., TAGER, J. M., GALJAARD, H., WESTERVELD, A. & REUSER, A. J. 1983. Assignment of the gene coding for human beta-glucocerebrosidase to the region q21-q31 of chromosome 1 using monoclonal antibodies. *Hum Genet,* 64**,** 227-31.

BARTON, N. W., BRADY, R. O., DAMBROSIA, J. M., DI BISCEGLIE, A. M., DOPPELT, S. H., HILL, S. C., MANKIN, H. J., MURRAY, G. J., PARKER, R. I., ARGOFF, C. E. & ET AL. 1991. Replacement therapy for inherited enzyme deficiency--macrophage-targeted glucocerebrosidase for Gaucher's disease. *N Engl J Med,* 324**,** 1464-70.

BARTUS, R. T., WEINBERG, M. S. & SAMULSKI, R. J. 2014. Parkinson's disease gene therapy: success by design meets failure by efficacy. *Mol Ther,* 22**,** 487-97.

BELMATOUG, N. S., J. 2012. *Gaucher Disease* [Online]. Available: http://www.orpha.net/consor4.01/www/cgi-bin/OC_Exp.php?lng=EN&Expert=355.

BERNS, K. I. & GIRAUD, C. 1996. Biology of adeno-associated virus. *Curr Top Microbiol Immunol,* 218**,** 1-23.

BITTON, A., ETZELL, J., GRENERT, J. P. & WANG, E. 2004. Erythrophagocytosis in Gaucher cells. *Arch Pathol Lab Med,* 128**,** 1191-2.

BLOM, S. & ERIKSON, A. 1983. Gaucher disease--Norrbottnian type. Neurodevelopmental, neurological, and neurophysiological aspects. *Eur J Pediatr,* 140**,** 316-22.

BOHLEGA, S., KAMBOURIS, M., SHAHID, M., AL HOMSI, M. & AL SOUS, W. 2000. Gaucher disease with oculomotor apraxia and cardiovascular calcification (Gaucher type IIIC). *Neurology,* 54**,** 261-3.

BOSCH, M. E., ALDRICH, A., FALLET, R., ODVODY, J., BURKOVETSKAYA, M., SCHUBERTH, K., FITZGERALD, J. A., FOUST, K. D. & KIELIAN, T. 2016. Self-Complementary AAV9 Gene Delivery Partially Corrects Pathology Associated with Juvenile Neuronal Ceroid Lipofuscinosis (CLN3). *J Neurosci,* 36**,** 9669-82.

BOSCH, M. E. & KIELIAN, T. 2015. Neuroinflammatory paradigms in lysosomal storage diseases. *Front Neurosci,* 9**,** 417.

BOUSTANY, R. M. 2013. Lysosomal storage diseases--the horizon expands. *Nat Rev Neurol,* 9**,** 583-98.

BOUSTANY, R. M. M., T. 2007. . *In:* RIMOIN, D. (ed.) *Emery and Rimoin's Principles and Practice of Medical Genetics* Elsevier.

BOUTIN, S., MONTEILHET, V., VERON, P., LEBORGNE, C., BENVENISTE, O., MONTUS, M. F. & MASURIER, C. 2010. Prevalence of serum IgG and neutralizing factors against adeno-associated virus (AAV) types 1, 2, 5, 6, 8, and 9 in the healthy population: implications for gene therapy using AAV vectors. *Hum Gene Ther,* 21**,** 704-12.

BRADBURY, A. M., GRAY-EDWARDS, H. L., SHIRLEY, J. L., MCCURDY, V. J., COLACO, A. N., RANDLE, A. N., CHRISTOPHERSON, P. W., BIRD, A. C., JOHNSON, A. K., WILSON, D. U., HUDSON, J. A., DE POMPA, N. L., SORJONEN, D. C., BRUNSON, B. L., JEYAKUMAR, M., PLATT, F. M., BAKER, H. J., COX, N. R., SENA-ESTEVES, M. & MARTIN, D. R. 2015. Biomarkers for disease progression and AAV therapeutic efficacy in feline Sandhoff disease. *Exp Neurol,* 263**,** 102-12.

BRADY, R. O. 2006. Enzyme replacement for lysosomal diseases. *Annu Rev Med,* 57**,** 283-96.

BROOKS, S. P. & DUNNETT, S. B. 2009. Tests to assess motor phenotype in mice: a user's guide. *Nat Rev Neurosci,* 10**,** 519-29.

BUSTOS, R., KOLEN, E. R., BRAITERMAN, L., BAINES, A. J., GORELICK, F. S. & HUBBARD, A. L. 2001. Synapsin I is expressed in epithelial cells: localization to a unique trans-Golgi compartment. *J Cell Sci,* 114**,** 3695-704.

CABRERA-SALAZAR, M. A., DERISO, M., BERCURY, S. D., LI, L., LYDON, J. T., WEBER, W., PANDE, N., CROMWELL, M. A., COPELAND, D., LEONARD, J., CHENG, S. H. & SCHEULE, R. K. 2012. Systemic delivery of a glucosylceramide synthase inhibitor reduces CNS substrates and increases lifespan in a mouse model of type 2 Gaucher disease. *PLoS One,* 7**,** e43310.

CAN, A., DAO, D. T., TERRILLION, C. E., PIANTADOSI, S. C., BHAT, S. & GOULD, T. D. 2012. The tail suspension test. *J Vis Exp***,** e3769.

CASTELHANO-CARLOS, M. J., SOUSA, N., OHL, F. & BAUMANS, V. 2010. Identification methods in newborn C57BL/6 mice: a developmental and behavioural evaluation. *Lab Anim,* 44**,** 88-103.

CASTLE, M. J., GERSHENSON, Z. T., GILES, A. R., HOLZBAUR, E. L. & WOLFE, J. H. 2014. Adeno-associated virus serotypes 1, 8, and 9 share conserved mechanisms for anterograde and retrograde axonal transport. *Hum Gene Ther,* 25**,** 705-20.

CEARLEY, C. N. & WOLFE, J. H. 2006. Transduction characteristics of adeno-associated virus vectors expressing cap serotypes 7, 8, 9, and Rh10 in the mouse brain. *Mol Ther,* 13**,** 528-37.

CHAN, K. Y., JANG, M. J., YOO, B. B., GREENBAUM, A., RAVI, N., WU, W. L., SANCHEZ-GUARDADO, L., LOIS, C., MAZMANIAN, S. K., DEVERMAN, B. E. & GRADINARU, V. 2017. Engineered AAVs for efficient noninvasive gene delivery to the central and peripheral nervous systems. *Nat Neurosci,* 20**,** 1172-1179.

CHANDLER, R. J., LAFAVE, M. C., VARSHNEY, G. K., TRIVEDI, N. S., CARRILLO-CARRASCO, N., SENAC, J. S., WU, W., HOFFMANN, V., ELKAHLOUN, A. G., BURGESS, S. M. & VENDITTI, C. P. 2015. Vector design influences hepatic genotoxicity after adeno-associated virus gene therapy. *J Clin Invest,* 125**,** 870-80.

CHANDLER, R. J., SANDS, M. S. & VENDITTI, C. P. 2017. Recombinant Adeno-Associated Viral Integration and Genotoxicity: Insights from Animal Models. *Hum Gene Ther,* 28**,** 314-322.

CHARROW, J., DULISSE, B., GRABOWSKI, G. A. & WEINREB, N. J. 2007. The effect of enzyme replacement therapy on bone crisis and bone pain in patients with type 1 Gaucher disease. *Clin Genet,* 71**,** 205-11.

CHENNA, R., SUGAWARA, H., KOIKE, T., LOPEZ, R., GIBSON, T. J., HIGGINS, D. G. & THOMPSON, J. D. 2003. Multiple sequence alignment with the Clustal series of programs. *Nucleic Acids Res,* 31**,** 3497-500.

CODERCH, L., LOPEZ, O., DE LA MAZA, A. & PARRA, J. L. 2003. Ceramides and skin function. *Am J Clin Dermatol,* 4**,** 107-29.

CONRADI, N. G., SOURANDER, P., NILSSON, O., SVENNERHOLM, L. & ERIKSON, A. 1984. Neuropathology of the Norrbottnian type of Gaucher disease. Morphological and biochemical studies. *Acta Neuropathol,* 65**,** 99-109.

COX, T., LACHMANN, R., HOLLAK, C., AERTS, J., VAN WEELY, S., HREBICEK, M., PLATT, F., BUTTERS, T., DWEK, R., MOYSES, C., GOW, I., ELSTEIN, D. & ZIMRAN, A. 2000. Novel oral treatment of Gaucher's disease with N-butyldeoxynojirimycin (OGT 918) to decrease substrate biosynthesis. *Lancet,* 355**,** 1481-5.

COX, T. M. 2001. Gaucher disease: understanding the molecular pathogenesis of sphingolipidoses. *J Inherit Metab Dis,* 24 Suppl 2**,** 106-21; discussion 87-8.

COX, T. M. 2010. Gaucher disease: clinical profile and therapeutic developments. *Biologics,* 4**,** 299-313.

COX, T. M. & CACHON-GONZALEZ, M. B. 2012. The cellular pathology of lysosomal diseases. *J Pathol,* 226**,** 241-54.

CRAWLEY, A. C. & WALKLEY, S. U. 2007. Developmental analysis of CNS pathology in the lysosomal storage disease alpha-mannosidosis. *J Neuropathol Exp Neurol,* 66**,** 687-97.

DAHL, M., DOYLE, A., OLSSON, K., MANSSON, J. E., MARQUES, A. R. A., MIRZAIAN, M., AERTS, J. M., EHINGER, M., ROTHE, M., MODLICH, U., SCHAMBACH, A. & KARLSSON, S. 2015. Lentiviral gene therapy using cellular promoters cures type 1 Gaucher disease in mice. *Mol Ther,* 23**,** 835-844.

DAVIDSON, B. L., STEIN, C. S., HETH, J. A., MARTINS, I., KOTIN, R. M., DERKSEN, T. A., ZABNER, J., GHODSI, A. & CHIORINI, J. A. 2000. Recombinant adeno-associated virus type 2, 4, and 5 vectors: transduction of variant cell types and regions in the mammalian central nervous system. *Proc Natl Acad Sci U S A,* 97**,** 3428-32.

DAYA, S. & BERNS, K. I. 2008. Gene therapy using adeno-associated virus vectors. *Clin Microbiol Rev,* 21**,** 583-93.

DAYTON, R. D., WANG, D. B. & KLEIN, R. L. 2012. The advent of AAV9 expands applications for brain and spinal cord gene delivery. *Expert Opin Biol Ther,* 12**,** 757-66.

DEACON, R. M. 2013. Measuring motor coordination in mice. *J Vis Exp***,** e2609.

DEEGAN, P. B. & COX, T. M. 2012. Imiglucerase in the treatment of Gaucher disease: a history and perspective. *Drug Des Devel Ther,* 6**,** 81-106.

DEKKER, N., VAN DUSSEN, L., HOLLAK, C. E., OVERKLEEFT, H., SCHEIJ, S., GHAUHARALI, K., VAN BREEMEN, M. J., FERRAZ, M. J., GROENER, J. E., MAAS, M., WIJBURG, F. A., SPEIJER, D., TYLKI-SZYMANSKA, A., MISTRY, P. K., BOOT, R. G. & AERTS, J. M. 2011. Elevated plasma glucosylsphingosine in Gaucher disease: relation to phenotype, storage cell markers, and therapeutic response. *Blood,* 118**,** e118-27.

DESNICK, R. J. & SCHUCHMAN, E. H. 2012. Enzyme replacement therapy for lysosomal diseases: lessons from 20 years of experience and remaining challenges. *Annu Rev Genomics Hum Genet,* 13**,** 307-35.

DEVEBER, G. A., SCHWARTING, G. A., KOLODNY, E. H. & KOWALL, N. W. 1992. Fabry disease: immunocytochemical characterization of neuronal involvement. *Ann Neurol,* 31**,** 409-15.

DEVERMAN, B. E., PRAVDO, P. L., SIMPSON, B. P., KUMAR, S. R., CHAN, K. Y., BANERJEE, A., WU, W. L., YANG, B., HUBER, N., PASCA, S. P. & GRADINARU, V. 2016. Cre-dependent selection yields AAV variants for widespread gene transfer to the adult brain. *Nat Biotechnol,* 34**,** 204-9.

DEVI, A. R., GOPIKRISHNA, M., RATHEESH, R., SAVITHRI, G., SWARNALATA, G. & BASHYAM, M. 2006. Farber lipogranulomatosis: clinical and molecular genetic analysis reveals a novel mutation in an Indian family. *J Hum Genet,* 51**,** 811-4.

DISEASE, A. W. G. O. M. O. P., KISHNANI, P. S., STEINER, R. D., BALI, D., BERGER, K., BYRNE, B. J., CASE, L. E., CROWLEY, J. F., DOWNS, S., HOWELL, R. R., KRAVITZ, R. M., MACKEY, J., MARSDEN, D., MARTINS, A. M., MILLINGTON, D. S., NICOLINO, M., O'GRADY, G., PATTERSON, M. C., RAPOPORT, D. M., SLONIM, A., SPENCER, C. T., TIFFT, C. J. & WATSON, M. S. 2006. Pompe disease diagnosis and management guideline. *Genet Med,* 8**,** 267-88.

DONSANTE, A., MILLER, D. G., LI, Y., VOGLER, C., BRUNT, E. M., RUSSELL, D. W. & SANDS, M. S. 2007. AAV vector integration sites in mouse hepatocellular carcinoma. *Science,* 317**,** 477.

DUQUE, S., JOUSSEMET, B., RIVIERE, C., MARAIS, T., DUBREIL, L., DOUAR, A. M., FYFE, J., MOULLIER, P., COLLE, M. A. & BARKATS, M. 2009. Intravenous administration of self-complementary AAV9 enables transgene delivery to adult motor neurons. *Mol Ther,* 17**,** 1187-96.

DVIR, H., HAREL, M., MCCARTHY, A. A., TOKER, L., SILMAN, I., FUTERMAN, A. H. & SUSSMAN, J. L. 2003. X-ray structure of human acid-beta-glucosidase, the defective enzyme in Gaucher disease. *EMBO Rep,* 4**,** 704-9.

ENQUIST, I. B., LO BIANCO, C., OOKA, A., NILSSON, E., MANSSON, J. E., EHINGER, M., RICHTER, J., BRADY, R. O., KIRIK, D. & KARLSSON, S. 2007. Murine models of acute neuronopathic Gaucher disease. *Proc Natl Acad Sci U S A,* 104**,** 17483-8.

ENQUIST, I. B., NILSSON, E., MANSSON, J. E., EHINGER, M., RICHTER, J. & KARLSSON, S. 2009. Successful low-risk hematopoietic cell therapy in a mouse model of type 1 Gaucher disease. *Stem Cells,* 27**,** 744-52.

ENQUIST, I. B., NILSSON, E., OOKA, A., MANSSON, J. E., OLSSON, K., EHINGER, M., BRADY, R. O., RICHTER, J. & KARLSSON, S. 2006. Effective cell and gene therapy in a murine model of Gaucher disease. *Proc Natl Acad Sci U S A,* 103**,** 13819-24.

ESCH, S. W., WILLIAMS, T. D., BISWAS, S., CHAKRABARTY, A. & LEVINE, S. M. 2003. Sphingolipid profile in the CNS of the twitcher (globoid cell leukodystrophy) mouse: a lipidomics approach. *Cell Mol Biol (Noisy-le-grand),* 49**,** 779-87.

EYAL, N., WILDER, S. & HOROWITZ, M. 1990. Prevalent and rare mutations among Gaucher patients. *Gene,* 96**,** 277-83.

FARFEL-BECKER, T., VITNER, E. B. & FUTERMAN, A. H. 2011a. Animal models for Gaucher disease research. *Dis Model Mech,* 4**,** 746-52.

FARFEL-BECKER, T., VITNER, E. B., KELLY, S. L., BAME, J. R., DUAN, J., SHINDER, V., MERRILL, A. H., JR., DOBRENIS, K. & FUTERMAN, A. H. 2014. Neuronal accumulation of glucosylceramide in a mouse model of

neuronopathic Gaucher disease leads to neurodegeneration. *Hum Mol Genet,* 23**,** 843-54.

FARFEL-BECKER, T., VITNER, E. B., PRESSEY, S. N., EILAM, R., COOPER, J. D. & FUTERMAN, A. H. 2011b. Spatial and temporal correlation between neuron loss and neuroinflammation in a mouse model of neuronopathic Gaucher disease. *Hum Mol Genet,* 20**,** 1375-86.

FERRARI, F. K., SAMULSKI, T., SHENK, T. & SAMULSKI, R. J. 1996. Second-strand synthesis is a rate-limiting step for efficient transduction by recombinant adeno-associated virus vectors. *J Virol,* 70**,** 3227-34.

FINK, J. K., CORRELL, P. H., PERRY, L. K., BRADY, R. O. & KARLSSON, S. 1990. Correction of glucocerebrosidase deficiency after retroviral-mediated gene transfer into hematopoietic progenitor cells from patients with Gaucher disease. *Proc Natl Acad Sci U S A,* 87**,** 2334-8.

FISCHER, A. H., JACOBSON, K. A., ROSE, J. & ZELLER, R. 2008. Hematoxylin and eosin staining of tissue and cell sections. *CSH Protoc,* 2008**,** pdb prot4986.

FOUST, K. D., NURRE, E., MONTGOMERY, C. L., HERNANDEZ, A., CHAN, C. M. & KASPAR, B. K. 2009. Intravascular AAV9 preferentially targets neonatal neurons and adult astrocytes. *Nat Biotechnol,* 27**,** 59-65.

FRANCO, L. M., SUN, B., YANG, X., BIRD, A., ZHANG, H., SCHNEIDER, A., BROWN, T., YOUNG, S. P., CLAY, T. M., AMALFITANO, A., CHEN, Y. T. & KOEBERL, D. D. 2005. Evasion of immune responses to introduced human acid alpha-glucosidase by liver-restricted expression in glycogen storage disease type II. *Mol Ther,* 12**,** 876-84.

FUKUDA, T., EWAN, L., BAUER, M., MATTALIANO, R. J., ZAAL, K., RALSTON, E., PLOTZ, P. H. & RABEN, N. 2006. Dysfunction of endocytic and autophagic pathways in a lysosomal storage disease. *Ann Neurol,* 59**,** 700-8.

FUTERMAN, A. H. & HARDY, J. 2016. Perspective: Finding common ground. *Nature,* 537**,** S160-1.

FUTERMAN, A. H. & VAN MEER, G. 2004. The cell biology of lysosomal storage disorders. *Nat Rev Mol Cell Biol,* 5**,** 554-65.

GAN-OR, Z., AMSHALOM, I., KILARSKI, L. L., BAR-SHIRA, A., GANA-WEISZ, M., MIRELMAN, A., MARDER, K., BRESSMAN, S., GILADI, N. & ORR-URTREGER, A. 2015. Differential effects of severe vs mild GBA mutations on Parkinson disease. *Neurology,* 84**,** 880-7.

GIROD, A., WOBUS, C. E., ZADORI, Z., RIED, M., LEIKE, K., TIJSSEN, P., KLEINSCHMIDT, J. A. & HALLEK, M. 2002. The VP1 capsid protein of adeno-associated virus type 2 is carrying a phospholipase A2 domain required for virus infectivity. *J Gen Virol,* 83**,** 973-8.

GOKER-ALPAN, O., LOPEZ, G., VITHAYATHIL, J., DAVIS, J., HALLETT, M. & SIDRANSKY, E. 2008. The spectrum of parkinsonian manifestations associated with glucocerebrosidase mutations. *Arch Neurol,* 65**,** 1353-7.

GOKER-ALPAN, O., SCHIFFMANN, R., PARK, J. K., STUBBLEFIELD, B. K., TAYEBI, N. & SIDRANSKY, E. 2003. Phenotypic continuum in neuronopathic Gaucher disease: an intermediate phenotype between type 2 and type 3. *J Pediatr,* 143**,** 273-6.

GOKER-ALPAN, O., STUBBLEFIELD, B. K., GIASSON, B. I. & SIDRANSKY, E. 2010. Glucocerebrosidase is present in alpha-synuclein inclusions in Lewy body disorders. *Acta Neuropathol,* 120**,** 641-9.

GOMBASH LAMPE, S. E., KASPAR, B. K. & FOUST, K. D. 2014. Intravenous injections in neonatal mice. *J Vis Exp***,** e52037.

GRABOWSKI, G. A. 2008. Phenotype, diagnosis, and treatment of Gaucher's disease. *Lancet,* 372**,** 1263-71.

GRABOWSKI, G. A. 2012. Gaucher disease and other storage disorders. *Hematology Am Soc Hematol Educ Program,* 2012**,** 13-8.

GRABOWSKI, G. A., GATT, S. & HOROWITZ, M. 1990. Acid beta-glucosidase: enzymology and molecular biology of Gaucher disease. *Crit Rev Biochem Mol Biol,* 25**,** 385-414.

GRABOWSKI, G. A. P., G.A.; KOLODNY, E.H. 2010. The Online Metabolic and Molecular Bases of Inherited disease. New York: Mc Graw Hill.

GRAEBER, M. B., STREIT, W. J., KIEFER, R., SCHOEN, S. W. & KREUTZBERG, G. W. 1990. New expression of myelomonocytic antigens by microglia and perivascular cells following lethal motor neuron injury. *J Neuroimmunol,* 27**,** 121-32.

GRAVES, P. N., GRABOWSKI, G. A., EISNER, R., PALESE, P. & SMITH, F. I. 1988. Gaucher disease type 1: cloning and characterization of a cDNA encoding acid beta-glucosidase from an Ashkenazi Jewish patient. *DNA,* 7**,** 521-8.

GRAY, S. J., FOTI, S. B., SCHWARTZ, J. W., BACHABOINA, L., TAYLOR-BLAKE, B., COLEMAN, J., EHLERS, M. D., ZYLKA, M. J., MCCOWN, T. J. & SAMULSKI, R. J. 2011. Optimizing promoters for recombinant adeno-associated virus-mediated gene expression in the peripheral and central nervous system using self-complementary vectors. *Hum Gene Ther,* 22**,** 1143-53.

GRIMM, D. & KAY, M. A. 2003. From Virus Evolution to Vector Revolution: Use of Naturally Occurring Serotypes of Adeno-associated Virus (AAV) as Novel Vectors for Human Gene Therapy. *Curr Gene Ther.,* 3**,** 281-304.

GUERTL, B., NOEHAMMER, C. & HOEFLER, G. 2000. Metabolic cardiomyopathies. *Int J Exp Pathol,* 81**,** 349-72.

GUNDERSEN, H. J., JENSEN, E. B., KIEU, K. & NIELSEN, J. 1999. The efficiency of systematic sampling in stereology--reconsidered. *J Microsc,* 193**,** 199-211.

GUPTA, N., OPPENHEIM, I. M., KAUVAR, E. F., TAYEBI, N. & SIDRANSKY, E. 2011. Type 2 Gaucher disease: phenotypic variation and genotypic heterogeneity. *Blood Cells Mol Dis,* 46**,** 75-84.

HADDAD, S. E., KHOURY, M., DAOUD, M., KANTAR, R., HARATI, H., MOUSALLEM, T., ALZATE, O., MEYER, B. & BOUSTANY, R. M. 2012. CLN5 and CLN8 protein association with ceramide synthase: biochemical and proteomic approaches. *Electrophoresis,* 33**,** 3798-809.

HALBERT, C. L., MILLER, A. D., MCNAMARA, S., EMERSON, J., GIBSON, R. L., RAMSEY, B. & AITKEN, M. L. 2006. Prevalence of neutralizing antibodies against adeno-associated virus (AAV) types 2, 5, and 6 in cystic fibrosis and normal populations: Implications for gene therapy using AAV vectors. *Hum Gene Ther,* 17**,** 440-7.

HARRIS, C. M., TAYLOR, D. S. & VELLODI, A. 1999. Ocular motor abnormalities in Gaucher disease. *Neuropediatrics,* 30**,** 289-93.

HOLLAK, C. E., VAN WEELY, S., VAN OERS, M. H. & AERTS, J. M. 1994. Marked elevation of plasma chitotriosidase activity. A novel hallmark of Gaucher disease. *J Clin Invest,* 93**,** 1288-92.

HOLLERAN, W. M., ZIEGLER, S. G., GOKER-ALPAN, O., EBLAN, M. J., ELIAS, P. M., SCHIFFMANN, R. & SIDRANSKY, E. 2006. Skin abnormalities as an early predictor of neurologic outcome in Gaucher disease. *Clin Genet,* 69**,** 355-7.

HONG, Y. B., KIM, E. Y., YOO, H. W. & JUNG, S. C. 2004. Feasibility of gene therapy in Gaucher disease using an adeno-associated virus vector. *J Hum Genet,* 49**,** 536-43.

HOROWITZ, M., WILDER, S., HOROWITZ, Z., REINER, O., GELBART, T. & BEUTLER, E. 1989. The human glucocerebrosidase gene and pseudogene: structure and evolution. *Genomics,* 4**,** 87-96.

HRUSKA, K. S., LAMARCA, M. E., SCOTT, C. R. & SIDRANSKY, E. 2008. Gaucher disease: mutation and polymorphism spectrum in the glucocerebrosidase gene (GBA). *Hum Mutat,* 29**,** 567-83.

HUIZING, M., HELIP-WOOLEY, A., WESTBROEK, W., GUNAY-AYGUN, M. & GAHL, W. A. 2008. Disorders of lysosome-related organelle biogenesis: clinical and molecular genetics. *Annu Rev Genomics Hum Genet,* 9**,** 359-86.

HUSAIN, T., PASSINI, M. A., PARENTE, M. K., FRASER, N. W. & WOLFE, J. H. 2009. Long-term AAV vector gene and protein expression in mouse brain from a small pan-cellular promoter is similar to neural cell promoters. *Gene Ther,* 16**,** 927-32.

JACKSON, K. L., DAYTON, R. D., DEVERMAN, B. E. & KLEIN, R. L. 2016. Better Targeting, Better Efficiency for Wide-Scale Neuronal Transduction with the Synapsin Promoter and AAV-PHP.B. *Front Mol Neurosci,* 9**,** 116.

JARDIM, L. B., VILLANUEVA, M. M., DE SOUZA, C. F. & NETTO, C. B. 2010. Clinical aspects of neuropathic lysosomal storage disorders. *J Inherit Metab Dis,* 33**,** 315-29.

JEYAKUMAR, M., DWEK, R. A., BUTTERS, T. D. & PLATT, F. M. 2005. Storage solutions: treating lysosomal disorders of the brain. *Nat Rev Neurosci,* 6**,** 713-25.

JMOUDIAK, M. & FUTERMAN, A. H. 2005. Gaucher disease: pathological mechanisms and modern management. *Br J Haematol,* 129**,** 178-88.

KANDEL, E. S., J. H.; JESSEL, T. 2012. *Principles of Neural Science*, McGraw-Hill Education.

KARLIN, S. & MRAZEK, J. 1996. What drives codon choices in human genes? *J Mol Biol,* 262**,** 459-72.

KIM, B. J., LEE, S. Y., KIM, H. W., PARK, E. J., KIM, J., KIM, S. J., SO, I. & JEON, J. H. 2009. Optimized immunohistochemical analysis of cerebellar purkinje cells using a specific biomarker, calbindin d28k. *Korean J Physiol Pharmacol,* 13**,** 373-8.

KIM, J. Y., GRUNKE, S. D., LEVITES, Y., GOLDE, T. E. & JANKOWSKY, J. L. 2014. Intracerebroventricular viral injection of the neonatal mouse brain for persistent and widespread neuronal transduction. *J Vis Exp***,** 51863.

KO, D. C., MILENKOVIC, L., BEIER, S. M., MANUEL, H., BUCHANAN, J. & SCOTT, M. P. 2005. Cell-autonomous death of cerebellar purkinje neurons with autophagy in Niemann-Pick type C disease. *PLoS Genet,* 1**,** 81-95.

KOIKE, M., SHIBATA, M., WAGURI, S., YOSHIMURA, K., TANIDA, I., KOMINAMI, E., GOTOW, T., PETERS, C., VON FIGURA, K., MIZUSHIMA, N., SAFTIG, P. & UCHIYAMA, Y. 2005. Participation of autophagy in storage of lysosomes in neurons from mouse models of neuronal ceroid-lipofuscinoses (Batten disease). *Am J Pathol,* 167**,** 1713-28.

KOPRIVICA, V., STONE, D. L., PARK, J. K., CALLAHAN, M., FRISCH, A., COHEN, I. J., TAYEBI, N. & SIDRANSKY, E. 2000. Analysis and classification of 304 mutant alleles in patients with type 1 and type 3 Gaucher disease. *Am J Hum Genet,* 66**,** 1777-86.

KOTIN, R. M., SINISCALCO, M., SAMULSKI, R. J., ZHU, X. D., HUNTER, L., LAUGHLIN, C. A., MCLAUGHLIN, S., MUZYCZKA, N., ROCCHI, M. & BERNS, K. I. 1990. Site-specific integration by adeno-associated virus. *Proc Natl Acad Sci U S A,* 87**,** 2211-5.

KOTTERMAN, M. A. & SCHAFFER, D. V. 2014. Engineering adeno-associated viruses for clinical gene therapy. *Nat Rev Genet,* 15**,** 445-51.

KOZAK, M. 2005. Regulation of translation via mRNA structure in prokaryotes and eukaryotes. *Gene,* 361**,** 13-37.

LAL, T. R. & SIDRANSKY, E. 2017. The Spectrum of Neurological Manifestations Associated with Gaucher Disease. *Diseases,* 5.

LEONE, P., SHERA, D., MCPHEE, S. W., FRANCIS, J. S., KOLODNY, E. H., BILANIUK, L. T., WANG, D. J., ASSADI, M., GOLDFARB, O., GOLDMAN, H. W., FREESE, A., YOUNG, D., DURING, M. J., SAMULSKI, R. J. & JANSON, C. G. 2012. Long-term follow-up after gene therapy for canavan disease. *Sci Transl Med,* 4**,** 165ra163.

LEVINE, B. & KLIONSKY, D. J. 2004. Development by self-digestion: molecular mechanisms and biological functions of autophagy. *Dev Cell,* 6**,** 463-77.

LISOWSKI, L., DANE, A. P., CHU, K., ZHANG, Y., CUNNINGHAM, S. C., WILSON, E. M., NYGAARD, S., GROMPE, M., ALEXANDER, I. E. & KAY, M. A. 2014. Selection and evaluation of clinically relevant AAV variants in a xenograft liver model. *Nature,* 506**,** 382-6.

LISOWSKI, L., TAY, S. S. & ALEXANDER, I. E. 2015. Adeno-associated virus serotypes for gene therapeutics. *Curr Opin Pharmacol,* 24**,** 59-67.

LIU, G., MARTINS, I., WEMMIE, J. A., CHIORINI, J. A. & DAVIDSON, B. L. 2005. Functional correction of CNS phenotypes in a lysosomal storage disease model using adeno-associated virus type 4 vectors. *J Neurosci,* 25**,** 9321-7.

LIU, Y., SUZUKI, K., REED, J. D., GRINBERG, A., WESTPHAL, H., HOFFMANN, A., DORING, T., SANDHOFF, K. & PROIA, R. L. 1998. Mice with type 2 and 3 Gaucher disease point mutations generated by a single insertion mutagenesis procedure. *Proc Natl Acad Sci U S A,* 95**,** 2503-8.

LLOYD-EVANS, E., PELLED, D., RIEBELING, C., BODENNEC, J., DE-MORGAN, A., WALLER, H., SCHIFFMANN, R. & FUTERMAN, A. H. 2003. Glucosylceramide and glucosylsphingosine modulate calcium mobilization from brain microsomes via different mechanisms. *J Biol Chem,* 278**,** 23594-9.

LOEB, J. E., CORDIER, W. S., HARRIS, M. E., WEITZMAN, M. D. & HOPE, T. J. 1999. Enhanced expression of transgenes from adeno-associated virus vectors with the woodchuck hepatitis virus posttranscriptional regulatory element: implications for gene therapy. *Hum Gene Ther,* 10**,** 2295-305.

LUKINA, E., WATMAN, N., ARREGUIN, E. A., DRAGOSKY, M., IASTREBNER, M., ROSENBAUM, H., PHILLIPS, M., PASTORES, G. M., KAMATH, R. S., ROSENTHAL, D. I., KAPER, M., SINGH, T., PUGA, A. C. & PETERSCHMITT, M. J. 2010. Improvement in hematological, visceral, and skeletal manifestations of Gaucher disease type 1 with oral eliglustat tartrate (Genz-112638) treatment: 2-year results of a phase 2 study. *Blood,* 116**,** 4095-8.

MANFREDSSON, F. P., RISING, A. C. & MANDEL, R. J. 2009. AAV9: a potential blood-brain barrier buster. *Mol Ther,* 17**,** 403-5.

MANNO, C. S., CHEW, A. J., HUTCHISON, S., LARSON, P. J., HERZOG, R. W., ARRUDA, V. R., TAI, S. J., RAGNI, M. V., THOMPSON, A., OZELO, M., COUTO, L. B., LEONARD, D. G., JOHNSON, F. A., MCCLELLAND, A., SCALLAN, C., SKARSGARD, E., FLAKE, A. W., KAY, M. A., HIGH, K. A. & GLADER, B. 2003. AAV-mediated factor IX gene transfer to skeletal muscle in patients with severe hemophilia B. *Blood,* 101**,** 2963-72.

MANNO, C. S., PIERCE, G. F., ARRUDA, V. R., GLADER, B., RAGNI, M., RASKO, J. J., OZELO, M. C., HOOTS, K., BLATT, P., KONKLE, B., DAKE, M., KAYE, R., RAZAVI, M., ZAJKO, A., ZEHNDER, J., RUSTAGI, P. K.,

NAKAI, H., CHEW, A., LEONARD, D., WRIGHT, J. F., LESSARD, R. R., SOMMER, J. M., TIGGES, M., SABATINO, D., LUK, A., JIANG, H., MINGOZZI, F., COUTO, L., ERTL, H. C., HIGH, K. A. & KAY, M. A. 2006. Successful transduction of liver in hemophilia by AAV-Factor IX and limitations imposed by the host immune response. *Nat Med,* 12**,** 342-7.

MARSHALL, J., SUN, Y., BANGARI, D. S., BUDMAN, E., PARK, H., NIETUPSKI, J. B., ALLAIRE, A., CROMWELL, M. A., WANG, B., GRABOWSKI, G. A., LEONARD, J. P. & CHENG, S. H. 2016. CNS-accessible Inhibitor of Glucosylceramide Synthase for Substrate Reduction Therapy of Neuronopathic Gaucher Disease. *Mol Ther,* 24**,** 1019-1029.

MARTINEZ-ARIAS, R., CALAFELL, F., MATEU, E., COMAS, D., ANDRES, A. & BERTRANPETIT, J. 2001. Sequence variability of a human pseudogene. *Genome Res,* 11**,** 1071-85.

MATTAR, C. N., WADDINGTON, S. N., BISWAS, A., JOHANA, N., NG, X. W., FISK, A. S., FISK, N. M., TAN, L. G., RAHIM, A. A., BUCKLEY, S. M., TAN, M. H., LU, J., CHOOLANI, M. & CHAN, J. K. 2013. Systemic delivery of scAAV9 in fetal macaques facilitates neuronal transduction of the central and peripheral nervous systems. *Gene Ther,* 20**,** 69-83.

MATTAR, C. N., WONG, A. M., HOEFER, K., ALONSO-FERRERO, M. E., BUCKLEY, S. M., HOWE, S. J., COOPER, J. D., WADDINGTON, S. N., CHAN, J. K. & RAHIM, A. A. 2015. Systemic gene delivery following intravenous administration of AAV9 to fetal and neonatal mice and late-gestation nonhuman primates. *FASEB J,* 29**,** 3876-88.

MAZZULLI, J. R., XU, Y. H., SUN, Y., KNIGHT, A. L., MCLEAN, P. J., CALDWELL, G. A., SIDRANSKY, E., GRABOWSKI, G. A. & KRAINC, D. 2011. Gaucher disease glucocerebrosidase and alpha-synuclein form a bidirectional pathogenic loop in synucleinopathies. *Cell,* 146**,** 37-52.

MCCARTY, D. M. 2008. Self-complementary AAV vectors; advances and applications. *Mol Ther,* 16**,** 1648-56.

MCCARTY, D. M., MONAHAN, P. E. & SAMULSKI, R. J. 2001. Self-complementary recombinant adeno-associated virus (scAAV) vectors promote efficient transduction independently of DNA synthesis. *Gene Ther,* 8**,** 1248-54.

MCEACHERN, K. A., NIETUPSKI, J. B., CHUANG, W. L., ARMENTANO, D., JOHNSON, J., HUTTO, E., GRABOWSKI, G. A., CHENG, S. H. & MARSHALL, J. 2006. AAV8-mediated expression of glucocerebrosidase ameliorates the storage pathology in the visceral organs of a mouse model of Gaucher disease. *J Gene Med,* 8**,** 719-29.

MCLEAN, J. R., SMITH, G. A., ROCHA, E. M., HAYES, M. A., BEAGAN, J. A., HALLETT, P. J. & ISACSON, O. 2014. Widespread neuron-specific transgene expression in brain and spinal cord following synapsin promoter-driven AAV9 neonatal intracerebroventricular injection. *Neurosci Lett,* 576**,** 73-8.

MEHTA, A. 2006. Epidemiology and natural history of Gaucher's disease. *Eur J Intern Med,* 17 Suppl**,** S2-5.

MELCHIORRI, D., PANI, L., GASPARINI, P., COSSU, G., ANCANS, J., BORG, J. J., DRAI, C., FIEDOR, P., FLORY, E., HUDSON, I., LEUFKENS, H. G., MULLER-BERGHAUS, J., NARAYANAN, G., NEUGEBAUER, B., POKROTNIEKS, J., ROBERT, J. L., SALMONSON, T. & SCHNEIDER, C. K. 2013. Regulatory evaluation of Glybera in Europe - two committees, one mission. *Nat Rev Drug Discov,* 12**,** 719.

MENDELL, J. R., ET AL. 2016a. Gene Therapy for Spinal Muscular Atrophy Type 1 Shows Potential to Improve Survival and Motor Functional Outcomes. *In:* INC., E. (ed.). The American Society of Gene & Cell Therapy.

MENDELL, J. R. A.-Z., S.; SHELL, R.; ARNOLD, W. D.; RODINO-KLAPAC, L.; KISSEL, J. T.; PRIOR, T.; MIRANDA, C; LOWES, L.; ALFANO, L.; BERRY, K.; PETEK, C.; CHURCH, K.; BRAUN, L.; CORCORAN, S.; MEYER, K.; LIKHITE, S.; BURGHES, A.; FOUST, K. D.; KASPAR, B. K. 2016b. Gene Therapy for Spinal Muscular Atrophy Type 1 Shows Potential to Improve Survival and Motor Functional Outcomes. *In:* THERAPY, M. (ed.) *The American Society of Gene & Cell Therapy.* Elsevier.

MIGNOT, C., DOUMMAR, D., MAIRE, I., DE VILLEMEUR, T. B. & FRENCH TYPE 2 GAUCHER DISEASE STUDY, G. 2006. Type 2 Gaucher disease: 15 new cases and review of the literature. *Brain Dev,* 28**,** 39-48.

MISTRY, P. K., LIU, J., YANG, M., NOTTOLI, T., MCGRATH, J., JAIN, D., ZHANG, K., KEUTZER, J., CHUANG, W. L., MEHAL, W. Z., ZHAO, H., LIN, A., MANE, S., LIU, X., PENG, Y. Z., LI, J. H., AGRAWAL, M., ZHU, L. L., BLAIR, H. C., ROBINSON, L. J., IQBAL, J., SUN, L. & ZAIDI, M. 2010. Glucocerebrosidase gene-deficient mouse recapitulates Gaucher disease displaying cellular and molecular dysregulation beyond the macrophage. *Proc Natl Acad Sci U S A,* 107**,** 19473-8.

MISTRY, P. K., SIRRS, S., CHAN, A., PRITZKER, M. R., DUFFY, T. P., GRACE, M. E., MEEKER, D. P. & GOLDMAN, M. E. 2002. Pulmonary hypertension in type 1 Gaucher's disease: genetic and epigenetic determinants of phenotype and response to therapy. *Mol Genet Metab,* 77**,** 91-8.

MIYAZAKI, J., TAKAKI, S., ARAKI, K., TASHIRO, F., TOMINAGA, A., TAKATSU, K. & YAMAMURA, K. 1989. Expression vector system based on the chicken beta-actin promoter directs efficient production of interleukin-5. *Gene,* 79**,** 269-77.

MORISOT, C., MILLAT, G., COESLIER, A., BOURGOIS, B., FONTENOY, E., DOBBELAERE, D., VEROT, L., HAOUARI, N., VAILLANT, C., GOTTRAND, F., BOGAERT, E., THELLIEZ, P., KLOSOWSKI, S., DJEBARA, A., BACHIRI, A., MANOUVRIER, S. & VANIER, M. T. 2005. [Fatal neonatal respiratory distress in Niemann-Pick C2 and prenatal diagnosis with mutations in gene HE1/NPC2]. *Arch Pediatr,* 12**,** 434-7.

MORRISON, C. 2015. $1-million price tag set for Glybera gene therapy. *Nat Biotechnol,* 33**,** 217-8.

NAGRAL, A. 2014. Gaucher disease. *J Clin Exp Hepatol,* 4**,** 37-50.

NALDINI, L. 2015. Gene therapy returns to centre stage. *Nature,* 526**,** 351-60.

NARITA, A., SHIRAI, K., ITAMURA, S., MATSUDA, A., ISHIHARA, A., MATSUSHITA, K., FUKUDA, C., KUBOTA, N., TAKAYAMA, R., SHIGEMATSU, H., HAYASHI, A., KUMADA, T., YUGE, K., WATANABE, Y., KOSUGI, S., NISHIDA, H., KIMURA, Y., ENDO, Y., HIGAKI, K., NANBA, E., NISHIMURA, Y., TAMASAKI, A., TOGAWA, M., SAITO, Y., MAEGAKI, Y., OHNO, K. & SUZUKI, Y. 2016. Ambroxol chaperone therapy for neuronopathic Gaucher disease: A pilot study. *Ann Clin Transl Neurol,* 3**,** 200-15.

NASO, M. F., TOMKOWICZ, B., PERRY, W. L., 3RD & STROHL, W. R. 2017. Adeno-Associated Virus (AAV) as a Vector for Gene Therapy. *BioDrugs*.

NATHWANI, A. C., REISS, U. M., TUDDENHAM, E. G., ROSALES, C., CHOWDARY, P., MCINTOSH, J., DELLA PERUTA, M., LHERITEAU, E., PATEL, N., RAJ, D., RIDDELL, A., PIE, J., RANGARAJAN, S., BEVAN, D.,

RECHT, M., SHEN, Y. M., HALKA, K. G., BASNER-TSCHAKARJAN, E., MINGOZZI, F., HIGH, K. A., ALLAY, J., KAY, M. A., NG, C. Y., ZHOU, J., CANCIO, M., MORTON, C. L., GRAY, J. T., SRIVASTAVA, D., NIENHUIS, A. W. & DAVIDOFF, A. M. 2014. Long-term safety and efficacy of factor IX gene therapy in hemophilia B. *N Engl J Med,* 371**,** 1994-2004.

NATHWANI, A. C., TUDDENHAM, E. G., RANGARAJAN, S., ROSALES, C., MCINTOSH, J., LINCH, D. C., CHOWDARY, P., RIDDELL, A., PIE, A. J., HARRINGTON, C., O'BEIRNE, J., SMITH, K., PASI, J., GLADER, B., RUSTAGI, P., NG, C. Y., KAY, M. A., ZHOU, J., SPENCE, Y., MORTON, C. L., ALLAY, J., COLEMAN, J., SLEEP, S., CUNNINGHAM, J. M., SRIVASTAVA, D., BASNER-TSCHAKARJAN, E., MINGOZZI, F., HIGH, K. A., GRAY, J. T., REISS, U. M., NIENHUIS, A. W. & DAVIDOFF, A. M. 2011. Adenovirus-associated virus vector-mediated gene transfer in hemophilia B. *N Engl J Med,* 365**,** 2357-65.

NAULT, J. C., DATTA, S., IMBEAUD, S., FRANCONI, A., MALLET, M., COUCHY, G., LETOUZE, E., PILATI, C., VERRET, B., BLANC, J. F., BALABAUD, C., CALDERARO, J., LAURENT, A., LETEXIER, M., BIOULAC-SAGE, P., CALVO, F. & ZUCMAN-ROSSI, J. 2015. Recurrent AAV2-related insertional mutagenesis in human hepatocellular carcinomas. *Nat Genet,* 47**,** 1187-93.

NEUMANN, J., BRAS, J., DEAS, E., O'SULLIVAN, S. S., PARKKINEN, L., LACHMANN, R. H., LI, A., HOLTON, J., GUERREIRO, R., PAUDEL, R., SEGARANE, B., SINGLETON, A., LEES, A., HARDY, J., HOULDEN, H., REVESZ, T. & WOOD, N. W. 2009. Glucocerebrosidase mutations in clinical and pathologically proven Parkinson's disease. *Brain,* 132**,** 1783-94.

NIH, G. H. R. 2017. *What is gene therapy?* [Online]. MD 20894, USA: National Institute of Health. Available: https://ghr.nlm.nih.gov/primer/therapy/genetherapy.

NILSSON, O. & SVENNERHOLM, L. 1982. Accumulation of glucosylceramide and glucosylsphingosine (psychosine) in cerebrum and cerebellum in infantile and juvenile Gaucher disease. *J Neurochem,* 39**,** 709-18.

NIXON, G. F. 2009. Sphingolipids in inflammation: pathological implications and potential therapeutic targets. *Br J Pharmacol,* 158**,** 982-93.

O'NEILL, R. R., TOKORO, T., KOZAK, C. A. & BRADY, R. O. 1989. Comparison of the chromosomal localization of murine and human glucocerebrosidase genes and of the deduced amino acid sequences. *Proc Natl Acad Sci U S A,* 86**,** 5049-53.

ORVISKY, E., SIDRANSKY, E., MCKINNEY, C. E., LAMARCA, M. E., SAMIMI, R., KRASNEWICH, D., MARTIN, B. M. & GINNS, E. I. 2000. Glucosylsphingosine accumulation in mice and patients with type 2 Gaucher disease begins early in gestation. *Pediatr Res,* 48**,** 233-7.

PAN, C., NELSON, M. S., REYES, M., KOODIE, L., BRAZIL, J. J., STEPHENSON, E. J., ZHAO, R. C., PETERS, C., SELLECK, S. B., STRINGER, S. E. & GUPTA, P. 2005. Functional abnormalities of heparan sulfate in mucopolysaccharidosis-I are associated with defective biologic activity of FGF-2 on human multipotent progenitor cells. *Blood,* 106**,** 1956-64.

PANDEY, M. K., RANI, R., ZHANG, W., SETCHELL, K. & GRABOWSKI, G. A. 2012. Immunological cell type characterization and Th1-Th17 cytokine production in a mouse model of Gaucher disease. *Mol Genet Metab,* 106**,** 310-22.

PARENTI, G., ANDRIA, G. & VALENZANO, K. J. 2015. Pharmacological Chaperone Therapy: Preclinical Development, Clinical Translation, and Prospects for the Treatment of Lysosomal Storage Disorders. *Mol Ther,* 23**,** 1138-48.

PARENTI, G., MORACCI, M., FECAROTTA, S. & ANDRIA, G. 2014. Pharmacological chaperone therapy for lysosomal storage diseases. *Future Med Chem,* 6**,** 1031-45.

PARFITT, D. A., AGUILA, M., MCCULLEY, C. H., BEVILACQUA, D., MENDES, H. F., ATHANASIOU, D., NOVOSELOV, S. S., KANUGA, N., MUNRO, P. M., COFFEY, P. J., KALMAR, B., GREENSMITH, L. & CHEETHAM, M. E. 2014. The heat-shock response co-inducer arimoclomol protects against retinal degeneration in rhodopsin retinitis pigmentosa. *Cell Death Dis,* 5**,** e1236.

PASSINI, M. A., WATSON, D. J., VITE, C. H., LANDSBURG, D. J., FEIGENBAUM, A. L. & WOLFE, J. H. 2003. Intraventricular brain injection of adeno-associated virus type 1 (AAV1) in neonatal mice results in complementary patterns of neuronal transduction to AAV2 and total long-term correction of storage lesions in the brains of beta-glucuronidase-deficient mice. *J Virol,* 77**,** 7034-40.

PASTORES, G. M. & HUGHES, D. A. 2015. Gaucher Disease. *In:* PAGON, R. A., ADAM, M. P., ARDINGER, H. H., WALLACE, S. E., AMEMIYA, A., BEAN, L. J. H., BIRD, T. D., FONG, C. T., MEFFORD, H. C., SMITH, R. J. H. & STEPHENS, K. (eds.) *GeneReviews(R).* Seattle (WA).

PASTORES, G. M. & MAEGAWA, G. H. 2013. Clinical neurogenetics: neuropathic lysosomal storage disorders. *Neurol Clin,* 31**,** 1051-71.

PASTORES, G. M., PATEL, M. J. & FIROOZNIA, H. 2000. Bone and joint complications related to Gaucher disease. *Curr Rheumatol Rep,* 2**,** 175-80.

PAXINOS, G. F., K. 2012. *Paxinos and Franklin's the Mouse Brain in Stereotaxic Coordinates*, Academic Press.

PELLED, D., LLOYD-EVANS, E., RIEBELING, C., JEYAKUMAR, M., PLATT, F. M. & FUTERMAN, A. H. 2003. Inhibition of calcium uptake via the sarco/endoplasmic reticulum Ca2+-ATPase in a mouse model of Sandhoff disease and prevention by treatment with N-butyldeoxynojirimycin. *J Biol Chem,* 278**,** 29496-501.

PEREIRA, D. J., MCCARTY, D. M. & MUZYCZKA, N. 1997. The adeno-associated virus (AAV) Rep protein acts as both a repressor and an activator to regulate AAV transcription during a productive infection. *J Virol,* 71**,** 1079-88.

PLATT, F. M. 2014. Sphingolipid lysosomal storage disorders. *Nature,* 510**,** 68-75.

PLATT, F. M. & LACHMANN, R. H. 2009. Treating lysosomal storage disorders: current practice and future prospects. *Biochim Biophys Acta,* 1793**,** 737-45.

PLATT, F. M., NEISES, G. R., DWEK, R. A. & BUTTERS, T. D. 1994. N-butyldeoxynojirimycin is a novel inhibitor of glycolipid biosynthesis. *J Biol Chem,* 269**,** 8362-5.

POLGREEN, L. E., TOLAR, J., PLOG, M., HIMES, J. H., ORCHARD, P. J., WHITLEY, C. B., MILLER, B. S. & PETRYK, A. 2008. Growth and endocrine function in patients with Hurler syndrome after hematopoietic stem cell transplantation. *Bone Marrow Transplant,* 41**,** 1005-11.

PRESSLER, R. & AUVIN, S. 2013. Comparison of Brain Maturation among Species: An Example in Translational Research Suggesting the Possible Use of Bumetanide in Newborn. *Front Neurol,* 4**,** 36.

PRINETTI, A., PRIONI, S., CHIRICOZZI, E., SCHUCHMAN, E. H., CHIGORNO, V. & SONNINO, S. 2011. Secondary alterations of sphingolipid metabolism in lysosomal storage diseases. *Neurochem Res,* 36**,** 1654-68.

RAHIM, A. A., WONG, A. M., HOEFER, K., BUCKLEY, S. M., MATTAR, C. N., CHENG, S. H., CHAN, J. K., COOPER, J. D. & WADDINGTON, S. N. 2011. Intravenous administration of AAV2/9 to the fetal and neonatal mouse leads to differential targeting of CNS cell types and extensive transduction of the nervous system. *FASEB J,* 25**,** 3505-18.

RASTALL, D. P. & AMALFITANO, A. 2015. Recent advances in gene therapy for lysosomal storage disorders. *Appl Clin Genet,* 8**,** 157-69.

RECZEK, D., SCHWAKE, M., SCHRODER, J., HUGHES, H., BLANZ, J., JIN, X., BRONDYK, W., VAN PATTEN, S., EDMUNDS, T. & SAFTIG, P. 2007. LIMP-2 is a receptor for lysosomal mannose-6-phosphate-independent targeting of beta-glucocerebrosidase. *Cell,* 131**,** 770-83.

REINER, O. & HOROWITZ, M. 1988. Differential expression of the human glucocerebrosidase-coding gene. *Gene,* 73**,** 469-78.

ROTH, P., SKLOWER BROOKS, S., POTAZNIK, D., COOMA, R. & SAHDEV, S. 2005. Neonatal Gaucher disease presenting as persistent thrombocytopenia. *J Perinatol,* 25**,** 356-8.

SANDHOFF, K. 2013. Metabolic and cellular bases of sphingolipidoses. *Biochem Soc Trans,* 41**,** 1562-8.

SARAIVA, J., NOBRE, R. J. & PEREIRA DE ALMEIDA, L. 2016. Gene therapy for the CNS using AAVs: The impact of systemic delivery by AAV9. *J Control Release,* 241**,** 94-109.

SCHMIDT, M., VOUTETAKIS, A., AFIONE, S., ZHENG, C., MANDIKIAN, D. & CHIORINI, J. A. 2008. Adeno-associated virus type 12 (AAV12): a novel AAV serotype with sialic acid- and heparan sulfate proteoglycan-independent transduction activity. *J Virol,* 82**,** 1399-406.

SCHOCH, S., CIBELLI, G. & THIEL, G. 1996. Neuron-specific gene expression of synapsin I. Major role of a negative regulatory mechanism. *J Biol Chem,* 271**,** 3317-23.

SCHOLZ, S. W. & JEON, B. S. 2015. GBA mutations and Parkinson disease: when genotype meets phenotype. *Neurology,* 84**,** 866-7.

SCHUELER, U. H., KOLTER, T., KANESKI, C. R., BLUSZTAJN, J. K., HERKENHAM, M., SANDHOFF, K. & BRADY, R. O. 2003. Toxicity of glucosylsphingosine (glucopsychosine) to cultured neuronal cells: a model system for assessing neuronal damage in Gaucher disease type 2 and 3. *Neurobiol Dis,* 14**,** 595-601.

SCOTT, J. E. & WILLETT, I. H. 1966. Binding of cationic dyes to nucleic acids and ther biological polyanions. *Nature,* 209**,** 985-7.

SEHARA, Y., FUJIMOTO, K. I., IKEGUCHI, K., KATAKAI, Y., ONO, F., TAKINO, N., ITO, M., OZAWA, K. & MURAMATSU, S. I. 2017. Persistent Expression of Dopamine-Synthesizing Enzymes 15 Years After Gene Transfer in a Primate Model of Parkinson's Disease. *Hum Gene Ther Clin Dev,* 28**,** 74-79.

SHACHAR, T., LO BIANCO, C., RECCHIA, A., WIESSNER, C., RAAS-ROTHSCHILD, A. & FUTERMAN, A. H. 2011. Lysosomal storage disorders and Parkinson's disease: Gaucher disease and beyond. *Mov Disord,* 26**,** 1593-604.

SHELTON, S. B., PETTIGREW, D. B., HERMANN, A. D., ZHOU, W., SULLIVAN, P. M., CRUTCHER, K. A. & STRAUSS, K. I. 2008. A simple, efficient tool for assessment of mice after unilateral cortex injury. *J Neurosci Methods,* 168**,** 431-42.

SIDRANSKY, E. 2004. Gaucher disease: complexity in a "simple" disorder. *Mol Genet Metab,* 83**,** 6-15.

SIDRANSKY, E., FARTASCH, M., LEE, R. E., METLAY, L. A., ABELLA, S., ZIMRAN, A., GAO, W., ELIAS, P. M., GINNS, E. I. & HOLLERAN, W. M. 1996. Epidermal abnormalities may distinguish type 2 from type 1 and type 3 of Gaucher disease. *Pediatr Res,* 39**,** 134-41.

SIDRANSKY, E. & LOPEZ, G. 2012. The link between the GBA gene and parkinsonism. *Lancet Neurol,* 11**,** 986-98.

SIEGL, G., BATES, R. C., BERNS, K. I., CARTER, B. J., KELLY, D. C., KURSTAK, E. & TATTERSALL, P. 1985. Characteristics and taxonomy of Parvoviridae. *Intervirology,* 23**,** 61-73.

SIMONARO, C. M., D'ANGELO, M., HASKINS, M. E. & SCHUCHMAN, E. H. 2005. Joint and bone disease in mucopolysaccharidoses VI and VII: identification of new therapeutic targets and biomarkers using animal models. *Pediatr Res,* 57**,** 701-7.

SINHA, G. 2014. Gaucher's disease oral therapy gets nod from FDA. *Nat Biotechnol,* 32**,** 970-1.

SNYDER, B. R., GRAY, S. J., QUACH, E. T., HUANG, J. W., LEUNG, C. H., SAMULSKI, R. J., BOULIS, N. M. & FEDERICI, T. 2011. Comparison of adeno-associated viral vector serotypes for spinal cord and motor neuron gene delivery. *Hum Gene Ther,* 22**,** 1129-35.

SORRENTINO, N. C., D'ORSI, L., SAMBRI, I., NUSCO, E., MONACO, C., SPAMPANATO, C., POLISHCHUK, E., SACCONE, P., DE LEONIBUS, E., BALLABIO, A. & FRALDI, A. 2013. A highly secreted sulphamidase engineered to cross the blood-brain barrier corrects brain lesions of mice with mucopolysaccharidoses type IIIA. *EMBO Mol Med,* 5**,** 675-90.

SPIEGEL, S. & MERRILL, A. H., JR. 1996. Sphingolipid metabolism and cell growth regulation. *FASEB J,* 10**,** 1388-97.

SRIVASTAVA, A., LUSBY, E. W. & BERNS, K. I. 1983. Nucleotide sequence and organization of the adeno-associated virus 2 genome. *J Virol,* 45**,** 555-64.

STARETZ-CHACHAM, O., LANG, T. C., LAMARCA, M. E., KRASNEWICH, D. & SIDRANSKY, E. 2009. Lysosomal storage disorders in the newborn. *Pediatrics,* 123**,** 1191-207.

STEPHENS, M. C., BERNATSKY, A., BURACHINSKY, V., LEGLER, G. & KANFER, J. N. 1978. The Gaucher mouse: differential action of conduritol B epoxide and reversibility of its effects. *J Neurochem,* 30**,** 1023-7.

STIRNEMANN, J., BELMATOUG, N., CAMOU, F., SERRATRICE, C., FROISSART, R., CAILLAUD, C., LEVADE, T., ASTUDILLO, L., SERRATRICE, J., BRASSIER, A., ROSE, C., BILLETTE DE VILLEMEUR, T. & BERGER, M. G. 2017. A Review of Gaucher Disease Pathophysiology, Clinical Presentation and Treatments. *Int J Mol Sci,* 18.

STONE, D. L., GINNS, E. I., KRASNEWICH, D. & SIDRANSKY, E. 2000a. Life-threatening splenic hemorrhage in two patients with Gaucher disease. *Am J Hematol,* 64**,** 140-2.

STONE, D. L. & SIDRANSKY, E. 1999. Hydrops fetalis: lysosomal storage disorders in extremis. *Adv Pediatr,* 46**,** 409-40.

STONE, D. L., TAYEBI, N., ORVISKY, E., STUBBLEFIELD, B., MADIKE, V. & SIDRANSKY, E. 2000b. Glucocerebrosidase gene mutations in patients with type 2 Gaucher disease. *Hum Mutat,* 15**,** 181-8.

SUMMERFORD, C. & SAMULSKI, R. J. 1998. Membrane-associated heparan sulfate proteoglycan is a receptor for adeno-associated virus type 2 virions. *J Virol,* 72**,** 1438-45.

TAMARGO, R. J., VELAYATI, A., GOLDIN, E. & SIDRANSKY, E. 2012. The role of saposin C in Gaucher disease. *Mol Genet Metab,* 106**,** 257-63.

TARDIEU, M., ZERAH, M., HUSSON, B., DE BOURNONVILLE, S., DEIVA, K., ADAMSBAUM, C., VINCENT, F., HOCQUEMILLER, M., BROISSAND, C., FURLAN, V., BALLABIO, A., FRALDI, A., CRYSTAL, R. G., BAUGNON, T., ROUJEAU, T., HEARD, J. M. & DANOS, O. 2014. Intracerebral administration of adeno-associated viral vector serotype rh.10 carrying human SGSH and SUMF1 cDNAs in children with mucopolysaccharidosis type IIIA disease: results of a phase I/II trial. *Hum Gene Ther,* 25**,** 506-16.

TESSITORE, A., DEL, P. M. M., SANO, R., MA, Y., MANN, L., INGRASSIA, A., LAYWELL, E. D., STEINDLER, D. A., HENDERSHOT, L. M. & D'AZZO, A. 2004. GM1-ganglioside-mediated activation of the unfolded protein response causes neuronal death in a neurodegenerative gangliosidosis. *Mol Cell,* 15**,** 753-66.

TRONCHE, F., KELLENDONK, C., KRETZ, O., GASS, P., ANLAG, K., ORBAN, P. C., BOCK, R., KLEIN, R. & SCHUTZ, G. 1999. Disruption of the glucocorticoid receptor gene in the nervous system results in reduced anxiety. *Nat Genet,* 23**,** 99-103.

TSUJI, S., MARTIN, B. M., BARRANGER, J. A., STUBBLEFIELD, B. K., LAMARCA, M. E. & GINNS, E. I. 1988. Genetic heterogeneity in type 1 Gaucher disease: multiple genotypes in Ashkenazic and non-Ashkenazic individuals. *Proc Natl Acad Sci U S A,* 85**,** 2349-52.

US FOOD AND DRUG ADMINISTRATION 2016. *Cellular & Gene Therapy Guidances* [Online]. MD 20993, USA. Available: https://www.fda.gov/BiologicsBloodVaccines/GuidanceComplianceRegulatoryInformation/Guidances/CellularandGeneTherapy/default.htm.

US FOOD AND DRUG ADMINISTRATION 2017. *FDA approves first treatment for a form of Batten disease* [Online]. Available: https://www.fda.gov/newsevents/newsroom/pressannouncements/ucm555613.htm.

VARDI, A., ZIGDON, H., MESHCHERIAKOVA, A., KLEIN, A. D., YAACOBI, C., EILAM, R., KENWOOD, B. M., RAHIM, A. A., MASSARO, G., MERRILL, A. H., JR., VITNER, E. B. & FUTERMAN, A. H. 2016. Delineating pathological pathways in a chemically induced mouse model of Gaucher disease. *J Pathol,* 239**,** 496-509.

VELLODI, A. 2014. Bone marrow transplantation for lysosomal storage disorders. *Expert Review of Endocrinology & Metabolism,* 1**,** 425-438.

VITNER, E. B., DEKEL, H., ZIGDON, H., SHACHAR, T., FARFEL-BECKER, T., EILAM, R., KARLSSON, S. & FUTERMAN, A. H. 2010. Altered expression and distribution of cathepsins in neuronopathic forms of Gaucher disease and in other sphingolipidoses. *Hum Mol Genet,* 19**,** 3583-90.

VITNER, E. B., FARFEL-BECKER, T., EILAM, R., BITON, I. & FUTERMAN, A. H. 2012. Contribution of brain inflammation to neuronal cell death in neuronopathic forms of Gaucher's disease. *Brain,* 135**,** 1724-35.

VITNER, E. B. & FUTERMAN, A. H. 2013. Neuronal forms of Gaucher disease. *Handb Exp Pharmacol***,** 405-19.

VITNER, E. B., SALOMON, R., FARFEL-BECKER, T., MESHCHERIAKOVA, A., ALI, M., KLEIN, A. D., PLATT, F. M., COX, T. M. & FUTERMAN, A. H. 2014. RIPK3 as a potential therapeutic target for Gaucher's disease. *Nat Med,* 20**,** 204-8.

WALKLEY, S. U. 2009. Pathogenic cascades in lysosomal disease-Why so complex? *J Inherit Metab Dis,* 32**,** 181-9.

WALTER, J., YOU, Q., HAGSTROM, J. N., SANDS, M. & HIGH, K. A. 1996. Successful expression of human factor IX following repeat administration of adenoviral vector in mice. *Proc Natl Acad Sci U S A,* 93**,** 3056-61.

WAN, L., HSU, C. M., TSAI, C. H., LEE, C. C., HWU, W. L. & TSAI, F. J. 2006. Mutation analysis of Gaucher disease patients in Taiwan: high prevalence of the RecNciI and L444P mutations. *Blood Cells Mol Dis,* 36**,** 422-5.

WANG, D. B., DAYTON, R. D., HENNING, P. P., CAIN, C. D., ZHAO, L. R., SCHROTT, L. M., ORCHARD, E. A., KNIGHT, D. S. & KLEIN, R. L. 2010. Expansive gene transfer in the rat CNS rapidly produces amyotrophic lateral sclerosis relevant sequelae when TDP-43 is overexpressed. *Mol Ther,* 18**,** 2064-74.

WANG, R. Y., BODAMER, O. A., WATSON, M. S., WILCOX, W. R. & DISEASES, A. W. G. O. D. C. O. L. S. 2011. Lysosomal storage diseases: diagnostic confirmation and management of presymptomatic individuals. *Genet Med,* 13**,** 457-84.

WATAKABE, A., OHTSUKA, M., KINOSHITA, M., TAKAJI, M., ISA, K., MIZUKAMI, H., OZAWA, K., ISA, T. & YAMAMORI, T. 2015. Comparative analyses of adeno-associated viral vector serotypes 1, 2, 5, 8 and 9 in marmoset, mouse and macaque cerebral cortex. *Neurosci Res,* 93**,** 144-57.

WEI, R. R., HUGHES, H., BOUCHER, S., BIRD, J. J., GUZIEWICZ, N., VAN PATTEN, S. M., QIU, H., PAN, C. Q. & EDMUNDS, T. 2011. X-ray and biochemical analysis of N370S mutant human acid beta-glucosidase. *J Biol Chem,* 286**,** 299-308.

WEST, M. J., SLOMIANKA, L. & GUNDERSEN, H. J. 1991. Unbiased stereological estimation of the total number of neurons in thesubdivisions of the rat hippocampus using the optical fractionator. *Anat Rec,* 231**,** 482-97.

WONG, K., SIDRANSKY, E., VERMA, A., MIXON, T., SANDBERG, G. D., WAKEFIELD, L. K., MORRISON, A., LWIN, A., COLEGIAL, C., ALLMAN, J. M. & SCHIFFMANN, R. 2004. Neuropathology provides clues to the pathophysiology of Gaucher disease. *Mol Genet Metab,* 82**,** 192-207.

WORGALL, S., SONDHI, D., HACKETT, N. R., KOSOFSKY, B., KEKATPURE, M. V., NEYZI, N., DYKE, J. P., BALLON, D., HEIER, L., GREENWALD, B. M., CHRISTOS, P., MAZUMDAR, M., SOUWEIDANE, M. M., KAPLITT, M. G. & CRYSTAL, R. G. 2008. Treatment of late infantile neuronal ceroid lipofuscinosis by CNS administration of a serotype 2 adeno-associated virus expressing CLN2 cDNA. *Hum Gene Ther,* 19**,** 463-74.

WU, J., ZHAO, W., ZHONG, L., HAN, Z., LI, B., MA, W., WEIGEL-KELLEY, K. A., WARRINGTON, K. H. & SRIVASTAVA, A. 2007. Self-complementary recombinant adeno-associated viral vectors: packaging capacity and the role of rep proteins in vector purity. *Hum Gene Ther,* 18**,** 171-82.

XU, Y. H., REBOULET, R., QUINN, B., HUELSKEN, J., WITTE, D. & GRABOWSKI, G. A. 2008. Dependence of reversibility and progression of mouse neuronopathic Gaucher disease on acid beta-glucosidase residual activity levels. *Mol Genet Metab,* 94**,** 190-203.

XU, Y. H., WENSTRUP, R. & GRABOWSKI, G. A. 1995. Effect of cellular type on expression of acid beta-glucosidase: implications for gene therapy in Gaucher disease. *Gene Ther,* 2**,** 647-54.

YOUNG-GQAMANA, B., BRIGNOL, N., CHANG, H. H., KHANNA, R., SOSKA, R., FULLER, M., SITARAMAN, S. A., GERMAIN, D. P., GIUGLIANI, R.,

HUGHES, D. A., MEHTA, A., NICHOLLS, K., BOUDES, P., LOCKHART, D. J., VALENZANO, K. J. & BENJAMIN, E. R. 2013. Migalastat HCl reduces globotriaosylsphingosine (lyso-Gb3) in Fabry transgenic mice and in the plasma of Fabry patients. *PLoS One,* 8**,** e57631.

ZEEVI, D. A., ALTARESCU, G., WEINBERG-SHUKRON, A., ZAHDEH, F., DINUR, T., CHICCO, G., HERSKOVITZ, Y., RENBAUM, P., ELSTEIN, D., LEVY-LAHAD, E., ROLFS, A. & ZIMRAN, A. 2015. Proof-of-principle rapid noninvasive prenatal diagnosis of autosomal recessive founder mutations. *J Clin Invest,* 125**,** 3757-65.

ZHANG, H., YANG, B., MU, X., AHMED, S. S., SU, Q., HE, R., WANG, H., MUELLER, C., SENA-ESTEVES, M., BROWN, R., XU, Z. & GAO, G. 2011. Several rAAV vectors efficiently cross the blood-brain barrier and transduce neurons and astrocytes in the neonatal mouse central nervous system. *Mol Ther,* 19**,** 1440-8.

ZHANG, S., TANG, M. B., LUO, H. Y., SHI, C. H. & XU, Y. M. 2017. Necroptosis in neurodegenerative diseases: a potential therapeutic target. *Cell Death Dis,* 8**,** e2905.

ZIEGLER, R. J., CHERRY, M., BARBON, C. M., LI, C., BERCURY, S. D., ARMENTANO, D., DESNICK, R. J. & CHENG, S. H. 2007. Correction of the biochemical and functional deficits in fabry mice following AAV8-mediated hepatic expression of alpha-galactosidase A. *Mol Ther,* 15**,** 492-500.

ZIMRAN, A. 2011. How I treat Gaucher disease. *Blood,* 118**,** 1463-71.